Université de Lille

Doctoral School **MADIS**
University Department **CRIStAL**

Thesis defended by

Sumit SOOD

on **7 December 2021**

In partial fulfilment of the requirements for PhD degree from Université de Lille

Academic field **Automatique et Informatique Industriel**

Multiphysics modelling for online diagnosis and efficiency tracking: Application to green H$_2$ production

Thesis supervised by

Supervisor:	Belkacem OULD-BOUAMAMA	-	Professor and Director of Research, Polytech Lille, University of Lille, Lille (France)
Co-supervisor:	Jean-Yves DIEULOT	-	Associate Professor (HDR), Polytech Lille, University of Lille, Lille (France)
	Mathieu BRESSEL	-	Dr. Lecturer Researcher, Junia, Lille (France)

Composition of jury

Referees:	Christophe TURPIN	-	Director of Research CNRS, Laplace Laboratory, Toulouse (France)
	Samir JEMEI	-	Professor, FEMTO-ST CNRS, IUT of Belfort-Montbéliard, Belfort (France)
Examiners:	Nadia STEINER	-	Professor, FEMTO-ST CNRS, IUT of Belfort-Montbéliard, Belfort (France)
President of jury	Betty SEMAIL	-	Professor and Director of L2EP, Polytech Lille, University of Lille, Lille (France)
	Jurriaan BOON	-	Dr. Senior Scientist, Sustainable Technologies for Industrial Processes (STIP), TNO, Petten (Netherlands)
Invited member:	Andrei KHODAKOV	-	Director of Research CNRS, UCCS Laboratory, University of Lille

Université de Lille

Ecole doctorale **MADIS**
Unité de recherche **CRIStAL**

Thèse présentée par

Sumit Sood

Soutenue le **07 décembre 2021**

En vue de l'obtention du grade de docteur de Université de Lille

Discipline **Automatique et Informatique Industriel**

Modélisation multiphysique pour le diagnostic et le suivi de l'efficacité en ligne : Application à la production d'H$_2$ vert

Thèse dirigée par

Directeur:	Belkacem OULD-BOUAMAMA	-	Professeur et Directeur de Recherche, Polytech Lille, Université de Lille, Lille (France)
Co-directeur:	Jean-Yves DIEULOT	-	Maître de Conférences (HDR), Polytech Lille, Université de Lille, Lille (France)
Co-encadrant:	Mathieu BRESSEL	-	Dr Enseignant Chercheur, Junia, Lille (France)

Composition de jury

Rapporteurs:	Christophe TURPIN	-	Directeur de Recherche CNRS, Laboratoire LAPLACE, Toulouse (France)
	Samir JEMEI	-	Professeur, FEMTO-ST CNRS, IUT de Belfort-Montbéliard, Belfort (France)
Examinateurs:	Nadia STEINER	-	Professeur, FEMTO-ST CNRS, IUT de Belfort-Montbéliard, Belfort (France)
Président du jury	Betty SEMAIL	-	Professeur et Directrice Laboratoire L2EP, Polytech Lille, Université de Lille, Lille (France)
	Jurriaan BOON	-	Dr. Scientifique senior, Sustainable Technologies for Industrial Processes (STIP), TNO, Petten (Pays-Bas)
Invité:	Andrei KHODAKOV	-	Directeur de Recherche CNRS, Laboratoire UCCS, Université de Lille

Acknowledgements

To my Grand-parents **Lt. Mr. Joginder Pal Sood** and **Lt. Mrs. Usha Sood**

Résumé

L'hydrogène vert est le vecteur d'énergie du futur le plus prometteur car il est d'une part capté par des sources renouvelables et inépuisables qui sont les énergies éolienne et/ou solaire et d'autre part permet de meilleurs transport et stockage de l'énergie sur le long terme en bouteilles haute pression par un électrolyseur pour produire ensuite de l'électricité par des piles à combustible sans émission d'aucun polluant. La nature intermittente des SER dégrade la performance et le fonctionnement dynamique des électrolyseurs PEM et leur couplage doit être étudié afin d'assurer la disponibilité opérationnelle et la pérennité du fonctionnement des équipements par une détection précoce des défauts et l'estimation de leurs durées de vie mais aussi le suivi en ligne des performances technico économiques.

L'objectif de la thèse réalisé dans le cadre du projet Européen Interreg-2 Mers E2C est de développer un modèle dynamique multi-physique d'un électrolyseur PEM, basé sur une approche Bond-Graph pour une utilisation générique pour d'autres types d'électrolyseur non seulement pour l'analyse mais aussi pour la conception de systèmes de supervision en ligne pour la détection et localisation de défauts. La modélisation des divers composants de l'électrolyseur a été réalisée sous forme de capsules Bond-Graph. Ces capsules peuvent être connectées en tenant compte de la structure du diagramme d'instrumentation pour obtenir un modèle dynamique global. Ce modèle est capable de représenter différentes configurations, du pilote de laboratoire jusqu'à l'échelle industrielle, et également de suivre l'efficacité en temps réel. Le modèle a été converti en MATLAB® Simulink pour implémentation, puis validé expérimentalement sur une cellule alimentée par une Plateforme Multi-Source Hybride comprenant des sources d'énergie solaire et éolienne. Le modèle a été adapté pour représenter et étudier la performance d'un électrolyseur à Membrane Echangeuse d'Anions, dont la configuration et l'architecture sont similaires, en collaboration avec l'Université d'Exeter. Le modèle permet également de développer des algorithmes de commande, diagnostic et pronostic ; ainsi, un diagnostic robuste des défauts est présenté dans ce travail. Une Interface Utilisateur Graphique pour la supervision en ligne incorpore le modèle et les algorithmes de diagnostic.

Mots clés: Modélisation multi-physique; Diagnostic robuste des défauts; Suivi de l'efficacité; Bond Graph; Electrolyser PEM; Hydrogène vert; Sources Intermittentes; Modélisation dynamique à base de graphes ; Simulation en temps réel

Abstract

Renewable Energy Sources (RES) have emerged as a sustainable alternative to carbon-based energy sources as the world is struggling in limiting the greenhouse effect in the coming years. The use of RES, such as solar and wind, alone is non-reliable due to their intermittent nature. The surplus electricity generated during off-peak hours must be stored to tackle the problem of the unavailability of energy. Green Hydrogen (GH_2) generation using electrolyser running on RES has seen an increase in recent years for the storage of this surplus energy due to its advantages over conventional methods (such as batteries and ultra-capacitors) for long term storage and transport. Proton Exchange Membrane (PEM) based electrolysers are better suited for the coupling with RES as compared to the alkaline electrolysers due to their faster start-up times and fast dynamic load changing capability. The intermittent nature of RES affects the performance and operation dynamics of the PEM electrolyser and must be analysed and studied in order to make these systems more reliable and safer to use. Mathematical modelling is one of the possible solutions for studying their behavior and developing supervision algorithms.

Under the framework of the E2C project of the European Interreg 2-Seas program, a generic dynamic multi-physics model of a PEM electrolyser has been proposed in this work based on Bond Graph (BG) approach. Various components of the PEM electrolyser have been modelled in the form of BG capsules. These capsules can be connected based on the piping and instrumentation diagram of the PEM electrolyser system to have a global model of the system. The developed model is capable of representing different configurations of PEM electrolysers ranging from laboratory scale to industrial scale. The model is also capable of facilitating efficiency tracking in real-time. The developed model in the BG form has been converted into MATLAB$^{\circledR}$ Simulink block diagram from the implementation point of view. The model was then validated using a single cell PEM electrolyser powered by a Hybrid Multi-source Platform (HMP) running on solar and wind energy at the University of Lille. The proposed model was also extended for the modelling and performance study of Anion Exchange Membrane (AEM) electrolysis cell, in collaboration with the University of Exeter of England, which shares a similar configuration and architecture.

The developed model for the PEM electrolysis system is also suitable for the development of control, diagnosis, and prognosis algorithms. Therefore, a model-based robust fault diagnosis for PEM water electrolyser has been proposed in this work. The proposed diagnosis algorithms and model have been then utilized for developing the graphical user interface for online supervision.

Key words: Multi-physics modeling; Robust fault diagnosis; Efficiency tracking; Bond Graph; PEM electrolyser; Green hydrogen; Intermittent sources; Graphical Dynamical modeling; Real time simulation.

Contents

ix

List of Figures

List of Tables

Nomenclature

α_k Charge transfer or symmetry factor coefficients for k^{th} electrode

β Transformer coefficient of the converter

ΔG_R Gibb's free energy of water dissociation reaction, J.mol^{-1}

ΔH_R Enthalpy Change of water dissociation reaction, J.mol^{-1}

ΔS_R Entropy change of water dissociation reaction, J.mol^{-1}.K^{-1}

$\dot{\xi}$ Rate of reaction flow, mol.s^{-1}

$\dot{H}$ Enthalpy rate, J.s^{-1}

$\dot{m}_i$ Mass flow rate of the ith species, kg.s^{-1}

$\dot{n}_i$ Gas mass flow rate for i^{th} species, kg.s^{-1}

$\dot{Q}$ Rate of heat flow, J.s^{-1}

γ Hydration of the membrane

ν_i Coefficient of stoichiometry for i^{th} species

ρ_w Water density, kg.m^{-3}

σ_M Conductivity of the membrane, S.m^{-1}

ε Efficiency

A_M Cross-sectional area of the membrane, m^2

$A_{sep,i}$ Cross-sectional area of the ith separator, m^2

a_{H_2O} Chemical activity of water

C_i Matter storage capacity of the ith species ($i = H_2, O_2, H_2O$), kg^2.J^{-1}

C_p Specific heat at constant pressure, J.kg^{-1}.K^{-1}

C_{cold}^{th} Thermal capacitance of cooling tank, J.K^{-1}

C_{cool}^{th} Thermal capacitance of cooling circuit, J.K^{-1}

$C_{dry,i}^{ch}$ Dryer's chemical capacitance of the purification unit for the ith species, mol.Pa^{-1}

C_{dry}^{th} Dryer's thermal capacitance of the purification unit, J.K^{-1}

C_{enc}^{th} Thermal capacity of the enclosure, J.K^{-1}

$C_{Hsep,i}^{ch}$ Chemical capacitance of hydrogen separator for the ith species, mol.Pa^{-1}

$C_{Osep,i}^{ch}$ Chemical capacitance of oxygen separator for the ith species, mol.Pa^{-1}

$C_{rec,k}^{th}$ Thermal capacitance of recirculation circuit (anode/cathode side), J.K^{-1}

C_{sep,H_2}^{fl-th} Field capacitance element representing fluidic capacitance and thermal capacitance of hydrogen separator

C_{sep,O_2}^{fl-th} Field capacitance element representing fluidic capacitance and thermal capacitance of oxygen separator

C_{stack} Thermal capacitance of the stack, J.K^{-1}

D_i Parameter for diffusion, $m^2.s^{-1}$

d_M Ratio of length to the cross-sectional area of the membrane, m^{-1}

$E_{act,k}$ Activation overvoltages for k^{th} electrode, V

E_{cell} Cell voltage, V

E_{ohm} Ohmic overvoltage, V

E_{rev} Reversible voltage, V

E_{rev}^0 Standard reversible cell voltage at STP, V

g Acceleration due to gravity, $m.s^{-2}$

H_i Henry's Parameter, $Pa.m^3.mol^{-1}$

I_{cell} Cell current, A

J Current density, $A.m^{-2}$

$J_{0,k}$ Standard current exchange density for k^{th} electrode, $A.m^{-2}$

L_M Length of the membrane, m

$L_{sep,i}$ Water level in Separators (HSV and OSV), m

$L_{sep,i}$ Water level of the ith separator, m

M_i Molar mass for i^{th} species, kg mol^{-1}

n_{eo} Electro-osmosis coefficient

P Pressure, Pa

p_i Partial pressure of ith species, Pa

R_c Coupling element for fluidic flow to thermal flow

$R_{act,k}$ Non linear activation resistance for k^{th} electrode

R_{ads} Coupling resistance of adsorbed water molar flow and the enthalpy flow towards dryer

$R_{diff,i}$ Diffusion resistance of the ith species, $Pa.s.kg^{-1}$

$R_{dry,enc}$ Thermal resistance between purification unit and enclosure, $K.s.J^{-1}$

R_{dry} Internal pneumatic resistance of the dryer, $Pa.s.kg^{-1}$

R_{enc} Thermal resistance between the enclosure and the atmosphere, $K.s.J^{-1}$

$R_{exhaust}$ Pneumatic resistance of the exhaust valve, Pa.s.kg^{-1}

$R_{Hrec,enc}$ Thermal resistance between hydrogen recirculation circuit and enclosure, K.s.J^{-1}

$R_{Hsep,enc}$ Thermal resistance between hydrogen separator and enclosure, K.s.J^{-1}

R_{htex} Thermal resistance of heat exchanger, K.s.J^{-1}

$R_{hyst,k}$ Internal fluidic resistance of the stack at th k_{th} electrode side, Pa.s.kg^{-1}

$R_{Lrec,k}$ Hydraulic resistance representing leakage in recirculation circuit (anode/cathode side), Pa.s.kg^{-1}

R_{ohm} Total ohmic resistance of the cell, Ω

$R_{Orec,enc}$ Thermal resistance between oxygen recirculation circuit and enclosure, K.s.J^{-1}

$R_{Osep,enc}$ Thermal resistance between oxygen separator and enclosure, K.s.J^{-1}

R_{others} Ohmic resistance of the cell except membrane, Ω

$R_{sep,hc}$ Pneumatic resistance between hydrogen separator and hydrogen circuit, Pa.s.kg^{-1}

$R_{sep,oc}$ Pneumatic resistance between oxygen separator and oxygen circuit, Pa.s.kg^{-1}

R_{sepv} Hydraulic resistance of the separator valve, Pa.s.kg^{-1}

R_{stack} Thermal resistance of the stack, K.s.J^{-1}

R_{tank} Hydraulic resistance between tank and oxygen Separator, Pa.s.kg^{-1}

T Temperature, K

$V_{Hsep,i}$ Volume of the ith species in HSV, m^3

$V_{Osep,i}$ Volume of the ith species in OSV, m^3

x_i Mass fraction of the ith species

μ_i Chemical potential of the ith species, J.kg^{-1}

A_i Chemical affinity of the ith species, J.mol^{-1}

C_{ads}^{ch} Water adsorption capacity of the purification unit, mol.Pa^{-1}

F   Faraday's constant, C.mol^{-1}

R   Ideal gas constant, J.mol^{-1}. K^{-1}

List of Abbreviations

AEM Anion Exchange Membrane. xii, xv, 3, 5, 16, 17, 19, 22, 24, 72, 106, 109–111, 113–118

AI Artificial Intelligence. 11

ARR Analytical Redundancy Relation. 14, 16, 17, 76, 79–82, 129–133

BG Bond Graph. xi–xiii, 9, 15–17, 39, 40, 47, 50–69, 71, 72, 74, 76, 85, 105, 106, 109–117, 119–127, 129–132

BoP Balance of Plant. 15, 35, 37, 40, 43, 45, 46, 53, 60, 105

BV Butler-Volmer. 28–32, 35, 37, 41, 43

CFD Computational Fluid Dynamics. 27, 31, 43, 45–47

CO$_2$ Carbon Dioxide. 2, 3

COG Causal Ordering Graph. 42, 44

CRIStAL Centre de Recherche en Informatique, Signal et Automatique de Lille. 1, 2, 4, 18

CTC Charge Transfer Coefficient. 30, 32

DBG Diagnostic Bond Graph. xi–xiii, 17, 50, 74, 76–80, 83–89, 99, 100, 103, 106, 107, 129–132

DC Direct Current. 19, 21, 38, 42, 73, 124

DME Dimethyl Ether. 3, 6

EDX Energy Dispersive X-ray Spectroscopy. 50

EEC Equivalent Electrical Circuit. 33, 35, 37–40, 42, 44, 46

EIS Electrochemical Impedance Spectroscopy. 37, 48–50

EMR Energetic Macroscopic Representation. 39, 40

ERDF European Regional Development Fund. 2

FDI Fault Detection and Isolation. 47, 74, 76, 99, 108

FSM Fault Signature Matrix. xiii, xv, 81–88, 100, 130, 133

FTC Fault Tolerant Control. 10, 14

GDL Gas Diffusion Layer. 20, 30, 37, 45–47

GH$_2$ Green Hydrogen. xi, 6, 15, 46, 105

GUI Graphical User Interface. xii, 5, 16, 18, 52, 100, 102, 103, 106

HMP Hybrid Multi-source Platform. xii, 5, 16–18, 100, 102, 106

General Introduction

Contents

1.1 Thesis framework

The results presented in this Ph.D. thesis are the outcome of the research work carried out at Centre de Recherche en Informatique, Signal et Automatique de Lille (CRIStAL), CNRS UMR 9189, under the supervision of Professor Belkacem Ould-Bouamama, Dr. Jean-Yves Dieulot and Dr. Mathieu Bressel. This research work was funded under Interreg 2 Seas E2C project (subsidiary contract no. 2S03-019).

1.2 General Context

The Paris Agreement, a new climate treaty adopted by 196 signatory parties of United Nations Framework Convention on Climate Change at COP-21 set the milestone for reducing global warming to keep the average global annual temperature increase below two degree Celsius which is to be achieved by the year 2100 through limiting the greenhouse house emissions using leading science and technology [1]. The world has seen the increase in the use of RES, while reducing the dependence on the conventional fuels, as one of the solutions to achieve this objective. Figure 1.1 shows the renewable energy generation around the world since 1965 using hydro power, solar power, wind power and other sources like geothermal and biomass based on the data published by bp in the 70th edition of the statistical review of world energy [2]. Hydro power has always been a leading renewable energy source and it can be seen that the use of wind and solar energy has seen considerable rise in last decade.

A lot of research has been carried out in order to make the harness of these RES more efficient, eco-friendly and cost effective so that they can compete with the conventional energy sources such as petroleum and coal to shift the balance towards green energy. France has also been actively working towards increasing the use of RES. Under Multi-annual Energy Program, targets have been set by the policymakers to be achieved by 2023 and 2028 (Shown in the table 1.1) for the development of the renewable energy infrastructure [3].
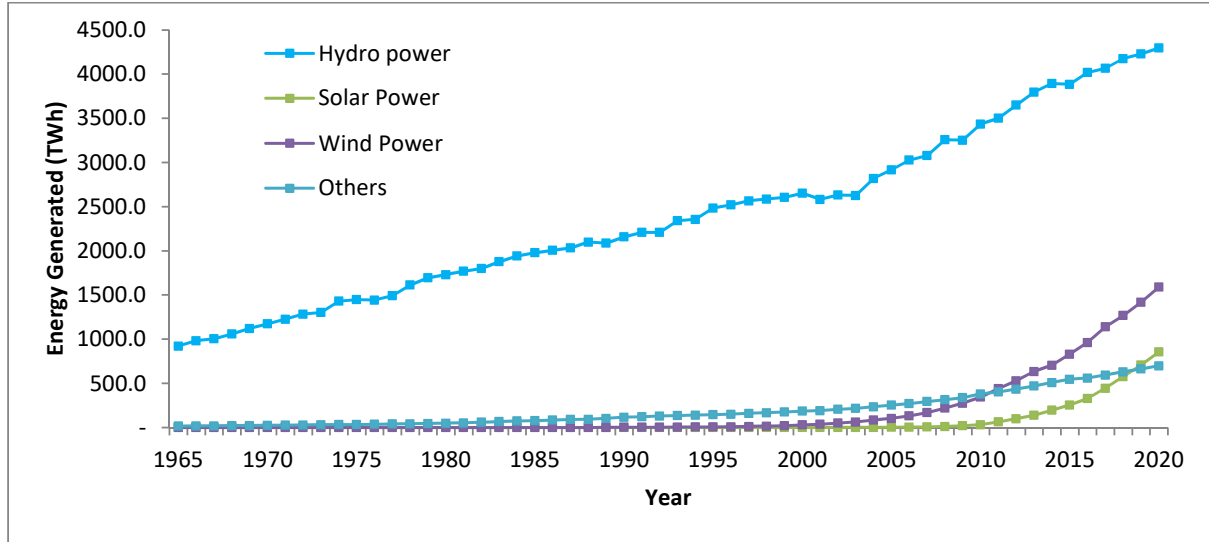
Figure 1.1: Renewable energy generation around the world

Renewable Energy Source	Targets to be achieved	
	by 2023	by 2028
Solar Energy	24.1 GW	33.2-44 GW
Wind Energy (Onshore)	24.1 GW	33.2-34.7 GW
Wind Energy (Offshore)	3.4 GW	5.2-6.2 GW
Hydroelectricity	25.7 GW	26.4-26.7 GW
Biomass	145 TWh	157-169 TWh
Geothermal Energy	2.9 TWh	4-5.2 TWh

Table 1.1: Renewable energy targets to be achieved by France.

France is also a part of European Territorial Cooperation Programme named Interreg 2 Seas 2014-2020 along with England, Belgium/ Flanders and the southern part of the Netherlands which also focuses on the development and implementation of low-carbon technologies in the 2 seas region in order to reduce the greenhouse gases emission and dependency on the conventional energy sources. The program is partially funded by the European Regional Development Fund (ERDF). Figure 1.2 shows the area covered by the Interreg 2 Seas programme. In July 2018, a project named **Electrons to high value Chemical products**, most commonly known as **E2C** project, was started under Interreg 2 Seas programme with the ambition of developing technologies for the conversion of Carbon Dioxide (CO_2) with the help of surplus renewable energy available in 2 Seas region into fuels and sustainable chemicals for the industry.

1.2.1 E2C Project

E2C project was officially started as a three year project on 1st July 2018, with Project budget of 7,184,812€ (including 4,310,887€ ERDF contribution). Due to the Covid-19 pandemic, the deadline has been shifted to 30th June 2022. The project is a collaborative effort of seven partners from 2 seas region, Energy Research Centre of the Netherlands (leading partner) and Technical University Delft from the Netherlands, University of Lille from France, University of Exeter and University of Sheffield from England and Flemish Institute for Technological Research and University of Antwerp from Belgium. From University of Lille Itself there are two research teams (CRIStAL and Unité de Catalyse et de Chimie du Solide de Lille (UCCS)) that

2
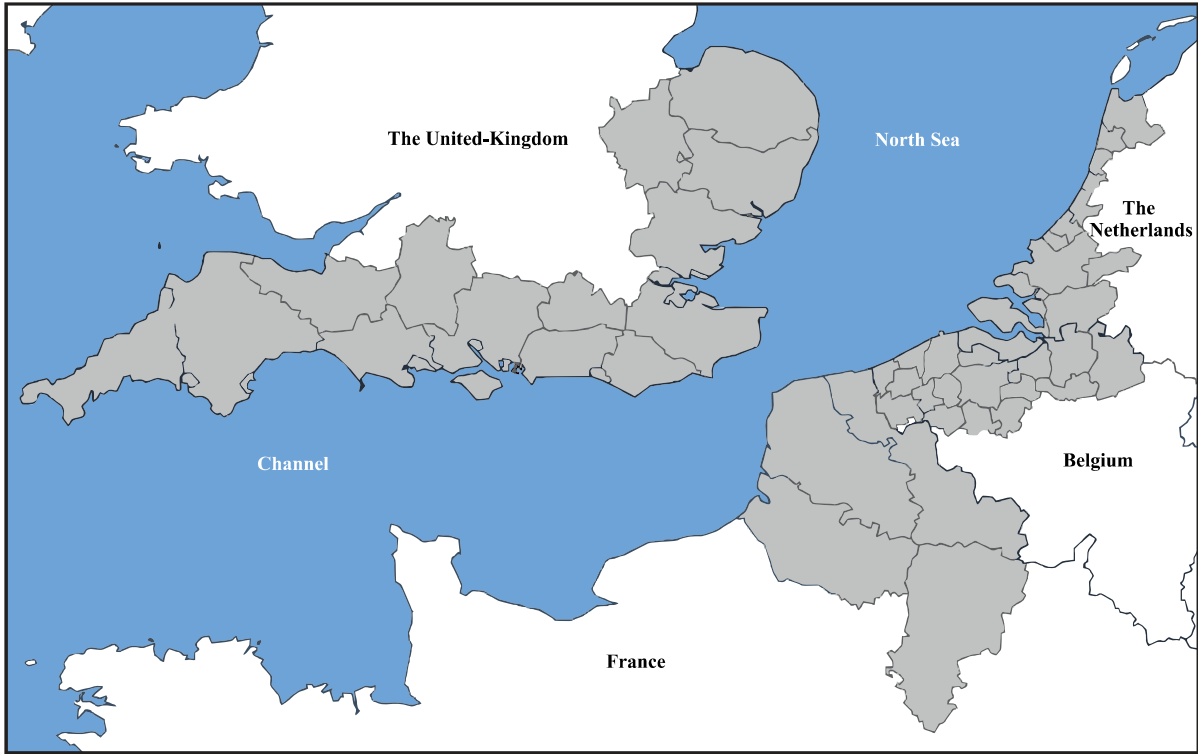
Figure 1.2: Interreg 2 Seas region

are working on this project with different objectives. The overall objective of the project is to develop two innovative Power-to-X technologies namely direct and indirect conversion processes to convert the CO_2 into formic acid and Dimethyl Ether (DME) respectively with the help of green electricity obtained from RES resulting in the reduction of carbon footprint as the CO_2 is used as a raw material. The key outcomes of the project are as follows

- Pilot demonstrator for each of the developed Power-to-X technologies i.e. one for direct process for the conversion of CO_2 and green electricity into formic acid and one for indirect process to convert CO_2 and green electricity into DME.

- A test bench installation for the testing and lifetime estimation for Anion Exchange Membrane (AEM) electrolysis cells.

- Report on the feasibility studies for the implementation of the developed Power-to-X technologies that include, road-mapping, calculations and planning for different scenarios for business and industrial implementation of the technologies.

Figure 1.3 shows the process of conversion of CO_2 into DME. The renewable energy in the form of green electricity is used for generating the hydrogen using an electrolyser. Oxygen is generated as a byproduct. The hydrogen is then utilized along with CO_2, which can be sourced from industries through CO_2 trapping, in a reactor where Sorption Enhanced Dimethly Ether Synthesis (SEDMES) process takes place. DME is the final product while water is produced as a byproduct. This whole process is termed as indirect line as the renewable energy is indirectly used to produce DME.

Figure 1.4 shows the process of converting CO_2 into formic acid. In direct conversion process, the green electricity is directly used to power electrochemical flow reactor in which the CO_2 is fed to the cathode side where Formic acid is formed and flows out with the unconsumed CO_2.

3
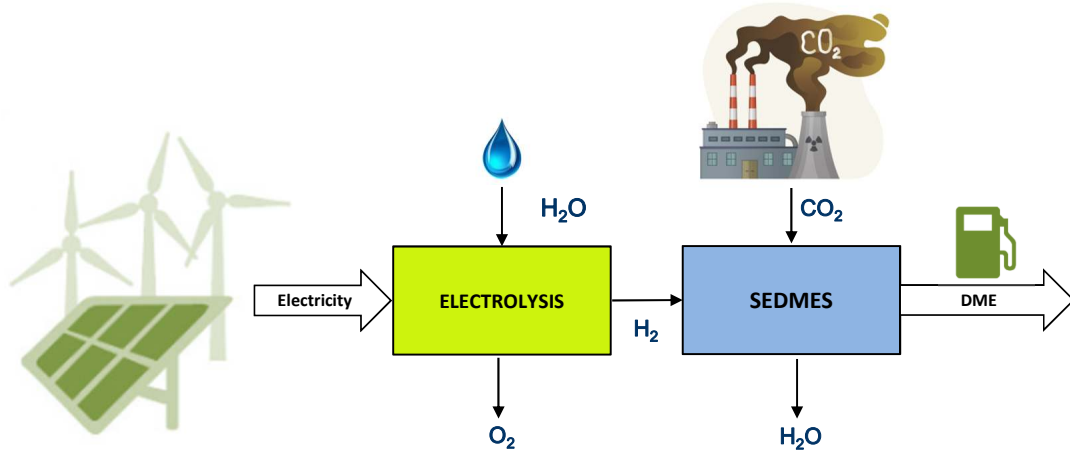
Figure 1.3: Indirect conversion process

Oxygen gas evolves through anode as a byproduct. The construction of the electrochemical flow reactor is similar to that of an electrolyser.
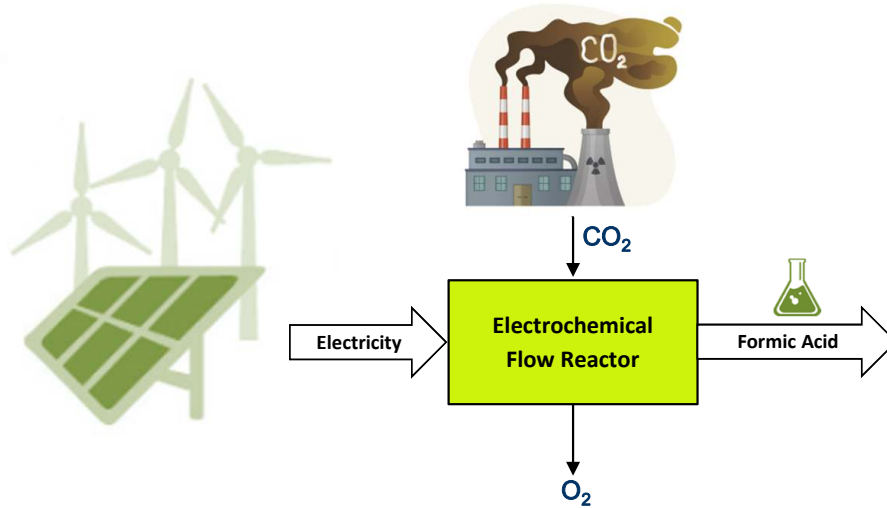
Figure 1.4: Direct conversion process

1.2.1.1 Contribution of CRIStAL in E2C Project

The PERennisation des Systèmes Industriels (PERSI) team of CRIStAL laboratory, specialised in modelling,control and supervision of complex multi-physics systems, has been a part of the project from the very beginning. The PERSI team is tasked to provide two deliverables for the project. These deliverables are

- **D1.3.1** PEM electrolyser system performance & lifetime modelling simulation tool.

- **D1.3.2** Report on modelling & simulation control strategies for direct and indirect conversion processes.

The first deliverable D1.3.1 was focused on the development of generic dynamic multi-physics model of PEM electrolyser running on intermittent sources (solar and wind energy) and its

and validation on the HMP available at University of Lille. The model was also extended to AEM electrolysis cell through the collaboration with University of Exeter (see appendix A). Diagnosis and prognosis (remaining useful life estimation) algorithms were also developed. A GUI for performance simulation and supervision of PEM electrolyser was constructed using MATLAB® Simulink. This deliverable was submitted in January 2021.

The second deliverable D1.3.2 is due for the end of December 2021. This deliverable focuses on the preparation of the report on control strategies for direct and indirect conversion processes (literature survey and possible solutions). It will also include the demonstration for Indirect process line in the form of simulations under various operating conditions and real-time demonstration under different scenarios on HMP for indirect conversion under intermittent sources (which is possible for electrolyser part only as the pilot for SEDMES is not available to be coupled with existing HMP at University of Lille.

1.2.2 Green Hydrogen as Energy Storage

Solar and wind energy are emerging as a clean and sustainable alternatives to the conventional energy sources, but, they lack a stable output as the availability of the energy cannot be ensured all the time and it depends on the climate conditions. Due to their intermittent nature, the availability of the energy is often unpredictable, makes the electricity production using these sources alone non-reliable. The electricity consumption in itself is only very partially controllable, hence the energy production must be able to adapt according to change in the demand. Figure 1.5 shows the monthly average solar energy and wind speed for year 2020 for one of the cities in north of France. It can be seen that the availability of these energy sources

(a)

(b)
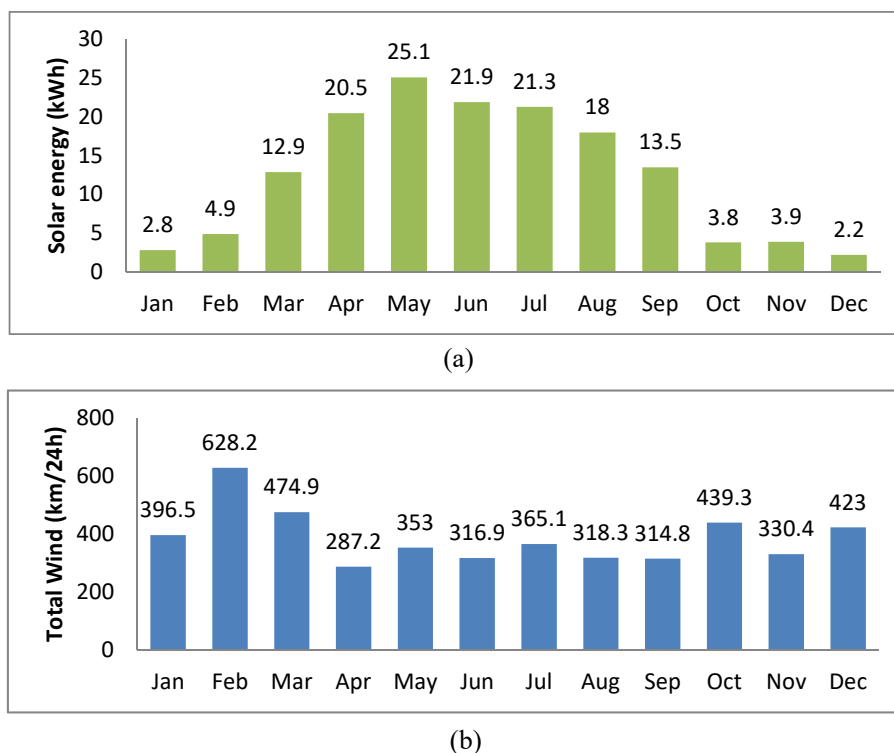
Figure 1.5: Availability of solar and wind energy in North France (59890) for 2020 [4]

vary throughout the year. Usually these energy sources are utilized with grid assistance in order to avoid the problem of energy unavailability. However, during off peak hours, the energy available through these RES could be surplus and must be stored in order to avoid the energy

5

wastage and minimize operating cost. Conventionally, batteries are used to store this surplus energy, but is it not a viable option in case the energy is required to be stored for a long time. Also, with increase in the amount of energy to be stored, the cost of storage increases as more batteries are required.

Using hydrogen as storage for surplus electricity from RES has gained popularity in recent years due to its numerous advantages. Hydrogen can be produced from water, which is available in abundance. It has the highest energy content while being the lightest and cleanest fuel [5]. The use of hydrogen as a fuel only results in water as the emission. Hydrogen production through electrolysis of water is a well-established technique and can be easily integrated with suitable electric sources [6]. GH_2 is a term that is used to represent the hydrogen that is generated using RES for water electrolysis. GH_2 is a better alternative to batteries for energy storage for long time [7]. Also, it can be transported easily over long distances in the form of pressurized gas. Figure 1.6 shows the potential applications of the hydrogen generated using RES. The surplus energy from RES is used to generate GH_2 using suitable water electrolysis. The produced GH_2 can be stored in the hydrogen storage tanks which can then later be utilized to regenerate electricity using fuel-cell to support electrical loads or to drive a fuel-cell equipped electric vehicle. The GH_2 can also be used in the industry for producing ammonia, oil refining
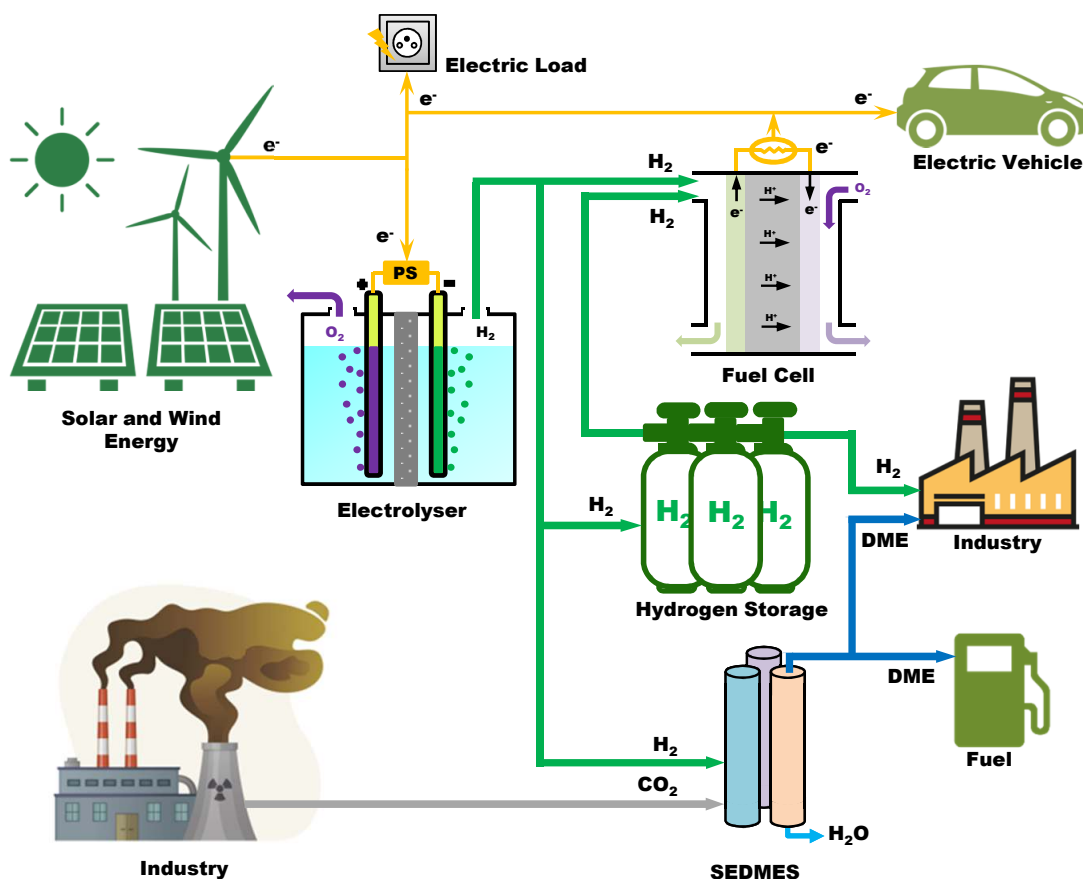
Figure 1.6: Generation, storage and application of GH_2

and methanol production. Figure 1.7 shows the increasing trend of global demand of pure hydrogen since 1975, major part of which is utilized for refining and ammonia production. The global demand of hydrogen is estimated to reach 212Mt by 2030 out of which 10% share is estimated to be of GH_2 [8]. In the case of the E2C project, it is used to generate DME using SEDMES process which can be used as a fuel and is also extensively used in chemical industry.

6
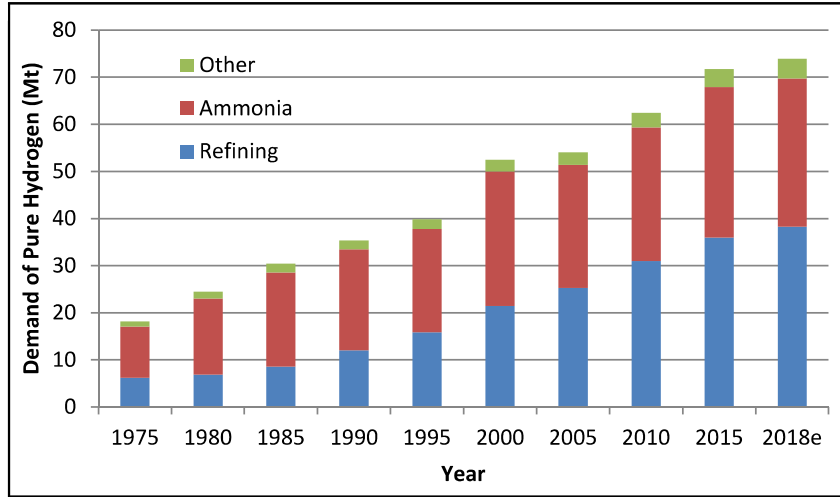
Figure 1.7: Global demand for pure hydrogen since 1975[9]

1.2.3 Technological Issues

Despite of numerous advantages of using hydrogen as storage, there are also some shortcomings that are needed to be addressed in order to make this energy storage method safe, economic, and reliable. As hydrogen is a light gas, energy density by volume at atmospheric pressure is very low. Therefore, the hydrogen needs to be compressed to make it an efficient energy storage method. This is achieved by producing the hydrogen at high pressure or by including the compression stage before storage. This increases the cost of the storage process. Hydrogen is also a highly flammable gas, therefore, its handling requires extreme care. The Hindenburg disaster is a proof of destruction that can be caused by minuscule accident or improper handling of hydrogen gas [10]. The electrolysers required to produce pure hydrogen at high pressure and production rate are also expensive as they use novel metals. Research is being carried out to make these devices less expensive by inventing new materials. Due to the intermittent nature of the RES, the dynamics of the electrolyser is affected and it becomes necessary to study the effect of the intermittency of the RES on the overall performance of the electrolyser even if the effect of the intermittency is reduced when the system is grid assisted. Indeed, the use of RES to operate the electrolyser poses various issues that need to be addressed. At very low power output from the source, when the power is barely enough to run the electrolyser, the rate of hydrogen production may be lower than the rate of gases crossover through the membrane which can be dangerous for the electrolyser as well as the operator [11]. Intermittent sources may also lead to the lower efficiency as the electrolyser might not be operating at the nominal temperature. Thus, it becomes necessary to study the effect of the intermittent sources on the performance of the electrolyser.

1.2.4 Why Bond Graphs for Dynamic Modelling of RES?

High cost of the electrolyser has always been a challenge for the researchers. New materials and cell design are being developed to reduce the overall cost of the electrolyser [12, 13]. There is also a need for developing the tools in order to test the electrolysers under different conditions to understand various phenomena taking place inside the electrolyser to predict the performance of the electrolyser in the cost effective way and to propose optimal sizing. Mathematical modelling plays a very crucial role towards this objective and acts as a dynamic connection between the electrolyser and the intermittent power source [14]. It also enables the researchers for the design

7

optimization and developing control for the system and online diagnosis to insure safety and availability of equipment [6].

Modelling and simulation are very powerful tools of modern engineering that can provide alternate means for design investigation and operating conditions optimization by spending less time and at relatively lower cost as compared to the physical experiments [15]. The importance of modelling and simulation increases many folds in case of dynamic multi-physics systems. Electrolysers are one such case in which complicated physico-chemical processes takes place. Modelling plays a significant role in quantifying such processes [16]. Also, system dynamics plays an important role in system performance during the operation of the electrolyser running on RES. The model should be able to capture the dynamics in order to predict the performance of the system over a required time window, according to the weather. It is particularly important if a hydrogen generator is connected directly to a chemical plant to supply the hydrogen at a steady rate based on the plant requirement. This is however partially achieved by using a buffer tank to temporally store the hydrogen and then supply it at the required pressure and flow-rate. While operating such systems, the main concern is to understand (diagnosis) or foresee (prognosis) abnormal situation so as to react as fast as possible so that the device can be either stopped in case of critical fault or to operate in degraded mode if the fault can be accommodated. Therefore, static models are not sufficient for this purpose and there is a requirement of a dynamical model.

Dynamical models once developed can serve multiple purposes ranging from understanding the phenomenon, developing control for the system as well as for diagnostics. For dynamic modelling of multi-physics system, a number of techniques have been developed over time to deal with the challenges posed by the requirements of a model to perform various tasks ranging from simulation to diagnosis. Different modelling techniques for dynamical systems can be broadly classified under two categories, namely equation based and graphical based modelling [17], as shown in figure 1.8.
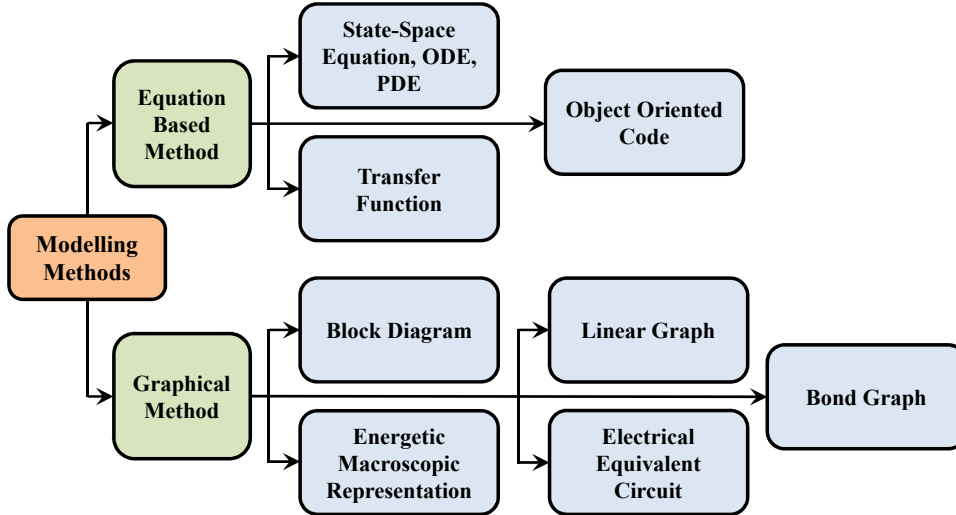
Figure 1.8: Different multidisciplinary modelling approach

In equation based modelling techniques, the system is represented in terms of ordinary differential equations. These approaches are very expressive and can easily handle most of the dynamical systems which include multi-physics systems. Furthermore, to use these approaches, the dynamical equations as well as the values of the parameters of the whole system are needed to be known by the modeller, these modelling techniques are less user friendly. In graphical based modelling approaches, the model is decomposed into graphical components (also called

as blocks or sub-models) that are connected with each other through ports. These blocks are assembled to represent the structure of the model that can exhibit the behaviour of the system. In the concept of graphical modelling, the user has the advantage of modifying and reusing the sub-models of different components which provides a user friendly way of modelling and flexibility in the modelling of the complex systems. Additionally, the graphical models have also the advantage of showing the topology of the represented system [17]. In opposition to the equation based modelling, there is no need of accurate parameters value. Although many approaches are available under the banner of graphical based modelling, BG is well suited for the multi-physics systems because of its many advantages.

BG is a unified multi-physics approach which involves four levels of modelling using only one tool (technological level, physical level, mathematical level and algorithmic level) [15]. Any system can be represented in terms of pictographic representation known as word BG that shows the main component of the system and the nature of exchange of power among them (Technological level). To deal with the enormous amount of equations describing the dynamic behaviour of the different phenomena occurring in the system (mathematical level), the BG (by its graphical nature) enables to display precisely the exchange of power in a system, including storage and transformation (physical level).The advantage here is to deduce systematically equations from a graphical description of the power exchange in the system (algorithmic level).

1.2.5 Prognostic and Health Management

In the safety–critical systems like electrolysis system running on intermittent sources, complete failure of any component or subsystem can be very dangerous or unsafe for the people and the environment. Therefore, real time health monitoring (diagnosis) of the system is essential for early detection of the fault and to identify the current health status of the components or system to ensure safe and reliable operation of the system. PHM is a new emerging technique that facilitates in performing predictive maintenance based on the prediction of degradation of the components and its trend and estimation of Remaining Useful Life (RUL) of the system and/or components. Figure 1.9 shows the various steps of the PHM.

Data Acquisition
- Collection of data from mentoring and extraction of the features.

Diagnosis
- Detection of occurrence of fault, its isolation and estimation of its severity.

Prognosis
- Calculation of the Remaining Useful Life.

Health Management
- Decision making based on the control laws for fault accommodation or maintenance.
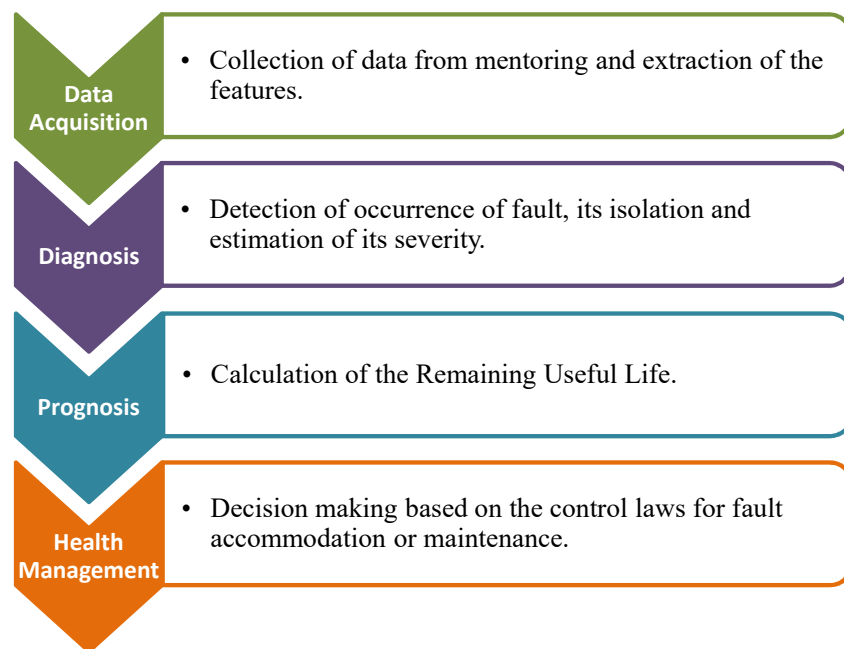
Figure 1.9: Various steps of the PHM

During data acquisition, the data is collected from the sensors placed throughout the system for various purposes such as feedback and control. The useful features are then extracted from this measurement data for monitoring the system health. Diagnosis step is very crucial for the reliable and safe operation of the system. At this step, the fault or degradation in the components of the system is detected. the fault is then isolated in order to determine the cause and its severity is estimated. Fault diagnosis in real-time is of critical importance for the complex systems so that the early detection of the fault could be performed. During prognosis step, once the degradation of the component/s of the system occurs, the estimation of the time is done for which the system can perform desired operations. This estimated time for which the system or component can remain functional is known as the RUL. This value of RUL is then used on the next step for health management. Based on the governing laws for the control of the system and RUL, appropriate action is taken by either scheduling the preventive maintenance or by completely stopping the operations of the system for further analysis and repair.

Hence, for improving Reliability, Availability, Maintainability and Safety (RAMS) of modern process engineering systems, prompt fault detection, robust faulty component isolation and effective RUL prediction of degrading components have become an active research area over the last few decades. More accurate integrated real time fault diagnosis and prognosis techniques are to be evolved according to the present demand of critical machinery performance for the predictive maintenance under PHM strategy.

1.2.5.1 Fault Diagnosis Tasks

There are generally four tasks for fault diagnosis, namely fault detection, fault isolation, fault identification and fault accommodation [18].

1. **Fault detection**: This is the first step of fault diagnosis tasks to detect the fault (if any) presence in the supervised system. It should be designed in such a way that it can detect the fault as early as possible when the process dynamics of the system is deviated beyond an acceptable limit from its nominal behaviour, which is very important before the fault to possibly causes a critical failure in the system. If an unacceptable behaviour is detected then an alarm state is declared.

2. **Fault isolation**: When any fault is detected and an alarm state is declared, then the aim of this stage to find out the initial set of fault candidates which is responsible for abnormal behaviour of the system. This stage further concerns the minimization of dimension of initial fault candidates by assuming that some of the fault candidates are robust or by using some other information.

3. **Fault identification**: The aim of this step is to find out the magnitude of the fault and its type. For abrupt fault, if multiple fault sets remain after fault isolation, then identification is required for each fault set and the fault set that matches the observations most closely is considered to be the true fault set. For incipient fault, the fault identification task is challenging since certain dynamic degradation behaviour for this fault must be assumed in advance and sometimes this prior knowledge is not easy to obtain. If the severity of the identified fault is acceptable, this severity will be used in the reconfiguration design of the system's control law.

4. **Fault accommodation**: Once the fault magnitude is estimated then the decision regarding whether the identified fault can be accommodated or not by suitably changing the control law is taken in this stage. Also degree of fault severity is used in this stage to determine whether to use system reconfiguration, Fault Tolerant Control (FTC) or manual supervision.

1.2.5.2 Fault Diagnosis Methodologies

Diagnosis search strategy is usually strongly dependent on the knowledge representation scheme which in turn is largely influenced by the kind of a priori knowledge available. Hence, the type of a priori knowledge used is the most important distinguishing feature in diagnostic systems. Diagnosis systems are classified based on a priori knowledge used. The basic of a priori knowledge that is needed for fault diagnosis is the set of failures and the relationship between the observations (symptoms) with the failures. A diagnostic system may have them explicitly, or it may be inferred from some source of domain knowledge. A priori domain knowledge may be developed from a fundamental understanding of the process using first principles knowledge. Such knowledge is referred to as deep, causal or model-based knowledge. On the other hand, it may be gleaned from past experience with the process. This knowledge is referred to as shallow, compiled, evidential or process history-based knowledge. Fault diagnosis methods can be broadly classified into two types: model based method and data driven method [18], as shown in figure 1.10.
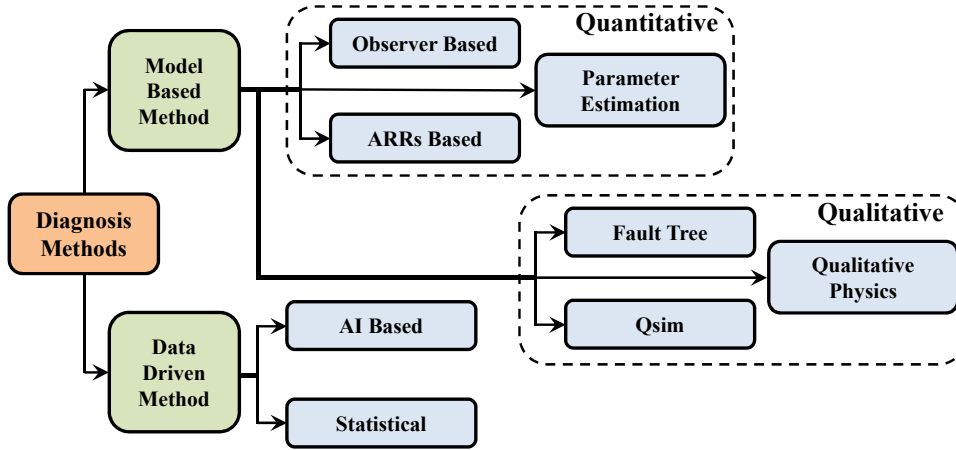
Figure 1.10: Classification of diagnosis methods

For model based methods, models serve as knowledge representation of a large amount of structural, functional and behavioural information and their relationship. This knowledge representation is capitalized to create complex cause-effect reasoning leading to construction of powerful and robust automatic diagnosis and isolation systems [18, 19]. In model-based, a priori knowledge can be broadly classified as qualitative or quantitative. The quantitative models represent mathematical functional relationships between the inputs and outputs of a system and they are evaluated numerically; while the qualitative models represent these relationships in terms of qualitative functions centered on different units in the system. Qualitative model based approach provides an alternative when a numerical model of the system is unavailable.

In contrast to the model-based approaches, where a priori knowledge about the model (either quantitative or qualitative) of the process is assumed, in process history-based methods, only the availability of large amount of suitably annotated historical process data are required. There are different ways in which this data can be transformed and presented as a priori knowledge to a diagnostic system. This is known as feature extraction. This can proceeds as either quantitative or qualitative feature extraction. In quantitative feature extraction, one can perform either a statistical or non-statistical feature extraction. Artificial Intelligence (AI) or statistical data-driven-based methods have some advantages, such as capturing complicated phenomenon without a priori knowledge, and performing faster than traditional system identification techniques in multivariate diagnosis/prognosis problems. However, the linkage between

11

fault degradation and changes in physical parameters is generally lost with data-driven models. Moreover, it is a tough and high cost task to collect abundant data. Many algorithms and data training models require a large amount of historic data, including normal state data and failure data that need to destroy the components/systems artificially.

There is always an overlap between the various approaches. For instance, it is clear that all models need data for estimating some of the parameters in the model and all the methods based on process data need to extract some form of a model to perform fault diagnosis. Different approaches for the diagnosis procedures have been developed, depending on the kind of knowledge used to describe the process model. Each system or process has its own complexities, which need to be described by following a specific methodology. Venkatasubramaniam et al. [20–22] have classified various fault detection and diagnosis methods into quantitative model based methods, qualitative model and search based methods and process history based methods. Further sub-classifications and detailed reviews on each approach are given therein. Thus, various approaches for diagnosis methods can be grouped into two types: model–based diagnosis and data–driven–based diagnosis. Nowadays, researchers integrate the advantages of various approaches to improve the diagnosis schemes, named as hybrid approaches.

1.2.5.3   Failure Prognosis Tasks

The term prognosis is well used in medical domain to describe the prediction of poor health of a patient by taking into account the actual diagnosis of a disease and its evolution compared with other similar observed cases. In industrial domain, the same reasoning of prognosis can be transposed to machines and components to answer the question about the remaining useful lifetime of a machine or a component once an impending failure condition is detected, isolated, and identified [23, 24]. Failure prognosis is used to determine how soon and likely a failure will occur. Prognosis could significantly reduce expensive downtime and maintenance costs. The prognosis is used to predict how much time is left before a failure occurs given the current machine condition and past operation profile. The time left before observing a failure is usually called RUL.

1.2.5.4   Failure Prognosis Methodologies

Failure prognosis methods can be broadly classified into three types, model-based prognosis, data-driven-based prognosis, experience-based or probability-based prognosis [23, 24]. Model-based prognosis consists in studying each component or subsystem in order to establish for each one of them a mathematical model of the degradation phenomenon. The derived degradation model is then used to predict the future evolution of the degradation. In this case, the prognosis consists in evolving the degradation model till a determined future instant from the actual deterioration state and by considering the future use conditions of the corresponding component. Three main steps are needed in the framework of model-based prognosis. The first step is related to the construction of an analytical dynamic model including the degradation mechanism or phenomenon, and the determination of failure thresholds. Follows, in the second step, a setup of a monitoring/diagnostic system is required which allows for estimating the actual value of degradation. Finally, a development or a selection of an adequate technique to solve the derived dynamic model (prediction step) is necessary. The main advantage of this approach dwells in the precision of the obtained results, as the predictions are achieved based on a mathematical model of the degradation. Data-driven-based prognosis approach consists in collecting information and data from the system and projecting them in order to predict the future evolution of some parameters, descriptors or features, and thus, predict the possible probable faults. The advantage of this approach is that, for a well monitored system, it is

possible to predict the future evolution of degradation without any need of prior mathematical model of the degradation. However, the results obtained by this approach suffer from precision and also very expensive due to the need of adequate information of data. Experience-based prognosis consists in using probabilistic or stochastic models of the degradation phenomenon, or the life cycle of the components, by taking into account the data and knowledge accumulated by experience during the whole exploitation period of the industrial system. The advantage of this approach is that it is not necessary to have complex mathematical models to do prognosis. Moreover, this approach is easy to apply on the systems for which significant data are stored in a same standard that facilitates their use. For example, a company which has conserved a production and maintenance database during a long period of time with some minor rules and standards for data storing, can easily get the estimation of the parameters of the probability laws. However, the main drawback of this approach dwells in the amount of data needed to estimate the parameters of the used laws. Indeed, huge and significant amount of exploitation data are needed in order to determine parameters degradation phenomenon or the life cycle of the concerned system. Consequently, this approach cannot be applied in the case of new systems for which data from experience feedback do not exist. The other kind of problem is that in most of cases, it is necessary to filter and pre-process the data to extract the useful ones, because the stored data are not always directly exploitable. Thus, prognosis methods intended for RUL prediction are grouped into three types: model–based prognosis, data–driven–based prognosis and experience or probability–based prognosis. Various approaches for process supervision can be integrated as hybrid approaches to improve the diagnosis and prognosis schemes for dynamical systems when the adequate data for the process is known for both normal and different faulty operating conditions. However, every method has its own advantages and drawbacks. Figure 1.11 shows the criteria for the selection of the approach for the process supervision based on the availability of the information.
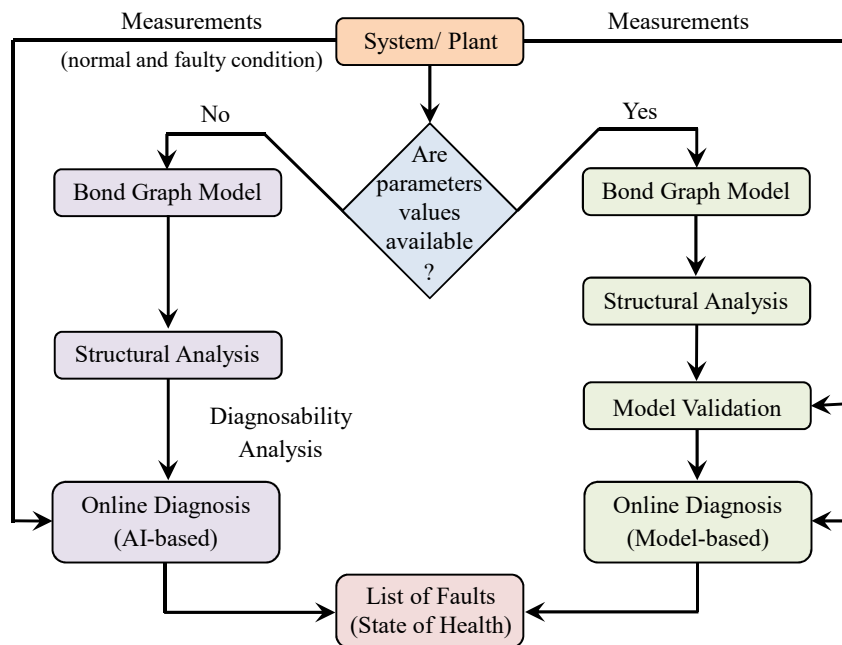
Figure 1.11: Process supervision based on the availability of the information

1.2.6 Online Supervision and Efficiency Tracking

Diagnosis and prognosis algorithms, once developed and validated for their effectiveness and robustness, are implemented in real-time in order to detect the occurrence of fault (if any) and to predict the RUL of the system or system components based on the condition of the system. As shown in figure 1.12, the inputs measurement from the real system using sensors is supplied as the input to the model of the system. The model estimates the nominal output of the system. These estimated outputs are compared to the actual outputs of the system. The difference between estimated and actual outputs are known as residuals and the numerical relation describing each residual is known as Analytical Redundancy Relation (ARR). For system oper-
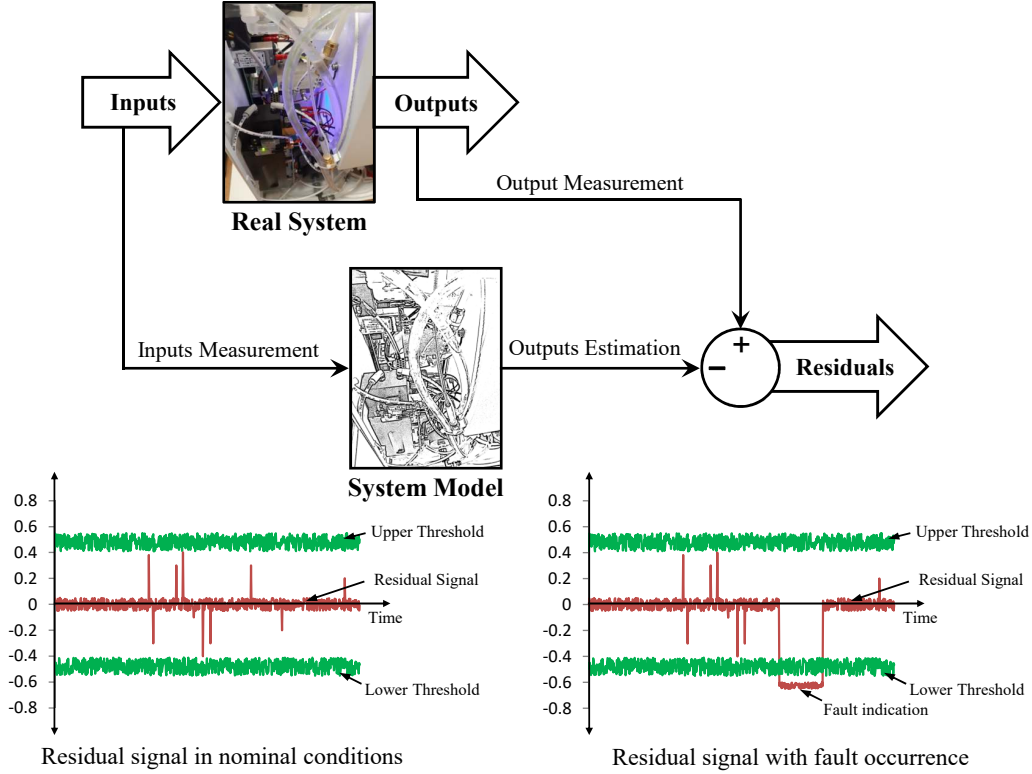
Figure 1.12: Online supervision of the system

ating normally, the value of the residual must be zero (ideal case). In the event of occurrence of fault, one or more of the residuals value becomes non zero as the estimated output and actual output does not match, which indicates the occurrence of fault in the system and the alarm is generated. However, due to the limitation of modelling in representing the actual system, uncertainties, disturbances etc. the value or residual is not equal to zero. In order to avoid false detection, the residuals are bounded by the upper and lower thresholds as shown in figure 1.12. Hence, even if the the residual value is non zero, the fault is not considered to be occurred unless the residual shoots out of one of the bounds as shown in figure 1.12. The thresholds can be set at a fixed value or adapt depending on the change in the operating conditions and are called as adaptive thresholds. Not all residuals are sensitive to the fault occurred. Therefore, knowing which residuals have crossed the thresholds it is possible to isolate and identify the fault. In case of the implementation of FTC, the control law is changed in order to accommodate the fault (if possible) using decision making tool based on fault signature matrix. and update the RUL of the system. For electrolysis systems running on RES, it is also very important to know when and how to operate the system in order to have desired performance. The instantaneous

efficiency of the system plays a critical role in fulfilling this objective.

Efficiency is one of the key factors to define the performance of the system. For a system that can be run in different operating modes and operating conditions, it is very important to know which operating conditions yields maximum efficiency in order to make the system operation efficient in terms of resources as well as the operating cost. The cost of the GH_2 is very critical point of comparison with the hydrogen obtained from other sources and conventional fuels. By 2030, the cost of GH_2 needs to be reduced by more than 50% (to \$2.0-\$2.5/kg) in order to make GH_2 a feasible alternative to the conventional fuels [25]. Production of GH_2, therefore, with the system which is non-efficient will be a great hindrance to achieve this objective. At plant level, the Balance of Plant (BoP) are not continuously working yet greatly affects the overall efficiency of the plant [26]. Therefore in order to have efficient GH_2 production, it is very important to track the efficiency of BoP as well as the overall efficiency of the system. The efficiency can also be used for making the controlling decision such as when to or when not to operate the system, in which operating mode and what operating conditions. However, for efficiency calculation, one needs to know the input power/ energy to the system, and output, which might not be always known at sub-components level due to lack of sensors. The mathematical model can be utilized for estimating the power losses and hence calculating the efficiency at various sub-components level. The BG models are again well suited for this task as the power is the common currency of exchange between different subsystems. Therefore, the power information can be easily obtained at subsystem levels. Figure 1.13 shows the schematics of model based online efficiency calculation. The power loss (P_{loss}) at various sub-components level is estimated using the model based on the input power (P_{in}) and operating conditions. The efficiency is then calculated as the ratio of the output power (P_{out}) to the input power.
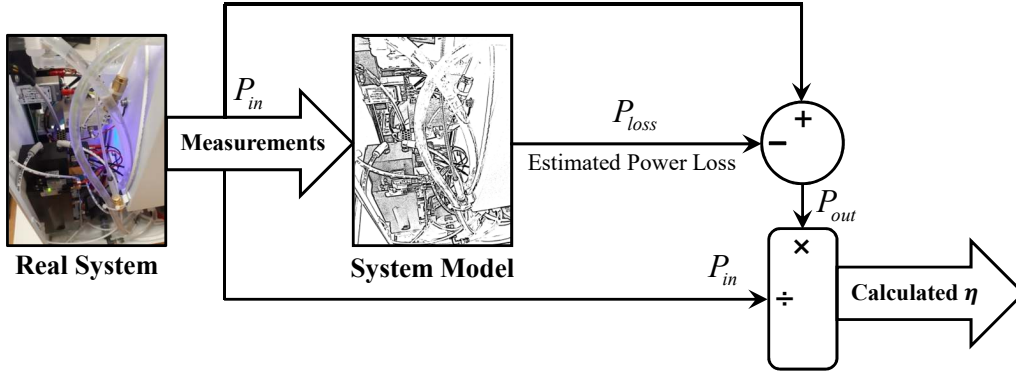
Figure 1.13: Online model-based η calculation

1.3 Problem Definition

GH_2 generation using RES is evolving very quickly with the world set towards the goal of limiting the green house gases emissions in the coming years. Efforts are being made to make this system more safer to use, reliable, efficient and cost effective so that it can compete with the existing alternatives. Due to the intermittent nature of the RES, and involvement of coupled multi-physical phenomena, the complexity increases many folds, therefore, tools are required to study and design these kind of systems. Mathematical modelling could be a great tool to provide the solution for studying the behaviour of these systems as well as to develop the supervision platform to monitor and control these systems in order to achieve desired objectives. Moreover, system performance degrades at different levels (components and subsystems levels)

due to ageing and dynamic operational behaviour. Such studies require a modular design approach, breaking the complete model into different sub-model levels, so that variation of different component parameters on the monitoring variables of the system can be analysed and tested easily and effectively. From the industrial perspective, the model should be adaptable with real monitoring of the system behaviour on suitable supervision platform. The model must have the following properties:

- The model should accurately reproduce the dynamical behaviour of the system without being too complex.

- The model should be easy to create and reuse.

- The model should be based on dimensional parameters.

- The model should be scalable to similar systems of different sizes.

- The model should be easily modifiable depending on the physical system configuration.

- The model should have multiple uses such as it should be suitable for developing control algorithms, diagnosis, prognosis and real-time implementation.

A look at the literature showed that most of the existing models are focused on behavioural studies and are system specific only and cannot be used for different configuration or size of the system or for real-time applications such as online diagnosis and control [6, 14]. Also, the efficiency of the system is a critical parameter for the performance evaluation and decision making for optimal operation. therefore, there is also a need of real-time efficiency monitoring of such system not only for optimal operation but also for the study of these system for economical aspects. The current approach uses the BG as a unified modelling approach for the development of a generic dynamical multi-physics model of the PEM electrolysis system represented in a modular fashion. Different subsystems of electrolyser process are first identified and then they are modelled using lumped parameters dynamics approach (showing different physical phenomena such as energy storage, dissipation and transformation). Based on BG model, different mathematical equations and ARRs are identified for the development of control, diagnosis and prognosis algorithm. Here, model builder of Symbol-Shakti is used for developing the generic PEM electrolyser model where the structural integrity of different components and sub-systems for the global system modelling is checked. Once the models of different sub-systems (capsules) are built, corresponding MATLAB® Simulink models are systematically derived from implementation point of view. The generic BG electrolyser model facilitates the formal model to adapt and to fit the different configurations of the electrolyser ranging from laboratory scale to industrial scale. Thus, this work is extended for the modelling and performance study of AEM electrolyser which share the similar configuration and architecture. The model is also capable of facilitating the efficiency tracking in real-time. The model was first validated using the HMP available at University of Lille. The model is then utilized along with developed diagnosis algorithms in order to develop the GUI for the real-time supervision of the HMP.

1.4 Thesis Organisation

The presented work in this PhD thesis has been segregated into six chapters in total and two appendices have been provided for additional information.

- After the current chapter of general introduction, the chapter 2 addresses the state of art of the modelling, diagnosis and prognosis of the PEM electrolyser. The existing models

of PEM electrolyser from the literature have been compared and exposed. The research gap identified from the state of art has also been defined.

- The chapter 3 focuses on the understanding of the BG based dynamic modelling of the PEM electrolyser. The model is presented in the form of sub-models that are assembled to achieve the global model of the PEM electrolyser. The mathematical equations governing the behaviour of the system are also presented in this chapter.

- Model based diagnosis and prognosis for PEM electrolyser has been presented in chapter 4. The faults that can occur in PEM electrolysis system running on RES are identified and analysed. The model presented in chapter 3 is used to develop DBG model in LFT form to make the diagnosis robust. The ARRs generated from the DBG model are also presented here.

- Chapter 5 focuses on the validation and online implementation of the model and algorithms developed in chapter 3 and 4. The model is first validated offline using the HMP available in the laboratory at University of Lille. The model and algorithms are then utilized for real-time implementation. The results obtained are analysed and discussed in this chapter.

- The conclusions, limitations and future prospects of the current work are summarised in chapter 6.

- The model developed in chapter 3 is adapted for AEM electrolyser (in collaboration with University of Exeter) is presented in appendix A as it is not a key output of the work presented in this thesis.

- BG approach for modelling, diagnosis and prognosis has been presented in appendix B

1.5 Results and Dissemination

The results obtained during the course of this PhD can be categorized as follows:

Fundamental Results

The quantifiable results of the thesis were disseminated through the following publications:

International Journal

- **Sood, S.**, Prakash, O., Boukerdja, M., Dieulot, J. Y., Ould-Bouamama, B., Bressel, M., & Gehin, A. L. (2020). Generic Dynamical Model of PEM Electrolyser under Intermittent Sources. Energies, 13(24), 6556.

- One publication is under preparation for the submission in an international journal for the dissemination of results for robust online diagnosis.

International Conferences

- **Sood, S.**, Bouamama, B. O., Dieulot, J. Y., Bressel, M., Li, X., Ullah, H., & Loh, A. (2020, September). Bond graph based multiphysic modelling of anion exchange membrane water electrolysis cell. In 2020 28th Mediterranean Conference on Control and Automation (MED) (pp. 752-757). IEEE.

- **Sood, S.**, Prakash, O., Boukerdja, M., Ould-Bouamama, B., Dieulot, J. Y., Bressel, M., & Gehin, A. L. (2021, July). Model-based diagnosis of proton exchange membrane water electrolysis cell: Bond graph based approach. In 2021 European Control Conference (ECC) (pp. 2139-2144).

- Prakash, O., **Sood, S.**, Boukerdja, M., Ould-Bouamama, B., Dieulot, J. Y., Gehin, A. L. & Bressel, M., (2021, July). A Model-based Prognosis approach to Proton Exchange Membrane Water Electrolysis System. In 2021 European Control Conference (ECC) (pp. 2133-2138).

- Boukerdja, M., Radi, Y., Prakash, O., **Sood, S.**, Ould-Bouamama, B., Chouder, A., Gehin, A. L., Dieulot, J. Y. & Bressel, M., (2021, August). LFT bond graph for online robust fault detection and isolation of hybrid multisource system. In 2nd International Conference on Clean and Green Energy Engineering (CGEE).

Application Results These results were obtained while working on the HMP.

- Development and implementation of a GUI for the supervision of HMP available at University of Lille based on the developed model and algorithms under the framework of E2C project.

- Hands on experience in the installation of the Programmable Logic Controller (PLC) and additional sensors into the HMP for improved monitorability and algorithms validation.

Project Management Results During the course of the PhD, I was also bestowed with the responsibility for the E2C project management tasks for CRIStAL team. Following are the results obtained during this time.

- Preparation and submission of the Deliverable D1.3.1 for E2C project in January 2021.

- Preparation and submission of the Deliverable D1.3.2 for E2C project (to be submitted in December 2021).

- Preparations of video presentation for the webinar at the 2nd stake holder meeting of E2C project. https://www.youtube.com/watch?v=syFeMBkafFc

- Organization of meetings for knowledge and information exchange between CRIStAL team and other project partners.

- Preparation and delivery of the presentations for various project update on CRIStAL team side and consortium meetings.

State of art

Contents

In this chapter a brief introduction to different electrolysis techniques and their comparison have been presented. The work that has been done in the literature for the modelling, diagnosis and prognosis of the PEM water electrolyser was reviewed for the positioning of the proposed work. A special attention has been given for the modelling work that has been performed for the PEM electrolyser running on RES.

2.1 Water Electrolysis

Water electrolysis is a well established technique by which the molecules of water are split under the influence of the electric current resulting in the production of hydrogen and oxygen gases given by the following reaction [27].

$$H_2O(liquid) + electricity \rightarrow H_2(gas) + \frac{1}{2}O_2(gas) \tag{2.1}$$
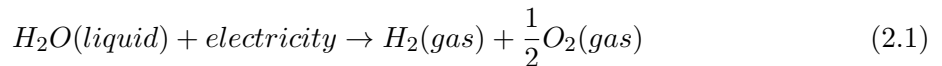
A water electrolysis system typically consists of two electrodes, one at which oxidation takes place is known as anode and the other at which the reduction reaction takes place is known as cathode, the electrolyte, a membrane to separate the produced gases and a Direct Current (DC) power source as shown in figure 2.1.

Based on the electrolyte used, the electrolysis can be classified into four types namely alkaline electrolysis, PEM water electrolysis, AEM water electrolysis and SOM water electrolysis. The first three methods are also known as low temperature water electrolysis methods as the temperature at which electrolysis takes place is below 100 ℃. SOM water electrolysis is a high temperature water electrolysis as the operating temperature ranges from 800–1000 ℃[28]. All four electrolysis methods are discussed briefly one by one. Figure 2.2 shows the schematics for different electrolysis methods.
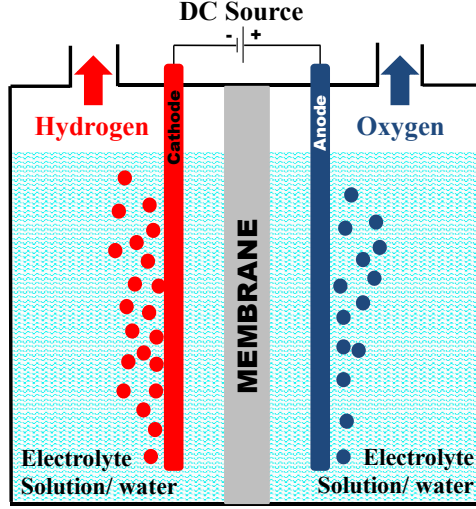
Figure 2.1: A simple water electrolysis cell

2.1.1 Alkaline Water Electrolysis

Alkaline water electrolysis is the most matured technology of hydrogen production and is commonly used electrolyser type in the industry [29]. Figure 2.2(a) shows the working principle of a zero gap alkaline electrolysis which is similar to the traditional alkaline electrolysis. The key difference is the use of porous electrodes in zero gap alkaline electrolyser that are compressed against the gas separator. This facilitates the produced gases to be released from the backside of the electrodes [30]. Electrodes are backed by the Gas Diffusion Layer (GDL) which acts as a bridge for the current between distribution (bipolar) plate and the electrode and also facilitates the movement of electrolyte solution to the electrode and the removal of produced gases from the reaction site. The electrolyte solution consisting of water and highly basic (pH 14) electrolyte (Potassium Hydroxide (KOH) and Sodium Hydroxide (NaOH) are the most commonly used electrolyte [30]) is pumped to both anode and cathode side. When the potential is applied across the electrodes the water is reduced at the cathode into hydrogen gas and hydroxyl radical (OH^-). The hydrogen gas escapes from the outlet at the cathode side and the OH^- ions moves through the porous gas separation membrane or diaphragm towards anode under the influence of the applied potential. Here the OH^- ions forms oxygen gas and water. The half-cell reactions for alkaline water electrolysis are as follows:

$$\textbf{Anode}: 2OH^- \rightarrow H_2O + \tfrac{1}{2}O_2 + 2e^-$$
$$\textbf{Cathode}: 2H_2O + 2e^- \rightarrow H_2 + 2OH^- \tag{2.2}$$
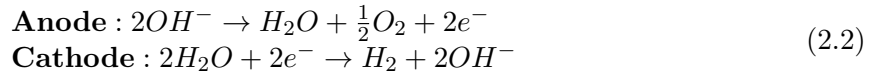
Alkaline water electrolysis cells are limited to operate on lower current densities due to the fact that higher current densities cause formation of bubbles in excess that causes resistance to the movement of electrons and ions [31]. This leads to bulkier system configuration for same hydrogen production rate as compared to PEM water electrolysis. The efficiency of the conventional alkaline water electrolysis cell is low, however, it ranges between 78-80% for zero gap configuration[31]. Also, due to the use of non-noble metals and their oxides as the catalysts, the cost of these electrolysis cells is quite less as compared to PEM water electrolysis. However, these electrolysis cells have low operational pressures due to which a compression step is required before storing the produced hydrogen, which acts as an additional cost for the operation of these systems. Corrosion due to alkalinity of the electrolyte is also a major issue [28].
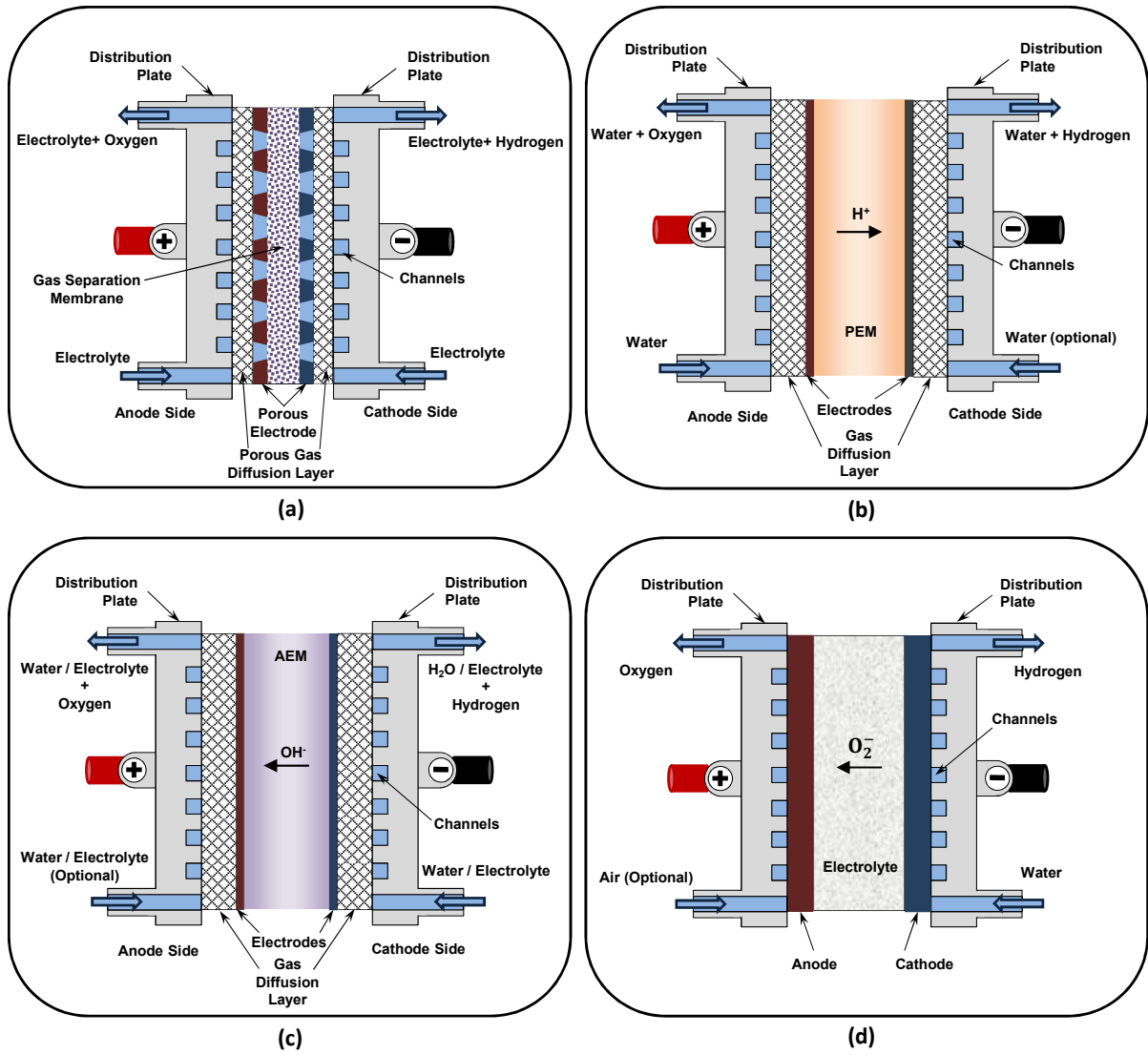
Figure 2.2: Schematics of (a) Zero gap alkaline water electrolysis, (b) PEM water electrolysis, (c) AEM water electrolysis and (d) SOM water electrolysis

2.1.2 PEM Water Electrolysis

PEM based water electrolysis has gained popularity in recent years due to its high performance as compared to the alkaline water electrolysis. Figure 2.2(b) demonstrates the basic working principle of the PEM electrolyser. PEM electrolyser cell consists of two half cells separated by a thin solid electrolyte membrane. The water is fed to the anode side of the cell where water is reduced to oxygen, positively charged hydrogen atoms (protons) and electrons. The oxygen produced during this half-cell reaction is removed with the unconsumed water. The protons move through the electrolyte membrane towards the cathode where they combine with the electrons from the DC power source and form the hydrogen gas. The water feed to the cathode side is optional as it is only there to facilitate the efficient removal of the hydrogen. These reactions take place at the catalyst layers coated on each electrode. The diffusion layer on each side helps in efficient current distribution and also connects the Membrane Electrode Assembly (MEA) to the distribution plates. Distribution plates aid toward structural integrity of the cell and facilitate water and gases transport. They also separate one cell from the other

when cells are assembled together in the form of a stack to deliver the required hydrogen flow rate. Half-cell reactions for each electrode (anode and cathode) are written as

$$\textbf{Anode}: H_2O \rightarrow 2H^+ + \frac{1}{2}O_2 + 2e^-$$
$$\textbf{Cathode}: 2H^+ + 2e^- \rightarrow H_2$$

(2.3)
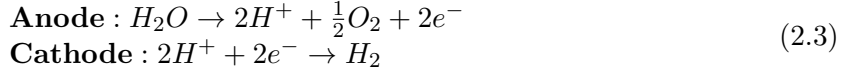
PEM water electrolysis provides greater safety and reliability over alkaline water electrolysis as there is no use of caustic electrolyte. These electrolysis cells are compact as compared to the alkaline electrolysis cells [31]. Also, the PEM water electrolysis can operate at high differential pressure across the membrane which helps in producing hydrogen at the required pressure for storing, thus eliminating the need of compression stage. PEM electrolyser has superiority over alkaline water electrolysis for load following when running on intermittent energy sources [32]. This is due to the fact that PEM water electrolysis has faster ion transportation than alkaline water electrolysis [28]. These electrolysis cells, therefore, also provide faster startup times. PEM water electrolysis offers very fast dynamic load change capability during its operation, without affecting it long-term performance [31]. PEM water electrolysis can operate at higher current densities as compared to the alkaline water electrolysis. Membrane of the PEM water electrolysis is the key limiting factor for the lifetime of the cell as the membrane is prone to the impurities in the water. Due to the acidic operation environment in MEA of PEM water electrolysis noble metals such as Platinum and irridium oxide are used as catalyst, the cost of these electrolysis cell is high as compared to the alkaline water electrolysis cells.

2.1.3 AEM Water Electrolysis

In the recent years, in order to benefit from the advantages of both alkaline and PEM electrolysis polymer based AEM have been developed. PEM electrolyser uses noble earth metals such as Ir, Ru, and Pt etc; which are expensive and limit its commercial applications. On the other hand, AEM electrolyser is based on alkaline electrolytes so, a wide range of earth-abundant transition metals and their oxides can be employed [33]. Schematic of an AEM water electrolysis cell is shown in figure 2.2 (c). The electrolyte is fed to the cell from the cathode side where the water is reduced into hydrogen and hydroxyl ions are formed. These negative ions transport through the membrane towards the anode where they recombine to release oxygen. The electrolyte acts as a reagent as well as it facilitates the removal of the hydrogen at cathode. The electrolyte or water can also be fed to the anode side to facilitate the removal of oxygen depending on the design of the cell. The half reactions on each electrode are given as [34]:

$$\textbf{Anode}: 4OH^- \rightarrow O_2 + 2H_2O + 4e^-$$
$$\textbf{Cathode}: 4H_2O + 4e^- \rightarrow 2H_2 + 4OH^-$$

(2.4)
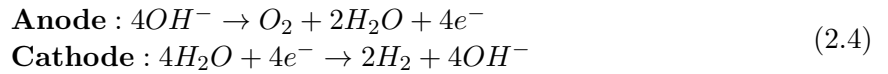
These membranes have made their way to the fuel cells but they are still under development for electrolysis [34]. To adapt AEM as a reliable technology for water electrolysis significant improvements are required[34]. Research is being carried out in order to achieve desirable properties for the membrane such as better mechanical stability, ionic conductivity, longer life, lower cost, for example by the E2C partners from University of Exeter. To finally assemble it into a functional and efficient electrolyser is another challenge.

2.1.4 SOM Water Electrolysis

SOM water electrolysis (schematics shown in figure 2.2 (d)) is a highly efficient water electrolysis method (electric efficiency of almost 100% [31]) whose working principle is complimentary to that of the SOM fuel-cells. In this method, a thin ceramic membrane, with high ionic conductivity at high temperatures, is used as electrolyte (most commonly yttria-stabilized zirconia

[28]) that allows the movement of oxide ions (O^{2-}). The water or steam is fed to the cathode side where the evolution of hydrogen takes place and O^{2-} ions are formed under the influence of the applied electric potential. The O^{2-} ions moves from cathode to anode side to form oxygen gas while releasing the electrons. Air is sometimes fed to the anode side to facilitate the removal of the produced oxygen gas. The half-cell reactions for anode and cathode side are [31]

$$\textbf{Anode}: 2O^{2-} \rightarrow O_2 + 4e^-$$
$$\textbf{Cathode}: 2H_2O + 4e^- \rightarrow 2H_2 + 2O^{2-} \tag{2.5}$$
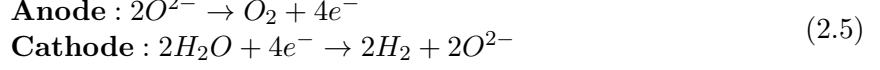
Due to the involvement of high temperatures the voltage required to operate the cell is quite low, in between 1.2 to 1.3V, with high current densities [31]. However, the higher operating temperatures also cause faster material degradation due to notable mechanical and thermal stresses. The life span of the SOM electrolysis cell is estimated to be around 2-3 years which is fairly low as compared to PEM and Alkaline electrolysis cells that lasts for almost 10 and 20 years[35]. This technology is also not available commercially at present but has been validated with the help of laboratory scale prototypes [28].

The comparison between these four water electrolysis techniques based on their key characteristics, advantages and disadvantages is shown in table 2.1 [12, 31, 34, 36–40].

2.2 PEM Water Electrolysis System

PEM water electrolysis system consists of one or more PEM electrolysis cell assembled together in the form of a stack. Stacking provides the best means of achieving the required quantities and rate of production of hydrogen while keeping the system compact. The cells can be stacked in two configurations as shown in figure 2.3. In mono-polar configuration each cell of the stack has two electrodes that are connected electrically in parallel. In this configuration, each cell has its own set of electrodes. This configuration is thus bulkier as compared to the latter. The overall voltage of the stack is equal to the voltage of a single cell and the total current flowing through the stack is the sum of current flowing through individual cell. In bi-polar configuration the cells share the electrodes with the adjacent cells except the two cells at the ends. Each contain one non shared electrode. The electrical power is supplied across the stack through these two non shared electrodes only. The shared electrodes between the cells act as anode for one cell and cathode for the other, hence the name bipolar (double polarity of single electrode). The cells are electrically in series connection. Therefore, the current flowing through each cell is same and the stack voltage can be calculated by adding the voltages of all the cells.

The power consumption by both configurations for similar operation is theoretically equal. The mono-polar configuration is suitable for small electrolysers in which the current requirement of the stack is not very high [41]. The Faradaic efficiency for this configuration is 100%. In case of bi-polar configuration due to the presence of parasitic current (i.e. current flowing through the bi-polar electrode that do not contributes towards actual electro-chemical reaction) Faradaic efficiency of the stack is reduced[41]. Also, the manufacturing of bi-polar stacks is complex and costly as compared to mono-polar stacks. Bi-polar configuration is the preferred choice for industrial scale electrolysers due to its compactness.

In addition to the cell/stack, an electrolyser has auxiliary components to ensure the proper functioning of the stack. These auxiliaries are essential to perform the following operations [15]:

- Electric power supply regulation to the stack depending on the requirement for hydrogen production.

- Regulation of the temperature of the stack to achieve desired efficiency.

Table 2.1: Comparison of Alkaline, PEM, AEM and SOM water electrolysis

	Name	Alkaline Water Electrolysis	PEM Water Electrolysis	AEM Water Electrolysis	SOM Water Electrolysis
Characteristics	Electrolyte	30% wt. KOH solution or 25% wt NaOH solution	Perfluorosulfonic acid	Quaternary ammonia polysulfone or optional dilute caustic solution	ZrO_2 ceramic stabalized with yttrium or scandium oxides
	Cathode	Ni, Ni-Mo alloys	Pt, Pt-Pd	Ni and Ni alloys	Ni-doped ceramic
	Anode	Ni, Ni-Co alloys	RuO_2, IrO_2	Ni, Fe, Co oxides	Transition metal oxides (perovskites)
	Half cell separation	Diaphragm (Zirfon Perl 500 μm)	Nafion 117 (e.g. 180 μm)	AEM (20-100 μm)	Thin ceramics (30–150 μm)
	Cell area	<4 m^2	<3 m^2	Lab testing cells	<0.06 m^2
	Current density	0.2-0.5 Acm^{-2}	0.6-2.0 Acm^{-2}	0.2-1.0 Acm^{-2}	0.3–1.0 Acm^{-2}
	Cell Voltage	1.8-2.40 V	1.75-2.20 V	1.8-2.2 V	1.2-1.3 V
	Operating pressure	<30 bar	<76 bar	<30 bar	<15 bar
	Temperature range	65-100 ℃	70-90 ℃	50-70 ℃	700–1000 ℃
	Hydrogen Purity	9.99-99.3 %	99.9999 %	99.99 %	99.5 %
	Cell Voltage η	52-69%	57-69%	~75%	~100%
	Estimated H_2 production cost	800-1300 €kg^{-1}	>1200 €kg^{-1}	Not available	Not available
	Lifetime of stack	<90000 h	<20000 h	Not available	<10000 h
	System response	Seconds	Milliseconds	-	seconds
	Development status	Matured technology	Matured for small scale application	Under developing/ Laboratory Scale	Under developing/ Laboratory Scale
Advantages		Well established technology Non-PGM catalysts Long-term stability Relative low cost Stacks in the MW range Cost effective	High current densities High voltage efficiency Good partial load range Rapid system response Compact cell design High gas purity Dynamic operation	Non-noble metal catalyst Noncorrosive electrolyte Compact cell design Low cost Absence of leaking High operating pressure	Efficiency up 100% Thermoneutral η >100% w/hot steam Non noble catalysts High pressure operation
Disadvantages		Low current densities Crossover of gases (degree of purity) Low partial load range Low dynamics Low operational pressures Corrosive liquid electrolyte	High cost of components Acidic corrosive environment Possibly low durability Commercialization Stacks below MW range	Laboratory stage Low current densities Low durability Membrane degradation Excessive catalyst loading	Laboratory stage Bulky system design Low mech. stability (brittle ceramics) No dependable Cost information

24
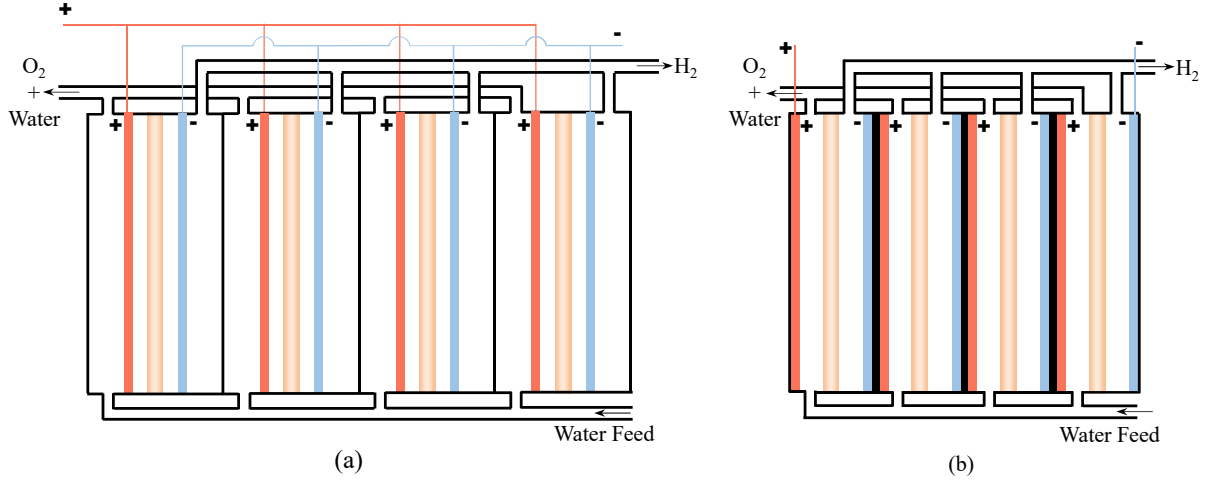
Figure 2.3: Stack configuration scheme: (a) Mono-polar (b) bi-polar

- Purification and flow control of the input water to the stack.

- Conditioning and purification of the produced hydrogen and output pressure regulation.

The general schematic of a PEM electrolyser is shown in Figure 2.4. Depending on the size and specification of the electrolyser, one or more components may or may not be present in the configuration. A power supply/voltage controller (electric converter) is used to regulate
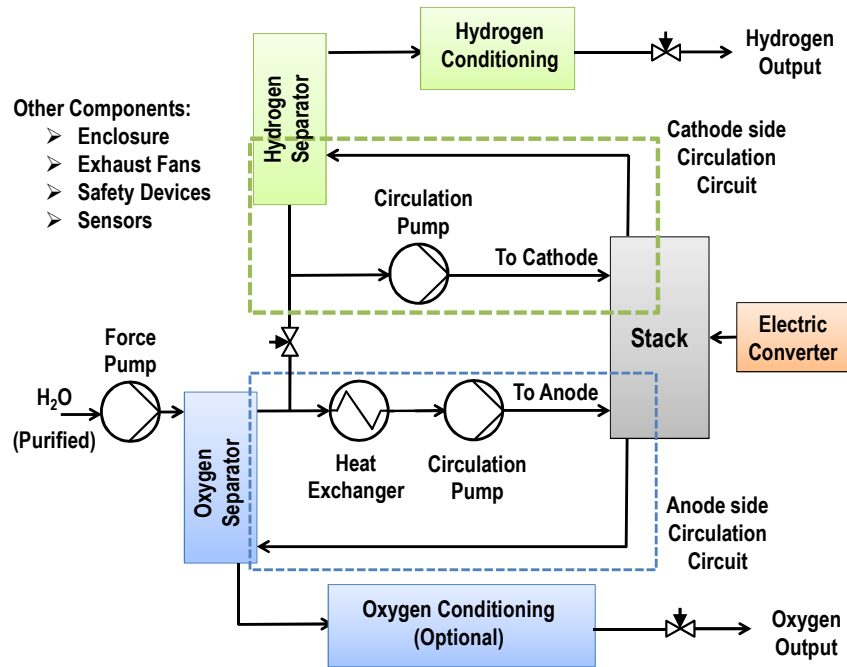
Figure 2.4: General schematic of a PEM electrolyser

the electric power supplied to the stack based on the set operating point (usually voltage is controlled to increase or decrease the hydrogen production). The water supplied to the stack is first purified and deionized before supplying it to the electrolyser in order to increase the longevity of the stack. Circulation circuit is implemented to feed the water to the anode side

for providing water for consumption in the electro-chemical reaction as well as to facilitate the removal of oxygen gas produced at the anode. This recirculation circuit is a closed loop and contains a pump to regulate the flow rate of water and a heat exchanger or a heater to regulate the temperature of the water flowing to the reaction site on the anode side. The flow rate of the water is always higher than the rate of consumption of water in order to avoid the damage to the membrane due to dryness. The recirculation circuit is sometimes also installed to the cathode side only to facilitate the removal of produced hydrogen gas. There are two outputs from the stack. First, on the anode side the excess water (which is not consumed during the electro-chemical reaction) and produced oxygen gas exits in the form of a bi-phasic fluid. The oxygen needs to be separated from the water before recirculating it to the stack. A liquid gas separator is used for this purpose. Second, on cathode side the liquid gas separator is used if the cathode side is fed with water. A controlled valve is used to regulate the level of water in the separators. Once the gases are separated from the water, depending on the required output conditions, the gases are purified, dried and compressed using output conditioning unit. There are other components in the PEM water electrolysis system to ensure the proper and safe functioning of the system. These include, safety devices, sensors, exhaust fans, enclosure, etc. [15]. All these auxiliary components also consume energy and directly affect the overall performance and efficiency of the electrolyser.

2.3   Models of PEM Electrolyser

PEM electrolyser is a complex system, an assembly of number of components (cell/stack, pumps, separators, etc.), that involves various multi-physics phenomena such as electro-chemical, thermo-electrochemical and thermo-fluidic phenomena. There exists a coupling between these phenomena, as they are dependent on each other, which further increases the complexity. Due to this, non-linear relations are required to describe its dynamics. Figure 2.5 shows various multi-physics phenomena involved in a PEM electrolysis cell.
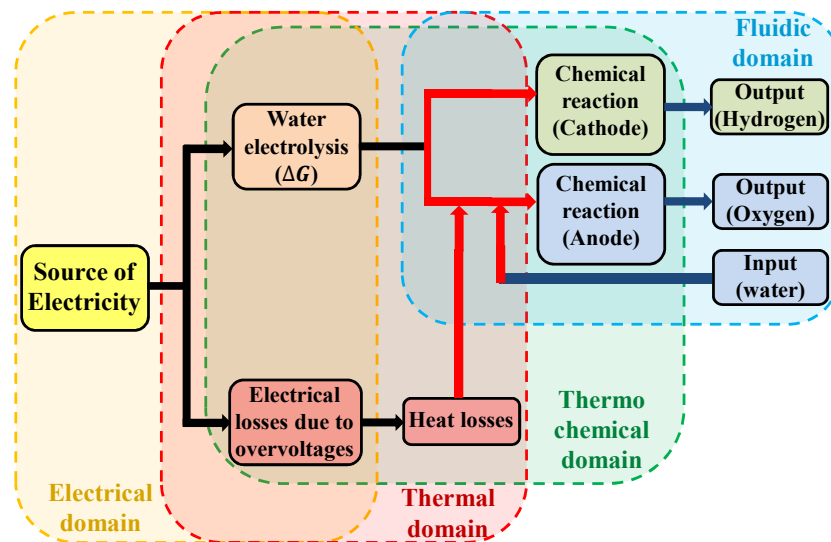
Figure 2.5: Multi-physics phenomena in PEM electrolyser cell/stack

PEM electrolyser coupled with renewable energy sources, such as solar energy and wind energy, is emerging as a reliable means of storage of surplus energy. Various installations all over the world have been done to integrate the RES and the electrolyser as a means of storage

[42]. A number of articles have been published for the study of effect of the coupling between the RES and the PEM water electrolyser on the performance of the system [7, 11, 43–65].

The intermittent nature of the RES also affects the performance of the electrolyser. To study these effects there is a need of deep analysis and understanding of the dynamical behaviour of the PEM electrolyser. This also enables the researchers to predict the performance of the PEM electrolyser under different operating scenarios such as running the electrolyser for a long time (say for days or months) on RES under different weather conditions. This study may include, but not limited to, estimating the overall hydrogen production, and predicting the stability, efficiency, flexibility and load tracking capability, produced gases quality, reliability and safety of the process against degradation of the components and possible system or component failure occurrences. This also enables the possibility of the system design, configuration improvement and development of supervision algorithms (for control, diagnosis and prognosis). Mathematical modelling is a powerful tool towards achieving these objectives. Therefore, it is necessary to have a PEM water electrolysis system model that can be used for the analysis of the dynamic behavior of the system under stress of intermittent nature of RES. Exhaustive reviews about PEM electrolyser modelling are available in the literature [6, 14, 66–69]. Bensmann provided a brief survey about the publications done on the modelling of PEM water electrolysis till 2016. The work on the modelling of these kind of electrolysers started in 1990s. In [67] the models used in the literature for the modelling of mass transport phenomenon for PEM water electrolysis were exposed. Olivier provided an excellent review about the modelling efforts done for the low temperature electrolysis (PEM and alkaline water electrolysis) [6]. Falcão provided a guide for the new researchers entering the field of modelling of PEM electrolyser, exposing the equations governing various phenomena in the PEM water electrolyser [14]. Yodwong exposed the models of PEM water electrolysis used for used for power electronics control [68]. As per literature review in reference [69], mostly the empirical and semi-empirical models for PEM electrolyser exist that can predict the behaviour of the electrolyser under varying operating conditions (for example, different temperatures and pressures). These models are mainly focused on phenomenon understanding and for developing control algorithms. These reviews, however, have not addressed all the articles on the modelling of the PEM water electrolysis. Therefore, a review of existing models for the PEM electrolyser is presented in the subsequent section to position the present work in comparison to the existing work in the literature. A brief review of the articles on the diagnosis and prognosis of the PEM water electrolyser is presented in section 2.4. Figure 2.6 shows the number of publications addressed in this state of art since 1992; 127 publications in total related to PEM water electrolysis modelling, 27 articles related to the modelling and study of coupling of PEM water electrolysis and RES and 25 articles related to diagnosis and prognosis of the PEM water electrolysers.

When compared to the PEM based fuel cells, there is not much work done on the modelling of PEM electrolyser as compared to the PEM fuel cell [6, 14]. However, the basic concept related to fuel cell can be adapted for modelling, control and optimisation of electrolyser due to structural and process similarity [53]. To explore the existing models for the PEM water electrolysis, the models have been segregated into the equation based models and graphical models as shown in the figure 2.7. The models used for the study of coupling between RES and PEM water electrolysis also belong to the first two categories, but have been classified separately in order to give special attention to them. The models developed for studying the monophasic or biphasic flows through the electrolysis cell, pressure and temperature distribution in the flow channels etc. using approaches such as Computational Fluid Dynamics (CFD), that are not categorized under equation based and graphical methods, have been discussed under miscellaneous models. The models under equation based and graphical models are further classified into static and dynamic models. The further classification is done based on the modelling method used.
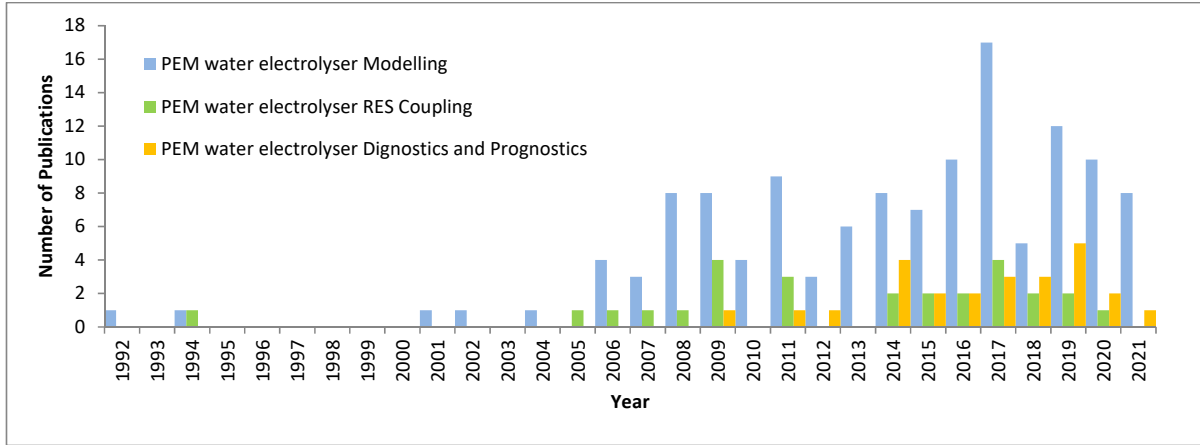
Figure 2.6: Number of relevant publications (year wise) for the modelling of PEM electrolysis, modelling/ study of coupling of PEM water electrolysis and RES and diagnosis and prognosis of the PEM water electrolysers

2.3.1 Equation Based Models

2.3.1.1 Equation Based Models: Static Models

2.3.1.1.1 Static Models: Analytical Models

An analytical two dimensional model for PEM electrolysis cell based on mass, charge and energy balance is proposed for the prediction of the performance of the PEM electrolysis cell [70]. The model is suitable for simulating the current and temperature distribution across the cell. The model is then extended to the prediction of the performance of the large stack by considering equivalent large single cell. Another simple analytical static model for PEM electrolysis cell was proposed by the authors which take into account the electrode kinetics and mass transport through MEA to predict the overpotentials of anode and cathode side [71]. A static theoretical model of PEM electrolyser based on Butler-Volmer (BV) equation for representing the electrode kinetics was used to analyse the Current-voltage (IV) curves [72]. The cell voltage was considered as the summation of four overvoltages depending on the operating current and reversible voltages calculated from Gibbs free energy. An analytical model was proposed for estimating the diffusion of gases through the membrane based on the Fick's law [73]. Henry's constants were considered as dependent on temperature and the diffusion coefficients were taken as dependent on temperature, pressure and concentration of the species.

A model was proposed in [74] for studying the transport of species through the membrane in high pressure PEM water electrolyser used for oxygen generation. The dusty-fluid model (DFM) was used for species transport considering the water flow to the cathode side. Simulation results were validated with the help of experimental data from the Hamilton Sundstrand's high pressure oxygen generating assembly (HPOGA) at different differential oxygen pressures. The authors found that the electro-osmotic drag has a significant influence over the dehydration of the membrane.

A multi-scale model for the PEM water electrolysis cell was proposed in [75]. The model was divided into nano-scale and micro-scale models. Nano-scale model dealt with two types of modelling; first, the zero dimensional modelling of the interaction between the catalyst surface and different chemical species and second, one dimensional modelling of the transport of chemical species and protons through the diffusion layer. The elementary kinetics for the electrochemical reaction was also presented. In micro-scale model two one-dimensional models were considered

28
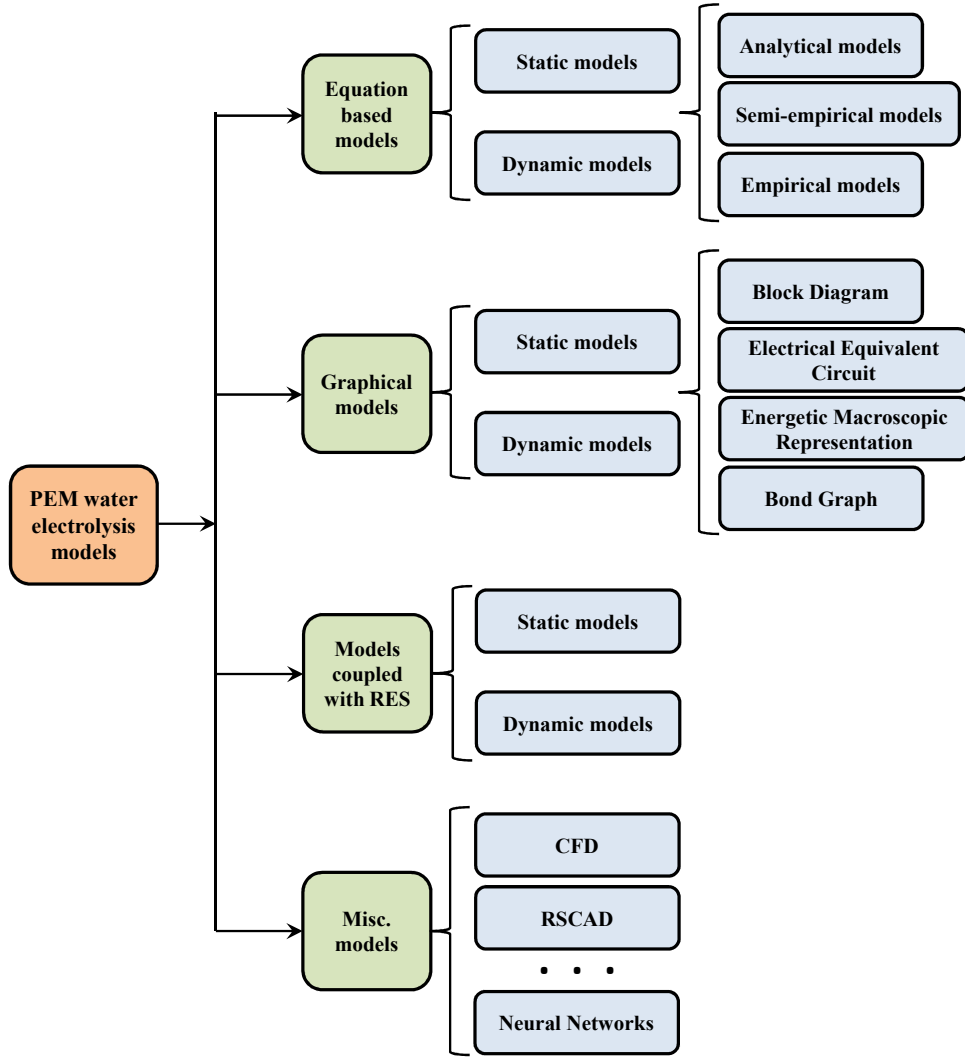
Figure 2.7: Models classification for the state of art.

to study the transport of the species. The model was validated against the experimental data as well as the experimental results published in the literature.

An analytical model for the electrochemical phenomenon based on Nernst equation and BV equations was adopted from the literature [76]. Empirical relation for calculating ionic conductivity as a function of temperature was utilised. Effects of various operating parameters over cell voltage were discussed in details with the help of simulations. The results were validated with the experimental data from the literature. There was no new contribution in the article.

An analytical model for the PEM water electrolysis with higher current densities was proposed [77]. A special focus was done on the ohmic and mass transport losses as they play a significant role at higher current densities. For calculating ohmic losses, an approach similar to [78] was implemented using resistance network model for the electrodes, flow channels and membrane. The model was validated against the experimental data for current density less than 3.5 Acm^{-2}. A uni-dimensional PEM electrolysis cell model coupled with the chemical degradation model was presented in [79]. The electrochemical model for estimating cell voltage was presented. For degradation modelling, the crossover of the oxygen from anode to cathode side was modelled. Similar work was also presented in [80].

Analytical modelling for performance evaluation of the PEM water electrolysis was per-

29

formed using Nernst and BV equations [81]. The gas crossover through the membrane was calculated based on the Fick's Law. The effect of different operating conditions on cell efficiency was also analysed. A numerical model for studying the effect of different operating variables on the Faradaic efficiency of the PEM electrolysis was proposed [82]. The Faradaic efficiency was expressed in terms of flux densities of hydrogen and oxygen across the membrane and rate of production of the gases. No experimental validation was performed.

A mathematical model was developed for the simulation of the behaviour of two phase flow of the PEM electrolyser under the variation of different properties of the gas diffusion layer such as porosity, angle of contact, humidity and size of the pores [83]. The model was coupled with the electrochemical model and equivalent resistance model for studying the effect on the cell efficiency and performance. The model was validated by comparing the IV characteristic curves obtained at different porosity and contact angles. A two-phase transport model for a PEM water electrolysis cell was proposed based on the porous media flow theory in [84]. The model also incorporates the electrochemical performance equations that can be used to predict the cell performance. The model is capable of simulating the effect of current density, angle of contact, porosity and the GDL thickness on the water transport, cell voltage and voltage efficiency. The model was validated against the experimental data for two cases with different pore sizes. A two dimensional multi-scale numerical model for the PEM water electrolysis was proposed in [85]. The model takes into account the heat and mass transfer (including the bubble flow), the transfer of charge through the membrane and electrochemical reaction. The authors considered the bi-phasic flow on the anode side to be non linear due to two bubbles regime (Coalesced and non coalesced bubbles regime) and the model was solved for both cases separately. The model was validated against the experimental characteristic polarization curve.

A mathematical model to study the effect of the loading of Pt and IrO$_2$ in catalyst layers of PEM water electrolysis cell was proposed [86]. The results from the model were compared with the experimental data from the experiments conducted by the authors. The model can be used for optimizing the performance of the cell by choosing the appropriate catalyst loading in order to achieve minimum cell voltage.

In [87], a two dimensional model for PEM water electrolyser was developed in the COMSOL® multi-physics software to simulate the effect of anode side catalyst on the characteristic curves. The model was validated against the experimental data from the literature. Effect of temperature, molar fraction distribution, thickness of membrane and length of current collector was compared for two different anode side catalysts.

The analytical electrochemical model was used by the authors to study the effect of cell temperature on the Charge Transfer Coefficient (CTC) and the effect of CTC on the cell voltage [88]. The model was validated against the experimental data from the literature. A similar work was also presented in [89]. The model was used for the study of various parameters on the CTC and the effect of CTC on the performance of the system and characterization of the performance of the PEM electrolysis cell. The model was validated against data from the literature.

An analytical electrochemical model was proposed for the PEM water electrolyser in [90] to study the effect of different parameters on the performance of the electrolyser by comparing the polarization curves, energy efficiency and exergy efficiency. These parameters include current density, membrane thickness, operating temperature, height and width of flow channels and pressure on cathode side. The effect of the concentration overvoltage was also considered with more accurate equation. The model was validated against the results from [91].

An analytical electrochemical model of PEM water electrolyser was used to study the influence of the parameters (porous transport layer material, structure and wettability) affecting the mass transport through the porous transport layers [92]. The model was validated against the experimental data for three different anode porous transport structures.

A mathematical model was proposed in [93] to calculate the overall system efficiency of the PEM water electrolyser while considering the effect of various operating conditions such as requirement of external heating, permeation through the membrane, operating pressure of the cell, membrane thickness and current density. The overall efficiency is defined as the product of three efficiencies; efficiency of hydrogen production, Faradaic efficiency and efficiency of compression of the produced gas.

A mathematical electrochemical model coupled with the transport model of bi-phasic flow was proposed in [94]. The model was implemented in OpenFOAM, which is open source CFD software. The model was validated only against the IV curve of the electrolyser. The model was used to compare the performance of the serpentine and parallel flow channels designs. The serpentine design performs better as compared to the parallel design at higher current densities.

In [95], an analytical electrochemical model of the PEM electrolyser coupled with mass transport (bi-phasic flow through porous media) and heat transfer (thermal equilibrium inside the cell) model was proposed. Two configurations were considered for modelling, one with and another without bipolar plates. The model was validated using polarization curve of a single cell PEM electrolyser.

A two dimensional mathematical model was presented in [96] to study the fluid transport phenomena in PEM electrolyser of 2-cell stack. The electrochemical phenomena were coupled with fluid transport phenomena in order to simulate the performance of the PEM electrolyser using porous liquid/gas diffusion layers.

In [97], an analytical dimensionless model for a PEM electrolyser (single cell) was proposed. A mathematical model in closed form for overpotential variation, current density distribution and water content distribution in membrane are obtained in non-dimensional form. The developed method offers a tool for the study of water management through the PEM electrolyser.

A three dimensional numerical model was proposed in [98] for the estimation of the effect of bi-phasic flow and heat transfer on the performance of a PEM water electrolysis cell. The model takes into account the coupling between liquid water saturation and temperature in the BV equation. In [99], a mathematical model was proposed for the bi-phasic water transport through the porous transport layer and PEM. The effect of different variables was then studied on the current density of the cell.

2.3.1.1.2 Static Models: Empirical Models

A first order regression model based on the experimental data for estimating the electrolyser voltage at different conditions of electrical load was presented based on key operating parameters, i.e. pressure, temperature and the flow of water. Two operating conditions (at current densities 0.1 and 1 Acm^{-2}) were considered for the presented study [100]. The study showed that the pressure and temperature affect the cell voltage predominantly in both cases, while the effect of flow of water is negligible.

A regression model based on the experimental data was proposed for the PEM electrolyser to estimate the electro-osmotic drag coefficient as a function of current density, pressure and temperature [101]. The objective of the study was to obtain the suitable operating condition with lower water transport through the membrane in order to achieve driest possible hydrogen at the cathode. According to their observations, the temperature had the least effect and the pressure had the most effect on the electro-osmotic drag.

2.3.1.1.3 Static Models: Semi-empirical Models

In [102], a hydrodynamic model for the PEM electrolysis cell was presented in order to estimate the moisture content of the membrane based on the water transport through porous

gas diffusion layer and effect of electric current and temperature over the water consumption and pressure generation on anode and cathode sides. A semi-empirical model of PEM water electrolysis cell to estimate the pressure drop across current collector and its effect on the IV curves was proposed [103]. The model is suitable for simulating IV curves only. Another semi-empirical model of PEM electrolyser stack comprised of 20 cells was developed to simulate the characteristic curves [104]. The effect of activation voltages and ohmic resistance on the overall potential was considered. The loss due to mass transport was neglected. A similar approach was adopted in [105], to develop a semi-empirical model for electrochemical phenomenon in PEM electrolysis cell. The effect of ion transport through membrane on ohmic resistance of the cell was also considered. A simple semi-empirical model for study the effect of different parameters, such as membrane thickness, current exchange density, on the characteristic curve of the PEM electrolysis cell was proposed [106]. The model is based on the BV equation for calculating the overpotentials and Nernst equation to calculate the reversible potential. The effect of anode and cathode overpotentials, ohmic resistance and interfacial overpotential were considered on the characteristic curve. The conductivity of the membrane was calculated empirically. The similar model was also presented in [107] by the same author in which the BV equation was simplified empirically. Another semi-empirical model was developed to study the dependence of CTC of anode side electrode on the operating temperature for a PEM electrolysis stack [108]. The reversible potential is calculated based on the Nernst equation and the activation overvoltages are calculated using Tafel equation for the electrochemical process. Ohmic overpotential was considered as a function of membrane thickness and conductivity. Overvoltage due to mass transport was neglected due to low operating current densities. A semi-empirical model was also proposed to simulate the performance of a PEM electrolysis stack [109]. The reversible potential was considered as dependent on the temperature. Membrane conductivity, anode and cathode side exchange current densities were estimated from the IV curves of the electrolyser using non linear curve fitting using Levenberg–Marquardt algorithm. The developed model was used for the development of model predictive control for the fuel-cell and electrolyser based space heating system for smart building [110].

A theoretical model for the estimation of the relationship between cell voltage and cell current in high pressure PEM water electrolysis was proposed [91]. The model takes into account the diffusion overvoltage and effect of different temperatures on anode and cathode side on the cell voltage. The mass balance within the cell was also considered. In [111], a semi-empirical static model for the PEM electrolyser was proposed that takes into account multiple phenomena, such as gas crossover, electro-osmosis drag, kinetics of the evolution of gases, and various geometric parameters of the PEM electrolysis cell. The model is suitable for studying the effect of different operating parameters (such as current density, temperature, pressure and flow rate of water) on overall cell efficiency, hydrogen production and heat generated during the operation. The results showed that the high pressure PEM water electrolysis is not suitable at current densities lower than $0.6 \mathrm{Acm}^{-2}$ as the Faradaic efficiency drops significantly below this threshold.

A semi-empirical model was proposed for the study of gas crossover in PEM electrolyser in differential pressure and balanced pressure operation and corresponding loss in system efficiency [112]. The model was validated against the in-situ measurements performed for the hydrogen content on the anode side. An efficiency comparison between pressurised PEM electrolyser operation and the depressurized operation with external compression was also performed.

A mathematical model for the PEM water electrolysis was presented based on the mass balance equations (for water on both anode and cathode sides and), transport of water through the membrane and detailed calculation of cell voltage [78]. The effects of activation, ohmic and diffusion overvoltage were considered over the cell voltage. The ohmic resistance of the

32

electrodes and the bipolar plates were calculated using Equivalent Electrical Circuit (EEC). The model parameters were identified from the experimental data through curve fitting using non linear least squares method.

A semi-empirical, steady state model for the asymmetric high pressure PEM water electrolyser was presented in [113]. The model utilized the equations from the published articles [91] and [78] for defining the electrochemical phenomena and mass balance. The electrical efficiency of the system was also considered when the losses are caused by the balance of plant components. The experimental data from a 9.6kW PEM electrolyser was then utilised to empirically estimate certain parameters. The model simulations showed satisfactory results.

A semi-empirical model for PEM water electrolyser was proposed by the author that includes the effect of bubbles on the cell voltage [114]. The model was presented in the form of submodels that represent different phenomena such as thermodynamical, electrochemical, thermal and fluidic and are coupled together to form the complete model. The model is governed by mass and momentum balance, current conservation and heat transfer equations describing the behaviour of the system in steady state. The unknown parameters for the model were calculated through capillary flow porometry and rotating disc electrode. The model was able to predict the characteristic curves for the PEM electrolysis cell for higher current densities (up-to $5 Acm^{-2}$). The model was then utilized to study the effect of different system parameters on the performance curves (these parameters include operating temperature, pressure, water flowrate at the inlet, porous transport layer thickness, porosity and pore size).

In [115], a semi-empirical model was used to study the effect of clamping pressure and operating pressure on the performance of an unitized regenerative fuel cell operating as an electrolyser. The interfacial resistance was modelled as a function of contact pressure using an empirical relation obtained from the fitted experimental data. The contact pressured was modelled using a three dimensional model developed in the ANSYS® software.

2.3.1.2 Equation Based Models: Dynamic Models

2.3.1.2.1 Dynamic Models: Analytical Models

An analytical model of PEM electrolyser plant was proposed that includes the modelling of the coupling between electrochemical and thermodynamic phenomena in the PEM electrolysis cell [116]. The key objective of the model was to study the thermodynamic performance of the PEM electrolyser system. The model was able to estimate the heat production due to overpotentials. The results showed that the PEM electrolysis cell operation is exothermic as the heat produced during the operation is more than the thermal energy required. Parametric study of the effect of various operating parameters on the energy efficiency was also performed.

One dimensional mathematical model for studying the mechanism of the formation, growth and the lifetime of the oxygen bubbles in a PEM water electrolysis cell was proposed in [117]. The model utilizes three different approaches to estimate the growth and lifetime of the oxygen bubbles; buoyancy driven bubbles, drag driven bubbles and nucleation driven bubbles. The effect of various operating parameters on the bubble overpotential and lifetime of the bubble was calculated and compared using these three approaches. The model was validated against the experimental data published in three different publications.

A PEM water electrolysis model was developed using the approach similar to that used by [118] and [119] for incorporating the effect of temperature of the stack on the overvoltage [120]. The thermal model used to predict the temperature of stack and water tank take into account the exchange of heat between the system and the environment by calculating the heat loss between the stack and the environment and the heat loss between the water tank and environment through conduction. The model parameters were identified using MATLAB® parameter

identification toolbox. The model was then validated against the IV curve, temperature profile for the stack and water tank of the experimental setup.

A two dimensional multi-physics dynamical model of the high temperature proton exchange membrane was proposed in [121]. The model includes the electrochemical phenomena, heat transport (heat balance equation for the cell), mass and momentum transport through porous electrodes. Dynamic response for different voltage inputs (step, multi-step and diagonal) were simulated and compared.

2.3.1.2.2 Dynamic Models: Semi-empirical Models

A semi-empirical dynamic model for PEM electrolyser was proposed [122]. The overall model consisted of two sub-models. First, a steady state electrochemical model to establish the relationship between the cell current and cell voltage. Second, a dynamic thermal model to predict the temperature of the cell. The unknown parameters for the electrochemical model were identified using non linear least squares method.

Another dynamical semi-empirical model for the PEM electrolyser was proposed in [123]. The model was subdivided into three sub-models; electrochemical, H_2 production and thermal sub-model. The first sub-model was utilized to estimate the cell voltage. The effects of activation overvoltages, diffusion overvotlage and ohimc resistance were considered. Dynamic hydrogen flowrate was considered temperature dependent and computed from theoretical hydrogen flowrate using first order system. The thermal model was used to estimate the temperature of the stack using lumped parameter approach. The thermal capacitance and the thermal resistance of the stack were estimated from the experimental data.

In [124], a semi-empirical model of the PEM electrolysis system was used to calculate the cell voltage of the PEM electrolyser and heat supplied for the electrolysis from external heat source. The electrolysis system efficiency was then calculated based on the model developed. The comparison between different configurations of PEM electrolyser (Based on the positioning of the heat exchanger) was also performed in order to find the optimum solution for overall performance. The effect of various parameters (membrane thickness, operating temperatures, water flow rate and effectiveness of heat exchanger) on the system efficiency was also studied.

One dimensional semi-empirical dynamic model was proposed for the high pressure PEM electrolysis system in [125]. The model takes into account the water transport and gas permeation through membrane, compressiblity and variation of gases in the flow channels of anode and cathode side and vaporization of the water. The unsteady mass balance and energy balance equations were written for anode and cathode side channels and membrane in the partial differential form. For simplifying the model, these partial differential equations were converted into ordinary differential equations using cubic spline collocation method. The model was further simplified considering that there is a simultaneous flow of water and gas at same speed. The model was not validated using any experimental setup/ data.

A mathematical model for the PEM electrolysis cell with approach similar to [126], [127] and [49] has been developed that incorporates electro-chemical reactions, gas transport mechanism and various physical phenomena [128]. Authors have also defined the thermal efficiencies to analyse the cell performance. The model was used for polarization curves simulation and efficiency estimation.

In [129], a simplified mathematical model based on zero-dimensional dynamics and multi-physics approach was proposed to avoid complex model with too many parameters. The model incorporates different multi-physics phenomena such as electro-chemical model, thermal model and fluid-dynamic model. The power consumption by the auxiliaries of the electrolyser has also been incorporated to study the expenditure of thermal and electrical energy. The model was validated against the experimental data from the literature.

A semi-empirical model was used to simulate the performance of the PEM electrolysis system [130]. Optimization of the seven operating parameters (temperature, water content of membrane, anodic and cathodic exchange current densities, anodic and cathodic pressures and membrane thickness) was performed using Taguchi's method. The proposed method aims to reduce the experimental cost to optimise the parameters by conducting experiments.

2.3.1.3 Equation Based Models: Summary

The equation based models found in the literature have been summarized in the table 2.2. The majority of the models are static and focused on the phenomena understanding, characteristic curves prediction/ simulation, efficiency calculation and mainly takes into account the electrochemical phenomenon. Nernst equation, BV equation sets the base for most of the models to represent the electrochemical phenomenon. Some models have been proposed for studying the effect of different operating parameters on the characteristic curves. Other phenomenon like mass transport, bi-phasic fluid flow inside the electrolysis cell/ stack, gas crossover through the membrane, oxygen bubbles formation and propagation have been modeled to gain deep understanding of their mechanism and to study their effects on the characteristics curves and efficiency of the PEM water electrolysis. A handful of dynamical equation based models exist that can simulate the dynamic behaviour of the PEM water electrolysis system such as the prediction of the temperature evolution, simulation of hydrogen production and flowrate. The scope of modelling of most of these articles is limited to the PEM electrolysis cell. Very few have considered the whole stack (mainly for performance simulation) and even fewer the effect of BoP on the system performance. BoP have a significant impact on the performance of the system and must be considered in order to have a good model of the complete electrolysis system. Most of these models are not suitable for the system control, monitoring and diagnosis.

2.3.2 Graphical Models

2.3.2.1 Graphical Models: Static Models

2.3.2.1.1 Static Models: Block Diagram

A MATLAB® Simulink model based on the EEC model similar to [131] and [132] was used by the authors to represent the electrochemical phenomenon of the PEM electrolysis cell [133]. The reversible cell voltage was calculated from Gibbs free energy and overvoltages were calculated as dependent on temperature and pressure using Tafel equations. The efficiency of the electrolysis system was also estimated as the ratio of useful power to input power.

One dimensional mathematical model of PEM water electrolyser and fuel-cell were proposed in [134]. Approach similar to [126] and [127] was used to model the PEM electrolyser. The model was divided into four sub-models; voltage (to calculate cell voltage). Anode, cathode and membrane (to calculate flow balance). The model was implemented in MATLAB® Simulink. The models were validated against the experimental data from [135].

2.3.2.1.2 Static Models: Electrical Equivalent Circuit

Equivalent circuit was proposed first in [71] for the calculation of the MEA electric resistance. For this the anode, cathode, membrane and inter-facial resistances were considered in series. The same model was also utilised in [106] and [107]. Another EEC model for a single cell PEM electrolyser was proposed in [131]. Experimental data for steady state operation was used to model the characteristic curves of the electrolyser. The internal resistance of the cell and the reversible potential were modelled as dependent on the temperature and pressure using

Table 2.2: Summary of equation based models

Year	Ref.	Modelling Method	Static/ Dynamic	Modelling scope			Phenomenon modelled						Purpose of the model
				Cell	Stack	BoP	Elec.	Elec.-chem.	Thrm	Fluidic	Gas Cross.	Bubbles	
1992	[102]	Semi-empirical	Static	✓				✓		✓			Performance analysis
2001	[103]	Semi-empirical	Static	✓				✓					Simulation of IV curve
2002	[70]	Analytical	Static	✓				✓					Simulation of current & temperature distribution
2004	[71]	Analytical	Static	✓				✓					Performance analysis
2005	[104]	Semi-empirical	Static		✓			✓					Simulation of IV curve
2006	[105]	Semi-empirical	Static	✓				✓					Phenomenon understanding
2007	[106]	Semi-empirical	Static	✓				✓					Performance analysis
2008	[108]	Semi-empirical	Static		✓			✓					Study of the dependence of overvoltages on Temperature
2008	[116]	Analytical	Dynamic	✓				✓	✓				Study of thermodynamic performance & efficiency
2008	[107]	Semi-empirical	Static	✓				✓					Performance analysis
2008	[109]	Semi-empirical	Static		✓			✓	✓				Phenomenon understanding
2008	[72]	Analytical	Static	✓				✓					Phenomenon understanding
2009	[91]	Semi-empirical	Static		✓			✓		✓			Performance analysis
2009	[122]	Semi-empirical	Dynamic	✓				✓	✓				Temperature prediction, performance analysis
2009	[100]	Empirical	Static		✓			✓					Phenomenon understanding
2010	[111]	Semi-empirical	Static	✓				✓	✓	✓	✓		Phenomenon understanding & efficiency estimation
2010	[101]	Empirical	Static		✓					✓			Operating conditions selection
2011	[73]	Analytical	Static	✓						✓			Phenomenon understanding
2012	[123]	Semi-empirical	Dynamic		✓			✓	✓				System behaviour simulation
2012	[124]	Semi-empirical	Static		✓	✓		✓					Performance prediction & efficiency calculation
2012	[74]	Analytical	Static	✓						✓	✓		Phenomena understanding
2013	[125]	Semi-empirical	Dynamic	✓				✓		✓	✓		System behaviour simulation
2013	[75]	Analytical	Static	✓				✓		✓			Phenomena understanding & parametric study
2013	[112]	Semi-empirical	Static	✓				✓			✓		Phenomena understanding & efficiency calculation
2014	[76]	Analytical	Static	✓				✓					Parametric study of cell voltage
2014	[78]	Semi-empirical	Static	✓				✓		✓			Polarization curves simulation
2014	[77]	Analytical	Static	✓				✓					Phenomena understanding
2014	[110]	Semi-empirical	Static		✓			✓	✓				Model predictive control
2015	[79]	Analytical	Static	✓				✓		✓			Cell degradation estimation
2016	[81]	Analytical	Static	✓				✓		✓			Phenomena understanding & efficiency calculation
2016	[82]	Analytical	Static	✓				✓		✓	✓		Efficiency calculation
2016	[83]	Analytical	Static	✓				✓		✓			Performance prediction & efficiency calculation
2017	[113]	Semi-empirical	Static		✓	✓		✓		✓			Phenomena understanding & efficiency calculation
2017	[84]	Analytical	Static	✓				✓		✓		✓	Performance prediction & phenomena understanding
2017	[85]	Analytical	Static	✓				✓	✓	✓		✓	Performance prediction & phenomena understanding
2017	[120]	Analytical	Dynamic		✓			✓	✓	✓			System behaviour simulation
2017	[114]	Semi-empirical	Static	✓				✓	✓	✓		✓	Phenomena understanding & polarization curves simulation
2017	[86]	Analytical	Static	✓				✓					System performance optimization
2017	[117]	Analytical	Dynamic	✓				✓				✓	Phenomena understanding & polarization curves simulation
2017	[115]	Semi-empirical	Static	✓				✓		✓			Performance prediction & phenomena understanding
2017	[87]	Analytical	Static	✓				✓					Polarization curves simulation
2018	[128]	Semi-empirical	Dynamic	✓				✓		✓			Polarization curves simulation & efficiency estimation
2018	[88]	Analytical	Static	✓				✓					Phenomena understanding & polarization curves simulation
2019	[129]	Semi-empirical	Dynamic		✓	✓		✓	✓	✓			System behaviour simulation & efficiency calculation
2019	[130]	Semi-empirical	Static	✓				✓		✓	✓		Performance simulation
2019	[90]	Analytical	Static	✓				✓		✓	✓		Performance comparison & efficiency calculation
2019	[89]	Analytical	Static	✓				✓					Performance characterization
2020	[121]	Analytical	Dynamic	✓				✓	✓	✓			System response simulation
2020	[92]	Analytical	Static	✓				✓					Phenomena understanding
2020	[93]	Analytical	Static	✓				✓					Efficiency calculation
2020	[94]	Analytical	Static	✓				✓		✓			Performance comparison
2020	[95]	Analytical	Static	✓				✓	✓	✓			System performance simulation
2021	[96]	Analytical	Static	✓			✓	✓		✓			System performance simulation
2021	[97]	Analytical	Static	✓				✓		✓			Phenomena understanding
2021	[98]	Analytical	Static	✓				✓	✓	✓			Performance simulation
2021	[99]	Analytical	Static	✓				✓		✓			Phenomena understanding

empirical relations. The model was able to predict the production rate of the hydrogen and overall electrolyser efficiency.

An EEC model for a single cell PEM electrolyser was also proposed in [132]. The characteristic curves of the electrolyser were modelled using experimental data for steady state operation. It was found that the hydrogen production rate varies proportionally to the current and logarithmically to the input power.

A semi-empirical model for the study of electrochemical performance of the PEM water electrolysis was proposed in [136]. The model incorporated a detailed ohmic loss model based on EEC for the cell by considering resistances of bipolar plates, electrodes, membrane and interfacial resistance of the MEA which was also presented in [137]. The effect of various design parameters on the performance of the PEM electrolysis cell was studied.

A mathematical model to study the effect of tunable GDL on the performance of the PEM electrolyser was proposed in [138]. The model considers the effect of porosity and pore diameter on interfacial contact resistance and surface roughness factor to calculate ohmic and activation overvoltage. A two dimensional EEC model was proposed to estimate the current distribution on the catalyst layers. The model was validated against different characteristics curves obtained at different operating conditions.

In [139], mass transport losses in a PEM electrolyser were modelled using Electrochemical Impedance Spectroscopy (EIS) for which a modified Randels EEC was utilized. The model takes into account the effect of pressure and water flow on the losses due to mass transport. Simulations of polarization curves as a function of water flowrate and pressure for both cathode and anode side were performed.

2.3.2.2 Graphical Models: Dynamic Models

2.3.2.2.1 Dynamic Models: Block Diagram

A dynamic mathematical model for PEM electrolyser was proposed based on the molar balance on the anode and cathode side [126]. The model consists of four blocks, representing anode, cathode, membrane and voltage blocks. The model also take into account the mass transport through the membrane. The operating voltage is considered to be only affected by reversible voltage, overvoltage and ohmic resistance of the MEA. The dynamics of the hydrogen storage was also modelled to simulation pressure evolution of storage bottle while filling it with hydrogen. In [140], a dynamic model for the reversible fuel cell system was proposed by the authors which includes the modelling of the balance of plant. The sub-model of the electrolyser is simple and static, which can only be used to calculate the overall cell voltage based on the Nernst equation.

A dynamic model for PEM electrolyser developed in MATLAB$^{\circledR}$ Simulink was presented in [127]. The modelling is based on the molar balance on the cathode and anode sides, Nernst and BV equations. The model was divided into four sub-models; anode, cathode, membrane and voltage. The model was validated against experimental data from the literature. The effect of temperature and pressure on the performance of the electrolyser was studied. An approach similar to that of [127] was presented for the modelling of PEM water electrolysis stack in [135]. The BoP such as water tank and pump, cooling fan, power supply and storage tank for hydrogen were also modelled to calculate the power loss. These losses are considered for evaluating the system performance during numerical simulations. It was found that the losses in the stack at higher current densities exceeds the losses of other components.

A dynamic model for PEM water electrolysis was developed in MATLAB$^{\circledR}$ Simulink in [141]. The model was divided into 5 ancillaries; voltage (to compute cell voltage using Nernst equation, activation overpotential and ohmic over potential), anode and cathode (to calculate

the partial pressures and flows of the species), membrane (to calculate the mass transport) and storage (to capture the dynamics of the filling of the hydrogen bottle taking into account the initial hydrogen content in the bottle and hydrogen's compressibility). The experimental study was performed for four different bipolar plate flow channel configurations. The developed model was then used to simulate the IV curves for different configurations and effect of water flow rate on the flowrates of the hydrogen and oxygen.

In [142], an enhanced model for the PEM water electrolysis cell was proposed. The model was divided into four parts (similar to what is done in [126] and [127]). Mass balance equations for the anode, cathode and membrane were utilized. For cell voltage calculation approach similar to [143] was used. The model was implemented in MATLAB® Simulink.

A MATLAB® Simulink model was proposed in [144] to simulate the performance of the PEM water electrolysis system by taking into account the effect of the dynamics of the water pump and temperature variation on the hydrogen generation.

2.3.2.2.2 Dynamic Models: Electrical Equivalent Circuit

An EEC model was proposed for the modelling of electrochemical characteristics of the PEM electrolyser [143]. The ohimc losses, activation losses and concentration losses were considered. The equivalent electrical components that were considered for the modelling are membrane resistance (to represent ohmic losses), charge transfer resistance (to represent losses due to activation), double layer capacitance (to represent the electric capacitance formed due to the applied electric field across the current collectors) and Warburg impedance (to represent concentration losses). Two different approaches were used to obtain the values of the parameters for the EEC, namely, normal voltage response and system identification technique. An equivalent circuit model similar to the one proposed in [143] was used to model the electrochemical characteristics of the PEM electrolysis cell [145]. The parameters for the model were obtained using current interrupt method.

A model for studying the transient behaviour of the PEM water electrolyser was proposed [146]. Two dependent Resistor–Capacitor (RC) circuits were considered coupled with the double layer capacitance of the electrolyser. The model was effective for studying startup transient dynamics, however, it cannot be used for steady state operation performance evaluation.

An EEC model (considering a single RC circuit in series with ohmic resistance and reversible cell voltage generator) was used for the study of sliding mode pulse width modulation approach for the voltage regulation for the PEM electrolyser [147]. The experimental validation of the model was not performed.

A dynamic EEC model for the PEM electrolyser was proposed [148]. Two RC circuits (representing heat losses and dynamics of anode and cathode side) in series with internal resistance. The model was validated against the three cell PEM water electrolyser. An extension to the EEC proposed in [148] was presented in [149] by considering the voltage generator in series to the RC circuit representing the power required for hydrogen production. Two different time constants were considered for modelling the dynamic behaviour of charge layers. A static relation to estimate the cell temperature was also proposed based on the calculated thermal resistance of the cell. In [150], a control strategy based on the energy efficiency (using proportional-integral controller) for the electrical power supply of PEM water electrolyser was proposed based on the three-level interleaved DC to DC buck converter. The dynamic EEC model of the PEM water electrolyser developed in [148] was used to test the developed control strategy. EEC model similar to the one in [149] for a PEM electrolyser was proposed for studying the influence of different operating conditions and power electronics ripples effect on the cell voltage [151]. The work is limited only for study of cell voltage modelling under static and dynamic operating conditions. In continuation to the previously published article [151] the EEC model of the PEMF

38

electrolyser cell was proposed to study static and dynamic operations [152]. The parameters of the model were estimated using experimental data in two ways; as constants and as a function of current.

In [153], a model based adaptive approach to estimate the values of time constants for the EEC model of PEM electrolyser (presented previously in [148] and [149]) was proposed. The time constant for the cathode side was calculated as dependent on the cell current, using the EEC topology. A simple EEC for the PEM electrolyser was proposed in [154] to use it as an emulator for the load for the stack interleaved buck converter. The constant values of resistances and capacitance were chosen to simplify the model based on the experimental data.

2.3.2.2.3 Dynamic Models: Energetic Macroscopic Representation

A graphical dynamic model for PEM water electrolysis stack was developed using Energetic Macroscopic Representation (EMR) modelling technique [118]. The model was able to simulate the temperature evolution of the stack and the water supplying tank with good accuracy. The model was then utilized to simulate the polarization curves ad different temperatures and validated against the experimentally recorded data. The parameters for the model were obtained from literature and curve fitting of the experimental data and measurements. The model was highly complex and required deep understanding of the multi-physics phenomena of the PEM electrolysis.

2.3.2.2.4 Dynamic Models: Bond Graph

A BG based multi-physics model was proposed for the PEM electrolysis stack [155]. The model is sub divided into sub-models that represents different phenomena of the stack. The model was able to simulate the temperature evolution of the stack and hydrogen flowrate. This work was further extended and presented in [15] in the form of a dynamical multi-physics model that includes the modelling of the auxiliary components. The global model of the stack was developed by combining different sub-models focused on various phenomena in the stack such as electrochemical phenomena, thermo fluidic phenomena, mass transport phenomena. The modelling of the auxiliaries include, gas separators, valves, purification system and enclosure of the system. The model parameters were identified using a 25kW industrial PEM electrolyser. The model simulations were compared to the experimental measurements which showed the effectiveness of the model in reproducing the behaviour of the system. Another BG based model was reported in [17]. The article concerns the modelling of the hybrid multi-source system for hydrogen generation using event driven hybrid bond graph approach. This approach is well suited for such systems as it can handle operation mode management very easily. The model used for the electrolyser was simple yet dynamic. Only the electrochemical phenomenon to calculate cell voltage and hydrogen production was modelled.

2.3.2.3 Graphical Models: Summary

A number of graphical models exist for PEM water electrolysis in the literature (both static and dynamic) that have been summarised in table 2.3. EEC and block diagram representation are the most used techniques for the modelling. Models developed using EEC mostly focuses on the electrochemical phenomena. In some articles EEC technique has been used to calculate the resistance of the PEM electrolysis cell by considering the resistance of individual components. These models are then coupled with the rest of the model developed using other techniques. The block diagram representation has been used for developing the dynamical models (mostly) of the PEM electrolyser for the system performance or system behaviour simulations. Some

Table 2.3: Summary of graphical models

Year	Ref.	Modelling Method	Static/Dynamic	Modelling scope			Phenomenon modelled				Purpose of the model
				Cell	Stack	BoP	Elec.	Elec.-chem.	Thrm	Fluidic	
2004	[71]	EEC	Static	✓				✓			Performance analysis
2006	[126]	Block Diagram	Dynamic		✓			✓		✓	Performance analysis & efficiency calculation
2007	[106]	EEC	Static	✓				✓			Performance analysis
2008	[107]	EEC	Static	✓				✓			Performance analysis
2008	[140]	Block Diagram	Dynamic	✓		✓		✓			Performance simulations
2011	[118]	EMR	Dynamic		✓	✓	✓	✓	✓	✓	Performance simulations
2011	[127]	Block Diagram	Dynamic		✓			✓		✓	Performance analysis
2011	[131]	EEC	Static	✓				✓			Hydrogen prod. estimation & efficiency calculation
2011	[132]	EEC	Static	✓				✓			Hydrogen prod. estimation & efficiency calculation
2013	[141]	Block Diagram	Dynamic	✓		✓		✓		✓	System behaviour simulation
2013	[143]	EEC	Dynamic	✓				✓			System behaviour simulation
2014	[133]	Block Diagram & EEC	Static	✓				✓			Polarization curves simulation & efficiency calculation
2014	[145]	EEC	Dynamic	✓				✓			System behaviour simulation
2015	[142]	Block Diagram & EEC	Dynamic	✓				✓		✓	System behaviour simulation
2015	[136, 137]	EEC	Static	✓			✓				Electrical losses estimation
2016	[135]	Block Diagram	Dynamic		✓	✓		✓			Performance analysis
2016	[155]	Bond Graph	Dynamic		✓			✓	✓	✓	System behaviour simulation
2017	[15]	Bond Graph	Dynamic		✓	✓		✓	✓	✓	System behaviour simulation
2017	[138]	EEC	Static	✓			✓	✓			Performance analysis
2018	[17]	Bond Graph	Dynamic	✓				✓			System behaviour simulation
2018	[148]	EEC	Dynamic		✓			✓			System behaviour simulation & efficiency calculation
2019	[149]	EEC	Dynamic		✓			✓	✓		System behaviour simulation & efficiency calculation
2019	[147]	EEC	Dynamic	✓			✓	✓			Polarization curves simulation & control
2019	[139]	EEC	Static	✓				✓			Polarization curves simulation
2019	[150]	EEC	Dynamic	✓				✓			Model based control
2020	[151]	EEC	Dynamic	✓				✓			System behaviour simulation
2020	[153]	EEC	Dynamic		✓			✓			System response simulation
2020	[154]	EEC	Dynamic		✓			✓			System behaviour emulation
2021	[152]	EEC	Dynamic		✓			✓			System response simulation
2021	[134]	Block Diagram	Static	✓				✓		✓	Performance analysis & efficiency calculation
2021	[144]	Block Diagram	Dynamic	✓				✓	✓	✓	System behaviour simulation

of these models have considered the BoP for the overall system modelling for the estimation of stack temperature, hydrogen production, etc. However, they do not consider all the key phenomena of the cell/ stack. Other notable work on the PEM water electrolysis modelling has been done using EMR. The model take into account the BoP to estimate the temperature of the stack and water supply tank temperature. The model is however, highly complex and required deep understanding of the multi-physics phenomena of the PEM electrolysis. The model cannot be easily scaled and adapted for other configurations of the electrolyser. This model is also not suited for system monitoring and diagnosis. Another significant work on the PEM electrolyser modelling was done using BG approach. The model takes into account BoP for the system dynamic behaviour simulation, for the power consumption estimation and temperature prediction. The model is again highly complex and cannot be directly scaled or configured for other types of electrolysers. Also the model was not exploited for the diagnosis and prognosis.

2.3.3 Models Coupled with RES

A number of publications in the literature have addressed the issues arising due to the coupling between the PEM electrolyser and the RES. In [11] various configurations for using PEM electrolyser with Photo-voltaic (PV) panels for grid assisted and grid independent operations were explored. The issues that arises due to the intermittent nature of RES were also highlighted. Various publications have used the models of PEM water electrolysers to study the performance of the PEM water electrolysers under the influence of RES.

2.3.3.1 Models Coupled with RES: Static Models

In [156], a simple static model of the PEM electrolyser was used to study the performance of the electrolyser as a component in the solar-hydrogen energy system. A one year simulation of the system was presented. State of the charge of battery was used for control in order to connect and disconnect the components.

A dynamic model of a wind powered hybrid generation system was presented to simulate the performance [7]. The electrolyser is used to store the excess power and during times when there is less wind energy than demand, fuel-cell supplies the required power. Ultra capacitor is used to support the load for short duration. A simple static electrical model of electrolyser was used. The model was implemented in MATLAB® Simulink.

An electrochemical model for the PEM electrolysis cell directly on the solar energy was proposed [157]. The model is based on the BV equation to represent the kinetics of the electrodes and transport resistance of the membrane. An equivalent circuit model was then proposed to calculate the cell voltage by considering the cell resistances in series with the open circuit voltage. A simple analytical model of PEM electrolyser was used that includes only the calculation of reversible potential and a single overpotential [45]. The key focus was on the modelling of the PV cell. The developed model is utilized to predict the operating points for the considered system. The model was implemented in MATLAB® Simulink.

A method for sizing the Photo-voltaic panels to use them with PEM electrolyser for converting solar energy into hydrogen energy was proposed [48]. The simple models of the PV panel and the PEM electrolysers were considered from the literature. The simulations were then utilized to calculate the point cloud for the maximum power points for the PV panels. The polarization curve for the electrolyser is then normalized and fitted through this point cloud to estimate the ideal ratio for the sizing of the components. The model of the electrolyser used is semi empirical and static.

In [49], a simple model of electrolyser was considered based on the Faraday's Law. The key focus of the article was on the development and validation of the overall control strategies for the electrolyser powered by the wind farm.

A neural network based maximum power point tracking algorithm was proposed for solar powered PEM electrolyser system [50]. A mathematical model of the PEM electrolyser adapted from the literature was used for the simulation in MATLAB® Simulink. The model calculates the overall cell voltage using Nernst Equation and temperature and pressure dependent equations for hydrogen and oxygen production rates.

A model for the analysis of solar panel assisted hydrogen based energy storage system was proposed in [58]. The model included the sub-models of PV panels, PEM fuel cell, PEM electrolyser and hydrogen gas compressor. The model of electrolyser was very simple to calculate the amount of hydrogen produced. The model was used to simulate the electric load variation depending on the availability of solar energy and demand, and production and consumption of hydrogen for four different months. The model was, however, not validated.

Coupling between the RES and the electrolyser was proposed in [51] using synchronous

DC-DC buck converter. The system was modelled using block diagram representation. The electrolyser was modelled as a nonlinear resistance. No notable contribution in terms of modelling of the electrolyser was presented. A coupling between PV panels and PEM was presented in [53]. A simple electrochemical model was proposed based on the previous works on the fuel-cell for calculating the overall cell voltage. A new relation for calculation of concentration loss as a function of current density was implemented. In [54], an analytical electrochemical model was proposed based on the previous works for the simulation of the performance of the PEM water electrolysis coupled with PV cells. The model was validated against the results from the published articles.The hydrogen production for various operating conditions was simulated. The authors proposed two configurations for electrolysers, one in series and the other in parallel, for winter and summer.

The model of PEM water electrolysis developed in [91] was used with the model of PV panel to study the effect of the coupling between solar energy and PEM water electrolysis [158]. The simulations were performed for different weather conditions.

A two dimensional finite element based thermo-fluidic model was proposed for the study of the performance of the PEM electrolyser running at high temperature and pressure coupled with photo voltaic multi-junctions solar cell [57]. The model is useful for simulating the temperature distribution inside the cell and estimating the performance characteristics.

A simple electrochemical model of PEM water electrolysis cell (for stack voltage calculation) was used for power hardware in loop simulation of a PEM water electrolyser as a part of a smart grid powered by solar and wind power [59]. The model was validated against the measurements from a commercial PEM electrolyser. This could be a great tool to simulate load for study of power supply for PEM electrolyser.

A very simple empirical model to represent the current voltage relationship for a PEM water electrolysis was proposed [62]. This model was coupled to the semi-empirical model of PV module to simulate the performance of the PEM electrolyser running directly on solar energy with the help of PV panel. The model was not able to reproduce the experimental results due to very simple PEM electrolyser model.

2.3.3.2 Models Coupled with RES: Dynamic Models

A dynamical model of electrolyser, running on wind energy and ultra capacitor as a buffer energy source, was developed for control using Causal Ordering Graph (COG) [43]. Empirical relations were used to calculate the operating voltage and hydrogen production. The operating temperature of the electrolyser was assumed as a constant. Hydrogen pressure was calculated based on the ideal gas law. other ancillaries of the system such as wind generator, electrical converters, fuel cell, compressor. hydrogen tank were also modelled. The model is only suitable for performing control (power flow control for the system, Pressure control for the electrolyser, and hydrogen flow for the compressor). Similar work was proposed in [46] where a model based on COG was developed for the electrolyser running on wind energy. The objective of the model was to simulate the hydrogen production and to develop control algorithm to ensure the storage of excess energy in the form of hydrogen energy. Three controls operations were performed: control of current, outlet pressure of the electrolyser and flow rate of the hydrogen. Model used for the electrolyser was based on empirical relations to estimate the cell potential and Faradaic efficiency. Partial pressures of the species were calculated using ideal gas law. The hydrogen storage was also modelled to calculate the evolution of storage pressure. The developed model was also used as an electrolyser emulator for Hardware-in-loop simulation.

An analytical model of PEM electrolyser to study the effect of current ripples on the performance and behaviour of the electrolyser running on RES was proposed [44]. The overvoltages were modelled using EEC and were linearized around the operating point to simplify the model.

The response of the electrolyser to current interrupts was studied. In [47], a dynamic model for the standalone hybrid solar powered system was proposed that uses an electrolyser for the hydrogen generation and PEM fuel cell to convert the hydrogen into electricity when required. The simplified equivalent circuit model for the electrolyser was used. The simulations shows the effectiveness of such systems to power a small family house with effective power tracking. Mathematical relations used by the authors for the modelling of the electrolyser can be used for PEM electrolyser also with suitable parameter values.

A mathematical model for the PEM electrolyser sunning on solar energy was proposed in [119] using the mathematical equations similar to the work presented in [118]. The model was subdivided into three parts; Electrical part to calculate Nernst potential, electrochemical part to calculate overvoltage due to activation (using BV equation), ohmic resistance and diffusion, thermal model to calculate the temperature evolution of cell and water supply tank based on a lumped parameter approach. The model was validated against the experimental data for the electrolysis cell and the temperature measurements of the water supply tank.

Four different models of PEM water electrolyser were compared in [52] for the performance simulation of the PEM water electrolyser coupled with wind energy. The power consumption, cell voltage, current and hydrogen generation based on four selected models were compared.

In [60], an equivalent circuit model similar to the one used in [131] and [133] was coupled the model of a horizontal wind turbine and buck converter. The model was simulated in MATLAB® Simulink and compared with the experimental data. An error of 3.4% was observed.

Analytical dynamic models of alkaline and PEM water electrolysers were developed to simulate the performance based on the data input sets for the solar and wind energy from northwest region of Germany [65]. The electrochemical phenomena, mass balance and thermal model representing temperature evolution were considered for modelling. Simulations were performed for three different stack capacities by scaling the model by considering the stack working at 40, 60 and 80% capacity at nominal conditions. The techno-economic analysis was also performed for both types of electrolysers. The models were not validated against any experimental data.

2.3.3.3 Models Coupled with RES: Summary

The models that have been used to simulate the coupling between PEM water electrolysis and RES have been considered separately and summarised in table 2.4. Most of the models have focused on the coupling between PV and PEM water electrolysis. The models used are mostly equation based and only electrochemical phenomenon have been considered. These models have been used to estimate the electrical load of the PEM water electrolyser, calculating hydrogen production rate, for developing control for the whole hybrid system or to simulate system response for dynamic inputs. None of the models have considered the BoP in the modelling except one in which the hydrogen storage tank was modelled to estimate the pressure of the storage tank.

2.3.4 Miscellaneous Models

A number of models exist in the literature that cannot be considered under the preciously mentioned categories. These models include the CFD models, neural network models, etc. These models have been briefly discussed below.

Numerical simulations for the study of three dimensional fluid flow of water in the anode side bipolar plate were performed using CFD [159]. Only monophasic flow was considered for simplifying the calculations. The flow was considered laminar and three dimensional Navier Stokes equations and continuity equations were solved for the simulations for every finite volume cell. The authors observed that there is a pressure drop between inlet and outlet along the

Table 2.4: Summary of models used with RES

Year	Ref.	RES	Modelling Method	Static/ Dynamic	Cell	Stack	BoP	Elec.	Elec.-chem.	Thrm	Fluidic	Purpose of the model
1994	[156]	Solar	Empirical	Static	✓				✓	✓		Performance analysis & efficiency Calculation
2006	[7]	Wind	Block diagram	Static	✓				✓			Performance analysis & control
2007	[43]	Wind	COG	Dynamic		✓	✓	✓	✓		✓	Model based control
2008	[157]	Solar	Analytical & EEC	Static	✓				✓			Performance analysis
2009	[44]		Analytical & EEC	Dynamic	✓				✓			Performance analysis & efficiency Calculation
2009	[45]	Solar	Analytical	Static	✓				✓			Operating point selection & efficiency calculation
2009	[47]	Solar	EEC	Dynamic	✓				✓			System behaviour sim.
2009	[46]	Wind	COG	Dynamic		✓	✓	✓	✓		✓	System behaviour sim. & model based control
2011	[48]	Solar	Semi-empirical	Static	✓				✓			Sizing of the components
2011	[49]	Wind	Analytical	Static								Power consumption estimation & control
2011	[50]	Solar	Neural Network & Block Diagram	Static	✓				✓			Performance prediction
2014	[119]	Solar	Analytical	Dynamic	✓				✓	✓		Polarization curve and temperature simulation
2014	[51]	Solar & wind	Block diagram	Static	✓			✓				System behaviour sim.
2015	[53]	Solar	Analytical	Static	✓				✓			Performance analysis & efficiency Calculation
2016	[54]	Solar	Analytical	Static	✓				✓			System performance sim.
2016	[158]	Solar	Semi-empirical	Static	✓				✓		✓	Performance analysis
2017	[57]	Solar	FEM	Static	✓				✓	✓	✓	Performance analysis & phenomena understanding
2017	[58]	Solar	Analytical	Static	✓							Hydrogen production calc.
2017	[59]	Solar	Analytical	Static		✓			✓			Electrical load emulation
2017	[60]	Wind	EEC	Dynamic	✓		✓		✓			System performance sim.
2018	[62]	Solar	Emperical	Static	✓			✓				Hydrogen production calc.
2020	[65]	Solar & wind	Analytical	Dynamic		✓			✓	✓	✓	System response sim.

diagonal direction. The velocity distribution across the flow channels was also observed to be highly non-uniform and back flow was present at the exit. No experimental validation was presented for these claims. A three dimensional CFD model was proposed to study the bi-phasic flow of water and oxygen through the anode side bipolar plate in a PEM electrolysis cell [160]. The mixture model for the simulation of bi-phasic was utilized. The validation of the model was performed using the measured values of the pressure drop in uni-phase fluid flow. Higher pressure drop at the exit was observed in the simulations with increase in the oxygen bubbles rate. Similarly, numerical simulations for the study of three dimensional fluid flow of water in the anode side bipolar plate were performed [161]. The design of the flow channels of the bipolar plate was different than the one used by the author in [160]. It was observed that there is a pressure drop between inlet and outlet along the diagonal direction. The velocity distribution and temperature distribution across the flow channels were observed to be highly non-uniform. The simulations were validated against the average pressure drop measured with the help of two pressure gauges placed at the inlet and outlet of the bipolar plate. Another, CFD based numerical model of bi-phasic flow in the anode side flow plate was proposed in [162]. The objective of the simulation was to study the effect of different oxygen bubbles rate on the pressure, velocity and volume fraction distribution across the flow plate.

A CFD analysis was performed in [163] for analysing the mass distribution of water in the in-house assembled PEM water electrolysis stack of 10 cells and 120 channels. The authors claim uniform water distribution across the channels and homogeneous pressure in all the cells. The study of system performance and efficiency was also performed to optimize the operations of BoP by varying different parameters. In [164], a three dimensional bi-phasic model was developed for analysing the transportation of oxygen bubbles through the porous transport layers of a PEM electrolyser. The movement at the gas and liquid interface, in the porous media saturated with water, was simulated using using Volume of Fluid technique. The model also included the water flow through the channels. The developed model was validated against the experimental microfluidic investigations performed previously. The effectiveness of oxygen bubbles removal was estimated using the validated model by calculating the variation in pressure inside the bubbles during their movement. The maximum value of the threshold capillary pressure was considered as the indicator for efficient oxygen bubbles removal. The developed model has a potential use for studying the effect of new materials on the effectiveness of oxygen bubble removal. A three dimensional steady state, non-isothermal CFD model was proposed in [165] to study the performance of a new spiral fluid flow fields by investigating the distribution of temperature, pressure drop and current density. The validation of the model was performed using experimental data. The model performance is acceptable for the operation of the cell at low to medium current densities. In [166], a non-isothermal three dimensional CFD model for high temperature PEM water electrolysis cell bases on finite volume method was proposed to study the effect of various parameters such as membrane thickness, GDL thickness, cell temperature and cathode side pressure on the energy and exergy efficiencies and exergy cost. The results obtained were extrapolated to the stack. A multi-physics model for PEM water electrolyser was proposed in [167] based on the CFD, taking into account the effect of thermo-fluidic and mass transport phenomena on the performance of the electrolyser. The model was validated against the Laboratory scale PEM electrolyser with the flow field of three serpentine shape.

Models for the prediction of hydrogen flow rate, stack and system efficiency were proposed using Adaptive Neuro-Fuzzy Inference Systems based on neural networks [168]. Various inputs, outputs and parameters of the system were recorded to prepare a database to train these models. The authors claims the simulation error of $\pm$ 3% when compared to the experimental data. The authors sees the scope for utilizing these models as virtual censors. The model is,

45

however, highly system dependent as experiments are needed to be performed to develop the database and train the model for the application to different systems.

A dynamic artificial neural network model was developed for PEM electrolyser using Multi-layer Perceptron Network technique [169]. The model was trained to predict the stack voltage based on the current density, temperatures of the stack. The error between the predicted and actual stack voltage was found to be 1.96%.

In [170], a stochastic model of the porous transport layer constructed from sintered titanium powder was developed using data from X-ray based micro scale computed tomography. The stochastic parameters of the model were studied for their effect on the model by comparing mean pore size and throat diameter of the GDL. This developed stochastic model was used for pore network modelling in [171] to study the effect of the micro-structure of the Porous transport layer on the transport properties of the bi-phasic flow in the PEM water electrolyser. The influence of various model parameters such as pore size, throat size an porosity on the transport properties was studied.

The work presented in [59] was further extended in [61]. The dynamics of the power hardware in loop simulator was verified to ensure its ability to simulate the fast power and current variation of an industrial scale electrolyser as a part of smart grid. The aim of these simulations is the power supply unit of the electrolyser.

In [172], a model of a large scale PEM electrolyser was proposed by the authors in the RSCAD$^{\circledR}$ software coupled with an infinite grid for the real-time digital simulation. The electrolyser stack was modelled as an ohmic resistance and the pump was the only component considered in the BoP. The BoP was modelled with the help of dynamic load model from the library of the software. The performance of the model was compared with the performance of small electrolysers from the literature. A generic model for the large PEM electrolyser was proposed in RSCAD$^{\circledR}$ for the real-time simulations to study the impact of the electrolyser on the stability of the power system [173]. A simple EEC was considered for the PEM electrolyser consisting of three resistances and a single double layer capacitance. The model was validated against PEM electrolyser of 1MW.

2.3.4.1 Miscellaneous Models: Summary

The models considered in this category have been summarised in table 2.5. A number of models have been developed using CFD in order to study the flow of liquid gas mixture through the flow channels in the flow plates and its effect on the characteristic curves. CFD is for better accuracy but also better understanding of what happens at the micro-scale, that other models are not able to do. Better understanding of the transport phenomenon, mainly flows, at the microscopic level is of a great help for designing the flow plates and also for macroscopic modelling for behaviour simulations. Models using neural network techniques have also been proposed to have simplistic models to estimate the hydrogen production and stack voltage. Some efforts have also been made to simulate the GDL characteristics using stochastic modelling. Most of the models considered are static.

2.3.5 Conclusion

The view into the literature of the modelling shows that there still exists a requirement of the model for PEM electrolyser that can capture the key dynamics of the PEM electrolyser and act as a generic tool for representing different types, configuration and sizes of the electrolyser. The model must take into account the BoP to be utilized as an effective digital twin for research studies related to the coupling between PEM electrolyser and RES or some other chemical plant for GH$_2$ consumption. The model must be able to calculate the efficiency as it is a key indicator

Table 2.5: Summary of the miscellaneous models

Year	Ref.	Modelling Method	Static/ Dynamic	Modelling scope			Phenomenon modelled					Purpose of the model
				Cell	Stack	BoP	Elec.	Elec.-chem.	Thrm	Fluidic	Bubbles	
2007	[159]	CFD	Static	✓						✓		Flow analysis
2008	[160]	CFD	Static	✓						✓	✓	Flow analysis
2009	[161]	CFD	Static	✓					✓	✓		Temperature and flow analysis
2010	[168]	Neural Networks	Static		✓							Hydrogen flow and efficiency prediciton
2010	[162]	CFD	Static	✓						✓	✓	Flow analysis
2011	[169]	Neural Networks	Dynamic		✓		✓					Stack voltage estimation
2013	[163]	CFD	Static		✓					✓		System performance study & efficiency calculation
2016	[174]	COMSOL										Polarization curve simulation
2016	[164]	CFD	Static	✓						✓	✓	Phenomena understanding & flow analysis
2017	[170]	Stochastic Modelling	Static	✓								Simulation of GDL
2018	[172]	CFD	Dynamic		✓	✓	✓					Realtime simulation
2019	[165]	CFD	Static	✓				✓		✓		Flow analysis & polarization curve simulation
2019	[166]	CFD	Static	✓	✓							Efficiency calculation & exergy cost analysis
2019	[171]	Pore Network Modelling	Static	✓						✓		Phenomena understanding & flow analysis
2020	[173]	RSCAD	Dynamic		✓			✓				System response simulation
2021	[167]	CFD	Static	✓				✓	✓	✓		System performance analysis

of the system performance. To answer this, a modular generic dynamical multi-physics model based on BG approach has been proposed in the present work that can be used for representing different configurations of PEM electrolyser.

BG is a well-developed graphical modelling technique in which the systems or subsystems can be modelled with few elements (*Se*: source of effort, *Sf*: source of flow, *R*: resistance (dissipation of energy), *C*: capacitance (potential energy storage), *I*: inductance (kinetic energy storage), *Tf*: transformer and *Gy*: gyrator (for energy conversion between different physical domains), etc.) that represent physical phenomena. Irrespective of the physical domain the nature of these elements remains unchanged. Half arrows known as power bonds are used to connect these elements. These bonds represent the power exchange between the elements where the power is a product of generalized effort and flow. Therefore, BG is a unified approach that can be used in a similar way for the systems that belongs to different physical domains. The basics of the BG technique and its application for the modelling and Fault Detection and Isolation (FDI) into process engineering are well defined throughout the literature [18, 175–177]. Powerful software like 20sim is available that can generate dynamic equations directly from the BG model. Moreover, the parameters used have a physical meaning and the BG model can be refined very easily by adding new elements without having to start again the modelling process. Also, due to its structural and causal properties, the BG is suitable for control analysis, sizing, and diagnosis analysis and health management of PEM electrolyser. The BG technique for modelling is presented briefly in the appendix B.

2.4 Diagnosis and Prognosis of PEM Electrolyser

A look into the literature showed that there is not much work done for the model based diagnosis and health management of the PEM electrolyser.

2.4.1 Diagnosis

A number of techniques have been implemented for the diagnosis of the PEM water electrolysis cell and degradation study but are limited to either offline implementation or requires specialized equipment. Different electrical and non-electrical techniques to inspect the proper functioning of the PEM water electrolysis were exposed in [178]. Electrical techniques includes polarization measurements, EIS and current distribution mapping. Non electrical techniques includes visual inspection, thermal imaging, nuclear magnetic resonance and beam interrogation. A brief review of the studies related to diagnosis and degradation study of PEM water electrolyser has been presented below.

The diagnosis of the PEM water electrolyser rely mostly on the offline testing of the electrolysis cell/stack. Various safety issues related to high pressure PEM water electrolysis were discussed in [73]. The cell geometry plays a vital role in water flow distribution across the cell. A homogeneous flow of water is desired in order to avoid the accumulation of gases inside the cell and to prevent the occurrence of hot spots on the membrane that can result in membrane damage. Another important safety factor is gas crossover through the membrane which is prominent in case of high pressure electrolysis. a maximum allowable oxygen crossover towards cathode is 4% by volume in order to avoid the flaming of hydrogen. A new technique based on non-disturbing tool for the mapping of current and temperature of the PEM water electrolysis was presented in [179]. This technique was adapted from the fuel cell. Pressure sensitive film is used for the mechanical characterization of the cell. Electrical characterization is done using EIS and linear scan voltammetry. Cyclic voltammetry helps in the electrochemical characterization of the MEA to determine the active surface area of the anode. Measurements were done using this technique to analyse the effect of mechanical stress on the performance of the water electrolysis cell. Use of EIS as a diagnostic tool for the PEM water electrolysis was proposed in [180]. The AC-impedance spectra were observed during the nominal operation of the electrolysis cell, which can be used to identify the component that is more affected from degradation. In the presented study the anode side polarization resistance saw a significant increase during 1000 hours of continuous operation at 3Acm^{-2} as compared to cathode side. The decrease in the series resistance was also observed which is associated with membrane polymer restructuring or membrane thinning. In [181], a study of hydrogen permeation through the MEA of PEM water electrolysis under the influence of different current densities and operating pressures (differential) was performed. Online mass spectrometry was used to make the measurements. It was found that the hydrogen permeation is more prominent at higher current densities and lower partial pressures. A method for internal voltage sensing for the PEM electrolysis cell with the help of gold ribbon wires was proposed in [182]. The proposed method helps in separating the total cell resistance into anodic, cathodic and catalyst coated membrane resistance, which could be useful to study the degradation and to diagnose the fault in the system. Experimental study of the failure of the PEM water electrolysis cell was performed [183]. The failure was studied in two steps. The first one is the perforation of the membrane and the second one is the mechanical failure due to the combustion of the hydrogen and oxygen in the electrolyser compartments. Various existing hypothesis for explaining the causes of these failures in the literature were exposed. A non destructive approach using analysis of acoustic emission was proposed to detect the size and relative number of oxygen bubbles formed locally in a PEM water electrolysis cell [184]. The methodology was validated using a transparent PEM water electrolysis cell with single channel and high speed imaging.

Only one article was found for the model based fault detection and monitoring of the PEM water electrolyser. A semi-empirical dynamical model was used to develop a basic monitoring system in order to detect system actuator and sensor faults by calculating the two residuals [122]. Data driven approach was proposed for the diagnosis of the faults for PEM water electrolyser

in [64]. This approach, however, requires a lots of measurement data in both normal and faulty operating conditions.

2.4.2 Prognosis

The prognosis of the PEM water electrolyser constitutes mainly of the study of the degradation in the MEA and its mechanisms. Accelerated degradation test was performed by the authors by using galvanostatic pulses [185]. The system ran for approximately 5500 hours till the short circuit in the cell was detected. It was found through the post-mortem analysis of the failed cell that the primary cause for the failure was the corrosion of the catalyst layer along with the migration of the dissolved platinum towards the membrane. The thinning of the membrane was also observed. A proton exchange membrane electrolysis stack of 9 cell and effective area of 160cm^2 was tested for 7800hour continuous operation [186]. The average increase of 35.5μVh^{-1} was observed in the individual cell voltage. The electron probe X-ray microanalyze test of the MEA revealed the deposition of cations in the ion exchange sites of the catalyst layer. The degradation was reversed by cleaning the catalyst layer with the help of 0.5M sulphuric acid. The cation impurities that caused this reversible degradation originated from the feed water and the components used in the electrolyser. Study of the effect of flow inside the PEM electrolysis cell on its electrochemical performance was done using thermal imaging, EIS and flow visualization (by implementing a transparent cell). A simple thermodynamic analysis of heat balance in the PEM electrolysis cell was discussed. Degradation of PEM water electrolysis cell was studied for the operation of 1000 hours [55]. The degradation rate was found to be 194μVh^{-1}. The study showed a significant contribution of increase in ohmic resistance of anode side catalyst layer towards detected degradation. Two aging protocols for studying the membrane degradation for PEM water electrolysis were evaluated at two different temperatures [56]. It was observed that the membrane degradation is more prone to elevated temperatures as compared to the higher current densities. In [187] the degradation of different components (catalyst layer, membrane, bipolar plates and current collectors) of the PEM water electrolysis cell was reviewed and various mechanisms for these degradation were summarized. The strategies to avoid these degradations were also presented in the article. The importance of accelerated stress testing in comparison to the real-time degradation tests was also presented. Five PEM water electrolysis cells were operated with different current density profiles to observe the degradation of the cell [188]. Two cells were operated at constant current densities (one at higher and another at lower) and three with dynamic profile. It was observed that all the cells except the one running at lower current density showed degradation. The cell operating at the higher current density degraded faster at the rate of 194μVh^{-1}. It was also observed that running the system by periodically decreasing the current density helps in improving durability by reducing ohmic losses buildup. In [189], a study of degradation of MEA in PEM water electrolysis was performed using electrochemical and physio-chemical techniques. The key reasons for the degradation were observed to be the presence of Fe (from testing equipment) in the water, dissolution of Ru from the catalyst, degradation of Ti plate on the cathode side, restructuring of the membrane due to decrease in ionomer content and membrane thinning. Various mitigation strategies were also discussed for these degradations. The stability of PEM water electrolysis cell running at high current density was studied using two identical cells for constant and intermittent operation [190]. Till 2Acm^{-2} both the cells showed stable operation. The similar degradation was observed in both cells due to increase in ohmic and mass transport resistance due to the detachment of the non-corrosive coating from porous transport layer. A characterization method was proposed in [191] to distinguish between different overvoltages in order to determine the cause of degradation in the PEM electrolysis cell. It has been found that the major part of the increase in cell voltage due to degradation is recoverable by reduc-

ing the applied cell voltage. The non-recoverable degradation arises due to the application of higher current densities or the operation for long time which increases the ohmic and mass transport overvoltage. The study of the degradation in PEM water electrolysis cell was performed using seven identical cells operated at seven different operating modes that include one constant current mode, three constant voltage modes (at different temperatures), two cyclic modes 10 and 100 seconds current cycling and one solar profile operation. Improvement in the cell performance was observed with faster cycling time. The dynamic operation (solar profile) leads to the performance improvement due to the membrane thinning due to the increased fuloride emission. The membrane thinning can result in the increase of gas crossover which is dangerous. A review of the degradation mechanisms for the components of the PEM water electrolysis cell was provided and their mitigation options were discussed [192]. To study the degradation of the PEM water electrolyser under dynamic operation conditions (such as during operation with intermittent sources) a commercial MEA was operated using cell potential varying from 1.4V to 1.8V with long and short hold times [193]. MEA was subjected to different electrochemical (EIS) and physio-chemical measurements (X-ray Diffraction (XRD), Scanning Electron Microscopy (SEM), X-ray Photoelectron Spectroscopy (XPS), Transmission Electron Microscopy (TEM)and Energy Dispersive X-ray Spectroscopy (EDX)) to identify the causes of degradation. Irreversible resistive losses were observed to be more prominent to kinetic losses due to degradation.

In [64], a model to calculate the PEM electrolysis cell voltage was coupled with the degradation model to calculate the remaining useful life. The health of the system is estimated through the monitoring of performance factor. The model for estimating the degradation was proposed in [79]. For estimating the degradation of the membrane, the crossover of the oxygen from anode to cathode side was modelled. This crossover leads to the formation of hydrogen peroxide and radical through the Fenton reaction which leads to the degradation of the membrane. The time evolution of the membrane thickness was also modelled to simulate the membrane thinning based on the Fluor release rate. Similar work was also reported in [80].

2.4.3 Conclusion

Existing diagnosis and degradation testing methods warrants for the use of specialised instrumentation which is not always available or possible to implement without modifying the structure of the electrolysis cell. Some methods of degradation testing (such as SEM, glsTEM,XRD, EDX) requires the disassembly of the electrolysis cell which is not an ideal approach for degradation monitoring for remaining useful life estimation. In present work, a model based diagnosis, using BG approach, for PEM water electrolyser has been proposed for the real-time monitoring and fault detection. BG technique is well suited and can be implemented to perform structural analysis in order to check the diagnosibility of the system even if the value of the parameters is not known. Moreover, LFT (i.e. to perform which fault which may affect the system can be detected and isolated with any need of numerical value of parameters) BG can be implemented for obtaining a robust diagnosis (for avoiding false alarm) by generating thresholds that are adaptable with respect to parameter uncertainties [194, 195]. The current work focuses on the implementation of BG model-based diagnosis and prognosis approaches as per the availability of the system information. For the development of diagnosis algorithms, BG model in derivative causality is preferred over integral causality (used for simulations and study of the system behaviour [196]). Causality represents the relationship between cause and effect in BG. Derivative causality does not require the knowledge of system initial conditions (initial conditions are not clearly known for diagnosis and hence avoided). In DBG model, the sensors are considered as a source of effort and source of flow elements. The BG technique for diagnosis and prognosis is presented briefly in the appendix B.

Dynamic Modelling of PEM Electrolyser

Contents

The modelling of complex multi-physics systems like PEM water electrolyser is one of the most crucial tasks for studying the real behaviour of components, subsystems and overall system behaviour under dynamic operations. Moreover, system performance degrades at different levels (components and subsystems levels) due to ageing and dynamic operational behaviour. Such studies require a modular design approach, breaking the complete model into different sub-model levels, so that variation of different component parameters on the monitoring variables of the system can be analysed and tested easily and effectively. From the industrial perspective, the model should be adaptable with real monitoring of the system behaviour on suitable supervision platform. Current study considers such aspect of modelling for the PEM electrolyser BG as a unified modelling approach [18, 197]. A generic dynamical model of the PEM electrolysis system has been presented in this chapter. Model is termed as generic in the way that the modelling has been done in a modular fashion for the components of the PEM water electrolyser in the form of subsystems/capsules. These capsules can be used to represent various configurations of the electrolyser by assembling the capsules to obtain the desired model. Each capsule have a number of input and output ports (some of them may be optional) that are required to be connected with like power ports (i.e. the connecting ports must belong to the same domain). This allows the user to have a structurally sound global model. The BG modelling of each component of the PEM water electrolyser for generating capsules is presented in the succeeding sections.

Before analytical representation of the real system behaviour, some modelling hypothesis are taken into account in order to reduce the complexity of the system and to neglect the fast dynamics when compared to slow dynamics of the system:

- The cells constituting the stack are identical in nature and connected in series. Thus, the stack with N cells can be modelled as an equivalent single cell that has the same dynamics of the stack.

- Uniform fluid flows and current distribution are considered between cells.

- The effects of gravity are ignored.

- Overpotential due to mass transport or diffusion is negligible with the assumption that PEM system usually operates at low current density.

- Electrolysis reaction kinetics is assumed firmly as a Faradic process and considers that there is no mass limitation problem in the system.

- Gases produced are assumed to have similar properties as that of an ideal gas and the partial pressures of these gases are governed by Dalton's law.

- Temperature is homogeneous throughout the stack. This hypothesis holds good for electrolysis cells and stacks with properly designed flow channels where the temperature is regulated through inlet water temperature. Also, this allows to simplify the model by considering the thermal capacitance of the stack as a constant value for the temperature estimation.

- Cell is operated below the boiling temperature of the water.

- The system parameters are considered as lumped parameters. Pumps and fans are assumed as perfect mass flow sources.

The structural, functional and causal properties of the BG models makes it easier to deduce a dynamic model of the the system in the form of block diagram representation from BG models for use in simulation and development of supervision algorithms and GUI for online diagnosis and control. For this reason, once the BG capsules of the components of PEM electrolysis system are developed, they are converted into block diagrams for implementation in MATLAB® Simulink. The various steps involved in developing BG capsules of the components of PEM electrolysis system are presented in subsequent sections.

3.1 Technological Representation

The first step in the modeling using BG approach is to develop a word BG of the system. This is done by making a BG of the system with words consisting of various components or subsystems and characterizing the nature of energy exchanges between them. The schematic architecture of the PEM electrolyser and the physical variables exchanged between its subsystems are shown by the word BG presented in figure 3.1 (inspired from [15]).

In figure 3.1, line with half arrow represents the exchanged power, where yellow bonds show the electrical energy (current and voltage are power variables), red bonds show the thermal energy (heat flow and temperature variables), blue bonds show the fluidic energy (mass flow and pressure variables), green bonds with a circle in the middle show the thermal-fluidic energy coupling (heat flow-temperature and mass flow-pressure as thermal and hydraulic power variables) towards hydrogen side. Likewise, orange bonds with a circle in the middle show the thermal-fluidic energy coupling towards the oxygen side.

3.2 Modular Representation (Development of Capsules)

BG capsules are used, from one part, to describe the inner components of the electrolyser, and from another part, to explicit the coupling between the different energies highlighted by the word BG. Various phenomena occurring inside the cell/stack of PEM electrolyser are modelled separately and then assembled to have a global model of the cell/stack. This provides the flexibility to the model to be modified easily in case any particular phenomena is needed to be neglected or a detailed model is required. The BG models for the cell/stack and the components

52

of BoP of a PEM electrolysis are presented subsequently and are discussed discussed one by one.
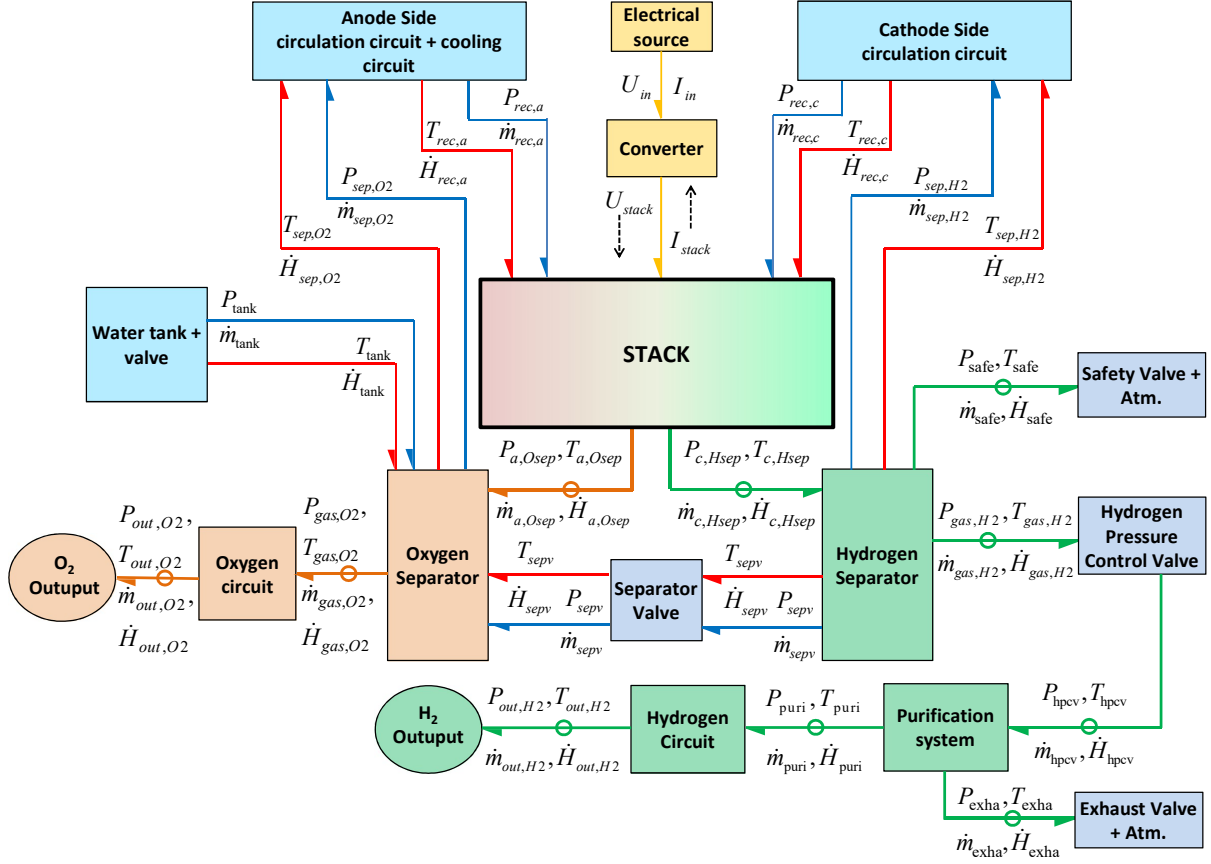

Figure 3.1: A word BG model of the electrolysis system.

3.2.1 Model of the Stack

The electrolysis cell/stack is often termed as a heart of the electrolyser. This is the most complex part in the electrolyser and greatly determines the dynamics of the system. Various coupled phenomena have been modelled as different sub-models (capsules) to provide more insight and are then assembled to have a complete model of the electrolysis cell/stack.

3.2.1.1 Electrochemical Sub-model of the Stack

The electrochemical sub-model is one of the crucial sub-models of the electrolysis system. It forms the basis to provide a relation between the cell current and cell voltage at different operating conditions, i.e. at different operating pressures and temperatures. The sum of all the electrochemical phenomena leads to a sub-model linking cell voltage and the current density, which is usually represented by a polarization curve. This sub-model explains the real kinetics of the reaction that occurs and gives the information about the amount of product flows according to the water consumed in the electrolysis system and also the production of heat in the stack system. This sub-model considers that electrochemical phenomenon occurs at steady state and thus the sub-model is responded with no time delay which means that there is instantaneous response with respect to change in any input to this sub-model. It is assumed that transient

response is very fast and dies out quickly, so it is neglected in model which is also well experimentally demonstrated by the work presented in [126, 142]. The electrochemical BG sub-model in the form of a capsule is shown in figure 3.2.
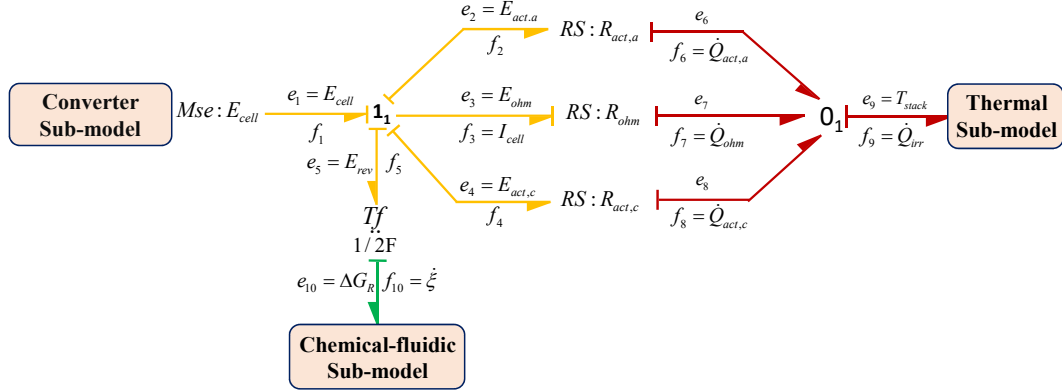

Figure 3.2: Electrochemical BG sub-model in capsule form.

This sub-model can also be used to find the required cell voltage, E_{cell}, at any operating condition with respect to reversible potential, E_{rev}, and different overpotentials which occur due to current flows in the cell results in irreversible heat dissipation. The reason of irreversible heat dissipation in the cell is due to the following: (i) the activation (Faradaic losses) voltages $E_{act,a}$ and $E_{act,c}$, respectively, occur at anode-electrolyte and cathode-electrolyte interfaces due to disturbance from the equilibrium chemical reaction and involved activation energies barriers in the preferred reaction. (ii) the electrical ohmic overpotential (non-Faradaic losses) due to internal cell resistance, i.e. it is proportional to the current which flows through electrodes, current collectors, bipolar plates and corresponding interconnections between them. Also, this overpotential occurs due to resistance offered by both electrolyte and membrane to the ions flow that separates both the electrodes. Generally, the electrode material in PEM electrolysers has high conductivity, so the flow of electrons is much faster as compared to ionic flow, and thus, usually the ohmic resistance due to ionic transport is considered. (iii) Overpotential due to mass transport or diffusion (non-Faradaic losses). It should be included in the model for a system having higher current density. Nernst equation is used to define the overpotential due to diffusion and it reveals that the diffusion limitation increases with increase in concentration of the product species at the reaction interface [28].

In this sub-model, E_{cell} is modelled as a modulated source of effort BG element, i.e. $Mse : E_{cell}$ and all the overpotentials are modelled by generalized RS (active multiport resistance able to generate and/or converts energy) coupled resistive elements as $RS : R_{act,a}$, $RS : R_{act,c}$ and $RS : R_{ohm}$ corresponding to anodic activation resistance, cathodic activation resistance and ohmic resistance, respectively. Here, the generalized RS coupled resistance element shows the coupled energy dynamics and links the electrical domain with the thermal domain. It acts as a source and transmits the generated heat or entropy to the thermal domain due to the current flow in electrical domain [17, 197]. Also, the transformation of electrical energy into chemical energy and vice a versa is modelled by transformer Tf generalized BG element, which describes the Faraday's law by linking the rate of reaction molar flow ($\dot{\xi}$) with the current flow through cell (I_{cell}), number of moles of electron transferred n (here $n = 2$) and Faraday's constant F; and, also by linking reversible cell voltage(E_{rev}) with free energy of water dissociation (ΔG_R), n and F, which are represented in equations 3.1 and 3.2. Based on causal bond graph model (figure 3.2) following equations (between flows and between efforts) can be deduced from the BG Tf element:

$$\dot{\xi} = \frac{I_{cell}}{n.F} \tag{3.1}$$

$$E_{rev} = \frac{\Delta G_R}{n.F} \tag{3.2}$$

Here E_{rev} is the reversible potential (minimum potential required for the electrolysis reaction). As per literature [6, 14], the reversible potential E_{rev} can be expressed by complex nonlinear equation as given in equation 3.3 at any operating temperature and pressure condition .

$$E_{rev} = E_{rev}^0 + \frac{R.T}{2.F} ln \left(\frac{p_{H_2}.p_{O_2}^{1/2}}{a_{H_2O}} \right) \tag{3.3}$$

where E_{rev}^0 is the standard reversible cell potential at standard operating conditions (at standard temperature and pressure), R is the ideal gas constant, p_i is the partial pressure of the ith species and a_{H_2O} is the chemical activity of water. The E_{rev}^0 is usually temperature dependent and is empirically defined as [6, 91, 118, 123].

$$E_{rev}^0 = 1.5184 - 1.5421 \times 10^{-3}T + 9.523 \times 10^{-5}T.ln\,(T) + 9.84 \times 10^{-8}T^2 \tag{3.4}$$

Activation overpotential: There is a relation between the kinetic part of the reaction, i.e. the current density, with the thermodynamic part, i.e. the overpotential. At equilibrium current exchange density (J_0) is defined and it is related with the exponential function of negative free Gibbs energy at equilibrium (ΔG_0). The value of the parameter J_0 or ΔG_0 should be obtained from the experiment. For the electrolysis process, i.e. possibility of occurring the dissociation of water, the cell voltage is usually more than the reversible standard voltage which results in overpotential because of current flow, and thus, it contributes to polarization. This current flow is usually the difference between anodic and cathodic currents at the non-equilibrium condition. The relation between the actual current and the overpotential is usually obtained by using Buttler-Volmer equation as given in equation 3.5 and used in many literature [59, 90, 91, 125, 198].

$$J_{cell} = J_{0,k} \left[\exp\left(\frac{\alpha_k.n.F}{R.T}.E_{act,\,k} \right) - \exp\left(-\frac{(1-\alpha_k).n.F}{R.T}.E_{act,\,k} \right) \right] \tag{3.5}$$

where $J_{cell} = I_{cell}/A_M$ is current density of cell, A_M is cross-sectional area of membrane. Also, $J_{0,k}$ and α_k represent the current exchange density and charge transfer or symmetry factor coefficient, respectively, at anode or cathode. Usually, symmetry factor is taken as 0.5; however it lies between 0 and 1. Thus, at $\alpha_k = 0.5$, the overpotential $E_{act,k}$ at anode or cathode (e_2 and e_4 in figure 3.2) can be expressed by equation 3.6 associated with BG multiport $RS : R_{act,a}$ and $RS : R_{act,c}$.

$$E_{act,k} = \frac{R.T}{F}\sinh^{-1}\left(\frac{J_{cell}}{2.J_{0,k}} \right) \tag{3.6}$$

In thermochemical model (figure 3.2), equation 3.6 is the constitutive relation for nonlinear resistive element $RS : R_{act,k}$ modulated by the variable parameter $J_{0,k}$ for each electrode and expressed as

$$J_{0,k} = J_{0,k}^{ref}.\exp\left(\frac{-\Delta G_{0,k}}{R.T} \right) \tag{3.7}$$

where, $J_{0,k}^{ref}$ and $\Delta G_{0,k}$ are estimated from the characteristic curves of the electrolyser through curve fitting and the temperature T is obtained from the thermal model of the stack.

Ohmic overpotential: This overpotential is modelled by the dissipative element, i.e. generalized BG resistive element $R : R_{ohm}$. According to the resistive causality in the BG sub-model (figure 3.2), the constitutive relation for $R : R_{ohm}$ is given as

$$I_{cell} = \frac{E_{ohm}}{R_{ohm}} \tag{3.8}$$

where E_{ohm} is the ohmic overpotential. The ohmic resistance R_{ohm} mainly includes the resistance offered by the membrane to ions flow and also includes the other ohmic resistance R_{other} offered by the internal cell components except the membrane. Thus, R_{ohm} is obtained from equation 3.9 that depends upon the properties (σ_M) and parameters of the membrane (L_M, A_M). σ_M represents the membrane conductivity, L_M and A_M, respectively, represent the length and cross-sectional area of the membrane. Moreover, the resistance R_{other} can be obtained from the experiments using model fitting technique.

$$R_{ohm} = \frac{d_M}{\sigma_M} + R_{other} \tag{3.9}$$

where d_M is the ratio of L_M to A_M and σ_M can be empirically defined as in equation 3.10. Membrane conductivity depends on cell temperature T and the membrane water content parameter γ.

$$\sigma_M = (0.005139.\gamma - 0.00326).exp\left[1268\left(\frac{1}{303} - \frac{1}{T}\right)\right] \tag{3.10}$$

The parameter γ value varies from 14 to 25, whose value depends on the nature of membrane hydration. For a poorly hydrated membrane, it is taken as 14 while for fully hydrated it is taken as 25 [28].

Based on BG causal properties and constitutive relations for different elements, different relations can be systematically obtained from the sub-model of electrochemical phenomenon. At junction 1_1 (refer figure 3.2), the conservative phenomenon can be written as in equation 3.11:

$$(e_1.f_1) - (.f_2) - (e_3.f_3) - (e_4.f_4) - (e_5.f_5) = 0 \tag{3.11}$$

Since, at junction 1_1 all the flows are equal, i.e., $f_1 = f_2 = f_3 = f_4 = f_5$. Thus, as per causality in sub-model (figure 3.2), $e_3 = E_{ohm}$ can be obtained from equation 3.11 as

$$E_{ohm} = e_1 - e_2 - e_4 - e_5 \tag{3.12}$$

where value of $e_1 = E_{cell}$, $e_2 = E_{act,a}$, $e_4 = E_{act,c}$, $e_5 = E_{rev}$. So, equation 3.12 becomes

$$E_{ohm} = E_{cell} - E_{act,a} - E_{act,c} - E_{rev} \tag{3.13}$$

where E_{cell} is derived from BG source element $Mse : E_{cell}$ as input causality. $E_{act,a}$, $E_{act,c}$ are derived from constitutive relations for BG elements $RS : R_{act,a}$, $RS : R_{act,c}$ as in equation 3.6 and E_{rev} is obtained from $Tf : 1/2F$ as in equation 3.2 or 3.3 . Thus, using BG sub-model, E_{ohm} can be systematically derived as

$$E_{ohm} = E_{cell} - \frac{R.T}{F}\sinh^{-1}\left(\frac{J_{cell}}{2.J_{0,a}}\right) - \frac{R.T}{F}\sinh^{-1}\left(\frac{J_{cell}}{2.J_{0,c}}\right) - E_{rev}^0 - \frac{R.T}{2.F}ln\left(\frac{p_{H_2}.p_{O_2}^{1/2}}{a_{H_2O}}\right) \tag{3.14}$$

Thus, using equation3.8, the cell current I_{cell} can be derived from the electrochemical BG submodel by using constitutive relation for $R : R_{ohm}$, which is used for controlling the hydrogen production by the cell. The required input cell voltage can also be derived by rearranging the equation3.14

$$E_{cell} = E_{ohm} + \frac{R.T}{F}\sinh^{-1}\left(\frac{J_{cell}}{2.J_{0,a}}\right) + \frac{R.T}{F}\sinh^{-1}\left(\frac{J_{cell}}{2.J_{0,c}}\right) + E_{rev}^0 + \frac{R.T}{2.F}ln\left(\frac{p_{H_2}.p_{O_2}^{1/2}}{a_{H_2O}}\right)$$

(3.15)

Likewise, using the property of junction 0_1 (refer figure 3.2), the conservative phenomenon can be written as:

$$(e_6.f_6) + (e_7.f_7) + (e_8.f_8) - (e_9.f_9) = 0$$

(3.16)

Since, at junction 0_1 all the efforts are equal, i.e., $e_6 = e_7 = e_8 = e_9$. Thus, as per causality in sub-model (figure 3.2), $f_9 = \dot{Q}_{irr}$ can be obtained from equation 3.16 as

$$\dot{Q}_{irr} = f_6 + f_7 + f_8$$

(3.17)

where value of $f_6 = \dot{Q}_{act,a}$, $f_7 = \dot{Q}_{ohm}$, $f_8 = \dot{Q}_{act,c}$. So, equation 3.17 becomes

$$\dot{Q}_{irr} = \dot{Q}_{act,a} + \dot{Q}_{ohm} + \dot{Q}_{act,c}$$

(3.18)

where $\dot{Q}_{irr}$ denotes the irreversible heat flow which is systematically derived from BG sub-model and obtained as the summation of activation losses at anode, cathode and ohmic loss.

3.2.1.2 Chemical-fluidic Sub-model of the Stack

In chemical-fluidic sub-model, the amount of hydrogen and oxygen production rates can be predicted with respect to consumed water. The BG chemical-fluidic sub-model in the form of a capsule is shown in figure 3.3. In the sub-model, transformers $Tf : \nu_i$ and $Tf : M_i$ generalized BG elements are used to find the rate of production of the products with respect to consumed reactant. Also, $C : C_i$ represent the storage of the matter for the ith species. The rate of produced mass for the ith species, i.e. $\dot{m}_i$, is obtained from the rate of reaction flow $\dot{\xi}$ from equation 3.19 as

$$\dot{m}_i = \nu_i.M_i.\dot{\xi} = \nu_i.M_i.\frac{I_{cell}}{n.F}$$

(3.19)

where ν_i and M_i, respectively, denote the coefficient of stoichiometry and molar mass of ith species.

3.2.1.3 Thermal Sub-model of the Stack

Thermal sub-model predicts the dynamic behaviour of the temperature evolution inside the stack which ultimately affects the relation between cell current and voltage. Thus, durability and efficiency of the electrolysis system is also affected. The complete thermal BG sub-model in the form of a capsule is represented in figure 3.4. The sub-model considers the major contribution of the heat from the different sources and phenomena such as heat input to stack by the water inflow towards anode and cathode side, heat taken away by the water outflow from stack towards hydrogen and oxygen separators, thermodynamics of chemical components during reaction (dissociation of water and production of gases) or endothermic nature of chemical reaction, Joule effect phenomenon due to circulation of charge/current, heat due to entropy change
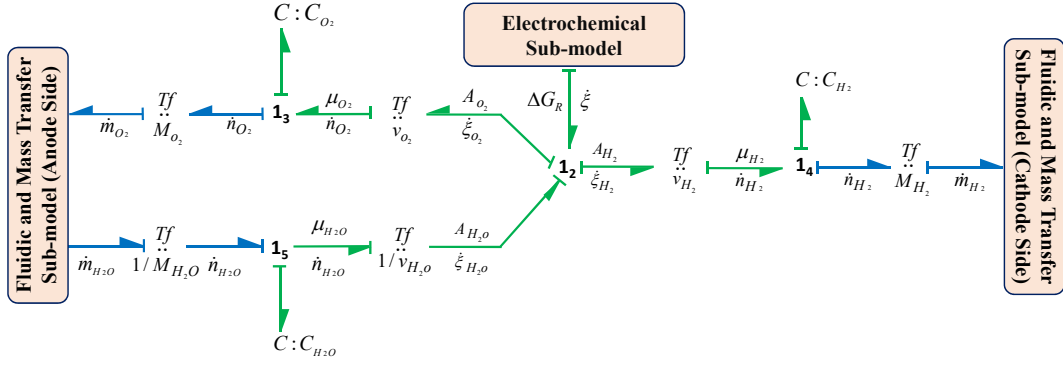
Figure 3.3: The BG chemical-fluidic sub-model in capsule form.

in reaction, thermal activated phenomenon due to mass transfer and diffusion and thermal effects due to system enclosure temperature. In the given figure, based on assigned causality, dashed arrows direction shows the input and output signal in the corresponding simulation block diagram deduced from BG model.
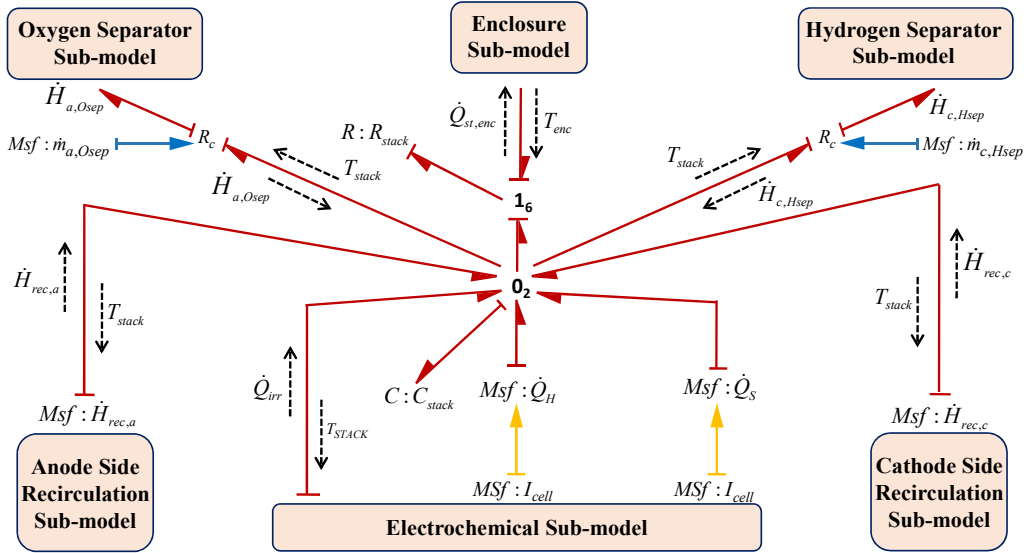

Figure 3.4: The BG thermal sub-model in capsule form.

This thermal sub-model is considered as a first order nonlinear model having one dynamic generalized BG capacitance C element. Here generalized $C : C_{stack}$ element, considered as a constant lumped parameter, models the thermal capacitance of the stack, and thus, it is assumed that temperature is homogenous throughout the stack. This lumped parameter can be estimated from the experiment using model fitting technique. From the BG thermal sub-model, the temperature of stack using constitutive relation of $C : C_{stack}$ and junction 0_2 is obtained as

$$T_{stack} = \frac{1}{C_{stack}} \int \left(\dot{H}_{rec,a} + \dot{H}_{rec,c} + \dot{Q}_{irr} + \dot{Q}_H + \dot{Q}_S - \dot{H}_{a,Osep} - \dot{H}_{c,Hsep} - \dot{Q}_{st,enc} \right) \mathrm{d}t \quad (3.20)$$

In equation 3.20, $\dot{H}_{rec,a}$, $\dot{H}_{rec,c}$ and $\dot{H}_{a,Osep}$, $\dot{H}_{c,Hsep}$ respectively, represent the enthalpy rate due to water inflow from recirculation circuit towards anode side, cathode side and water outflow from the stack towards oxygen and hydrogen separator side. These enthalpy flows are related with the molar enthalpy (H_i) and molar flow rate $(\dot{n}_i)$ of the involved species in the reaction. $\dot{Q}_{irr}$

is irreversible heat flow due to activations and ohmic losses, $\dot{Q}_H$ $\left(\text{i.e., } \dot{Q}_H = I_{cell}.\Delta H_R/2.F\right)$ denotes heat flow rate due to chemical components during reaction or endothermic nature of reaction (dissociation of water and production of gases), $\dot{Q}_S$ $\left(\text{i.e., } \dot{Q}_S = -I_{cell}.\Delta S_R/2.F\right)$ denotes the heat flow rate due to entropy change and $\dot{Q}_{st,enc}$ denotes heat transfer from stack to system enclosure due to temperature difference.

3.2.1.4 Fluidic and Mass Transfer Sub-model of the Stack

The global behaviour and the efficiency of cell can be affected due to the phenomena of fluidic motion and mass transfer and these cannot be ignored while developing the model of the electrolysis system. Thus, the phenomenon of fluidic motion and mass transfer must be integrated within thermal and electrochemical sub-models. It is assumed that there is no accumulation of fluid inside the stack and the product produced is continuously evacuated from the stack. This sub-model includes the transfer of water from anode to cathode by considering the electro-osmosis phenomenon and also considers the transfer in reverse direction, i.e. from cathode to anode, by the process of diffusion. This sub-model also includes the crossover of produced gases, i.e. oxygen and hydrogen gas flows towards the opposite electrode with respect to the electrode where they produce. The BG sub-model of fluidic and mass transfer phenomenon in the form of a capsule is shown in figure 3.5.
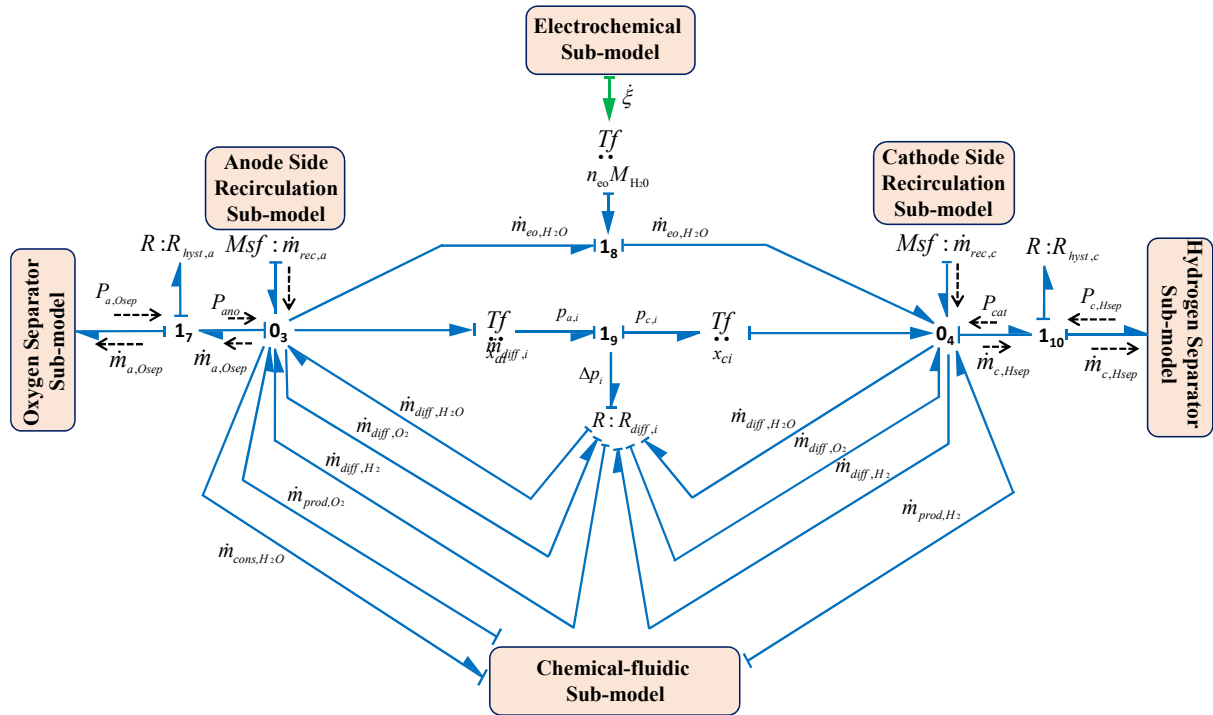

Figure 3.5: BG sub-model of fluidic and mass transfer phenomenon in capsule form.

In this sub-model, resistive generalized BG field element $R : R_{diff,i}$, i.e. $R : R_{diff,H_2O}$, $R : R_{diff,O_2}$, $R : R_{diff,H_2}$, and generalized transformer element $Tf : n_{eo}.M_{H_2O}$ are used, respectively, to model the crossover or diffusion flows due to water diffusion, oxygen diffusion, hydrogen diffusion and electro-osmosis diffusion. $R_{Hyst,a}$ and $R_{Hyst,c}$ are the hydraulic resistances at anode and cathode side, respectively. Thus, the model provides the rate of mass outflow of the mixture from the stack at the anode and cathode sides using constitutive relation

of junction 0_3 and 0_4 as given by equations 3.21 and 3.22, respectively.

$$\dot{m}_{a,Osep} = \dot{m}_{rec,a} + \dot{m}_{prod,O_2} - \dot{m}_{cons,H_2O} - \dot{m}_{eo,H_2O} + \dot{m}_{diff,H_2} + \dot{m}_{diff,H_2O} - \dot{m}_{diff,O_2} \quad (3.21)$$

$$\dot{m}_{c,Hsep} = \dot{m}_{rec,c} + \dot{m}_{prod,H_2} + \dot{m}_{eo,H_2O} + \dot{m}_{diff,O_2} - \dot{m}_{diff,H_2O} - \dot{m}_{diff,H_2} \quad (3.22)$$

where, $\dot{m}_{rec,a}$, $\dot{m}_{rec,c}$, respectively, denote rate of inflow masses from recirculation circuit to anode and cathode side. $\dot{m}_{prod,O_2}$, $\dot{m}_{prod,H_2}$ and $\dot{m}_{cons,H_2O}$, respectively, denote production of oxygen, hydrogen and water consumed which are obtained from electrochemical model. Also, $\dot{m}_{eo,H_2O}$ denotes the rate of water mass flow due to electro-osmosis, however, this phenomenon does not depend on thickness of the membrane. The electro-osmosis flow, $\dot{m}_{eo,H_2O}$, mainly depends on the magnitude of electric current flow during electrolysis process and the number of dragged water molecules by a proton ion as given in equation 3.23. This number is denoted by n_{eo} and called as electro-osmosis coefficient [91, 127]. This flow, $\dot{m}_{eo,H_2O}$, is obtained by using the generalized transformer element Tf: $n_{eo}.M_{H_2O}$ in the fluidic model which is coupled with the rate of reaction $\dot{\xi}$ of the thermochemical model.

$$\dot{m}_{eo,H_2O} = n_{eo}.M_{H_2O}.\dot{\xi} = n_{eo}.M_{H_2O}.\frac{I_{cell}}{n.F} \quad (3.23)$$

Also, $\dot{m}_{diff,i}$ denotes the flow of diffusion for the ith species through membrane and this flow for i^{th} species is obtained from the constitutive relation of the generalized resistive element $R : R_{diff,i}$. This sub-model shows that the diffusion flow for the ith species is proportional to the change in partial pressure at the both side of the membrane Δp_i and also the resistance $R_{diff,i}$ depends on the length of membrane L_M, diffusion parameter D_i and the Henry's parameter H_i [73, 79] as represented in equations 3.24 and 3.25, respectively.

$$\dot{m}_{diff,i} = \frac{|\Delta p_i| \,.\text{sign}\,(p_i - p_j)}{R_{diff,i}} \quad (3.24)$$

$$R_{diff,i} = \frac{H_i.L_M}{D_i.M_i.A_M} \quad (3.25)$$

Thus, the global model of the stack, as represented in figure 3.6, is obtained by integrating all the sub-models (capsules) such as electrochemical, chemical-fluidic, thermal, fluidic and mass transfer sub-models.

3.2.2 Models of the Components of BoP

BoP plays an important role in operating the electrolyser at desired operating points. The components of the BoP also contributes to the overall dynamics of the system and greatly effects the overall performance. The components of BoP varies depending on the configuration of the electrolyser. The common components as prescribed in word BG (see figure 3.1) such as: electrical converter, hydrogen and oxygen separator vessels, heat exchanger, cooling and recirculation systems, purification system, the pneumatically controlled hydraulic valves and the stack enclosure have been modelled in the form of the capsules and are presented below.

3.2.2.1 Converter Sub-model

Converter provides the control power input to the stack according to the operational point of the electrolyser. Usually, converter has a very fast response time (less than 0.1s); thus, the dynamic model of the converter has instantaneous power output. This sub-model is shown in figure 3.7.
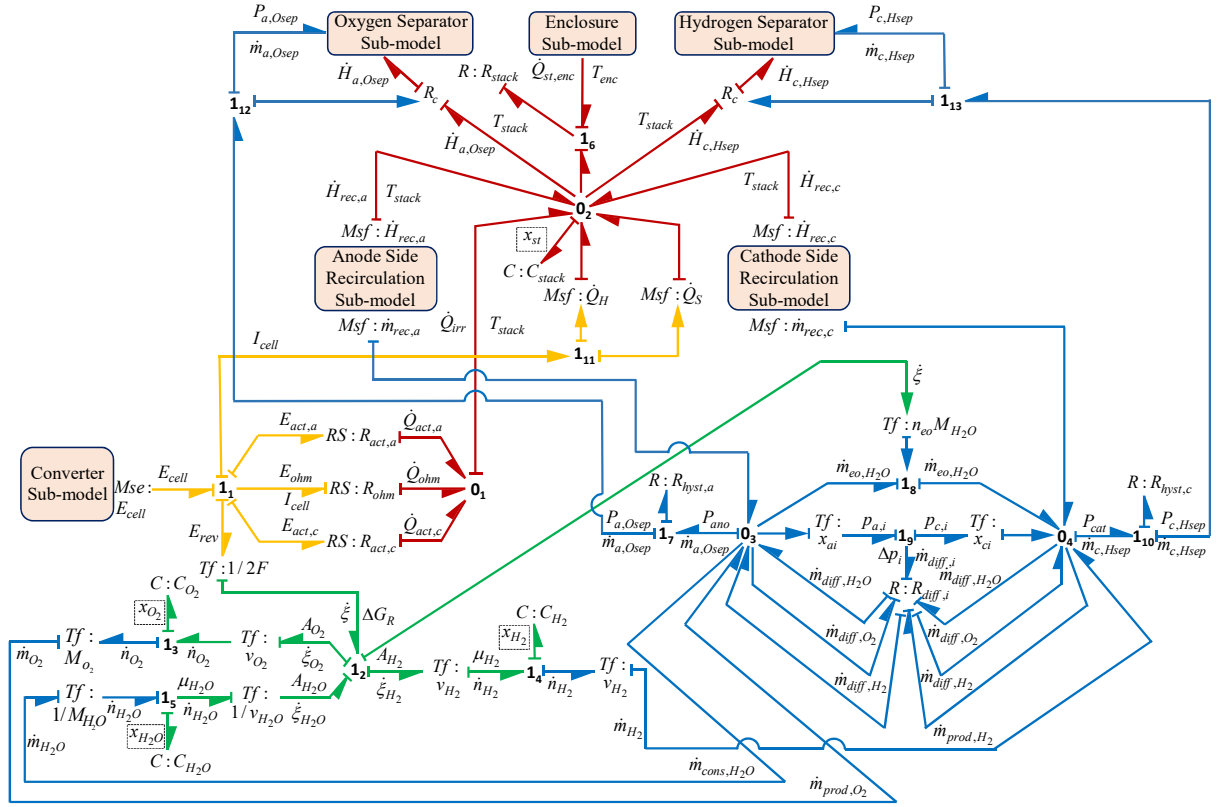
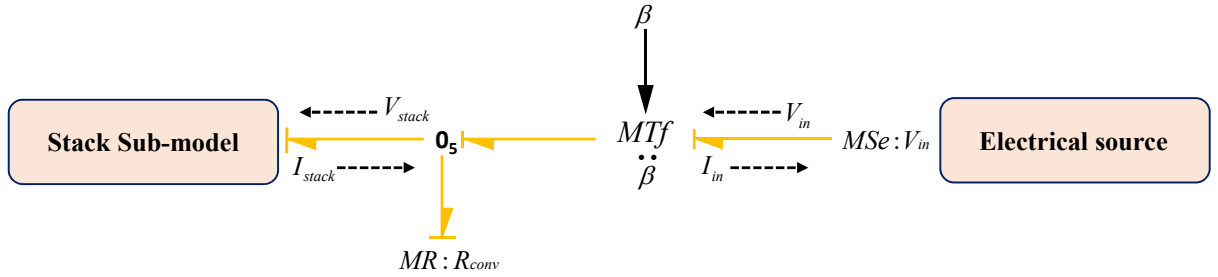Figure 3.6: The global model of the stack of the PEM electrolysis system.

Figure 3.7: BG sub-model of converter subsystem.

Here, physical phenomena of the converter is modelled by using a modulated transformer ($MTf : \beta$) and resistive ($R : R_{conv}$) generalized BG elements. In the model, $Mse : V_{in}$ is the input voltage to the converter from the electrical source (solar and/or wind source) and V_{stack} is the output of the converter which is fed in to the electrolyser for water dissociation. Thus, using dynamic BG sub-model (figure 3.7), constitutive relations can be derived as

$$V_{stack} = \beta . V_{in} \tag{3.26}$$

$$P_{in} = P_{stack} + P_{conv} \tag{3.27}$$

$$P_{conv} = P_{in} \left(1 - \varepsilon_{conv}\right) \tag{3.28}$$

where β is the coefficient of transformer, $P_{in} = V_{in}.I_{in}$ denotes input power, $P_{stack} = V_{stack}.I_{stack}$

denotes output power from the converter which is input to the stack, P_{conv} denotes the dissipation power of the converter due to its internal resistance and ε_{conv} denotes converter efficiency.

3.2.2.2 Separator Sub-models

Usually gas is collected over water in a vessel and due to the light weight of the gas it goes up and can be separated from the water. When the gas pressure reaches a certain fixed preset value in the separator it comes out from the separator vessel to the storage tank. In the electrolysis system, two separators are used for gas liquid separation: (i) hydrogen separation and (ii) oxygen separation. The separator subsystem includes the interaction of fluidic, thermal and chemical phenomena. In the modelling of each separator, it is assumed that the vessel is in cylindrical shape having a cross-sectional area $A_{sep,i}$. The BG sub-models of the hydrogen and oxygen separators are shown in Figs. 3.8(a) and 3.8(b), respectively.

Separator fluidic Phenomena: The hydraulic pressures or the water levels in the Hydrogen Separator Vessel (HSV) and Oxygen Separator Vessel (OSV) are determined from the continuity equations and these phenomenons are modelled in the sub-models as in Figs. 3.8(a) and 3.8(b), respectively.

The hydraulic capacity as a lumped parameter for i^{th} separator ($i = H_2, O_2$) is denoted by $C_{sep,i}^{fl} = A_{sep,i}/g$, where g is gravity. First the entire phenomena are discussed for HSV, and then likewise these are presented for OSV. Thus, for HSV from figure 3.8(a), using constitutive relation of $C : C_{sep,H_2}^{fl}$ and junction 0_6, HSV pressure can be obtained as

$$P_{sep,H_2} = \frac{1}{C_{sep,H_2}^{fl}} \int \left(\dot{m}_{cw,Hsep} - \dot{m}_{sepv} - \dot{m}_{sep,H_2} \right) .dt \tag{3.29}$$

where, $P_{sep,H_2} = \rho_w . g . L_{sep,H_2}$ is water pressure in HSV, L_{sep,H_2} is water level in HSV, ρ_w is water density, $\dot{m}_{cw,Hsep}$ is the water mass flow which is the product of known mass fraction of water $x_{c,w}$ and the mass flow of mixture, $\dot{m}_{c,Hsep}$ (obtained in equation 3.22), $\dot{m}_{sepv}$ is the water mass flow from the HSV to OSV through the separator valve (modelled using modulated resistive element $MR : R_{sepv}$). The sub-model of the separator valve [199] is highlighted in the figure 3.8(a). $\dot{m}_{sep,H_2}$ is the water mass flow out from the HSV to cathode side recirculation circuit.

Separator thermal Phenomena: The thermal capacity of the vessel is modelled by using lumped parameter, $C : C_{sep,i}^{th}$, whose value depends on cross-sectional area $A_{sep,i}$ and water level $L_{sep,i}$ in the vessel. Also, it is assumed that the coefficient of heat transfer of the vessel is constant. Thus, for HSV from figure 3.8(a), using constitutive relation of $C : C_{sep,H_2}^{th}$ and junction 0_7, HSV temperature can be obtained as

$$T_{sep,H_2} = \frac{1}{C_{sep,H_2}^{th}} \int \left(\dot{H}_{c,Hsep} - \dot{H}_{sepv} - \dot{H}_{sep,H_2} - \dot{H}_{hpcv} - \dot{H}_{safe} - \dot{Q}_{Henc} \right) .dt \tag{3.30}$$

where, T_{sep,H_2} temperature inside HSV, $\dot{H}_{c,Osep}$ is the enthalpy flow of the water and gas mixture from the cathode side of the stack to HSV and $\dot{H}_{sep,H_2}$ is the enthalpy flow out from the HSV to cathode side recirculation circuit and $\dot{Q}_{Henc}$ is the rate of heat loss due to temperature gradient between HSV and system enclosure. Note that all the enthalpy flow is correlated with their respective mass flow of water and mixture. The value of the enthalpy flows $\dot{H}_{gas,i}$ and $\dot{H}_j$ coupled with mass flows $\dot{m}_{gas,i}$ and $\dot{m}_j$ ($i = O_2, H_2; j = tank$) can be obtained from the expression as presented in equations 3.31 and 3.32, respectively. This coupling between thermal and fluidic phenomena is represented by generalized R_c element.
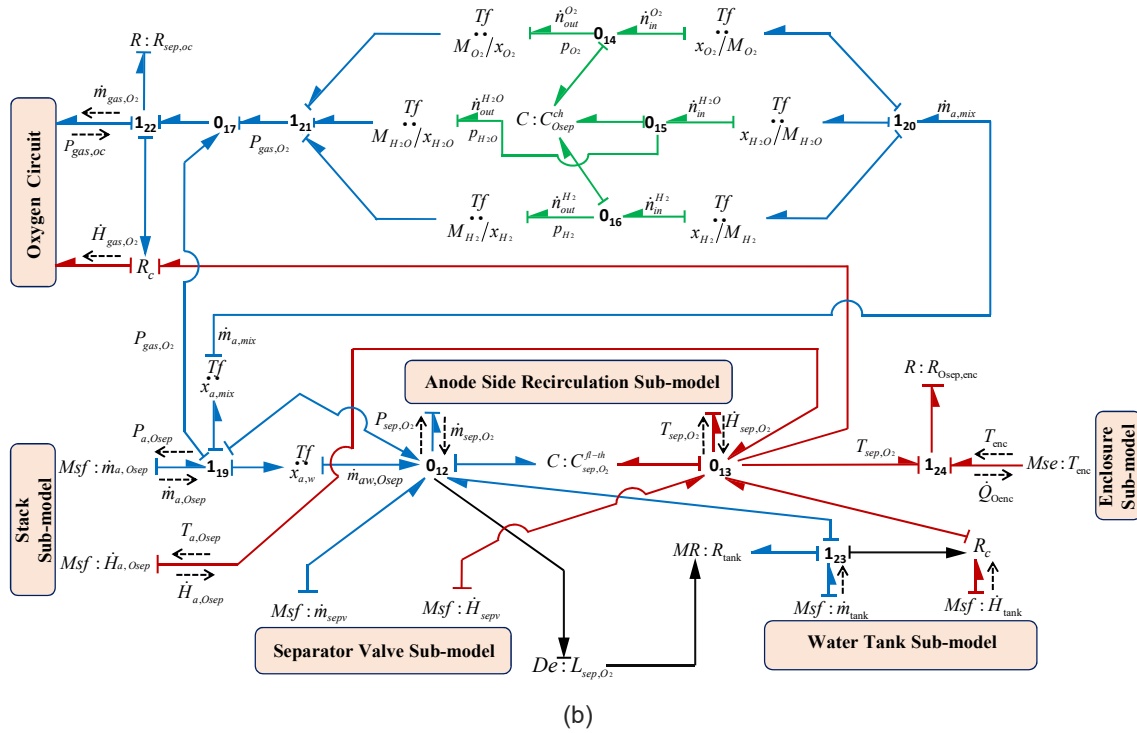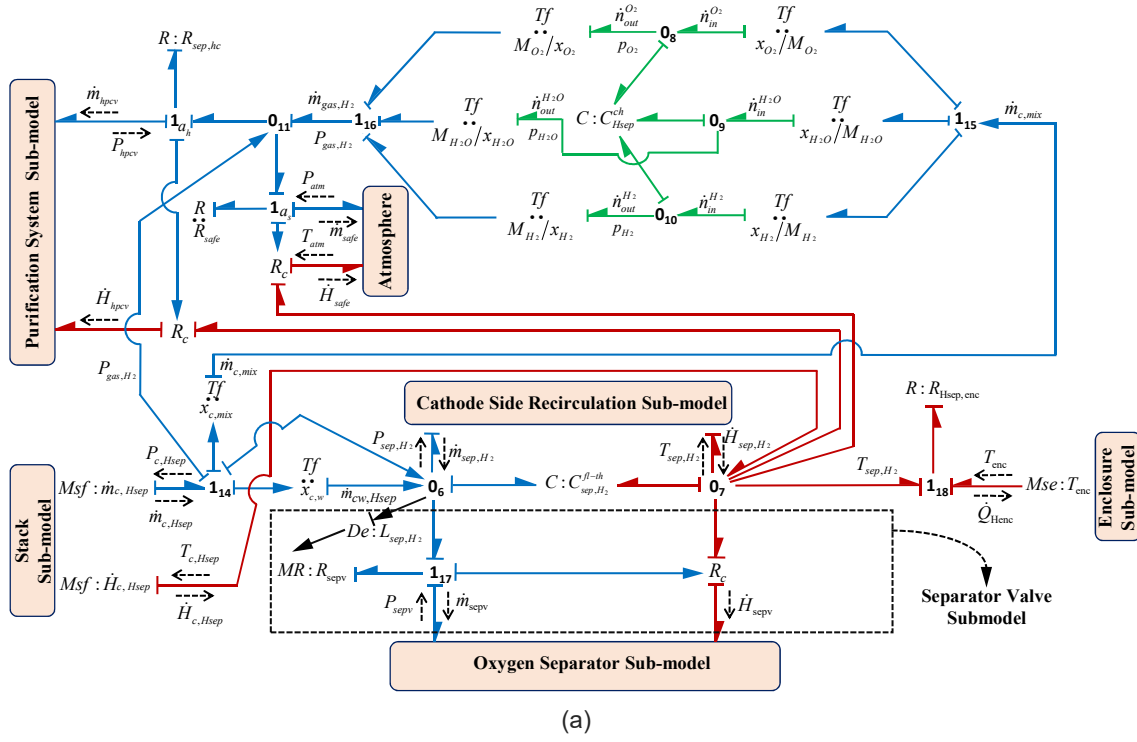
Figure 3.8: BG sub-models (a) hydrogen separator and (b) oxygen separator

$$\dot{H}_{gas,i} = \dot{m}_{gas,i} \cdot \left(\sum_i C_{pi} \right) \cdot T_{gas,i} \tag{3.31}$$

$$\dot{H}_j = \dot{m}_j \cdot C_{pj} \cdot T_j \tag{3.32}$$

where C_{pj} and $\sum\limits_i C_{pi}$, respectively, denote specific heat constant of water and gas. The thermal loss, $\dot{Q}_{Henc}$, is modelled by generalized BG resistive element $R : R_{Hsep,enc}$. Also, the system enclosure temperature is modelled as BG modulated source of effort element as $Mse : T_{enc}$, which is obtained from the thermal sub-model of the enclosure. Moreover, generalized detector element $De : L_{sep,H_2}$ is used which shows the measurement of separator water level that is further utilized by the controller for controlling the percentage opening of separator valve as per level set value.

Separator chemical Phenomena: For calculation of partial pressure, $P^{ch}_{Hsep,i}$, of the ith species, the chemical capacitance is modelled by using lumped parameter, $C : C^{ch}_{Hsep,i}$ at cathode side separator, whose value depends on molar mass M_i, volume $V_{Hsep,i}$ of the ith species, temperature $T_{Hsep,i}$ and the gas constant R which is obtained from equation 3.33.

$$C^{ch}_{Hsep,i} = \frac{M_i \cdot V_{Hsep,i}}{R \cdot T_{Hsep,i}} \tag{3.33}$$

Thus, for HSV from figure 3.8(a), using constitutive relation of $C : C^{ch}_{Hsep,i}$ and junction $0_8/0_9/0_{10}$, gases partial pressures can be obtained as

$$P^{ch}_{Hsep,i} = \frac{1}{C^{ch}_{Hsep,i}} \int \dot{n}_{ci} \cdot dt = \frac{1}{C^{ch}_{Hsep,i}} \int \left(\dot{m}_{c,Hsep} \cdot x_{c,mix} \cdot \frac{x_{c,i}}{M_i} - \dot{m}_{gas,H_2} \cdot \frac{x_{c,i}}{M_i} \right) \cdot dt \tag{3.34}$$

where $\dot{n}_{ci}$ denotes gas mass flow rate at cathode side, $x_{c,i}$ and $x_{c,mix}$, respectively, denote mass fraction of ith species and gas mixture (hydrogen, oxygen and water vapor) leaving from cathode side of stack to HSV, $\dot{m}_{gas,H_2}$ is the output gas flow towards purification system. The total pressure $P_{sep,H2}$ of the oxygen separator can be obtained from the summation of all the partial pressures of the gases according to Dalton's law. The valve and the pipe resistances are modelled using R elements.

Likewise, the fluidic, thermal and chemical phenomena for the OSV can be represented by equations 3.35-3.37, respectively. For OSV from figure 3.8(b), using constitutive relation of $C : C^{fl}_{sep,O_2}$ and junction 0_{12}, OSV pressure can be obtained as can be written as

$$P_{sep,O2} = \frac{1}{C^{fl}_{sep,O_2}} \int \left(\dot{m}_{tank} + \dot{m}_{sepv} + \dot{m}_{aw,Osep} - \dot{m}_{sep,O_2} \right) \cdot dt \tag{3.35}$$

where, $P_{sep,O_2} = \rho_w \cdot g \cdot L_{sep,O_2}$ is water pressure in OSV, L_{sep,O_2} is water level in OSV, $\dot{m}_{tank}$ is the water mass flow from water tank to OSV. $\dot{m}_{aw,Osep}$ is the water mass flow from the anode side of the stack to OSV and $\dot{m}_{sep,O_2}$ is the water mass flow out from the OSV to anode side recirculation circuit. The water mass flow $\dot{m}_{aw,Osep}$ can be obtained using the product of known mass fraction of water $x_{a,w}$ and the mass flow of mixture, $\dot{m}_{a,Osep}$, obtained in equation 3.21.

For OSV from figure 3.8(b), using constitutive relation of $C : C^{th}_{sep,O_2}$ and junction 0_{13}, OSV temperature can be obtained as

$$T_{sep,O_2} = \frac{1}{C^{th}_{sep,O_2}} \int \left(\dot{H}_{tank} + \dot{H}_{sepv} + \dot{H}_{a,Osep} - \dot{H}_{sep,O_2} - \dot{H}_{gas,O_2} - \dot{Q}_{Oenc} \right) \cdot dt \tag{3.36}$$

where, T_{sep,O_2} temperature inside OSV, $\dot{H}_{tank}$ is the enthalpy flow from water tank to OSV, $\dot{H}_{sepv}$ is the enthalpy flow from the HSV to OSV through the separator valve, $\dot{H}_{a,Osep}$ is the enthalpy flow of the water and gas mixture from the anode side of the stack to OSV and $\dot{H}_{sep,O_2}$ is the enthalpy flow out from the OSV to anode side recirculation circuit, $\dot{H}_{gas,O_2}$ is the heat flow output from OSV towards oxygen circuit and $\dot{Q}_{Oenc}$ is the rate of heat loss due to temperature gradient between OSV and system enclosure.

For OSV from figure 3.8(b), using constitutive relation of $C : C^{ch}_{Hsep,i}$ and junction $0_{14}/0_{15}/0_{16}$, gases partial pressures can be obtained as

$$P^{ch}_{Osep,i} = \frac{1}{C^{ch}_{Osep,i}} \int \dot{n}_{ai}.dt = \frac{1}{C^{ch}_{Osep,i}} \int \left(\dot{m}_{a,Osep}.x_{a,mix}.\frac{x_{a,i}}{M_i} - \dot{m}_{gas,O_2}.\frac{x_{a,i}}{M_i} \right).dt \qquad (3.37)$$

3.2.2.3 Cooling and Recirculation Circuits

The desired temperature of the stack is automatically maintained by the cooling and the recirculation system by getting the information of hydrogen and oxygen production along with the information of heat flow in this system. The recirculation system has its own process and instrumentation diagram which is used to feed the water at desired rate to the stack. In the current model the recirculation of water is done in each side of the cell, i.e. anode and cathode side using a recirculating controlled pump. However at anode side, a heat exchanger along with its own cooling system is also incorporated which mainly maintains the stack temperature by controlling the input water temperature for the stack. The BG sub-model of this system for anode and cathode sides in capsule forms are shown in Figs. 3.9(a) and 3.9(b), respectively.

The modelling of the cooling unit of the heat exchanger is also shown in figure 3.9(a). In the sub-model presented in figure 3.9(a), different pumps are model as the modulated source of flows $Msf : \dot{m}_{rec,a}$ and $Msf : \dot{m}_{cool}$, respectively, represent the anode side recirculating pump and the pump used for cooling of heat exchanger itself. The thermal capacity is modelled by the lump parameter $C : C^{th}_{rec,a}$. Thus, from the figure 3.9(a), using constitutive relation of $C : C^{th}_{rec,a}$ and junction 0_{19}, anode side recirculation temperature can be obtained as

$$T_{rec,a} = \frac{1}{C^{th}_{rec,a}} \int \left(\dot{H}_{sep,O_2} - \dot{H}_{rec,a} - \dot{Q}_{Orec,enc} - \dot{Q}_{cool} \right).dt \qquad (3.38)$$

where the enthalpy flows in the anode side recirculation system $\dot{H}_{sep,O_2}$ and $\dot{H}_{rec,a}$ are calculated from the equation 3.32. The heat dissipation, $\dot{Q}_{Orec,enc}$, due to temperature gradient between recirculation system and enclosure is modelled by BG generalized resistive element $R : R_{Orec,enc}$ and $\dot{Q}_{cool}$ is the extracted rate of heat flow by the heat exchanger which is modelled by using resistive element $R : R_{htex}$. In order to calculate the $\dot{Q}_{cool}$, the Number of Transfer Unit (NTU) technique is used for heat exchanger [200].

Likewise, for the sub-model of cooling unit of the heat exchanger in figure 3.9(a), using constitutive relations of $C : C^{th}_{cool}$, $C : C^{th}_{cold}$ and junctions 0_{20}, 0_{21} temperatures T_{cool}, T_{cold} can be obtained as

$$T_{cool} = \frac{1}{C^{th}_{cool}} \int \left(\dot{H}_{cold} - \dot{H}_{cool} + \dot{Q}_{cool} \right).dt \qquad (3.39)$$

$$T_{cold} = \frac{1}{C^{th}_{cold}} \int \left(\dot{H}_{cool} - \dot{H}_{cold} - \dot{Q}_{cold} \right).dt \qquad (3.40)$$

where T_{cool}, T_{cold} and C^{th}_{cool}, C^{th}_{cold} are the temperatures and thermal heat capacities of cooling system of heat exchanger and cooling tank for the coolant, respectively. In sub-model of cool-
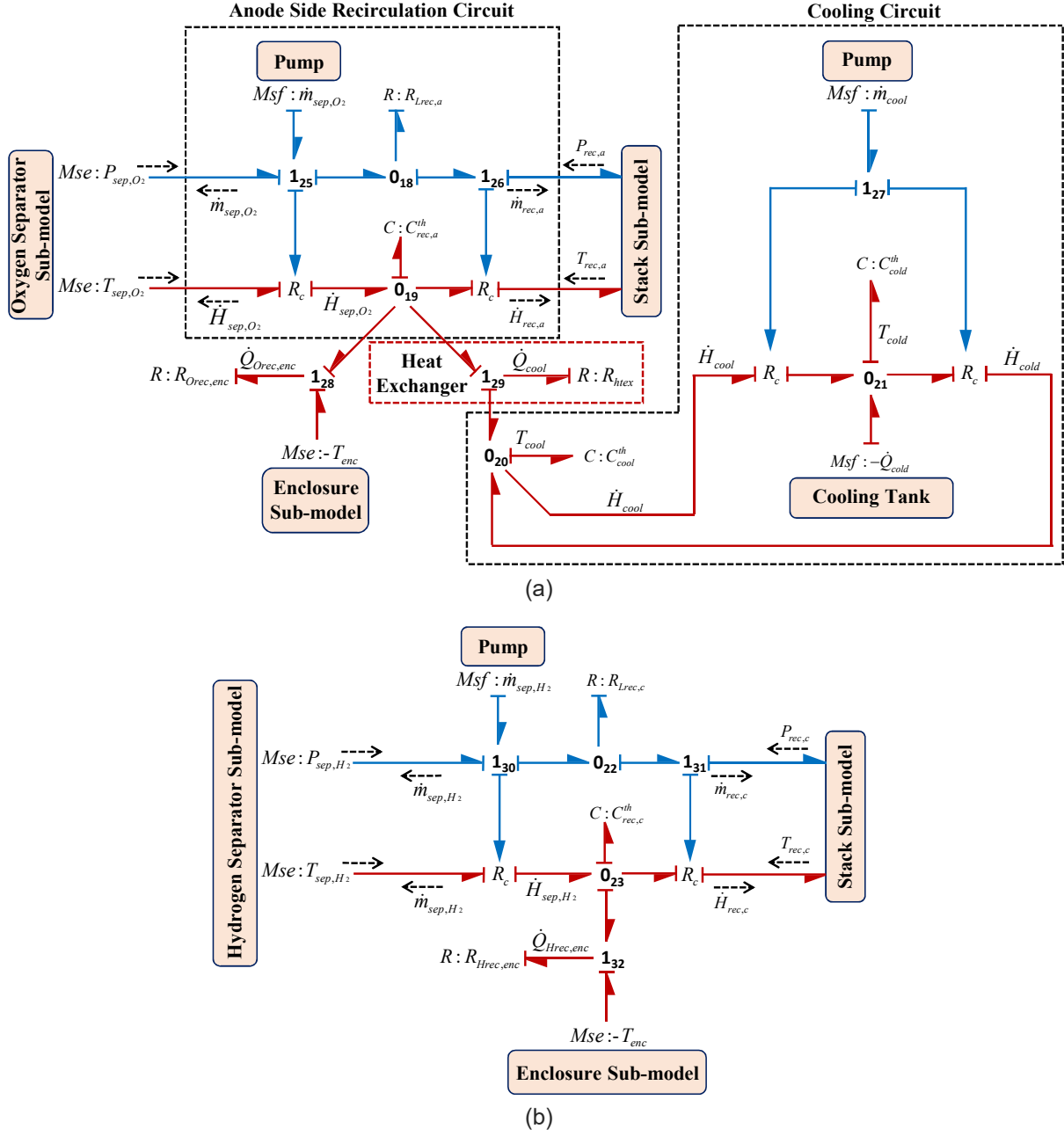
Figure 3.9: BG recirculation sub-models (a) anode side including cooling circuit and (b) cathode side.

ing unit in figure 3.9(a), $Msf : \dot{m}_{cool}$ represents the coolant mass flow which is used for the calculation of $\dot{H}_{cool}$ and $\dot{H}_{cold}$ using equation 3.32 with temperatures T_{cool} and T_{cold}, respectively.

Likewise, using the sub-model of recirculation system in cathode side as shown in figure 3.9(b), using constitutive relation of $C : C_{rec,c}^{th}$ and junction 0_{23}, cathode side recirculation temperature can be obtained as

$$T_{rec,c} = \frac{1}{C_{rec,c}^{th}} \int \left(\dot{H}_{sep,H_2} - \dot{H}_{rec,c} - \dot{Q}_{Hrec,enc} \right).\mathrm{dt} \tag{3.41}$$

where the enthalpy flows in the cathode side recirculation system $\dot{H}_{sep,H2}$ and $\dot{H}_{rec,c}$ are calculated from the equation 3.32. The lump parameter $C : C_{rec,c}^{th}$ is used to model its thermal capacity towards the cathode side.

3.2.2.4 Hydrogen Purification Subsystem

This unit purifies the gas according to the preset hydrogen purity level required for the particular application. A dryer is used which removes the unwanted moisture from the gas by adsorbing the fraction of water content in it. The modelling of this unit requires the coupling of thermal, chemical and fluidic phenomena. The BG sub-model of the purification subsystem is shown in figure 3.10. The lump parameters $C : C_{dry}^{th}$, $R : R_{dry,enc}$, $R : R_{dry}$, $R : R_{exhaust}$, $C : C_{dry}^{ch}$, $C : C_{ads}^{ch}$ and $RS : R_{ads}$ are, respectively, used to model the thermal capacity, thermal resistance, internal pneumatic resistance, exhaust resistance, dryer chemical capacity, water adsorption capacity and the adsorption resistance of the unit. Here, element $RS : R_{ads}$ is used to couple the chemical and thermal phenomena of the unit. According to figure 3.10, using constitutive relation of $C : C_{dry}^{th}$ and junction 0_{28}, dryer temperature T_{dry} can be obtained as

$$T_{dry} = \frac{1}{C_{dry}^{th}} \int \left(\dot{H}_{hpcv} + \dot{H}_{ads} - \dot{H}_{puri} - \dot{Q}_{dry,enc} - a_e \dot{Q}_{exha} \right).\mathrm{dt} \tag{3.42}$$

where $\dot{H}_{hpcv}$ is the enthalpy flow coming through hydrogen pressure control valve, $\dot{H}_{ads} = \dot{n}_{ads}^{H2O}.\Delta H_{ads}$ is the enthalpy flow due to fraction of water adsorption with molar flow $\dot{n}_{ads}^{H2O}$ in the reaction, $\dot{H}_{puri}$ enthalpy flow out from the purification system toward hydrogen production, $\dot{Q}_{dry,enc}$ is the rate of heat loss due to temperature gradient between dryer unit and system enclosure and $\dot{H}_{exha}$ is the enthalpy flow when the exhaust valve is on ($a_e = 1$).

Likewise, according to figure 3.10, using constitutive relations of $C : C_{dry,i}^t$ and junction $0_{24}/0_{26}$ for partial pressures $p_{dry,i}$ of oxygen and hydrogen gases, respectively, and $C : C_{dry,j}^{ch}$ and junction 0_{25} for partial pressure $p_{dry,j}$ of water vapour can be obtained as

$$p_{dry,i} = \frac{1}{C_{dry,i}^{ch}} \int \left(\dot{m}_{hpcv}.\frac{x_i}{M_i} - \dot{m}_{puri}.\frac{x_i}{M_i} \right).\mathrm{dt} \tag{3.43}$$

$$p_{dry,j} = \frac{1}{C_{dry,j}^{ch}} \int \left(\dot{m}_{hpcv}.\frac{x_j}{M_j} - \dot{m}_{puri}.\frac{x_j}{M_j} - \dot{n}_{ads}^j \right).\mathrm{dt} \tag{3.44}$$

where $\dot{m}_{hpcv}$ is the mass inflow coming through hydrogen pressure control valve, $\dot{m}_{puri}$ mass outflow from the purification system towards hydrogen production, x_i and x_j are the respective mass fractions. The capacities $C_{dry,i}^{ch}$ and $C_{dry,j}^{ch}$ can be similarly obtained from equation 3.33 for the different species. The total pressure P_{dry} of the dryer is the summation of partial pressure of the gases.
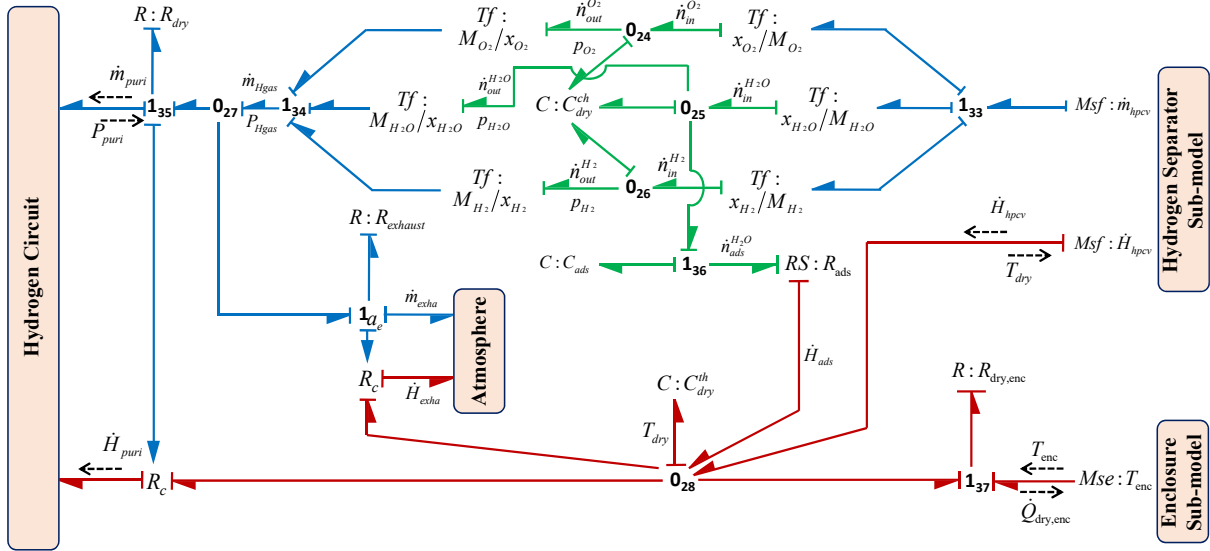
Figure 3.10: BG sub-model purification subsystem

3.2.2.5 System Enclosure

The major subsystems of the electrolysis system are kept inside an enclosure which is designed according to the environmental requirements and the different functions of the subsystems. The enclosure temperature is maintained at desired temperature by designing the proper venting system and providing the fan/blower for its cooling. The BG sub-model of the system enclosure is shown in figure 3.11. In this sub-model, the fan is modelled by the source of flow generalized BG element ($MSf : \dot{m}_{fan}$) to represent the mass flow of air and the atmospheric temperature is modelled as the source of effort generalized BG element ($MSe : T_{atm}$). The thermal capacity and the thermal resistance are modelled by the lumped parameters using $C : C_{enc}^{th}$ and $R : R_{enc}$. Thus, from figure 3.11, using constitutive relation of $C : C_{enc}^{th}$ and junction 0_{29}, enclosure temperature T_{enc} can be obtained as

$$T_{enc} = \frac{1}{C_{enc}^{th}} \int \left(\dot{Q}_{sbs} + \dot{H}_{in,fan} - \dot{H}_{out,fan} - \dot{Q}_{enc,atm} \right) .\mathrm{dt} \tag{3.45}$$

where $\dot{Q}_{sbs}$ is the summation of all the rate of heat losses from the different subsystems to the enclosure, $\dot{H}_{in,fan}$ and $\dot{H}_{out,fan}$ are the rate of heat enthalpy in to the enclosure and out from it which depend on the specific heat ($C_{P,air}$) and the mass flow of air ($\dot{m}_{fan}$). Also, $\dot{Q}_{enc,atm}$ is the rate of heat loss to the atmosphere.

3.3 Efficiency of the PEM Electrolysis System

For analyzing the performance of the electrolysis system, efficiency is also the one of the most important parameters whose definition mainly depends on the different operating conditions and the system designs. Here, the efficiency is defined in the two levels: (i) cell/stack level (ii) system level including the auxiliaries. Here, it is also assumed that the cell operating voltage is always greater than the thermal-neutral voltage. Also, operating temperature is below the boiling point of water and water supplied in the liquid form. The real output of the system is only the useful hydrogen produced. Oxygen is not considered as a real output of the system, however it is also produced along with hydrogen.
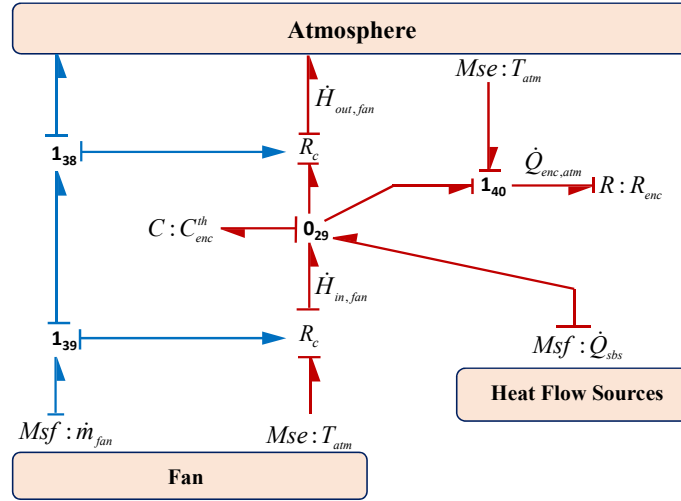
Figure 3.11: BG sub-model of system enclosure in capsule form.

3.3.1 Efficiency of Cell/stack

For the dissociation of water in electrolysis process, a fixed amount of energy is required, which is equal to the summation of Gibbs free energy, ΔG_R, and energy due to entropy change, $T\Delta S_R$, and this summed energies is called the enthalpy, ΔH_R, of the electrolysis reaction. Here ΔG_R is the minimum amount of energy that must be supplied by the electrical input by assuming the rest of energy is thermally contributed by $T\Delta S_R$ term. The change in enthalpy (ΔH_R) and Gibbs free energy (ΔG_R) can be obtained from the chemical kinetics of the reaction as 286 kJ/mol and 237 kJ/mol, respectively, at standard temperature and pressure conditions, that equivalently represented in the form of standard electrode potential as 1.23 V and thermo-neutral potential as 1.48 V, respectively [93]. In the calculation of standard electrode potential in reversible condition, it is assumed that all the thermal energy along with electrical energy are contributed in the electrolysis reaction based on Lower Heating Value (LHV) that does not include enthalpy of evaporation of water. However, in the calculation of thermo-neutral potential it is assumed that only electrical energy is contributed in the electrolysis reaction based on Higher Heating Value (HHV) that includes enthalpy of evaporation of water. Thus, the efficiency calculation of an electrolysis system is based on either the HHV or the LHV and it should be quoted while mentioning the efficiency of the system. Thus, the efficiency can be defined as the ratio of energy or power content of the hydrogen produced based on HHV or LHV and the input electrical energy or power to the system. Usually, HHV is preferred over LHV to calculate the efficiency of an electrolysis system supplied with liquid water, as the enthalpy of evaporation has to be provided by the process and it is represented as in equation 3.46 [28].

$$\varepsilon_{cell}^{HHV} = \frac{HHV.\dot{\eta}_{H_2}}{P_{elec}} = \frac{HHV.\dot{\eta}_{H_2}}{E_{cell}.I_{cell}} \tag{3.46}$$

where $\dot{\eta}_{H_2}$ is molar flow of hydrogen and P_{elec} is electrical DC input power to the electrolysis cell.

Efficiency (ε_{diss}) for water dissociation can also be defined as the ratio of energy requirement in reversible condition (En_{rev}) to the energy requirement in irreversible condition (En_{irrev}).

$$\varepsilon_{diss} = \frac{En_{rev}}{En_{irrev}} \tag{3.47}$$

Thus, based on equation 3.47, other important efficiencies such as: voltage efficiency and current

or Faradaic efficiency are also defined. Voltage efficiency can be obtained as the ratio of thermal-neutral voltage to the actual cell voltage at any operating condition, assuming the cell is always operating at a voltage above the thermal-neutral voltage. Thus, voltage efficiency is given as

$$\varepsilon_{volt} = \varepsilon_{diss} = \frac{En_{rev}}{En_{irrev}} = \frac{nFE_{tn}}{nFE_{cell}} = \frac{E_{tn}}{E_{cell}} \tag{3.48}$$

Voltage efficiency as defined in equation 3.48 can be analytically represented in the form of any operating temperature $T < 393.15$K as [201, 202]

$$\varepsilon_{volt} = \frac{1.485 - 1.49 \times 10^{-4} (T - T_0) - 9.84 \times 10^{-8}(T - T_0)^2}{E_{cell}} \tag{3.49}$$

The voltage efficiency as presented in equation 3.48 is valid with the assumption that the current supplied to the cell is fully converted into electro-chemical reaction of water dissociation. However, this is not the real situation in the cell operation due to the presence of some stray current in the cell and the unintended side reactions. Furthermore, gases permeation through PEM and successive recombination to water and leakage of gas leads to a loss of actual production of hydrogen. To consider this, the current or Faradaic efficiency ε_{curr} is defined, which is the ratio of actual hydrogen produced ($\dot{\eta}_{H_2,act}$) to the theoretically hydrogen produced ($\dot{\eta}_{H_2,th}$) based on Faraday's law.

$$\varepsilon_{curr} = \frac{\dot{\eta}_{H_2,act}}{\dot{\eta}_{H_2,th}} = \frac{\dot{\eta}_{H_2,act}}{(I/nF)} \tag{3.50}$$

Thus, the overall cell efficiency can be obtained by multiplying voltage and current efficiency as

$$\varepsilon_{cell} = \varepsilon_{volt}.\varepsilon_{curr} \tag{3.51}$$

3.3.2 Efficiency of System Including the Auxiliaries

Electrolysis system includes the various other supporting subsystems and auxiliaries for the production of green hydrogen. Every auxiliaries and subsystems have their own efficiency which can be estimated or supplied by the manufacturer. It is assumed that an imaginary boundary is considered that includes the electrolysis cell and the supporting auxiliaries for defining the system efficiency. Here, solar and/or wind subsystems are excluded for defining the system efficiency. Thus, the efficiency of the complete system is ratio of the energy content of hydrogen produced and the total amount of energy consumed and it is given as

$$\varepsilon_{syst}^{HHV} = \frac{HHV.\dot{\eta}_{H_2}}{P_{syst}} = \frac{HHV.\dot{\eta}_{H_2}}{P_{elec/\varepsilon_{conv}} + P_{pump} + P_{htex} + P_{other}} \tag{3.52}$$

where P_{syst} is the total amount of energy or power consumed in the considered system, P_{elec} denotes electrical DC input power and ε_{conv} denotes converter efficiency, P_{pump} denotes pump input power, P_{htex} denotes input power to heat exchanger and P_{other} denotes input power to other auxiliaries. However, there is always confusion and misunderstanding which heating value, i.e. LHV or HHV, should be used in efficiency calculation. To eliminate this confusion, efficiency can be represented in terms of power consumed by the electrolysis system, which represents the amount of electrical energy consumed by the system to produce one kilogram (kWh/kg of H_2) or one normal cubic meter (kWh/Nm^{-3} of H_2) of hydrogen.

It is noted that the efficiency calculation is constant when the electrical power input is constant. But, due to use of intermittent and time varying input sources (solar and/or wind power), the value of efficiency changes with time. Thus, this needs the instantaneous calculation of efficiency [26].

3.4 Global Model and Block Diagram Representation

Once the sub-models of all the components are developed using BG in the capsule form, they provides a model library to develop the global model for the PEM electrolysis. Depending on the configuration of the system, these sub-models can be assembled in order to represent the global model of the system. Figure 3.12 shows the global model of the PEM electrolysis system developed under BG approach. However, it is not possible to show a detailed global BG model for whole electrolyser here due to readability issue.
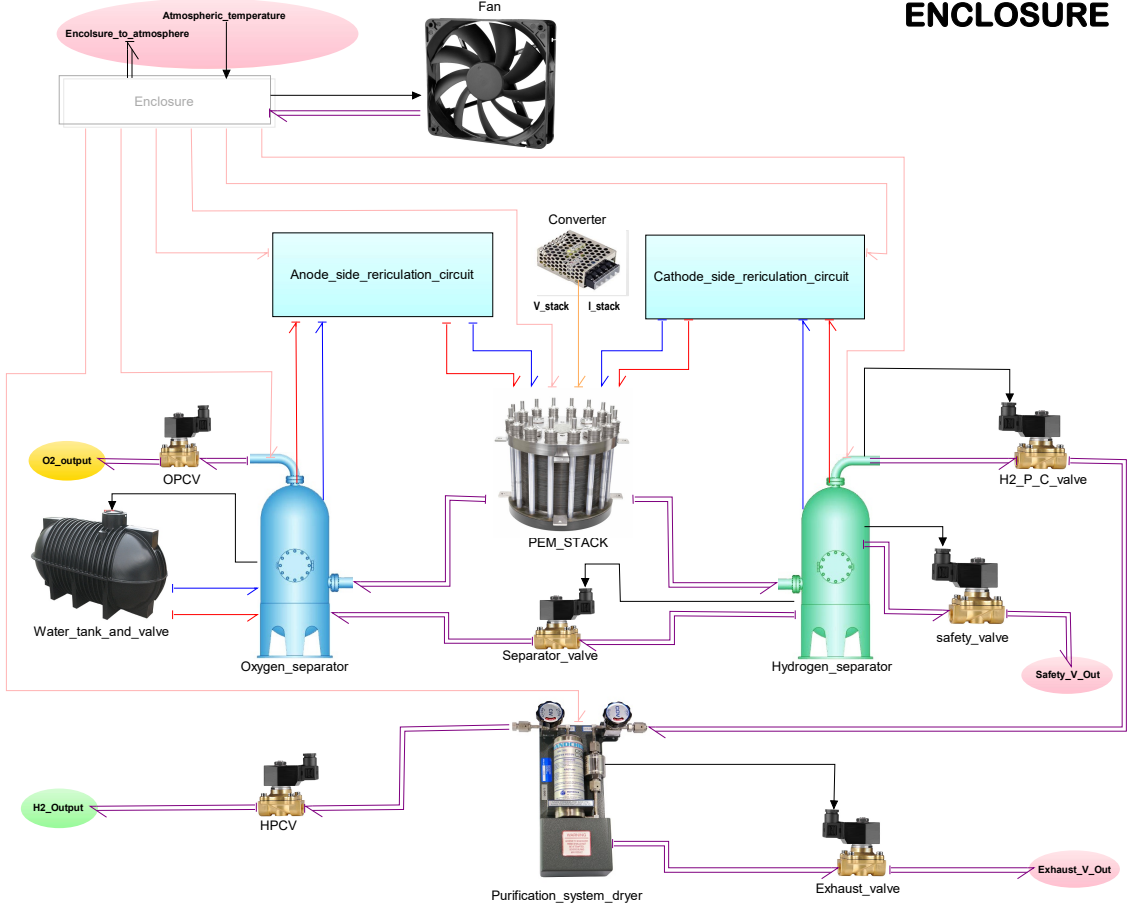
Figure 3.12: Global BG model of a PEM electrolysis system.

From implementation point of view, these BG models are also converted into block diagram representation in MATLAB® Simulink. As an example, figure 3.13 shows the block diagram representation of the PEM electrolysis stack in MATLAB® Simulink. The sub-models in the block diagram representation also then serves as a library to assemble the global model of the PEM electrolyser directly in the MATLAB® Simulink.

3.5 Conclusion

A generic dynamical multi-physics model of PEM electrolyser was presented in this chapter. The modular approach using BG technique was implemented to develop the capsules representing the sub-components of the PEM water electrolyser. The global model of the PEM water electrolyser is obtained by connecting the capsules as per the system configuration. The developed model is
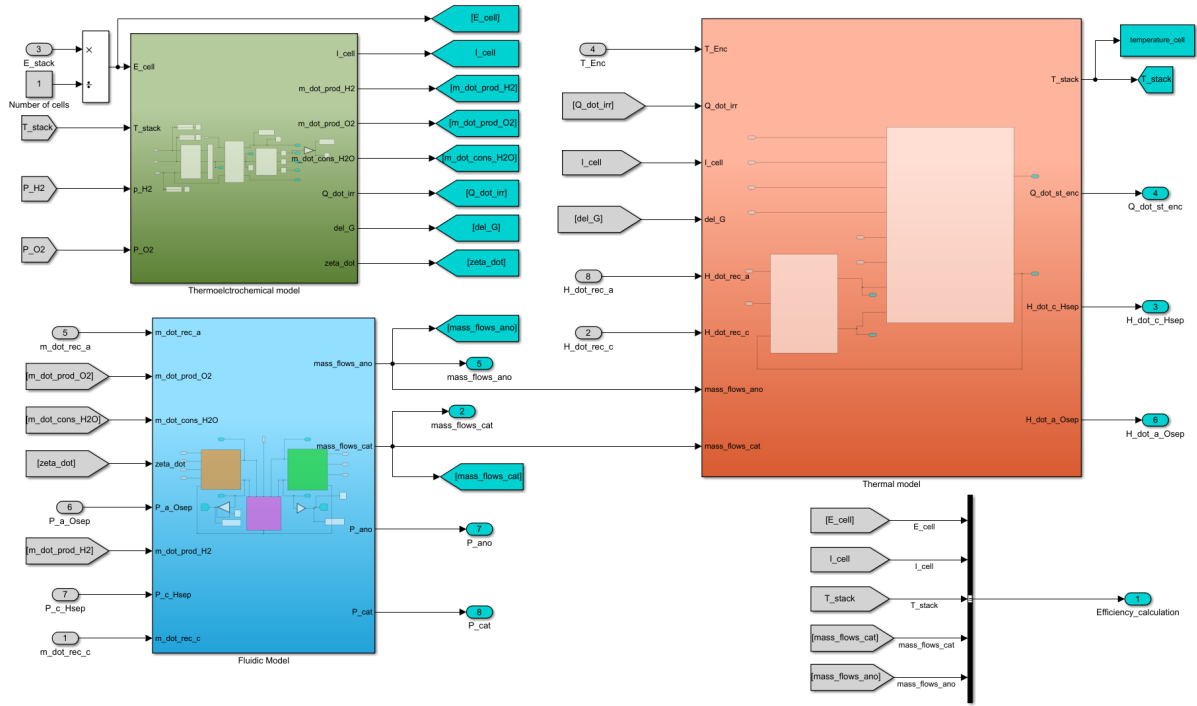
Figure 3.13: Block diagram representation of the PEM stack.

also converted into block diagram in MATLAB® Simulink environment from implementation point of view. The parameter estimation, validation and application of the developed model is discussed in chapter 5. The model was also extended to the AEM electrolysis cell (see appendix A). The developed model is further utilized for the development of diagnosis algorithms for PEM water electrolysis system. The BG model based robust diagnosis for PEM water electrolysis system is discussed in the next chapter.

CHAPTER 4

Model based robust diagnosis for PEM Electrolyser

Contents

PEM based water electrolysis is a widely used technique due to its high reliability and performance. PEM electrolyser clubbed with renewable energy sources is emerging as a great way of storing surplus green electricity in the form of hydrogen that can be used later to either regenerate electrical energy or for various industrial applications. Monitoring of these systems for faults is of uttermost importance in order to ensure the correct operation and safety of the system as well as of its surroundings. PEM electrolysers are susceptible to numerous faults that need to be detected on time. Some of these faults are very critical and if they are not detected on time, can cause damage to the electrolyser itself as well as its surroundings. Figure 4.1 shows the basic schematics of a PEM water electrolyser. When the DC is applied across
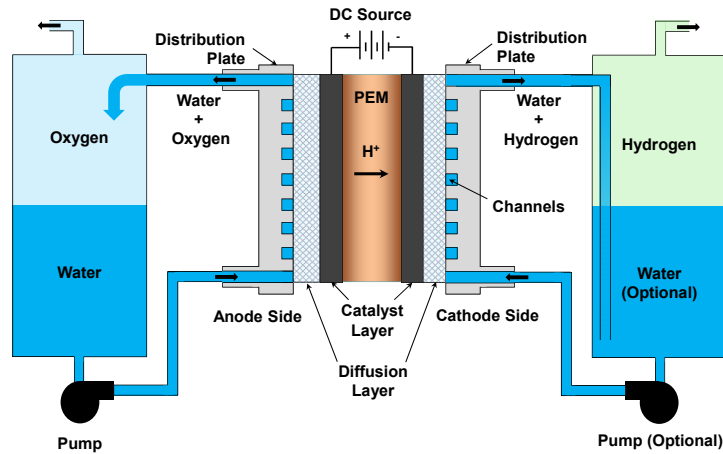
Figure 4.1: Schematics of a PEM water electrolyser

the cell, the water gets split into positive hydrogen atoms, oxygen gas, and free electrons at the anode. These positive hydrogen atoms move through the PEM towards the cathode where they receive electrons from the DC source and forms hydrogen gas. The working principle of PEM electrolysis is well illustrated in section 2.1 and can also be read in detail from [12, 203]. The PEM electrolysis cell/stack receives water on the anode side, through a pump, as a consumable as well as a carrier for the generated oxygen. The water feeding to the cathode side is optional. The electric converter provides the required electric power to the cell for electrolysis.

4.1 Diagnosis Background for PEM Water Electrolysers

The fault can occur at different components level although the cell/ stack has been the area of interest for previous studies as it is more susceptible to faults due to its complexity [64, 73, 122, 204, 205]. The cell/stack has non-linear behavior and includes multi-physics phenomena (such as electrical, chemical, thermal, fluidic) coupled together which adds to its complexity.

The MEA in the PEM electrolysis cell is the most common point of failure due to a number of reasons such as drying of the membrane, perforation of the membrane, mechanical failure of the cell due to improper handling, corrosion, overheating [202]. Most of the faults in the cell tend to change the cell voltage and thus reducing efficiency. The degradation of the cell also shows the same effect but the change is gradual. The fault in the cell could also be a result of the fault in some other components. For example, the drying of the membrane could be the result of the leakage in the cell, or recirculation circuit, or it can occur due to the failure of the pump feeding water to the cell [178]. Therefore, it becomes absolutely necessary to take into account the faults in the auxiliaries in addition to the stack. Table 4.1 summarises the possible faults in a PEM electrolyser and their indicators.

A look into the literature on the diagnosis of PEM electrolyser shows that most of the work is based on the monitoring of the system using different techniques that include electrical measurements, electrochemical impedance spectroscopy measurements, thermal imaging, visual inspection etc. [178, 205, 206]. These methods are usually offline, invasive, and costly as specific equipment are required for diagnosis. Also, sometimes the modification of the system is required in order to be able to perform the detection of a fault. Thus, there is a need for software-based diagnosis that can be implemented for the PEM electrolyser with the existing sensors. The aim of a suitable diagnostic approach is to detect and isolate system faults in real-time. This is done by continuously comparing the measured data from the system with the expected values according to the operating conditions [64].

Different diagnostic approaches can be crudely classified into model-based and non-model based/ data-driven approaches, Model-based approaches take advantage of the knowledge of the physical laws that govern the system. The residuals are evaluated from the measured data and the output of the model [122]. The change in the residual is the fault indicator. In non-model based approaches the information of the fault is obtained through the signal processing based on the database available for both normal and faulty operating conditions [64]. Non-model based techniques are faster and require less computational power for real-time monitoring as compared to the model-based techniques, but, it is very difficult and expensive to generate a database for all faulty operating conditions. Model based diagnosis approaches, on the other hand, helps in robust fault detection [175]. There is not much work done on the model based diagnosis for PEM electrolysers. Lebbal and Lecœuche have proposed a parity space based diagnosis algorithm which considers a simple static electrical model and thermal dynamics only [122]. Thus, it can be used for detecting a limited range of faults. A lot of work has been done for the modelling of PEM electrolysers but most of the work is limited to phenomena understanding and performance evaluation [6, 128, 152]. Graphical dynamical models have also been proposed for modelling the complex dynamics of the PEM electrolysers, but have not been exploited for model-based diagnosis [6, 15]. BG is a powerful tool that is used for developing the FDI algorithms for complex multi-physics systems [175]. BG delivers a robust FDI by exploiting the structural and causal properties of the model.

A model-based multi level diagnosis, using the model developed in 3, under BG paradigm for real-time monitoring of PEM electrolyser is proposed in this chapter. The schematics of the multi-level diagnosis approach is presented in figure 4.2. The DBG model (derivative causality) for each subsystem can be obtained from its corresponding BG model (integral causality).

Table 4.1: List of possible faults that can occur in PEM electrolyser

Faults in Electrolyser Subsystems		
Subsystem	**Fault**	**Fault Indicator**
Membrane (Stack)	Resistance Change due to contamination of foreign chemical pollutants in the flow of water	Voltage and Current
	Resistance Change due to chemical corrosion	Voltage and Current
	Decomposition of the polymer chain i.e. chemical attack on membrane material.	Voltage and Current
	Membrane shrinking/swelling that depends on the cyclic changes in the hydration level	Voltage and Current
	Pinhole formation due to cyclic shrinkage and swelling (crossover increase)	Voltage and Current
	Cell short-circuit	Voltage and Current
	Physical damage due to freezing	Voltage and Current
	Degradation due to intermittent and flexible operation	Voltage and Current
	Overheating causes membrane materia ldegradation	Voltage and Current
Catalysts Layers (Stack)	Loss of catalytic sites due to surface contamination and corrosion	Voltage and Current
	Washed out catalyst particles during operation	Voltage and Current
	Degradation due to H2–O2 recombination with platinum catalyst at cathode	Voltage and Current
Micro-porous and Gas Diffusion Layers (Stack)	Surface/interface degradation due to corrosion	Voltage and Current
	Increase in contact resistance due to degradation	Voltage and Current
Bipolar Plates with Flow channels (Stack)	Surface degradation due to corrosion vs oxidation in contact with deionized water	Voltage and Current
	Increase in contact resistance due to degradation and uneven current distributions	Voltage and Current
	Mechanical failure due to ageing effects	Voltage and Current
Gasket and seals (Stack)	Mechanical failures due to ageing and compression	Voltage and Current
Compression or End Plates (Stack)	Mechanical failures due to inappropriate handling	Voltage and Current
Hydrogen Separator	Separator valve not working (stuck-on or stuck-off)	Increase in the level of water than set value.
	Leakage of Water	Not enough pressure
	Leakage of gas	Not enough pressure
Oxygen Separator	Same faults as of Hydrogen Separator	
Cathode side recirculation circuit	Pump Is faulty	Not enough flow rate
	Leakage of water	Not enough Pressure
	Blockage	Not enough flow rate
Anode side recirculation circuit with cooling circuit	Pump Is faulty	Not enough flow rate
	Leakage of water	Not enough Pressure
	Heat exchanger (cooling Unit) not working	Temp. not maintained
	Blockage due to foreign object	Not enough flow rate
Purification Unit	Leakage of hydrogen	Not enough Pressure
	Dryer not working	Moisture in the output gas
Enclosure	Fan not working	Increase in system temp.

These DBG models capsules can be assembled to obtain a global diagnostic model of the PEM electrolyser. The global model can be used for the overall detection of the fault in the electrolyser when the electrolyser is a subsystem of another system such as in the case of PEM electrolyser running on the RES. Also, each DBG model of the subsystems can be used for the diagnosis at the subsystem level, if the subsystem can be decoupled from rest of the system by knowing the inputs and outputs (by measurement) to the subsystem concerned.
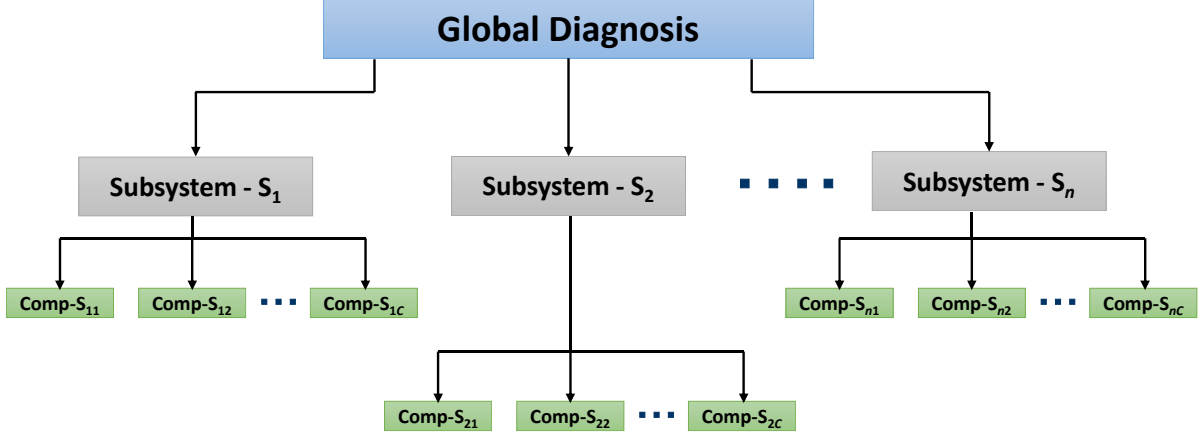
Figure 4.2: Multi level diagnosis for PEM electrolyser

For FDI the residuals are generated from ARRs systematically deduced from the BG model of PEM electrolyser. For strengthening the FDI algorithm against uncertainties, LFT BG is utilised [194, 195]. ARRs are the relations that are obtained from the junction equations in DBG and are expressed in the terms of known variables and parameters of the system. Numerical computation of these ARRs gives the residuals that are used to detect the occurrence of the fault (during normal operation, and without any disturbances and uncertainties, the numerical value of the ARR is equal to zero).

4.2 Model based diagnosis using BG

BG is a well-developed graphical modelling technique in which the systems or subsystems can be modelled with few elements (Se: source of effort, Sf: source of flow, R: resistance (dissipation of energy), C: capacitance (potential energy storage), I: inductance (kinetic energy storage), Tf: transformer and Gy: gyrator (for energy conversion between different physical domains), etc.) that represent physical phenomena. Irrespective of the physical domain the nature of these elements remains unchanged. Half arrows known as power bonds are used to connect these elements. These bonds represent the power exchange between the elements where the power is a product of generalized effort and flow. Therefore, BG is a unified approach that can be used in a similar way for the systems that belongs to different physical domains. The basics of the BG technique and its application for the modelling and FDI into process engineering si presented in appendix B. Moreover, LFT BG can be implemented for obtaining a robust diagnosis (for avoiding false alarm) by generating thresholds that are adaptable with respect to the degree of uncertainties in the parameters [194, 195].

4.2.1 Diagnostic BG model of PEM electrolysis cell/stack

For the development of diagnosis algorithms, BG model in derivative causality is preferred over integral causality (used for simulations and study of the system behaviour [196]). Causality

represents the relationship between cause and effect in BG. Derivative causality does not require the knowledge of system initial conditions (initial conditions are not clearly known for diagnosis and hence avoided). In DBG model, the sensors are considered as a source of effort and source of flow elements. The DBG model of the cell/stack of PEM water electrolysis is shown in Figure 4.3, where different sub-models related to electro-chemical, chemical, thermal and fluidic phenomena have been highlighted.
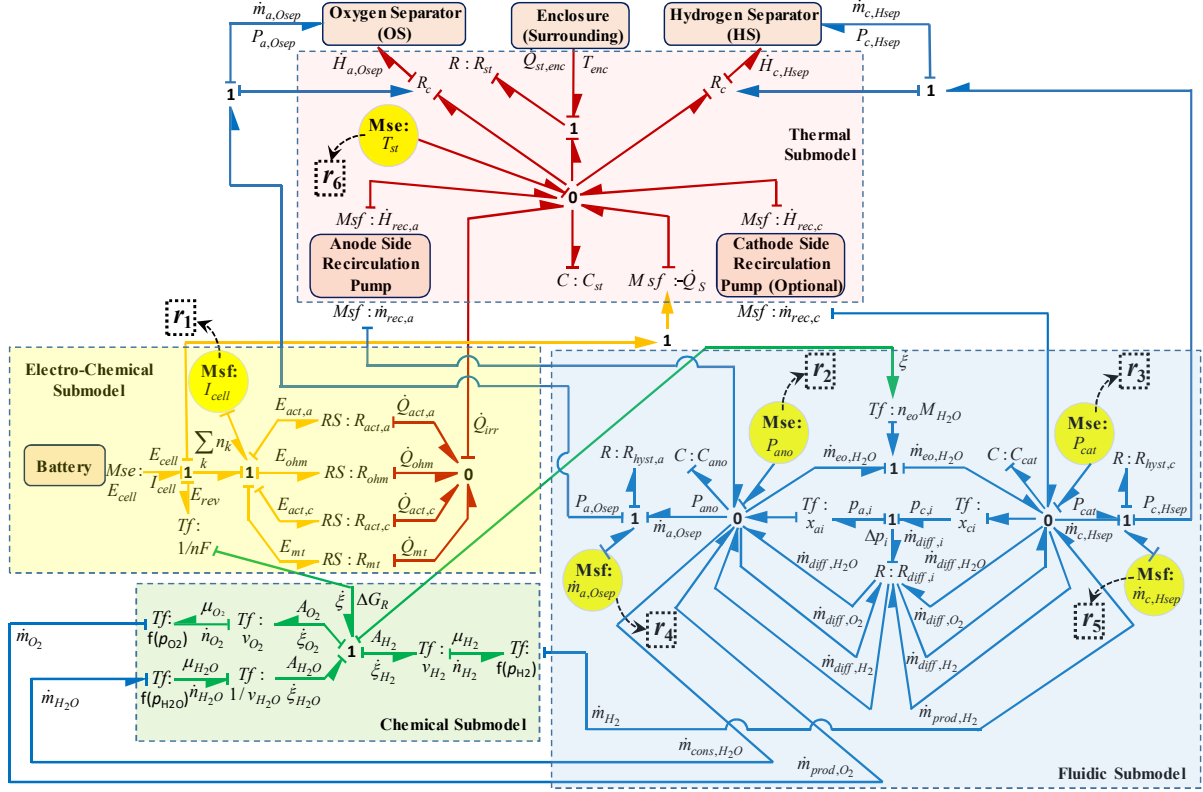

Figure 4.3: DBG model of the cell/stack of PEM water electrolyser

4.2.1.1 Electro-chemical Sub-model

Electrical sub-model represents the relationship between the voltage applied to the cell (E_{cell}) and the voltage required for actual electrolysis known as reversible voltage (E_rev). A significant amount of the applied voltage is lost due to the losses (such as activation losses, ohmic losses and mass transport losses) which occur in the cell/stack. These losses are termed as overvoltages. The relation of different overvoltages with E_{cell} is modelled using 1-junction. Different overpotential losses are modelled by two-port RS resistive elements, i.e. R_{ohm}, $R_{act,a}$, $R_{act,c}$ and R_{mt}, respectively, denote Ohmic loss (E_{ohm} from membrane, electrolyte, etc.), anode activation loss ($E_{act,a}$), cathode activation loss ($E_{act,c}$) and mass transport loss (E_{mt}) whose relations are given as [194]

$$E_{\text{ohm}} = I_{cell}.R_{\text{ohm}} \tag{4.1}$$

$$E_{\text{act, }k} = \frac{\text{R}.T_{st}}{\alpha_k.n.F}.\text{arcsinh}\left(\frac{I_{cell}}{2.I_{0,\ k}}\right); k = a,\ c \tag{4.2}$$

$$E_{\text{mt}} = \frac{\text{R}.T_{st}}{2.\beta.F}\ln\left(1 + \frac{I_{cell}}{I_L}\right) \tag{4.3}$$

where α_k and $I_{0,k}$ are, respectively, the symmetry factor and standard current exchange density at k^{th} electrode, R is the ideal gas constant, T_{st} is the cell/stack temperature, β is the diffusion constant and I_L is limiting current due to mass transport. Here, RS elements couple the electrical energy domain with the thermal energy domain, where $\dot{Q}_{irr}$ is the cumulative irreversible rate of heat due different losses in resistors R_{ohm}, $R_{act,a}$, $R_{act,c}$ and R_{mt}. Also, the phenomena related to electrical and chemical are coupled by using $Tf : 1/2F$ element that connects reaction rate $\dot{\zeta}$ with cell current I_{cell} and thermo-dynamical potential (E_{rev}) with Gibb's free energy (ΔG_R) using Faraday's law as

$$\dot{\zeta} = \frac{I_{cell}}{n.F}, E_{rev} = \frac{\Delta G_R}{n.F} \qquad (4.4)$$

where n is number of electrons and F is Faraday's constant.

4.2.1.2 Chemical Sub-model

Chemical sub-model helps in establishing the relations for the generation of hydrogen and oxygen and consumption of water. In the chemical sub-model, ΔG_R relation with the different affinity (A_i) is modelled by using 1-junction and rate (mol/s) of consumed reactant and produced gases by $Tf : v_i$ as

$$\Delta G_R = A_{H2} + A_{O2} - A_{H2O} \qquad (4.5)$$

$$\dot{n}_i = \nu_i.\dot{\zeta} = \nu_i.\frac{I_{cell}}{n.F} \qquad (4.6)$$

where $\dot{n}_i$ is the molar flow and v_i is the stoichiometry co-efficient. Also, $Tf : f(p_i)$ is the transformation from fluidic to chemical potential, $\mu_i(T_{st}, p_i) = \mu_i^0 + RTln(a_i)$, chemical activity a_i is equal to partial pressure (p_i) of the ith species.

4.2.1.3 Fluidic Sub-model

Fluidic model is based on the conservation of mass flows on both anode and cathode sides. In fluidic sub-model, $C : C_{ano}$ and $C : C_{cat}$ are, respectively, the capacity of storage of matters at anode and cathode side, field resistive element $R : R_{diff,i}$, i.e. $R : R_{diff,H2}$, $R : R_{diff,O2}$, $R : R_{diff,H2O}$, transformer $Tf : n_{eo}.M_{H2O}$ model the resistances for hydrogen crossover, oxygen crossover, water crossover from cathode to anode, electro-osmosis drag from anode to cathode, respectively. The mass flow conservations at anode and cathode are modelled by respective 0-junctions, where $\dot{m}_{a,Osep}$, $\dot{m}_{c,Hsep}$ and $\dot{m}_{rec,a}$, $\dot{m}_{rec,c}$, are the fluid outflows from the stack and the pumped water at the anode and cathode side, respectively; and $\dot{m}_{cons,H2O}$, $\dot{m}_{prod,H2}$, $\dot{m}_{prod,O2}$ and $\dot{m}_{eo,H2O}$, respectively, are the consumed water, hydrogen produced, oxygen produced and electro-osmosis drag water. The constitutive relations for element $R : R_{diff,i}$ and electro-osmosis drag are given as [194]

$$\dot{m}_{diff,i} = \frac{\Delta P_i}{R_{diff,i}} \qquad (4.7)$$

$$\dot{m}_{eo,H2O} = n_{eo}.M_{H2O}.\dot{\zeta} = n_{eo}.M_{H2O}.\frac{I_{cell}}{n.F} \qquad (4.8)$$

where $\Delta P_i = (p_{c,i} - p_(a,i)$ is the difference in partial pressure at cathode and anode, x_{ci} and x_{ai} are the respective mass fractions (for calculating partial pressures), n_{eo} is the electro-osmosis drag coefficient and M_i is the molar mass of the ith species. Also, in the DBG model, $R_{hyst,a}$ and $R_{hyst,c}$ denote the internal hydraulic resistances at anode and cathode sides of fluidic flows, respectively.

4.2.1.4 Thermal Sub-model

In thermal sub-model, $C : Cst$ and $R : Rst$ model the stack's thermal capacity and dissipative resistance, respectively. Thermal capacity $C : Cst$ is associated with the stack temperature using different enthalpy rates such as $\dot{H}_{rec,a}$), $\dot{H}_{rec,c}$ and $\dot{H}_{a,Osep}$, $\dot{H}_{c,Hsep}$ due to pumped water from OS, from HS (optional) and fluid exit to OS and exit to HS from stack, respectively, and $\dot{Q}_{irr}$ due to irreversible losses, $\dot{Q}_S$ due to entropy change in endothermic reaction and $\dot{Q}_{st,enc}$ due to temperature gradient between stack and enclosure. The R_C element shows coupling of fluidic to thermal flows.

4.2.1.5 Pump Sub-model

The pump that is used to feed the water to the cell from the separator tank is modelled as a source of flow with the following characteristic equations

$$\dot{m}_P = \Phi(I_{cell}) = \begin{cases} k.I_{cell} & \text{for} \quad 0 < I_{cell} \leq I_{\max} \\ k.I_{\max} & \text{for} \quad I_{cell} > I_{max} \\ 0 & \text{otherwise} \end{cases} \tag{4.9}$$

where $\dot{m}_P$ is the flow imposed by the pump, I_{max} is the saturation current.

4.2.2 ARR generation using LFT BG

ARRs are the relations that are obtained from the junction equations in DBG and are expressed in the terms of known variables and parameters of the system. Numerical computation of these ARRs gives the residuals that are used to detect the occurrence of the fault. During normal operation, and without any disturbances and uncertainties, the numerical value of the ARR is equal to zero. However, practically the value is non-zero due to sensor noise and parameter uncertainties. Hence it is required to use adaptive thresholds to account for robust diagnosis. Also, in the presence of high noise in the measurement data, the signals need to be filtered. The systematic extraction of ARRs from DBG has been discussed in B.2 and can be found elsewhere in details [175]. The real measurements obtained from the different sensors, such as cell current (I_cell), stack temperature (T_st), pressures at anode (P_{ano}) and cathode (P_{cat}), mass flows from stack to oxygen separator ($\dot{m}_{a,Osep}$) and to hydrogen separator ($\dot{m}_{c,Hsep}$) are the inputs to the DBG model. As developed in [128], the candidate ARRs are represented by conservative law equation deduced from "1" (sum of efforts = 0) and "0" junction (sum of flows = 0) associated with at least one sensor in considered junction. The unknown variables are then eliminated using causal covering paths. Based on this, the following candidate ARRs can be generated:

$$\text{ARR}_1 = E_{rev} + E_{ohm} + E_{act,a} + E_{act,c} + E_{mt} - E_{cell} \tag{4.10}$$

$$\text{ARR}_2 = \begin{aligned} \dot{m}_{a,Osep} - \dot{m}_{rec,a} - \dot{m}_{prod,O2} + \dot{m}_{cons,H2O} + C_{\text{ano}}.\tfrac{\mathrm{d}P_{ano}}{\mathrm{d}t} + \dot{m}_{eo,H2O} \\ - \dot{m}_{diff,H2} - \dot{m}_{diff,H2O} + \dot{m}_{diff,O2} \end{aligned} \tag{4.11}$$

$$\text{ARR}_3 = \begin{aligned} \dot{m}_{c,Hsep} - \dot{m}_{rec,c} - \dot{m}_{prod,H2} - \dot{m}_{eo,H2O} + C_{\text{cat}}.\tfrac{\mathrm{d}P_{cat}}{\mathrm{d}t} - \dot{m}_{diff,O2} \\ + \dot{m}_{diff,H2O} + \dot{m}_{diff,H2} \end{aligned} \tag{4.12}$$

$$\text{ARR}_4 = P_{a,Osep} - P_{ano} - \dot{m}_{a,Osep}.R_{hyst,a} \tag{4.13}$$

$$\text{ARR}_5 = P_{c,Hsep} - P_{cat} - \dot{m}_{c,Hsep}.R_{hyst,c} \tag{4.14}$$

$$\text{ARR}_6 = C_{st}.\frac{\mathrm{d}T_{st}}{\mathrm{d}t} - \dot{H}_{rec,a} - \dot{H}_{rec,c} - \dot{Q}_{irr} + \dot{Q}_S + \dot{H}_{a,Osep} + \dot{H}_{c,Hsep} + \dot{Q}_{st,enc} \tag{4.15}$$

ARR7 is obtained from the characteristic equation of the pump ($\phi(I_{cell})$) used for feeding water to the anode side and the measurement through the flow sensor Q_P and is written as

$$\text{ARR}_7 = \Phi\left(I_{cell}\right) - Q_P \tag{4.16}$$

The pump on the cathode side is optional and depends on whether the water is fed to the cathode side or not. ARR can be generated in a similar way if the pump for the cathode side also exists (not considered here).

However, ARR_i ($i = 1, 2..., 7$) presented in equations 4.10 to 4.16 show the nominal part of ARRs. To account for different uncertainties in parameters, system is usually modeled in LFT, called DBG-LFT model [195]. For example, uncertainties in the parameter $RS : R_{ohm}$ and current sensor I_{cell} can be detached from their nominal part and can be presented as

$$R^*_{\text{ohm}} = R_{\text{ohm}} \pm \Delta R_{\text{ohm}} \tag{4.17}$$

$$I^*_{\text{cell}} = I_{\text{cell}} \pm \Delta I_{\text{cell}} \tag{4.18}$$

where R^*_{ohm}, I^*_{cell} are the real and R_{ohm}, I_{cell} are the ideal resistance and current, respectively; $\Delta R_{\text{ohm}} = \delta_{R_{\text{ohm}}}.R_{\text{ohm}}$ and ΔI_{cell} are the respective uncertainties. Thus, constitutive relation for R^*_{ohm} is given by the Ohm's law as

$$\begin{aligned} E^*_{\text{ohm}} &= I^*_{\text{cell}}.R^*_{\text{ohm}} = (I_{\text{cell}} \pm \Delta I_{\text{cell}}).(R_{\text{ohm}} \pm \Delta R_{\text{ohm}}) \\ &\approx (I_{\text{cell}}.R_{\text{ohm}} \pm \Delta I_{\text{cell}}.R_{\text{ohm}}) \pm (I_{\text{cell}}.\delta_{R_{\text{ohm}}}.R_{\text{ohm}}) \\ &\approx (E_{\text{ohm}} \pm \Delta I_{\text{cell}}.R_{\text{ohm}}) \pm w_{R_{\text{ohm}}} \\ &\approx E'_{\text{ohm}} \pm w_{R_{\text{ohm}}} \end{aligned} \tag{4.19}$$

Hence, the real Ohmic loss E_ohm^* in real cases is represented by LFT model as shown in figure 4.4. Likewise, uncertainties in other parameters can be modelled (the methodology has been discussed in B.2).

Thus, the residual evaluated with real measurements and parameters is presented as

$$r_i = r_{ni} \pm \Delta r_i \tag{4.20}$$

where r_{ni} is the nominal part and Δr_i is the uncertain part. The uncertain part provides the residual bounds, called as adaptive thresholds. During normal operation residual is within the adaptive thresholds and in case of any degradation in any part residual crosses the adaptive thresholds.

After replacing all the unknown variables in terms of known parameters and measurements variables of the system, the residuals, equations 4.10 to 4.15, are rewritten as

$$r_1 = \begin{aligned} &E^0_{rev} + \frac{R.T_{st}}{n.F}ln\left(\frac{(P_{H2})^{\nu H2} \cdot (P_{O2})^{\nu O2}}{(a_{H2O})^{\nu H2O}}\right) + I_{cell}.R_{ohm} + \frac{R.T_{st}}{\alpha_a.n.F}\text{arcsinh}\left(\frac{I_{cell}}{2.I_{0,\ a}}\right) \\ &+ \frac{R.T_{st}}{\alpha_c.n.F}\text{arcsinh}\left(\frac{I_{cell}}{2.I_{0,\ c}}\right) + \frac{R.T_{st}}{2.\beta.F}\ln\left(1 + \frac{I_{cell}}{I_L}\right) - E_{cell} \pm \Delta r_1 \end{aligned} \tag{4.21}$$
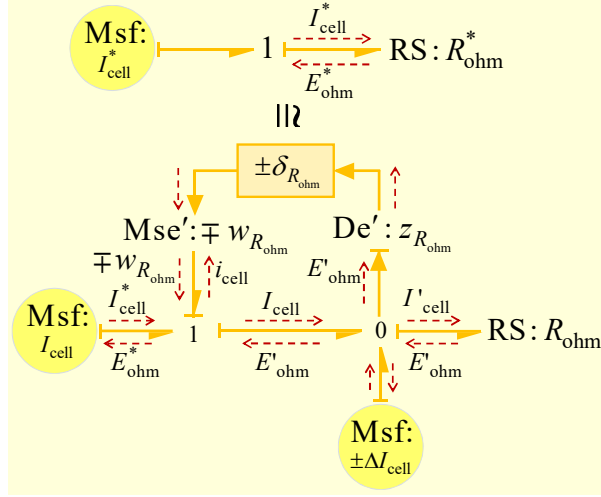
Figure 4.4: A LFT model for uncertainties in resistor and current sensor

$$r_2 = \begin{aligned} &\dot{m}_{a,Osep} - \dot{m}_{rec,a} - \nu_{O2}.M_{O2}.\frac{I_{cell}}{n.F} + \nu_{H2O}.M_{H2O}.\frac{I_{cell}}{n.F} + C_{ano}.\frac{dP_{ano}}{dt} \\ &+ n_{eo}.M_{H2O}.\frac{I_{cell}}{n.F} - \frac{\Delta P_{H2}}{R_{diff,H2}} - \frac{\Delta P_{H20}}{R_{diff,H20}} + \frac{\Delta P_{O2}}{R_{diff,O2}} \pm \Delta r_2 \end{aligned} \tag{4.22}$$

$$r_3 = \begin{aligned} &\dot{m}_{c,Hsep} - \dot{m}_{rec,c} - \nu_{H2}.M_{H2}.\frac{I_{cell}}{n.F} - n_{eo}.M_{H2O}.\frac{I_{cell}}{n.F} + C_{cat}.\frac{dP_{cat}}{dt} \\ &- \frac{\Delta P_{O2}}{R_{diff,O2}} + \frac{\Delta P_{H20}}{R_{diff,H20}} + \frac{\Delta P_{H2}}{R_{diff,H2}} \pm \Delta r_3 \end{aligned} \tag{4.23}$$

$$r_4 = P_{a,Osep} - P_{ano} - \dot{m}_{a,Osep}.R_{hyst,a} \pm \Delta r_4 \tag{4.24}$$

$$r_5 = P_{c,Hsep} - P_{cat} - \dot{m}_{c,Hsep}.R_{hyst,c} \pm \Delta r_5 \tag{4.25}$$

$$r_6 = \begin{aligned} &C_{st}.\frac{dT_{st}}{dt} - \dot{m}_{rec,a}.C_{P,H2O}.T_{rec,a} - \dot{m}_{rec,c}.C_{P,H2O}.T_{rec,c} - I_{cell}^2.R_{ohm} \\ &- \frac{R.T_{st}}{\alpha_a.n.F}\text{arcsinh}\left(\frac{I_{cell}}{2.I_{0,\,a}}\right).I_{cell} - \frac{R.T_{st}}{\alpha_c.n.F}\text{arcsinh}\left(\frac{I_{cell}}{2.I_{0,\,c}}\right).I_{cell} \\ &- \frac{R.T_{st}}{2.\beta.F}\ln\left(1 + \frac{I_{cell}}{I_L}\right).I_{cell} + \frac{I_{cell}}{n.F}.T_{st}.\Delta S_R + \dot{m}_{a,Osep}.C_{P,fluid}.T_{a,Osep} \\ &+ \dot{m}_{c,Hsep}.C_{P,fluid}.T_{c,Hsep} + \frac{T_{st}-T_{enc}}{R_{st}} \pm \Delta r_6 \end{aligned} \tag{4.26}$$

$$r_7 = \Phi\left(I_{cell}\right) - Q_P \tag{4.27}$$

4.2.3   FSM and Coherence Vector

FSM is the matrix that shows the relationship between the faults and ARRs [207]. The elements of the FSM can take a value of either 0 or 1 depending on the following condition

$$FSM_{ji} = \begin{cases} 1 & \text{when } ARR_i \text{ is sensitive to parameter } P_j \\ 0 & \text{otherwise} \end{cases} \tag{4.28}$$

Each row of the FSM represents the signature for the considered fault. According to different sensitivity of residuals, equations 4.21 to 4.27, FSM for the system can be obtained [128, 206]. FSM for the PEM water electrolysis cell/stack is shown in Table 4.2. The column I_D represents the detectability or monitorability of the fault. If the value of $I_D = 1$, the fault is detectable in the corresponding row component; and if the value of $I_D = 0$, it is non-detectable. The

Table 4.2: FSM for PEM electrolyser cell/stack

Phenomenon↓	ARR→ Fault↓	r_1	r_2	r_3	r_4	r_5	r_6	r_7	I_D	I_C
Electro-chemical	R_{ohm}	1	0	0	0	0	1	0	1	0
	$R_{act,a}$	1	0	0	0	0	1	0	1	0
	$R_{act,c}$	1	0	0	0	0	1	0	1	0
	R_{mt}	1	0	0	0	0	1	0	1	0
Fluidic	$R_{diff,H2}$	0	1	1	0	0	0	0	1	0
	$R_{diff,O2}$	0	1	1	0	0	0	0	1	0
	$R_{diff,H2O}$	0	1	1	0	0	0	0	1	0
	n_{eo}	0	1	1	0	0	0	0	1	0
	C_{ano}	0	1	0	0	0	0	0	1	1
	C_{cat}	0	0	1	0	0	0	0	1	1
	$R_{hyst,a}$	0	0	0	1	0	0	0	1	1
	$R_{hyst,c}$	0	0	0	0	1	0	0	1	1
	$F_{pump,a}$	0	0	0	0	0	0	1	1	1
Thermal	R_{st}	0	0	0	0	0	1	0	1	1

column I_C denotes the faulty component's isolability index. If the value of the $I_C = 1$, the faulty component is isolable and if the value of $I_C = 0$ it is non-isolable.

Table 4.2 shows the FSM for the PEM electrolyser.

The column I_D of table 4.2 represents the monitorability of the faults. Value of 1 means that the fault is monitorable and 0 means non-monitorable. As it can be seen from the table all the faults considered are monitorable. The column I_b of table 4.2 represents the isolability of the faults. Value of 1 means that the fault is isolable and 0 means non-isolable. The faults cannot be isolated if the signatures of more than one fault are the same.

For the real-time monitoring of the system, the ARRs values/residuals are continuously monitored using a coherence vector (in binary format), represented as in (4.29), and whose elements c_i are evaluated using (4.30)[207].

$$C = [c_1, c_2, c_3 .... c_m] \tag{4.29}$$

$$c_i = \begin{cases} 0 & \text{if} - \varepsilon_i \leq \text{Eval[ARR]} \leq \varepsilon_i \\ 1 & \text{otherwise} \end{cases} \tag{4.30}$$

where ε_i and $-\varepsilon_i$ are the upper and lower threshold bounds for i^{th} residual obtained from its uncertain part. The value of every element of the coherence vector is 0 for a healthy system. Each element of the coherence vector is continuously monitored and if the value of any element becomes one, a fault is said to have occurred. For isolation of the fault, the coherence vector is compared with FSM.

Different parameters presented in FSM (table 4.2) related to different type of faults. Increase of $R_{ohm} \uparrow$ reflects membrane degradation by corrosion, contamination, etc. Increase of $R_{act,k} \uparrow$ reflects possible degradation in catalyst layer (sluggish reaction), which depends on change in charger transfer coefficient (α_k) or current exchange density ($I_{0,k}$). Usually, anode catalyst layer is more susceptible to such degradation due to high working overpotential. Increase of $R_{mt} \uparrow$ reflects the partial blockage of reactant flow due to bubbles formation at high operational current density , which depends on change in limiting current (I_L). Likewise, decrease in $R_{diff,i} \downarrow$ reflects the increase of crossover diffusion flow due to phenomenon of gas-cross permeation through membrane. The catalytic recombination of hydrogen-oxygen due to crossover diffusion

is one of the dangerous phenomenon which causes membrane burning, especially at cathode side, $R_{diff,O2} \downarrow$, due to presence of platinum catalyst [122]. The change in n_{eo} is responsible for identifying the hydration level in the membrane. The decrease $n_{eo} \downarrow$ or increase $n_{eo} \uparrow$ value shows the drying or flooding degradation of the membrane. Parameters C_{ano} and C_{cat} reflect change in capacity of storage of matters. Increase of $R_{hyst,k} \uparrow$ reflects the scaling formation in pipe due to fluid contamination. Decrease of $R_{st} \downarrow$ reflects the change in heat dissipation limitation of the stack during ageing. The $F_{pump,a}$ denotes pump fault at anode side. However pump in cathode side is optional and depends on whether the water is fed to the cathode side or not. Thus fault in pump at cathode side is not considered. However, it can be included in a similar way if the pump for the cathode side also exists. It is clear that for the PEM water electrolyser cell/stack, all the degradations in the components are detectable and the related phenomenon is isolable using FSM. But, according to current instrumentation of the system, only parameters $R_{hyst,a}$, $R_{hyst,c}$, C_{ano}, C_{cat} and R_{st} are directly isolated from FSM after fault detection. However, a second level of isolation technique, i.e. parameter estimation, can be triggered for others as given in [206].

4.2.4 DBG Model for the BoP

Using the same approach as demonstrated above, the DBG model for the auxiliaries can be obtained in order to generate the residuals and FSM for each subsystem.

4.2.4.1 DBG Model for Anode Side Recirculation Circuit (Including Cooling Circuit)

In the DBG model (figure 4.5) of the anode side recirculation circuit which includes the cooling circuit, four sensors are considered to be installed in order to measure water flow rate to the stack ($\dot{m}_{rec,a}$), temperature of the recirculating water ($T_{rec,a}$), temperature of cooling system for heat exchanger(T_{cool}) and temperature of the coolant tank (T_{cold}). Four residuals are obtained
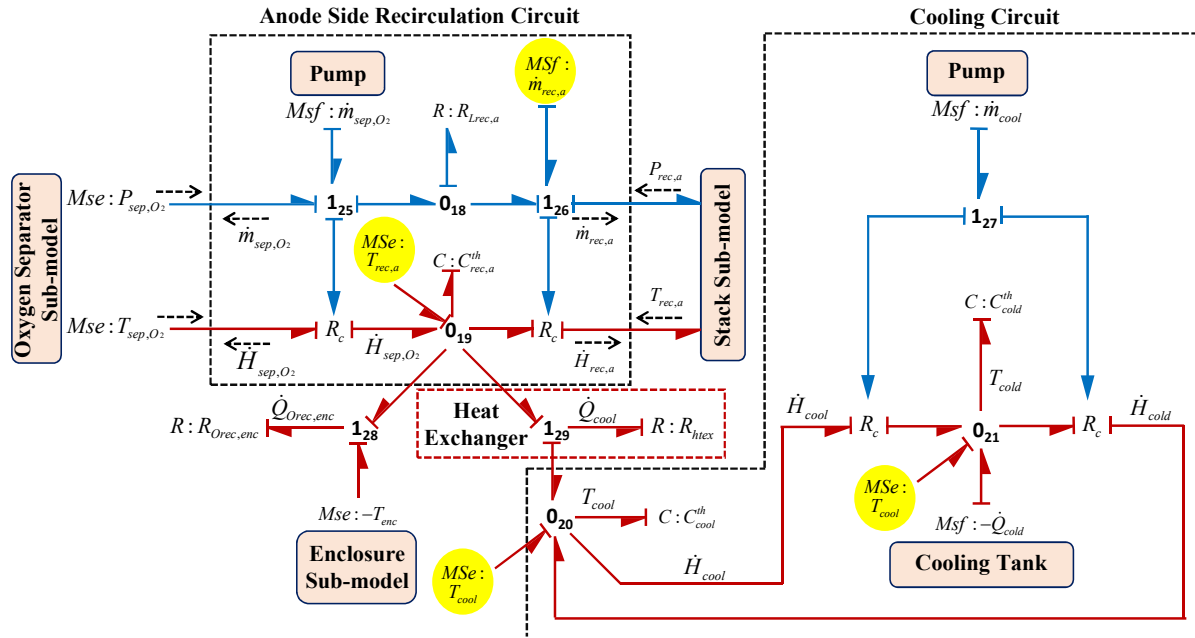
Figure 4.5: DBG model of the anode side recirculation circuit (including cooling circuit)

Table 4.3: FSM for anode side recirculation circuit (including cooling circuit)

Phenomenon↓	ARR→ Fault↓	r_1	r_2	r_3	r_4	I_D	I_C
Fluidic	$R_{Lrec,a}$	1	0	0	0	1	1
Thermal	$C_{rec,a}^{th}$	0	1	0	0	1	0
	R_{htex}	0	1	1	0	1	1
	$R_{orec,enc}$	0	1	0	0	1	0
	C_{cold}^{th}	0	0	0	1	1	1
	C_{cool}^{th}	0	0	1	0	1	1

(equations 4.31 to 4.34) from the junction equations where the sensors are placed.

$$r_1 = P_{rec,a} - R_{Lrec,a}.\dot{m}_{sep,O_2} \pm \Delta r_1 \tag{4.31}$$

$$r_2 = \begin{aligned} \dot{m}_{sep,O_2}.C_{P,fluid}.T_{Sep,O_2} - C_{rec,a}^{th}.\frac{dT_{rec,a}}{dt} - \dot{m}_{rec,a}.C_{P,fluid}.T_{rec,a} - \frac{T_{rec,a}-T_{cool}}{R_{hetx}} \\ -\frac{T_{rec,a}-T_{enc}}{R_{Orec,enc}} \pm \Delta r_2 \end{aligned} \tag{4.32}$$

$$r_3 = \frac{T_{rec,a}-T_{cool}}{R_{hetx}} + \dot{m}_{cool}.c_{P,coolant}.T_{cold} - C_{cool}^{th}.\frac{dT_{cool}}{dt} - \dot{m}_{cool}.c_{P,coolant}.T_{cool} \pm \Delta r_3 \tag{4.33}$$

$$r_4 = \dot{m}_{cool}.c_{P,coolant}.T_{cool} - \dot{Q}_{cold} - C_{cold}^{th}.\frac{dT_{cold}}{dt} - \dot{m}_{cool}.c_{P,coolant}.T_{cold} \pm \Delta r_4 \tag{4.34}$$

The FSM for the considered parametric faults is shown in table 4.3. Decrease in $R_{Lrec,a} \downarrow$ represents the leakage in the recirculation circuit. Increase in $R_{hetx} \uparrow$ represents the inefficient heat exchange due to fault in heat exchanger. Change in the parameters C_{cold}^{th} and C_{cool}^{th} represents the fault in cooling circuit. It can be seen from the table 4.3 that all the values in column I_D are 1. Therefore, all the faults are monitorable. The values in the column I_C shows that all the faults $C_{rec,a}^{th}$ and $R_{orec,enc}$ can be isolated as they have same signature. The pump faults were not considered in the presented DBG model, but can be easily detected using their characteristic equation as done in the case of stack DBG model.

4.2.4.2 DBG Model for Cathode Side Recirculation Circuit

Similar to DBG model of anode side recirculation circuit, DBG model for the cathode side recirculation circuit is shown in figure 4.6. Two sensors are considered in recirculation circuit. One flow sensor to measure the flow in the recirculation circuit $\dot{m}_{rec,c}$ and another for measuring the temperature of the fluid in the recirculation circuit.

The residuals are calculated as

$$r_1 = P_{rec,c} - R_{Lrec,c}.\dot{m}_{sep,H_2} \pm \Delta r_1 \tag{4.35}$$

$$r_2 = \dot{m}_{sep,H_2}.c_{P,fluid}.T_{Sep,H_2} - C_{rec,c}^{th}.\frac{dT_{rec,c}}{dt} - \dot{m}_{rec,c}.c_{P,fluid}.T_{rec,c} - \frac{T_{rec,a}-T_{enc}}{R_{Hrec,enc}} \pm \Delta r_2 \tag{4.36}$$

The FSM for the cathode side recirculation circuit is shown in table 4.4.

4.2.4.3 DBG Model for Hydrogen Separator

The key faults in the hydrogen separator is the leakage faults (leakage of gas and leakage of water). The leakage fault directly affects the thermal capacity also as the two phenomenon are coupled. DBG model of the hydrogen separator is shown in figure 4.7. Three sensors have
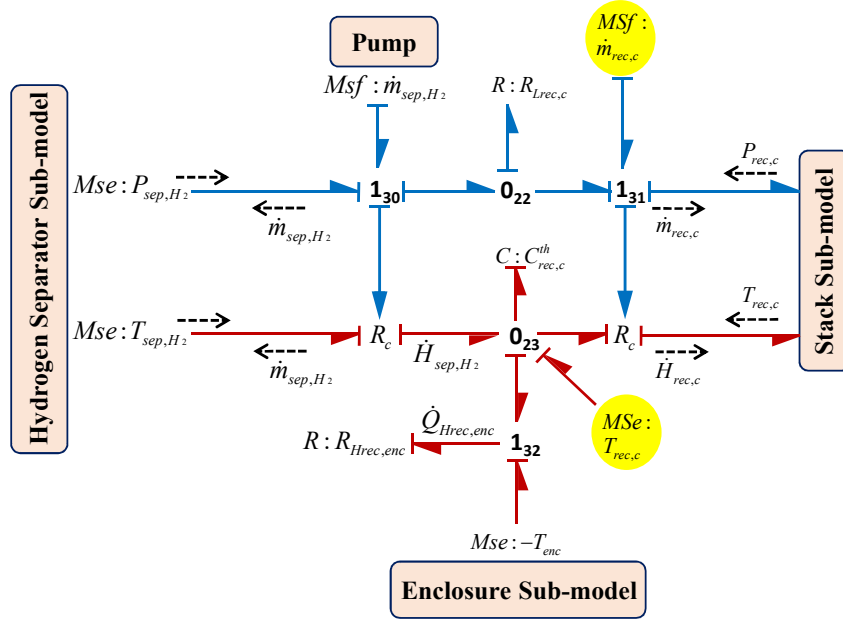
Figure 4.6: DBG model of the cathode side recirculation circuit

Table 4.4: FSM for cathode side recirculation circuit

Phenomenon↓	ARR→ Fault↓	r_1	r_2	I_D	I_c
Fluidic	$R_{Lrec,c}$	1	0	1	1
Thermal	$C_{rec,c}^{th}$	0	1	1	0
	$R_{Hrec,enc}$	0	1	1	0

been considered in the hydrogen separator. One flow sensor to measure the gas flow at the output of the hydrogen separator ($\dot{m}_{hpcv}$), one pressure and one temperature sensor at the outlet towards the recirculation circuit. If the BG model cannot be represented completely in derivative causality, it means that it is not possible to eliminate at least one unknown variable and that the system is not monitorable. For the chemical part of the hydrogen separator model, it is not possible to write $C : C_{Hsep}^{ch}$ in derivative causality without causing causality conflict at junction 1_16. Therefore the first residual of this subsystem is a hardware based. This residual is written as

$$r_1 = \dot{m}_{hpcv}^* - m_{hpcv} = \dot{m}_{hpcv}^* - \left(\frac{P_{gas,H_2} - P_{hpcv}}{R_{sep,hc}} \right) \pm \Delta r_1 \tag{4.37}$$

where m_{hpcv}^* is the sensor measurement. P_{gas,H_2} is calculated from the chemical compliance element $C : C_{Hsep}^{ch}$. As this element represent the physical volumetric capacity of the separator vessel, it is considered to be a robust parameter. The other two residuals are written as

$$r_2 = x_{cw}.\dot{m}_{c,Hsep} - \dot{m}_{sep,H_2} - C_{sep,H_2}^{fl} \frac{\mathrm{d}P_{sep,H_2}}{\mathrm{dt}} - \left(\frac{P_{sep,H_2} - P_{sepv}}{R_{sepv}} \right) \pm \Delta r_2 \tag{4.38}$$

$$r_3 = \begin{aligned} & C_{sep,H_2}^{th} \frac{\mathrm{d}T_{sep,H_2}}{\mathrm{dt}} + \dot{H}_{sep,H_2} - \dot{H}_{c,Hsep} + \dot{m}_{hpcv}.c_{P,fluid}.T_{sep,H_2} \\ & + \left(\frac{P_{gas,H_2} - P_{atm}}{R_{safe}} \right).c_{P,fluid}.T_{sep,H_2} + \left(\frac{T_{sep,H_2} - T_{enc}}{R_{Hsep,enc}} \right) \\ & + \left(\frac{P_{sep,H_2} - P_{sepv}}{R_{sepv}} \right).c_{p,water}.T_{sep,H_2} + \Delta r_3 \end{aligned} \tag{4.39}$$
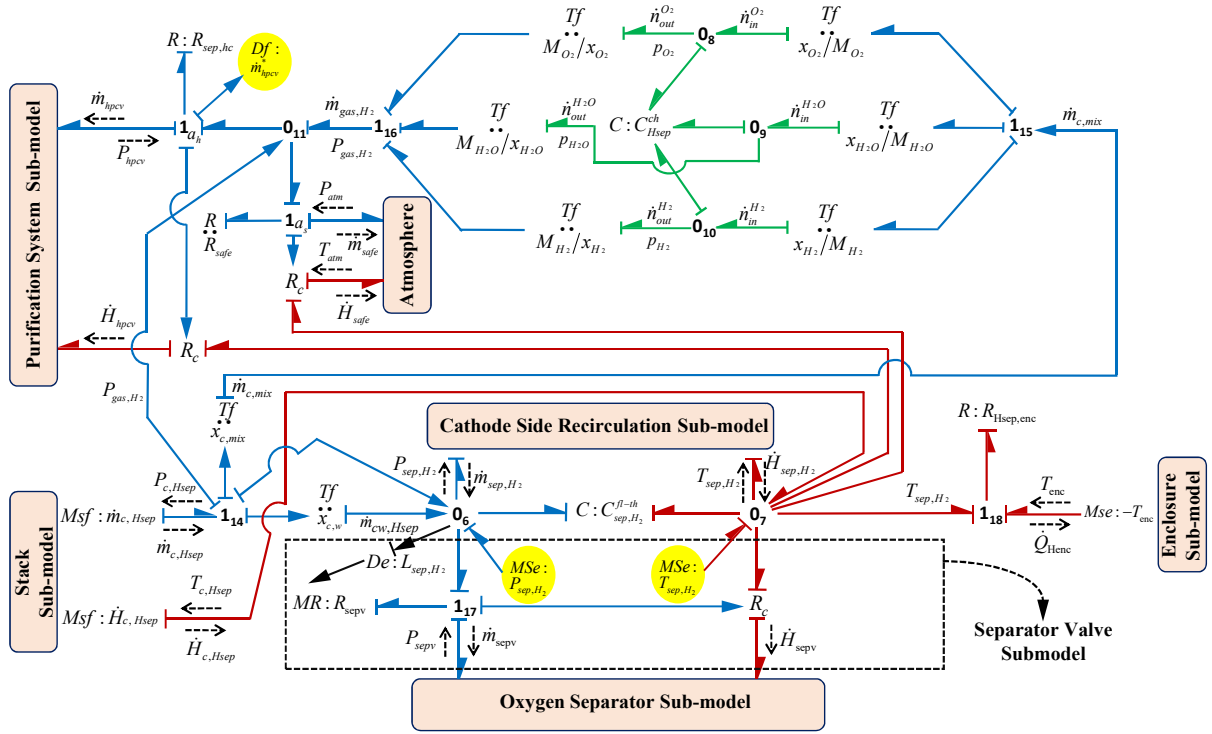
Figure 4.7: DBG model of the hydrogen separator

The FSM for the hydrogen separator is shown in the table 4.5. out of four, only two faults are isolable.

Table 4.5: FSM for hydrogen separator

Phenomenon↓	ARR→ Fault↓	r_1	r_2	r_3	I_D	I_C
Fluidic	$R_{sep,hc}$	1	0	0	1	1
	R_{sepv}	0	1	1	1	1
	R_{safe}	0	0	1	1	0
Thermal	$R_{Hsep.enc}$	0	0	1	1	0

4.2.4.4 DBG model for Oxygen Separator

The DBG model for the oxygen separator (shown in figure 4.8) is similar to that of hydrogen separator. Three sensors were considered in the similar configuration as that of hydrogen separator.

The residuals for the oxygen separator are

$$r_1 = \dot{m}^*_{gas,oc} - m_{gas,oc} = \dot{m}^*_{gas,oc} - \left(\frac{P_{gas,O_2} - P_{gas,oc}}{R_{sep,oc}} \right) \pm \Delta r_1 \tag{4.40}$$

$$r_2 = x_{aw}.\dot{m}_{a,Osep} + \dot{m}_{sep,v} + \dot{m}_{\text{tank}} - C^{fl}_{sep,O_2} \frac{\mathrm{d}P_{sep,O_2}}{\mathrm{d}t} - \dot{m}_{sep,O_2} \pm \Delta r_2 \tag{4.41}$$

$$r_3 = \begin{aligned} &C^{th}_{sep,O_2} \frac{\mathrm{d}T_{sep,O_2}}{\mathrm{d}t} + \dot{H}_{sep,O_2} - \dot{H}_{sepv} - \dot{H}_{\text{tank}} + \left(\frac{T_{sep,O_2} - T_{enc}}{R_{Osep,enc}} \right) \\ &+ \dot{m}_{gas,oc}.c_{P,fluid}.T_{sep,O_2} - \dot{H}_{a,Osep} \pm \Delta r_3 \end{aligned} \tag{4.42}$$
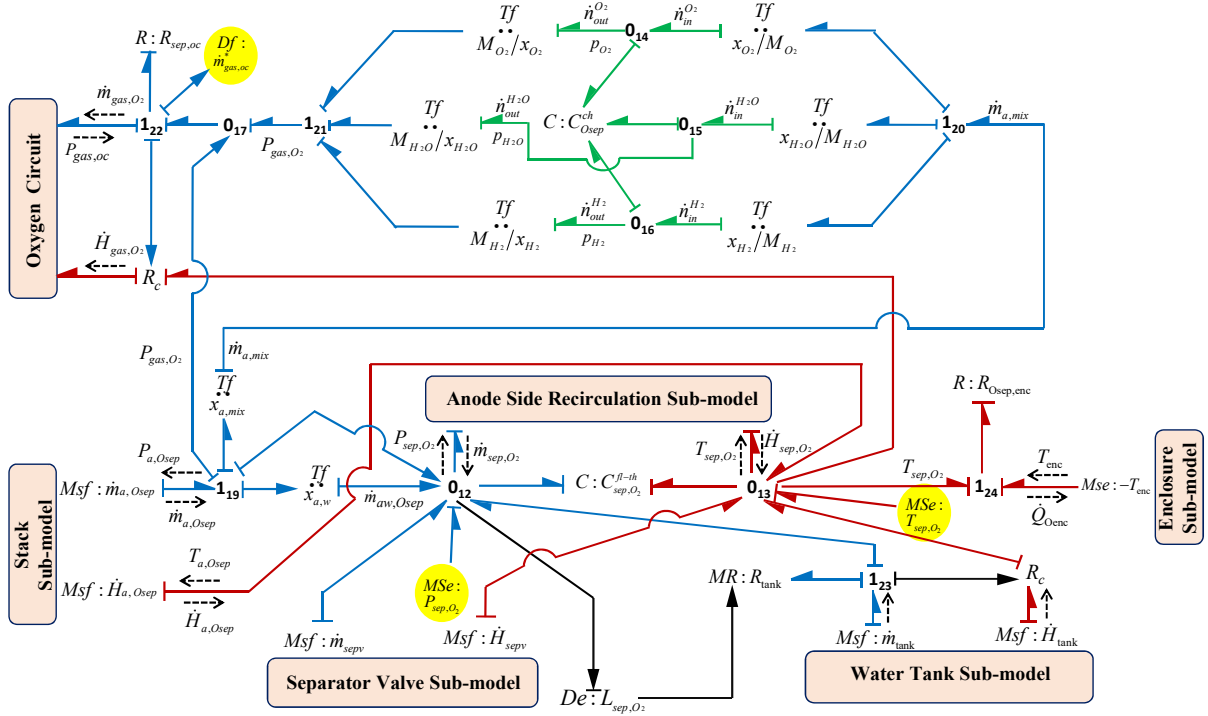
Figure 4.8: DBG model of the oxygen separator

Table 4.6: FSM for oxygen separator

Phenomenon↓	ARR→ Fault↓	r_1	r_2	r_3	I_D	I_C
Fluidic	$R_{sep,oc}$	1	0	0	1	1
Fluidic	C_{sep,O_2}^{fl}	0	1	0	1	1
Thermal	$R_{Hsep.enc}$	0	0	1	1	0
Thermal	$C_{sep,O2}^{th}$	0	0	1	1	0

The FSM for the oxygen separator is given in table 4.6.

4.2.4.5 DBG model for Purification Subsystem

The DBG model of purification sub system is shown in figure 4.9. Two sensors were considered to be installed in this subsystem. First sensor is the flow sensor installed at the outlet in order to detect the leakage or blockage fault. Second sensor is the temperature sensor to measure the temperature of the drying column.

The residuals for the purification subsystem are written as

$$r_1 = \dot{m}_{puri}^* - m_{puri} = \dot{m}_{puri}^* - \left(\frac{P_{Hgas} - P_{puri}}{R_{dry}} \right) \pm \Delta r_1 \tag{4.43}$$

$$r_2 = \begin{array}{c} C_{dry}^{th} \frac{dT_{dry}}{dt} + \left(\frac{P_{Hgas} - P_{atm}}{R_{exhaust}} \right).c_{P,fluid}.T_{dry} + \dot{m}_{puri}.c_{P,fluid}.T_{dry} \\ -\dot{H}_{ads} - \dot{H}_{hpcv} + \frac{T_{dry} - T_{enc}}{R_{dry,enc}} + \pm \Delta r_2 \end{array} \tag{4.44}$$

The FSM for the purification system is shown in table 4.7.
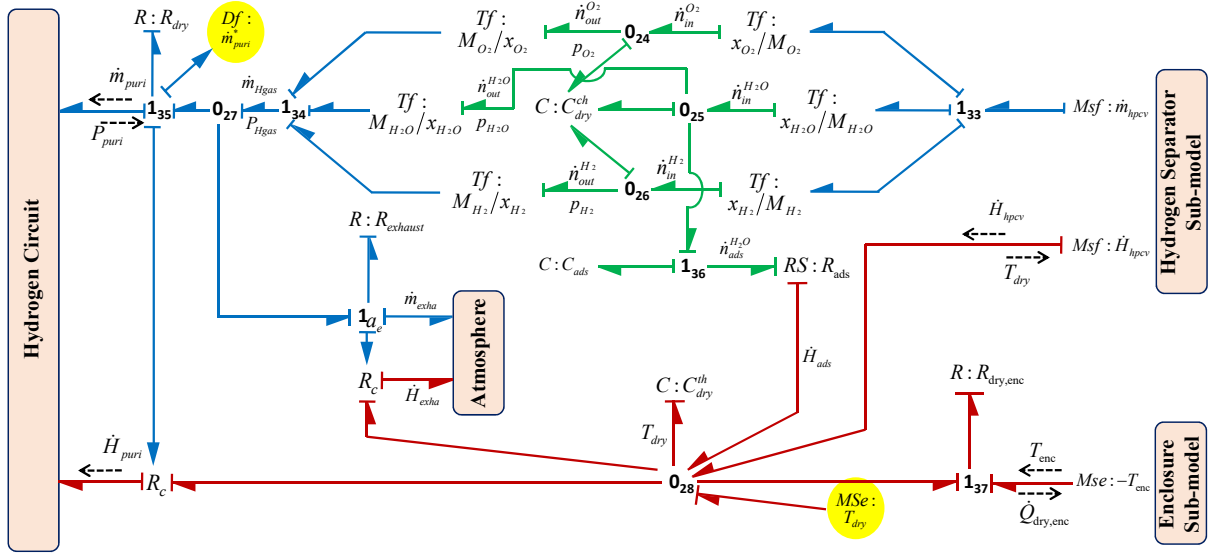
Figure 4.9: DBG model of the purification subsystem

Table 4.7: FSM for purification subsystem

Phenomenon↓	ARR→ Fault↓	r_1	r_2	I_D	I_C
Fluidic	R_{dry}	1	0	1	1
	$R_{exhaust}$	0	1	1	0
Thermal	C_{dry}^{th}	0	1	1	0
	$R_{dry,enc}$	0	1	1	0

4.2.4.6   DBG Model of System Enclosure

The DBG of the system enclosure is shown in figure 4.10. A temperature sensor is considered in the enclosure in order to measure the interior temperature. It is assumed that the temperature is homogeneous. The fault may occur due to the failure of the fan or clogging of the ventilation holes. Both faults will result in the increase of the temperature. The residual for the concerned system is written as

$$C_{enc}^{th}\frac{\mathrm{d}T_{enc}}{\mathrm{d}t} + \dot{m}_{fan}.c_{P,air}.T_{enc} + \left(\frac{T_{enc} - T_{atm}}{R_{enc}}\right) - \dot{Q}_{sbs} - \dot{m}_{fan}.c_{P,air}.T_{atm} \tag{4.45}$$

The FSM for the system enclosure is shown in table 4.8.

Table 4.8: FSM for system enclosure

Phenomenon↓	ARR→ Fault↓	r_1	I_D	I_C
Thermal	C_{enc}^{th}	1	1	0
	R_{enc}	1	1	0
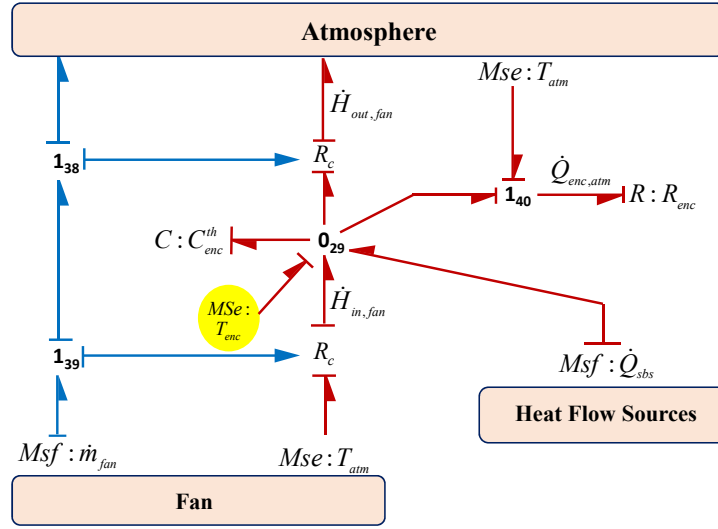
Figure 4.10: DBG model of the system enclosure

4.3 Conclusion

Model-based robust diagnosis was presented in this chapter. The modular approach that was used to develop the generic dynamical model of the PEM water electrolyser was also adapted in the diagnosis of PEM water electrolyser. The DBG models of the components of the PEM electrolyser were developed and the structural analysis was performed to know which faults are linked with physical interpretation of model and known patterns of degradation and are detectable and isolable. The diagnosis results for both offline and online diagnosis are presented in chapter 5.

Contents

This chapter focuses on the implementation of the model developed in chapter 3 and diagnosis algorithms developed in 4 to a laboratory scale single cell PEM electrolyser powered by solar and wind energy. The model was first validated and then utilised for the performance simulations. The diagnosis algorithms were tested offline and then incorporated into a supervision platform developed for the experimental test bench under consideration.

5.1 Experimental Setup

The experimental setup utilized for the present study was commercially supplied by the Heliocentris®. It consists of a laboratory scale, commercial, single cell PEM electrolyser of 300W connected to a hybrid multi-source platform as shown in figure 5.1.
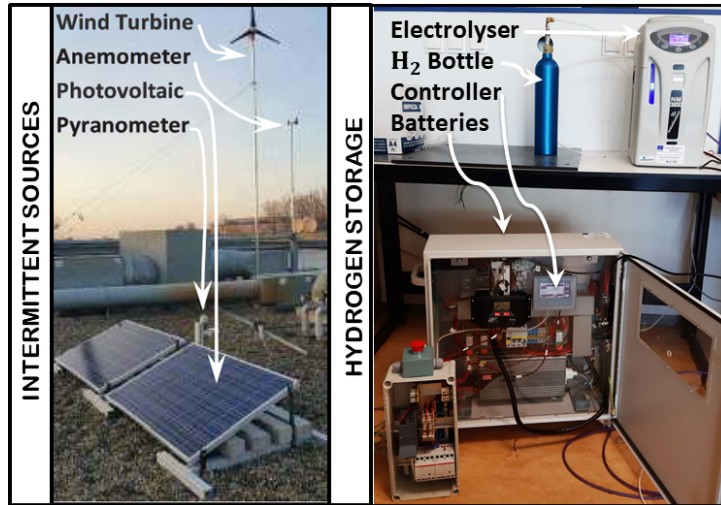
Figure 5.1: Experimental platform of the PEM electrolyser running on intermittent sources.

The platform is powered by two photo-voltaic panels (200W power per panel), permanent magnet type wind turbine (350-400W power) and two batteries (act as buffer with 55Ah capacity per battery). The PEM electrolysis cell is fed with water at the anode side only with a constant flow rate of 0.017 kg s^{-1} and the produced hydrogen (pressure range 1.4-10.7 bar) is stored in the metal hydride canister (H_2 bottle) of 760 standard liter capacity. The block diagram representation of the single cell PEM electrolyser is shown in the figure 5.2.

By default, one can only measure the hydrogen production rate of the electrolyser and the measurements from other sensors (such as internal and external pressure sensors) is used by
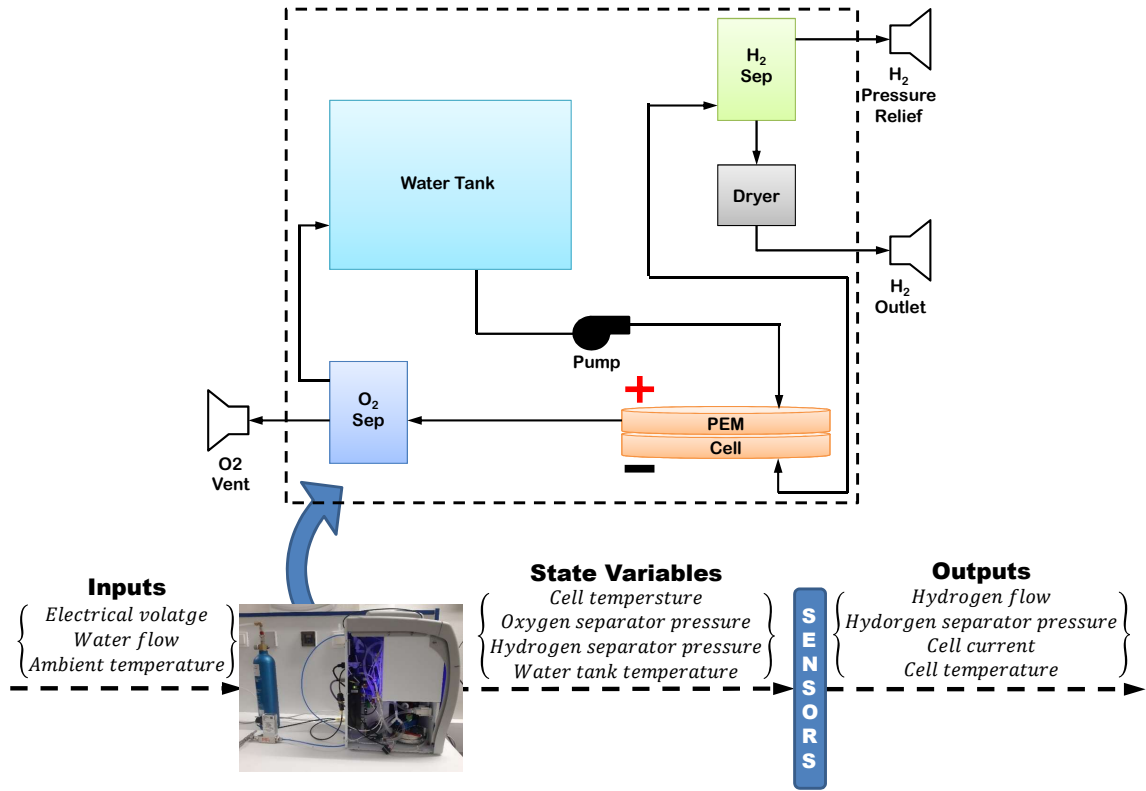
Figure 5.2: Block diagram representation of single cell PEM electrolyser.

the black box controller (to which we do not have an access) for the operation and safety of the system. Therefore, in order to acquire the data from the electrolyser and to increase the monitorability of the system, four sensors (flow sensor to measure hydrogen output flow rate, temperature sensor to measure water tank temperature, current and voltage sensors to measure electrical input to the cell) were placed in the electrolyser as shown in figure 5.3.
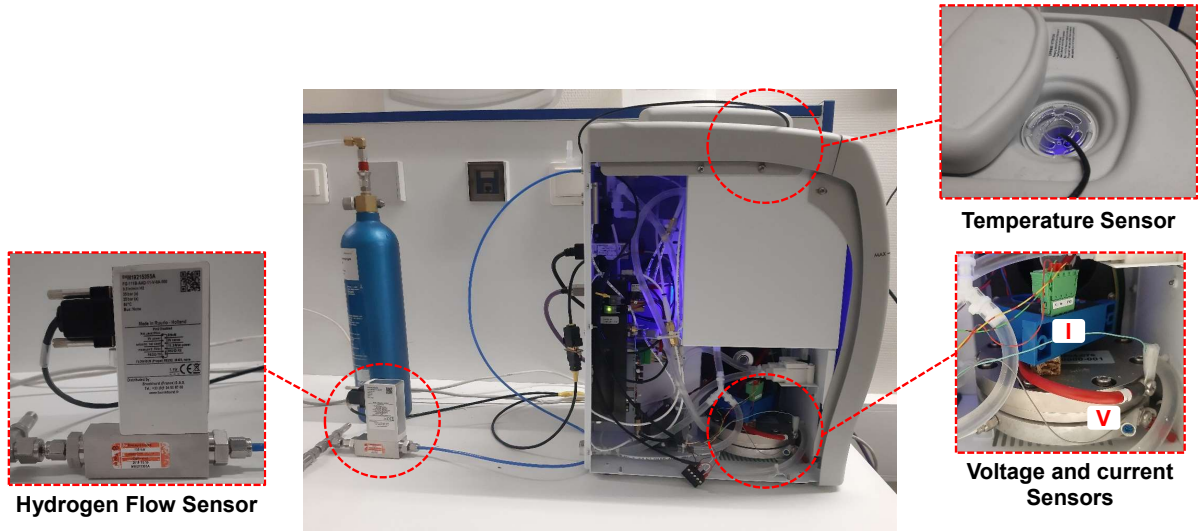
Figure 5.3: Positioning of the sensors installed.

The process for data acquisition is illustrated in figure 5.4. For the data acquisition, a PLC

was used to receive the analogue signals from the sensors and convert it into measurements. The measurements are then transmitted to the MATLAB® Simulink.
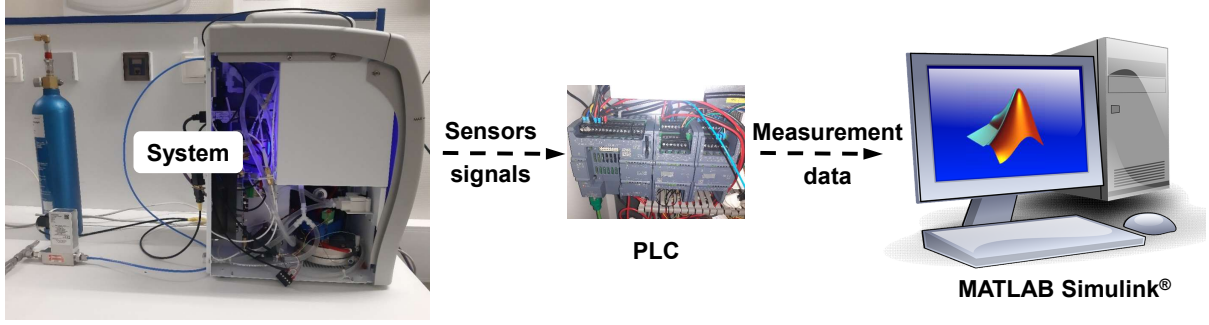
Figure 5.4: Data acquisition system.

5.2 Experimental validation and simulations of PEM electrolyser model

In order to reduce the complexity, only the model of the single cell PEM electrolyser was considered for the presented study and the intermittent sources were considered as an electrical source with signal noise (to represent intermittent nature). The model of the electrolyser was first tuned with the help of experimental data. The key parameters for the cell were identified
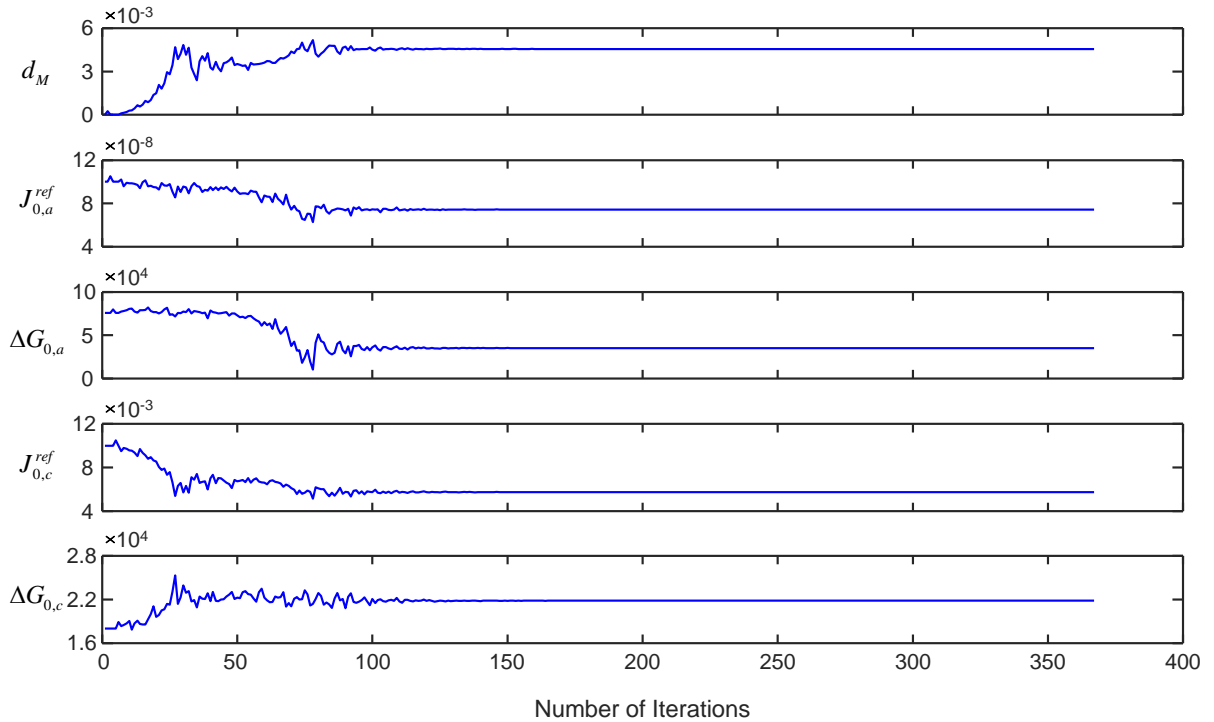
Figure 5.5: Parameter estimation for the sub-model of the stack.

using non-linear least square error optimization technique with the help of MATLAB's built-in function "Fminsearch". The objective it to find the values of d_M, $J_{0,a}^{ref}$, $\Delta G_{0,a}$, $J_{0,c}^{ref}$, $\Delta G_{0,c}$,

to minimize the difference between experimentally measured characteristic curve and the one generated by the model using equation 3.15. The estimation of these parameters is shown in figure 5.5.

The bounds for the parameters values are taken based on the values form the literature for better estimation [12, 15, 28, 202]. Other parameter values such as recirculation pump flow, height and cross-sectional area of hydrogen separator are taken based on the system specification provided by the manufacturer. The polarisation (characteristic) curve from the actual measurements and the one estimated using the developed model are shown in figure 5.6. The mean absolute percentage error between simulation and experimental data is found to be 4.8% which is reasonable and well within the acceptable limit for simulations and for the development of control and diagnosis algorithms.
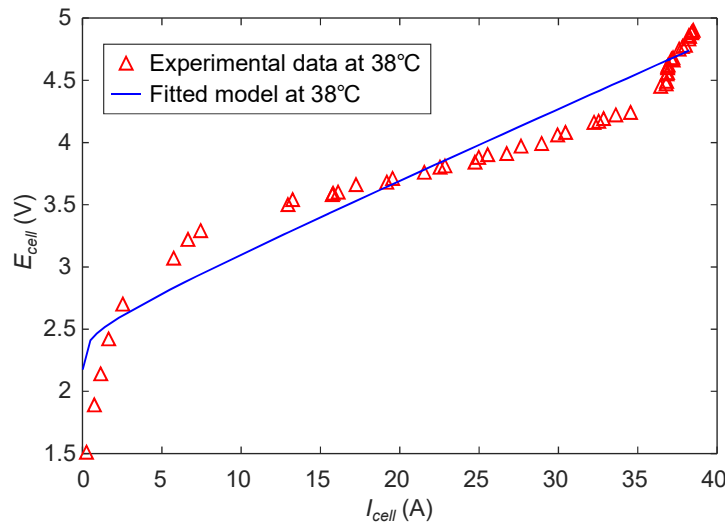
Figure 5.6: Comparison of experimental data and estimated polarization curve at 38℃.
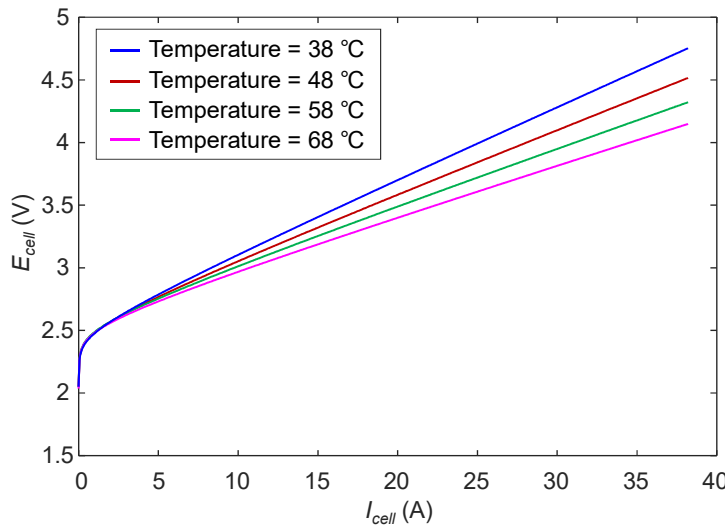
Figure 5.7: Simulation of polarisation curve for different temperatures.

Figure 5.7 shows the predicted characteristic curve at different temperatures. It can be seen that with the increase in the cell temperature the required cell voltage for electrolysis

decreases. The predicted performance is in good agreement with the expected behaviour of the electrolyser found in the literature [15, 28, 128]. In comparison, the model offers prediction as good as classical models but more scalable or physical is an asset.
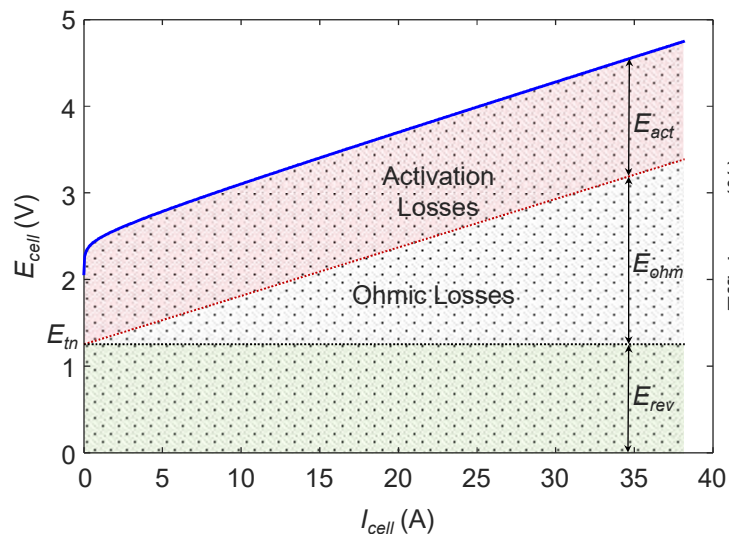
Figure 5.8: Contribution of different overvoltages in polarization curve.

Figure 5.8 shows the contribution of different overvoltages in the overall cell voltage. It can be seen that with increase in the current the ohmic losses increases linearly. The contribution of the activation losses in the overall cell voltage remains almost constant. The losses due to mass transportation is negligible for small electrolysis cells and hence it is neglected.

Figure 5.9 shows the variation of the cell efficiency with respect to the cell voltage.The efficiency of the cell is constant till the cell voltage is less than thermo-neutral voltage. Once the cell voltage exceeds the thermo-neutral voltage, the efficiency decreases continuously. However, the efficiency at the system level can be calculated as discussed in section 3.3.2, but, due to the limited number of the sensors placed in the experimental platform, the power consumed by different auxiliaries cannot be measured. Hence, the system level efficiency is not shown.
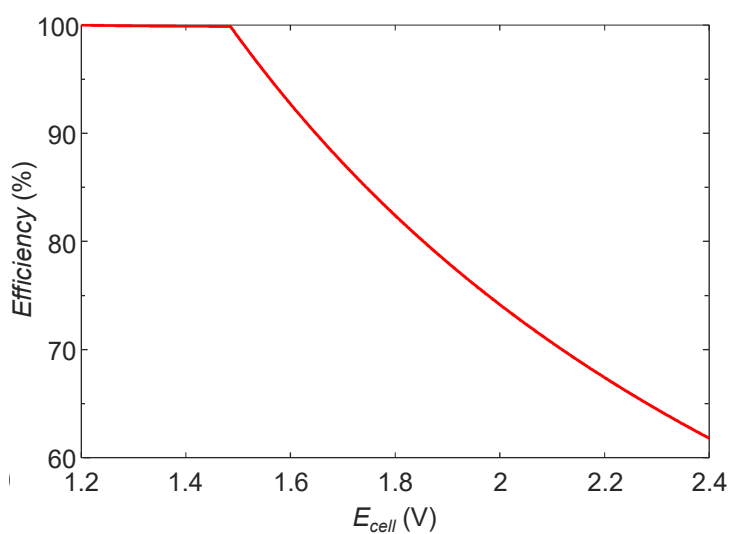
Figure 5.9: Efficiency vs cell voltage for PEM electrolysis cell

95

Figure 5.10 shows the prediction of the temperature evolution of the cell from the thermal sub-model. The temperature starts rising from the ambient temperature and attains a constant value when the steady state of the operation is reached.
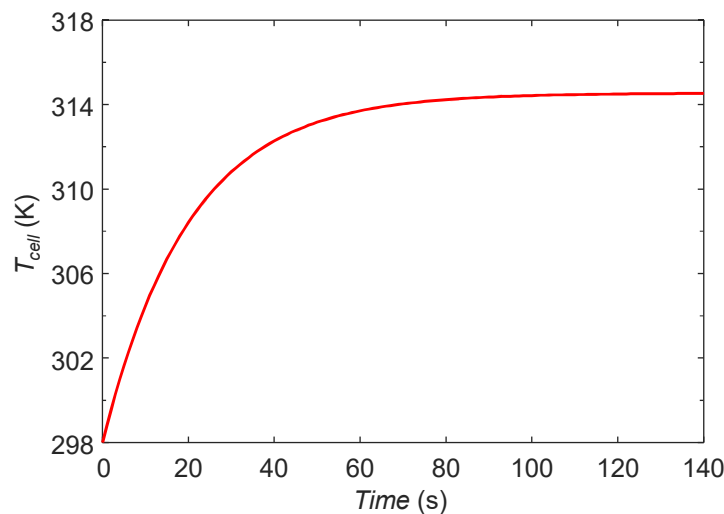
Figure 5.10: Predicted temperature evolution of PEM electrolysis cell

To predict the performance of the electrolyser powered by intermittent sources, a simulation of the electrolyser directly powered by the combination of solar and wind energy is performed. Figure 5.11(a) shows the total power fed to the cell by the converter and this figure also shows the individual contribution of each intermittent source. Figure 5.11(b) shows the input voltage to the electrolyser model with the objective of achieving high rate of hydrogen production and maintaining the hydrogen output pressure at 11 bars.
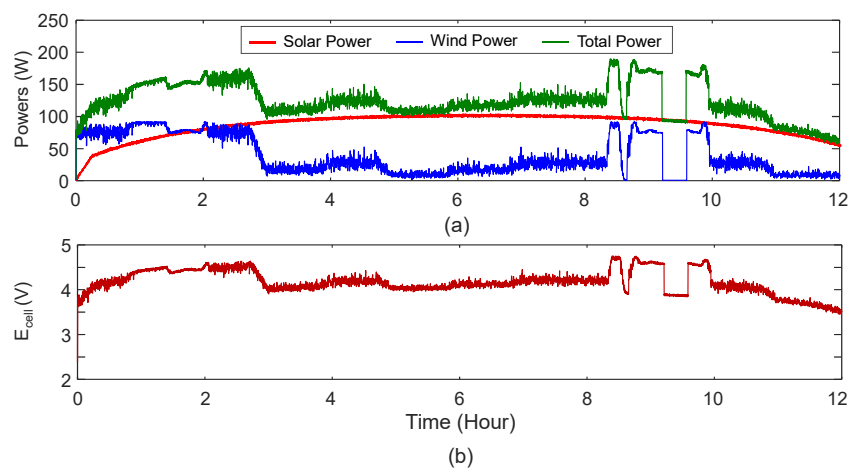
Figure 5.11: (a) Powers consumed by the cell for 12 hours run and (b) Input voltage for the cell running on intermittent sources.

Most of the part of this voltage is lost due to overvoltages. Figure 5.12 shows the contribution of each overvoltage and reversible voltage in the overall cell voltage for 12 hours operation.

The current drawn by the cell and the corresponding hydrogen production are shown in the figures 5.13(a) and 5.13(b), respectively. It can be seen from the figure 5.13(c), the efficiency of the cell is about 40%. This is due to the fact that the current electrolyser is designed to run at
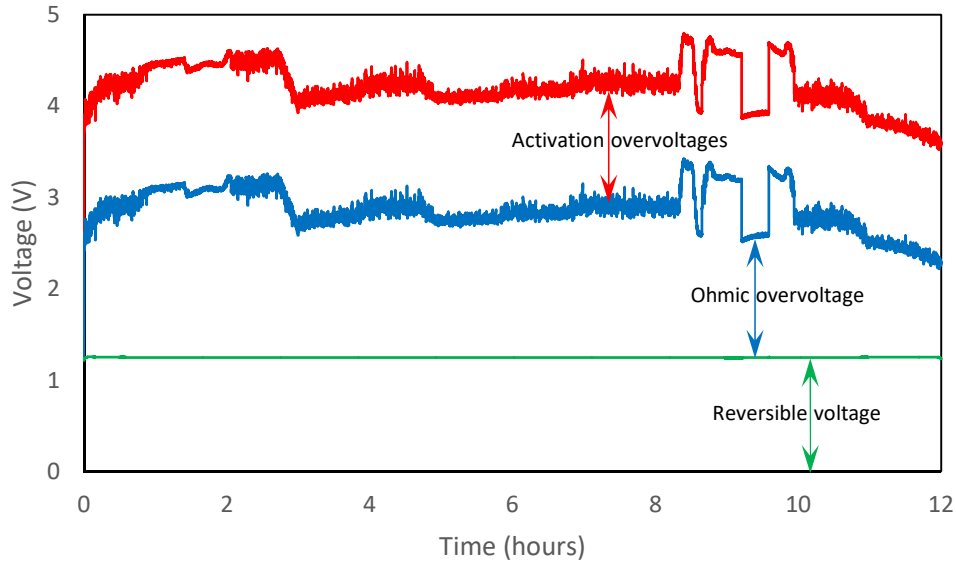
Figure 5.12: Contribution of different overvoltages in cell voltage.
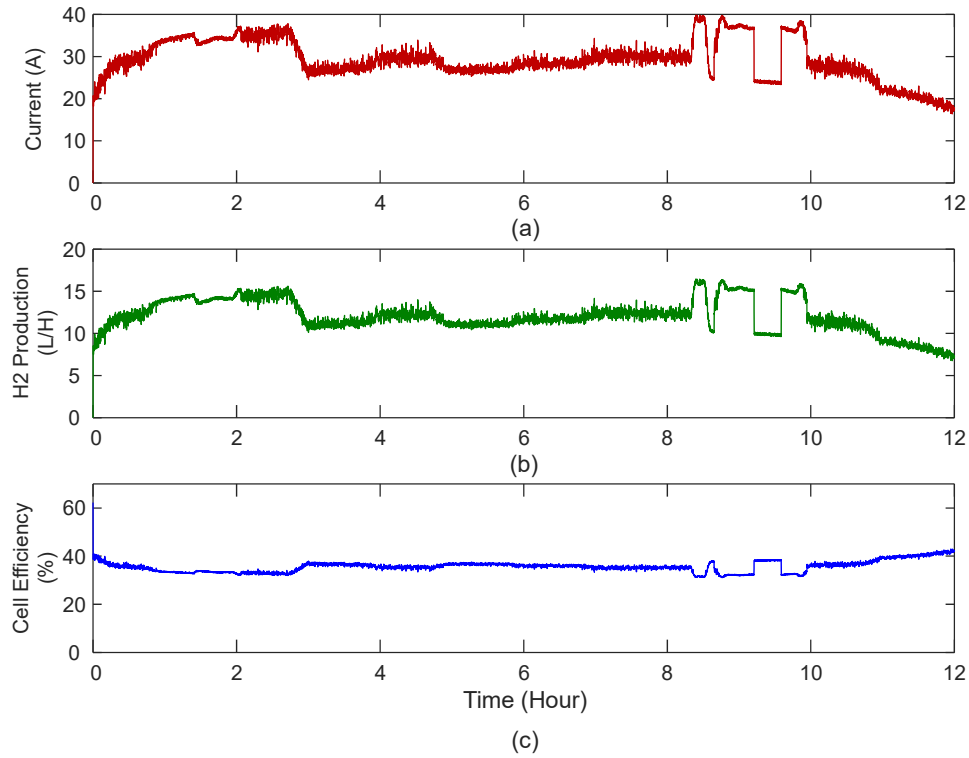
Figure 5.13: (a) Current drawn by the cell during 12 hours of operation, (b) hydrogen production and (c) corresponding cell efficiency for the cell.

particular set point with the objective of delivering continuous hydrogen flow at higher rates. This is achieved by running the electrolyser at higher voltage (around 4 to 5V) which results in reduced efficiency. The predicted cell temperature profile for considered 12 hours operation is shown in figure 5.14

The estimated pressure on anode side (P_ano) and cathode side (P_cat) are shown in figure

97
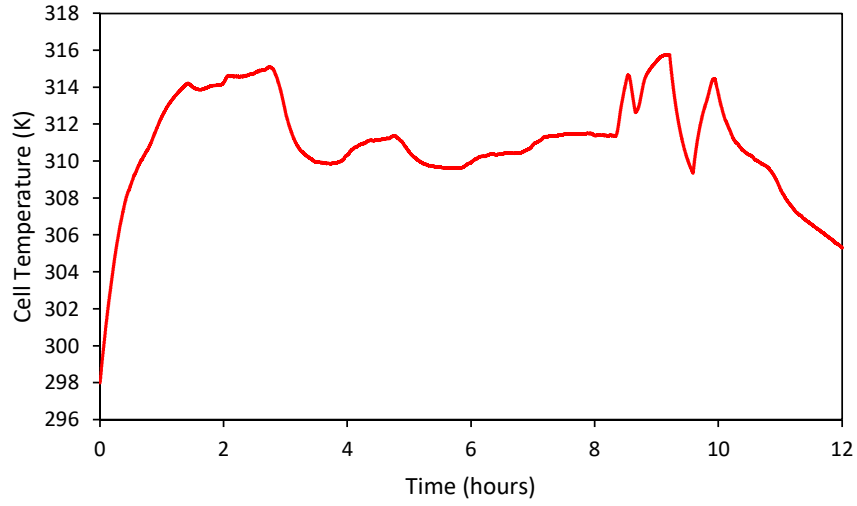
Figure 5.14: Evolution of temperature of the cell during 12 hours of operation.

5.15. The anode side pressure is maintained around atmospheric pressure. The cathode side pressure is maintained around the set point of 11 bars with the help of the on-off valve.
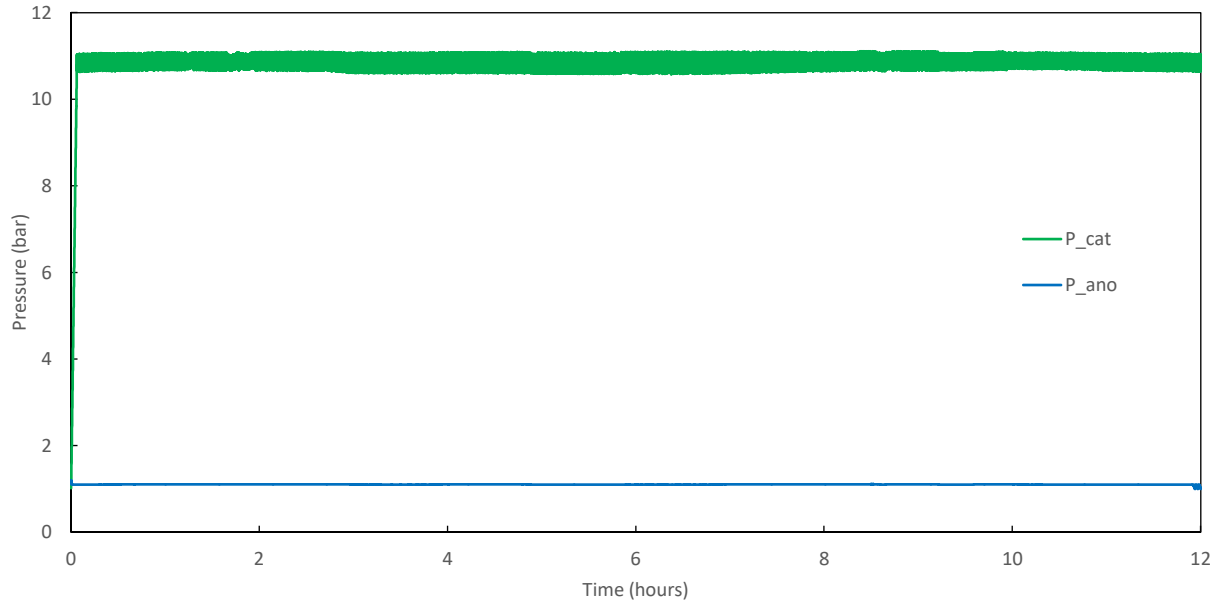
Figure 5.15: Pressure at anode and cathode for 12 hours operation.

The evolution of the pressure of hydrogen storage bottle is shown in figure 5.16. The internal volume of the storage bottle was considered to be 38 liters and it was assumed that the filling takes place at constant ambient temperature.

In order to improve both efficiency and hydrogen production rate, the number of electrolysis cells should be increased. In the current study, intermittent power is directly taken as an input for the model to predict the electrolyser's performance. However, in real electrolysis system running on RES, the controller with buffer power source (battery) with operating mode management is always present [17]. This is important to maintain the constant input power to the cell in reference to the set point for stable operation and to avoid faster degradation of the cell membrane.
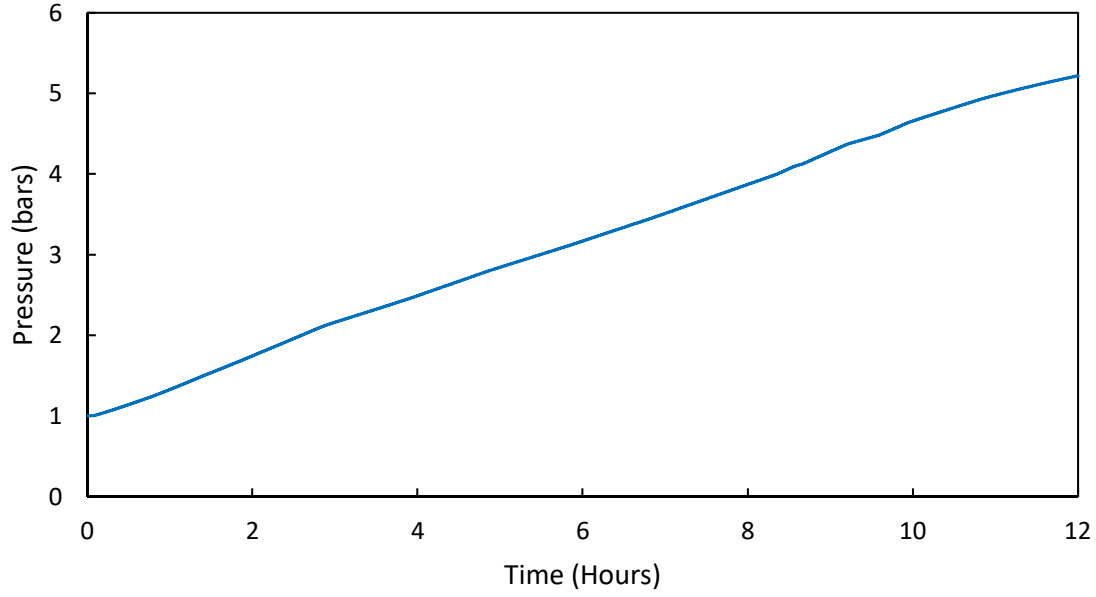
Figure 5.16: Evolution of the pressure of hydrogen storage bottle during 12 hours operation.

5.3 Offline diagnosis of the PEM electrolyser

For testing the FDI developed in 4.2, three parametric faults in the electrolysis cell were considered. Simultaneous occurrence of multiple faults is a very rare event but the sequential fault is very common in the industry. Therefore, it is assumed that these faults occurred one at a time. To perform the FDI at the subcomponent level, DBG model of electrolysis cell was considered. To emulate the actual system, the model developed in 3 was used under MATLAB® Simulink environment as shown in figure 5.17. This allows the possibility of testing different fault scenarios without endangering the actual system.
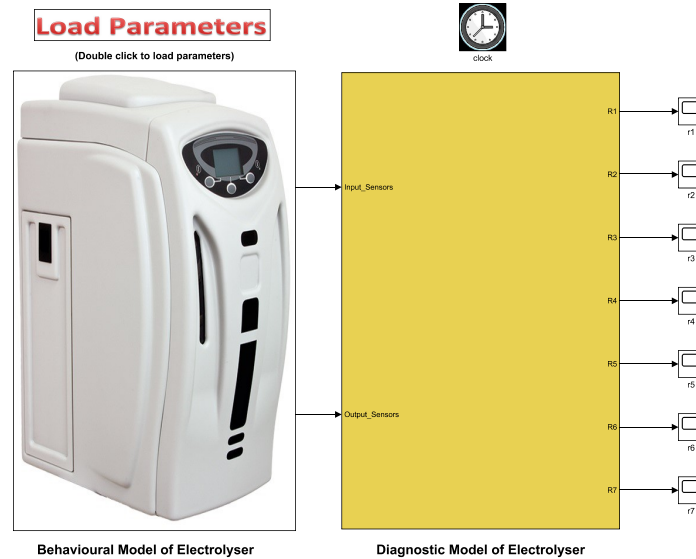
Figure 5.17: Offline diagnosis in MATLAB® Simulink environemnt

Faults were injected in the model itself to test the effectiveness of the developed FDI. As the fault were injected in the model, it is possible to revoke failures, not only change in a resistance

but even sometimes disappearance of an eltment. The first fault considered is a membrane fault which causes a 50% increase in R_{ohm}. It occurred abruptly between 50 to 100 seconds. The second fault is also assumed to be abrupt with the increase of 20% in the thermal resistance R_{st} of the cell that causes overheating of the electrolysis cell. This fault is injected from 200 to 250 seconds. The third fault is considered due to the oxygen crossover from anode to the cathode side. This fault is assumed to appear gradually between 300 to 350 seconds and causes changes in $R_{diff,O2}$.

Figure 5.18 shows the plots for the residuals monitored during the simulation. It can be seen from this figure that all the faults have been successfully detected.

In order to isolate the faults, the coherence vector is checked at the time at which the faults occur and the value of residual/s crosses the thresholds. The overshoot of the residuals r_1 and r_6 is due to the initial conditions taken to run the model. At time 50 seconds, it can be seen that r_1 and r_6 crosses thresholds. Thus, the coherence vector becomes [1,0,0,0,0,1,0]. Now comparing it with the FSM from table 4.2 shows that its signature matches with that of the first four faults as they all have same signature. Therefore, the fault was successfully detected, but cannot not be isolated as the similar fault indication could have been the result of any of first four faults. In order to make the fault isolable, either additional sensors are needed to be placed or estimation technique could be used to calculate the parameter values from the residual to compare it with the known good parameter values.

Similarly, at 200 seconds, when second fault occurred, the coherence vector is [0,0,0,0,0,1,0], which is unique when compared to the FSM. Therefore the second fault can not only be successfully detected but also be isolated from other faults.

Although, the third fault starts appearing gradually at 300 seconds, the values of the r_2 and ARR_3 cross the thresholds at 304.8 seconds. The coherence vector at this time is [0,1,1,0,0,0,0]. When it is compared with the FSM, it can be seen that its signature matches with more than one fault. Thus, is it not possible to isolate this fault, but, after estimation of the suspected faults using residuals values, the true fault can be isolated, which is the fault in $R_{diff,O2}$. Using the similar approach, the offline diagnosis for all the subcomponents of the PEM electrolyser can be performed using DBG models proposed in 4.2.4.

5.4 Online diagnosis

To implement the developed algorithms on the experimental platform, a GUI (shown in figure 5.19) was developed with the help of team members of PERSI. The GUI allows the monitoring of various components of the HMP including the electrolyser.

For performing the online diagnosis, the real-time measurements of the system is fed to the DBG model in order to compute the residuals and these residuals are monitored for fault detection. It is not easy to introduce an actual fault in the system as it can cause permanent damage to the system or could be hazardous to the surroundings, no actual, component level fault could be introduced into the system. A fault was emulated (as shown in figure 5.20) in the real system by manually turning off the outlet Valve without stopping the hydrogen production.

This disrupts the hydrogen flow from the electrolyser to the bottle. This fault directly affects the cell voltage and this can be seen from the monitoring of the residual r_1 obtained in 4.2.1 for electrochemical part as shown in figure 5.21.

The valve was closed at 45 seconds. The residual start moving towards lower threshold limit and crosses the threshold at 50 seconds. At 65 seconds the valve is opened again and the residual goes back within threshold limits at 70 seconds. The same fault is re-injected at 120 seconds and removed at 135 seconds. The successful detection of the fault can be seen from
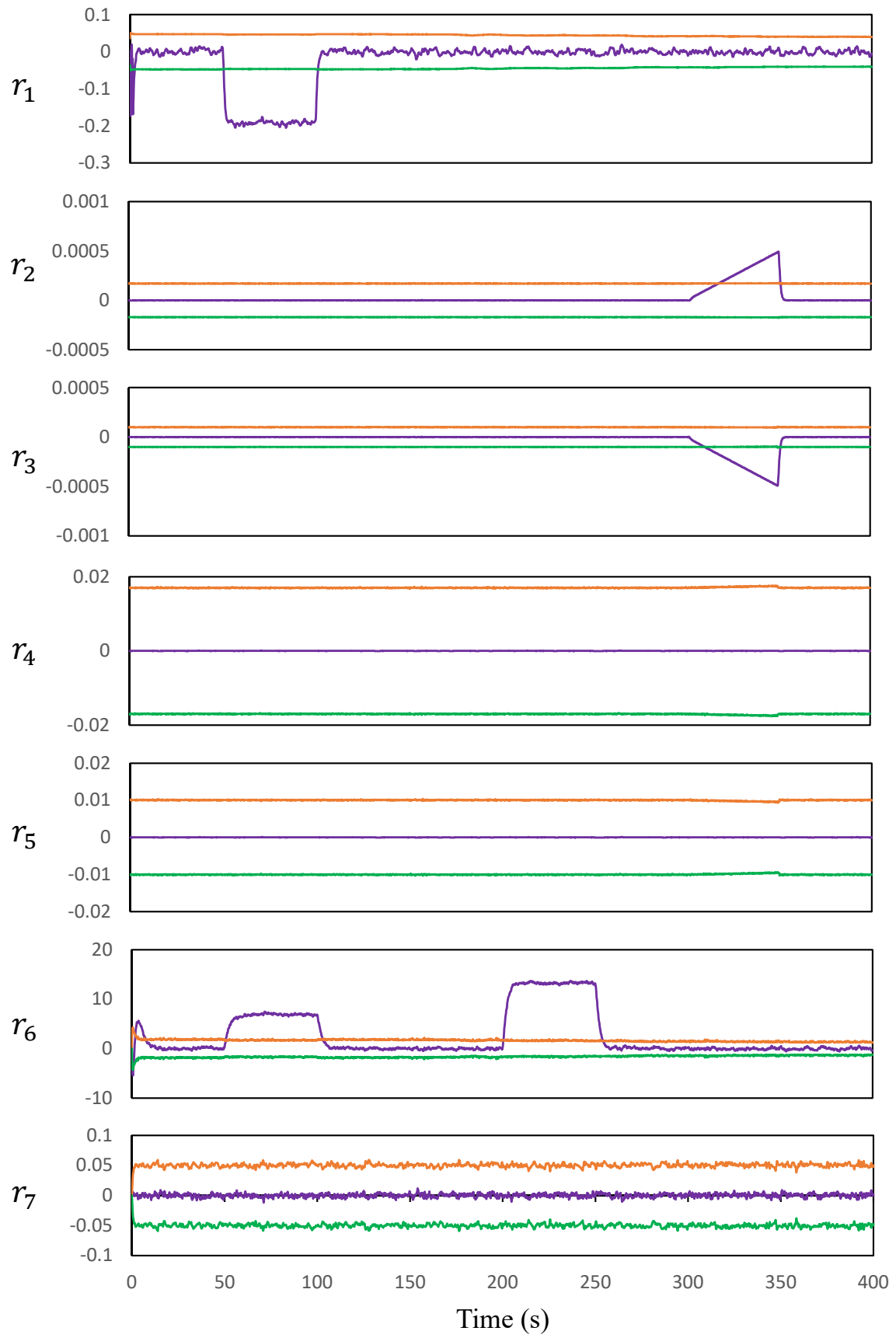
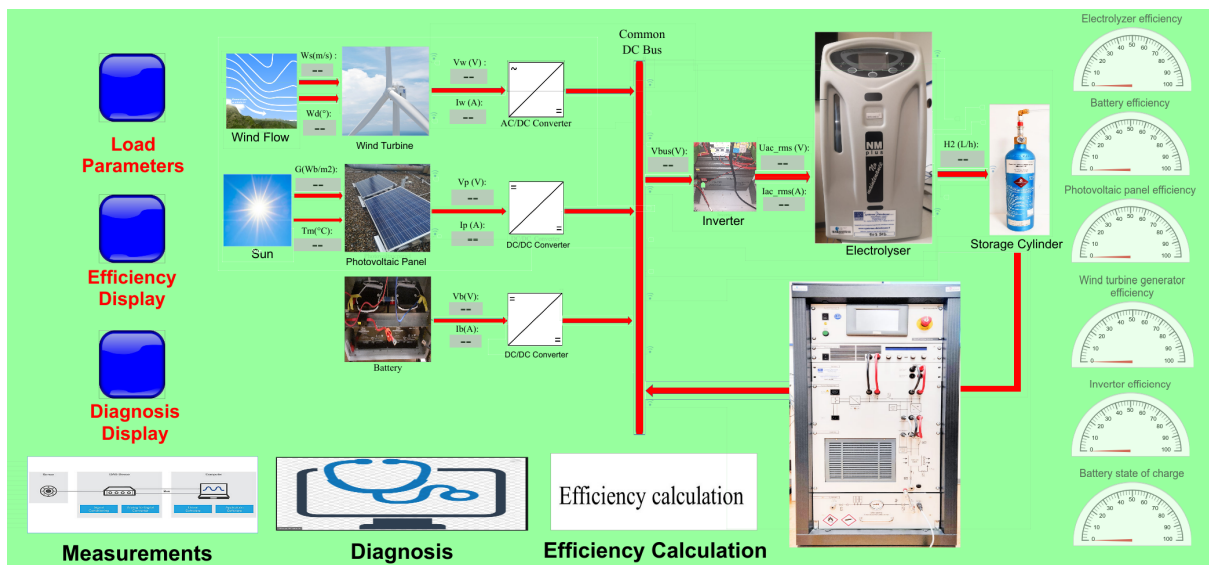Figure 5.18: ARRs monitoring and respective thresholds

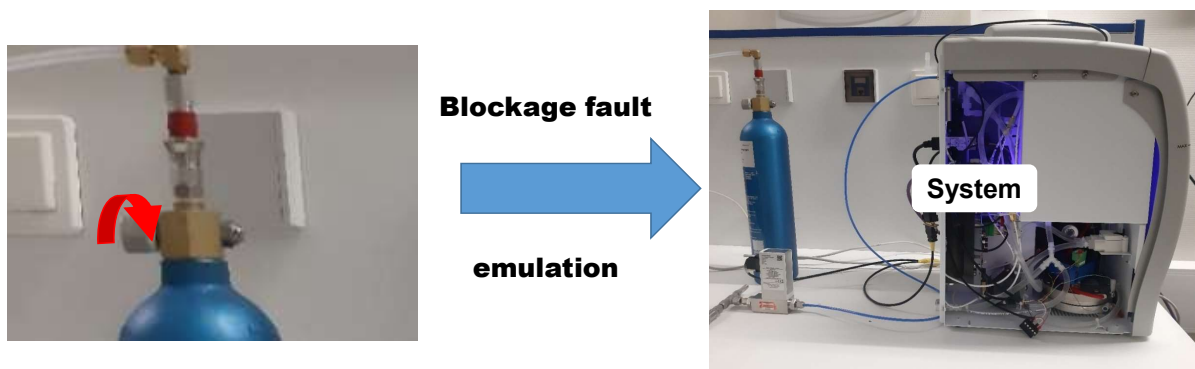Figure 5.19: GUI for HMP supervision

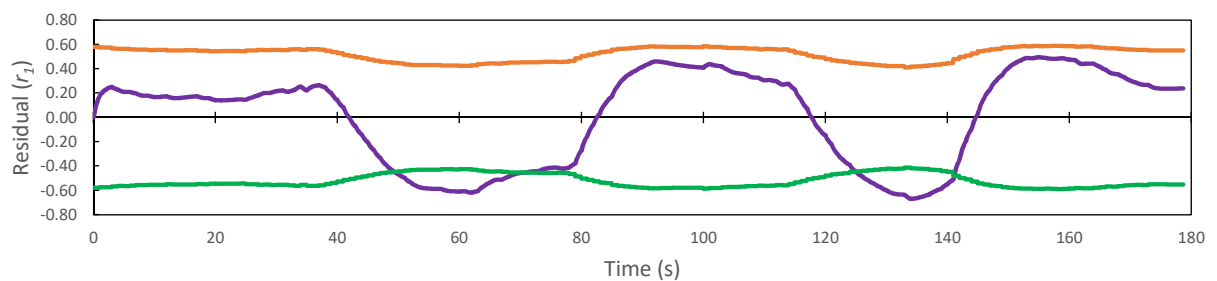Figure 5.20: Emulation of blockage fault in the electrolyser

Figure 5.21: Online blockage fault detection

the figure 5.21. Although, the fault occurred in a hydrogen purification part, but the effect was seen on the electrolysis cell itself. This is due to the coupling of different subsystems. The further diagnosis can be carried out using modular approach if the affected subsystem can be decoupled as mentioned earlier by knowing the good inputs and outputs of the subsystem. Once the affected subsystem is identified. The fault isolation could be performed.

5.5   Conclusion

The generic dynamic model of PEM electrolyser was adapted for a commercial laboratory scale electrolyser running on intermittent sources. The model parameters were calculated using non-linear optimization technique. The model was then validated against experimental data. simulations were then performed for the electrolyser running on intermittent sources for 12 hours. Offline diagnosis test was also performed for the developed DBG model in order to check the effectiveness of the diagnosis algorithms. The results have also been published in an international conference European Control Conference (ECC 2021). A GUI was also developed for the supervision of the experimental setup. To test the online diagnosis, blockage fault (interruption of hydrogen flow) was emulated in the actual system and was successfully detected by the developed diagnosis algorithms.

General Conclusion and outlook

Contents

6.1 General Conclusion

GH_2 has emerged as a strong candidate for the storage of surplus electrical energy available from RES such as solar and wind. It aligns perfectly with the global need of limiting the green house effect by reducing the use of carbon based fuels. GH_2 is the most promising energy vector for the future as it is pollution free and allows better transport and long term storage in the pressurized containers. The intermittent nature of RES, however, degrades the performance and affects the dynamic operation of the electrolysers. Therefore, it becomes necessary to study the coupling between the electrolysers and the RES in order to improve the performance and reliability of the equipment. The work presented in this thesis was funded by the E2C project under European Interreg 2-Seas program (subsidiary contract nr. 2S03-019). The project focuses on the development of two Power-to-X technologies to produce fuel and high value chemical from the green electricity generated through RES.

6.1.1 Overview of the Literature and Main Contributions

The key focus of this work was to develop a dynamical model for the PEM electrolyser that can not only be used for the performance analysis of the PEM electrolyser running on RES, but also for the design of online supervision systems for the detection and isolation of faults. It was observed from the literature survey that most of the models already developed are equation based, static and primarily focuses on the phenomena understanding and therefore cannot be used for the performance study in dynamic operations. There also exist dynamical models for PEM electrolysers, but very few of them have considered the effects of the BoP (auxiliaries) on the overall performance of the system. Further, very few of them have addressed the coupling between the electrolyser and RES. A notable work was presented by Pierre Olivier in 2017 in the form of a dynamical BG based model of an industrial scale PEM electrolyser. The model included the BoP of the system and was capable of reproducing the dynamical behaviour of the industrial scale PEM electrolyser. The model was highly complex, non generic and was not tested for the smaller electrolysers. The model also lacked the calculation of the efficiency of the system which is a great performance indicator. The model was also not exploited for the development of supervision algorithms for the fault detection and isolation for the electrolysers and needed improvements in terms of BG modelling. The look into the literature also showed that there is not much work done on the diagnosis and health management of PEM electrolysers. The most of the work has been done for the diagnosis degradation study of the cell/ stack using offline methods that involves the use of expensive instruments. Most of the time the electrolysis cell and stack is disassembled for visual inspection and performing microscopic analysis. A

negligible work was found on the model based diagnosis of PEM electrolysers that could be used for the detection of the faults in real-time.

A generic dynamical multi-physics model for the PEM electrolyser was proposed in chapter 3 based on the BG approach. The modelling of the key components of the electrolyser was carried out in the form of capsules (sub-models). These capsules are based on the physical structure of the component and therefore have certain inputs and outputs and can be connected to other capsules in the similar way the actual component is connected to other components physically. These capsules are assembled based on configuration of the electrolyser in order to obtain the global model. This allows the model to be adapted for different configurations of PEM electrolysers without starting from the beginning. New capsules can also be added, if required, in order to represent the components not presented in this work. Modification of the capsules is also possible in order to capture more accurately the behaviour of the component without disturbing the global model. The generic nature of the model allows it to be sized and scaled to fit different sizes of PEM electrolyser ranging from laboratory scale to industrial scale. The model also incorporates the calculation of system efficiency for the performance analysis. As the modelling is based on the exchange of power between different components/ subsystems, therefore the instantaneous efficiency of any component can be estimated. The developed model was converted into block diagram in MATLAB$^{®}$ Simulink for implementation. The model was then validated experimentally on a single cell PEM electrolyser powered by a HMP that utilizes the solar and wind power. The simulations were then carried out to estimate the performance of the considered PEM electrolyser for 12 hours operation when it is directly powered by solar and wind energy. This work has been published as a journal paper in MDPI Energies. In collaboration with University of Exeter under the framework of E2C project, the model was adapted to represent and study the performance of an AEM electrolysis cell, which has a similar configuration and architecture as that of small PEM electrolyser (shown in appendix A). The results were presented in Mediterranean Conference on Control and Automation (MED 2020).

Thanks to the BG approach ,because of its specific causal and structural properties, it is possible to use the presented model for the development of control, diagnosis and prognosis algorithms. Therefore, a robust fault diagnosis with respect to parameter uncertainties based on the developed model was also presented in this work in chapter 4. Based on the developed model, the DBG models for all the subsystems of the PEM electrolyser were proposed. Modular approach in diagnosis allows it to be used for different configurations of the PEM electrolyser. The developed DBG model can also be used for structural analysis of the configuration which helps in deciding if additional sensors placement is required. To make the diagnosis robust LFT BG was used to calculate the adaptive thresholds. This helps in avoiding the false alarm generation due to the presence of parametric and measurement uncertainties. The proposed diagnosis approach allows a multilevel diagnosis, by performing the diagnosis for the whole system in order to detect the fault or abnormality at the system level. Due to modular approach used for the diagnosis also, diagnosis for the subsystem alone can be performed if the subsystem can be decoupled from the system. The decoupling is possible if the inputs and outputs of the subsystem are known or measured. The proposed diagnosis algorithm was tested offline for testing its effectiveness for detecting the faults in the PEM electrolysis cell. The developed model was used to simulate the behaviour of the system and the faults were injected into the model itself. This provides a safe testing environment for the diagnosis algorithms without causing any damage to the actual system which could be sometimes irreversible and expensive. The faults injected in the virtual system were successfully detected. These results were published in a conference paper in European Control Conference (ECC 2021).

The developed model and diagnosis algorithms were used to develop a GUI for online monitoring of the single cell PEM electrolyser running on solar and wind energy through a HMP.

As the platform and the electrolyser were commercially acquired, it was not possible to gain access to the controller of the system in order to access data from the senors of the platform and electrolyser for monitoring. Therefore, additional sensors were placed in the electrolyser to increase the monitorability and a PLC based data acquisition was implemented. As, it is very difficult to introduce actual faults in the system without causing permanent damage, only one fault was tested for online fault detection. The blockage fault was introduced by closing the outlet valve of the electrolyser manually while the system was operational. The fault was successfully detected online.

6.1.2 Limitations of the proposed work

A number of limitations were identified for the proposed work. The developed PEM electrolyser model still depends on the parameter fitting in addition to the physical parameters in order to represent the behaviour of the system. This makes the model experimental data dependent for representing the system behaviour. The presented model does not take into account the degradation of the components. This limits the use of the developed model for long term (say months or years) performance prediction accurately. The capsules are needed to be assembled manually according to the configuration of the electrolyser which needs some understanding of the system inputs and outputs and interaction between different components. Therefore, certain skill set is required in order to adapt the model to different configurations. The developed model cannot capture fast dynamics of the system as the fast dynamics were neglected during the modelling when compared to slower dynamics. As mentioned previously, the model can be used for PEM electrolysers of different scale and configuration, but the model was not validated against any other electrolyser of different scale or configuration. The validation of the sub-models was not performed due to lack of sensors in the actual system.

The proposed diagnosis also have its limitations. The system parameter values are required to perform the diagnosis effectively. While developing the DBG models, different sensors were assumed to be placed in the actual system in order to detect different faults. This might not be true for actual system and the actual system may lack those sensors. Also, all the faults that were considered while developing the diagnosis algorithm are not isolable (this is however the hardware limitation of the system due to lack of sensors). Online validation for all the faults was not performed as it is very difficult to introduce the fault into the actual system safely. These limitations have set the path for the future work.

6.2 Future Perspectives

Based on the limitations of the presented work in previous section, there is a lot of possibilities for improvements and new applications for the proposed work. These possibilities have been summarised in the form of a list below

- Proposed PEM electrolyser model

    1. An attempt can be made to make the model dependent on the physical perimeters only, thus, eliminating the need of parameters fitting based on experimental data.
    2. The degradation of the components can be modelled into the capsules in order to simulate the long term operations more accurately. The model will also be then helpful for the techno economic analysis.
    3. A new interface can be developed in which the user enters the piping and instrumentation diagram of the system and the capsules gets automatically connected in the required configuration.

4. Detailed modelling of the subsystem could be performed in order to have various versions of the capsules which can be selected as per the requirement of the simulation being done. For example, certain phenomena can be neglected for smaller electrolyser but not in the large electrolysers. Therefore, the capsule of the required complexity can be selected.

5. The model can be used to develop a digital twin, e.g. Neural Networks. The digital twin can be then used for the testing and designing of the other components such as power electronics or renewable energy sources without investing into an actual electrolyser.

6. The model validation for scale-up can be performed-using large electrolysers.

7. Coupling of the PEM electrolyser with chemical plants could be studied using the developed model. Once such application can be seen in the E2C project where the hydrogen produced by the PEM electrolyser is directly fed into another chemical process known as SEDMES.

- Proposed model-based diagnosis

  1. The proposed diagnosis algorithms can be validated online by introducing the faults either in the system itself or by considering the equivalent electrical circuit or a digital twin in which the faults can be easily injected.

  2. The parameter estimation techniques could be incorporated in order to isolate the faults which are not isolable otherwise and the sensor placement is not possible.. For example the faults in the MEA are non isolable as per the configuration considered and it is not possible to install sensors inside the existing MEA that can help in isolating the faults.

  3. A hybrid diagnosis approach can be developed in which the developed model based diagnosis can be coupled with the data driven approach. This could be really helpful for the diagnosis of the systems in which parameters for some components cannot be calculated or estimated for model based diagnosis.

  4. Another important perspective in framework of the research activity in the PERSI group is the use of developed model for digital twin technology which is a software - based virtual replica of the process including its process equipment, instrumentation, control, supervision and online efficiency tracking. This digital twin simulator can be used for predictive maintenance and prognosis PHM (for earlier fault detection and isolation and estimation of equipment degradation). The interest is that the digital twin can be used for deep learning in the case of no model based FDI or for the testing of model based FDI (using observers, analytical redundancy relations...).

Nevertheless this work set a first step in the model based prognostic of this complex system as a collaborative work based on the proposed model has been presented in European Control Conference (ECC 2021) under the title "A Model-based Prognosis approach to Proton Exchange Membrane Water Electrolysis System".

Modelling of AEM Electrolysis Cell

This work is an attempt to develop and validate a graphical dynamical model of an AEM electrolysis cell based on BG, an energy based tool that allows to represent multi-physics systems. The model of the cell lays a foundation for developing a complete representation for AEM electrolysers which can be used for simulation as well as for developing control algorithms and fault diagnosis. Parameter identification and model validation is achieved using experimental data provided by University of Exeter in the framework of European e2C project. This work has been published in 28th Mediterranean Conference on Control and Automation (MED'2020).

A.1 Introduction

Hydrogen has emerged as a carbon neutral way of storing surplus electricity available from renewable energy resources at off peak hours due to its intermittent nature. Hydrogen is in abundance (can be produced from water), can be stored with ease and is the clean and lightest fuel with highest energy density [5]. Hydrogen production through water electrolysis is the most matured technology and can be easily coupled with any source of electricity [6].

Electrolysis is the technique through which the water molecules are split into hydrogen and oxygen gases under the influence of the electric current [208]. Two types of electrolysis techniques, namely alkaline electrolysis and PEM electrolysis are well developed and highly used on the commercial scale [209]. These two techniques have numerous advantages and disadvantages which are shown in Table A.1.

In the recent years, in order to benefit from the advantages of both alkaline and PEM electrolysis polymer based AEM have been developed. PEM electrolyser uses noble earth metals such as Ir, Ru, and Pt etc; which are expensive and limit its commercial applications. On the other hand, AEM electrolyser is based on alkaline electrolytes so, a wide range of earth-abundant transition metals and their oxides can be employed [33]. These membranes have made their way to the fuel cells but it is still under development for electrolysis [209]. To adapt AEM as a reliable technology for water electrolysis significant improvements are required [209]. Research is being carried out in order to achieve desirable properties for the membrane such as better mechanical stability, ionic conductivity, longer life, lower cost etc. To finally assemble this into a functional and efficient electrolyser is yet another challenge.

Table A.1: Advantages and disadvantages of alkaline, PEM and AEM electrolysis [209]

Alkaline	PEM	AEM
Advantages		
Mature technology	Higher performance	Non-noble metal catalyst
Non-PGM catalyst	Higher voltage efficiency	Noncorrosive electrolyte
Long term stability	Good partial load	Compact cell design
Low cost	Rapid system response	Low cost
Megawatt range	Compact cell design	Absence of leaking
Cost effective	Dynamic operation	High operating pressure
Disadvantages		
Low current densities	High cost of components	Laboratory stage
Crossover of gas	Acidic corrosive components	Low current densities
Low dynamic	Possible low durability	Durability
Low operating pressure	Noble metal catalyst	Membrane degradation

Modelling and simulation are very powerful tools of modern engineering that can also contribute towards these goals by providing alternate means for design investigation and operating conditions optimization by spending less time and at relatively lower cost as compared to the physical experiments [15]. The importance of modelling and simulation increases many folds in case of dynamic multi-physics systems. AEM electrolysis cell is one such case in which complicated physio-chemical processes takes place. Modelling plays a significant role in quantifying such processes [210]. Models once developed can also be used for understanding the phenomenon, developing control for the system as well as for diagnostics. Numerous modelling techniques have been developed by the researchers that can be broadly classified under two categories, namely equation based and graphical based modelling.

In equation based modelling techniques, the system is represented in terms of ordinary differential equations. These techniques are less user friendly and difficult to modify or update as the dynamic equations of the whole system are needed beforehand [17]. Distributed parameters dynamic models represented by Partial Differential Equations (PDE are also used for deep analysis, but this kind of models are not suited for control and diagnosis tasks. The models (complex and resolved using finite elements) are used mainly for sizing, chemical and thermal process design and analysis [70].

In graphical based modelling approaches, the model of the system is represented by connecting the graphical models of subsystems (known as blocks) through ports based on their physical interactions. It is easy to understand the physical structure as well as the behaviour of the system through such models. These approaches are more user friendly and are based on physical phenomenon.

Many graphical modelling techniques are available out of which BG is of significant interest. BG is based on power exchange between the components of the system and is domain independent which makes it well suited for multi-physics systems. This one single tool can be used for four different levels of modelling [15]. Another key advantage of using BG is that the same model can be used for simulation as well as for control,sizing, diagnosis and prognosis.

Due to the maturity of the alkaline and PEM electrolysis techniques a lot of research has been done on the modelling of these type of electrolysers. A review proposed by Olivier et al. [6] exposed the existing models for the alkaline and low temperature PEM electrolysers. It shows that majority of the models are equation based (empirical or analytical) and are focused on understanding phenomena (including degradation mechanisms), characterization of performance, development of control for the system,diagnostic and prognostic (long-term

durability evaluations). A very few graphical models exist for PEM electrolysers. Agbli et al. [118] proposed a graphical model based on energetic macroscopic representation (EMR) that can simulate the evolution of the temperature and included electro-chemical, electrical and thermal phenomena. They neglected the fluidic phenomenon. Zhou et al. [46] proposed a causal ordering graph (COG) based model to develop control algorithms for real time implementation in order to control power flow and hydrogen flow in a hybrid system containing electrolyser. A BG model proposed by Olivier et al. [15] for an industrial scale PEM electrolyser includes the auxiliaries of the electreolyser (Balance of plant). Different phenomenon like electro-chemical, thermal, fluidic, mass transfer have been incorporated into single model in order to study the effect on the overall performance of the model.

As AEM electrolysis in a new technique and is still being developed, there is not much work done on the modeling of such systems. There is only one mathematical model proposed by L. An et al. [210] that incorporates mass transport, charge transport and electro-chemical reaction in order to predict the performance of AEM electrolyser running on pure water. The model was validated by the experimental data available in the literature [211].

The lack of availability of a good model for AEM electrolyser warrants for the research in this area. The configuration of AEM electrolysis cell is similar to that of PEM [212]. There are some distinct differences such as the feed side, core chemical reactions etc. Because of this, models already developed for PEM can be modified and can be Incorporated for AEM. The work presented in this paper is an attempt to take a step towards achieving this objective. A dynamic multi-physic model based on BG theory has been developed for AEM electrolyser cell. Once the BG model is generated, MATLAB Simulink model is systematically constructed through it for the simulations. Parameter identification and model validation is performed using experimental data from actual AEM cell.

A.1.1 AEM Water Electrolysis

Schematic of an AEM water electrolysis cell is shown in Fig.A.1. The electrolyte is fed to the cell
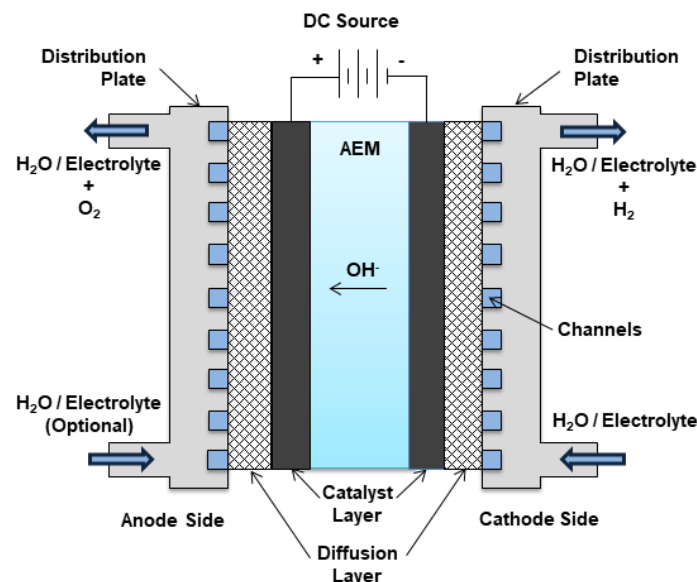
Figure A.1: Schematics of AEM water electrolysis

from the cathode side where the water is reduced into hydrogen and hydroxyl ions are formed. These negative ions transport through the membrane towards the anode where they recombine

to release oxygen. The electrolyte acts as a reagent as well as it facilitates the removal of the hydrogen at cathode. The electrolyte or water can also be fed to the anode side to facilitate the removal of oxygen depending on the design of the cell. The half reactions on each electrode and overall reaction is given as [209]:

$$\textbf{\textit{Anode}} : 4OH^- \rightarrow O_2 + 2H_2O + 4e^- \quad E_0 = 0.41\,V \tag{A.1}$$

$$\textbf{\textit{Cathode}} : 4H_2O + 4e^- \rightarrow 2H_2 + 4OH^- \quad E_0 = -0.828\,V \tag{A.2}$$

$$\textbf{\textit{Overall}} : H_2O(l) \rightarrow H_2(g) + \frac{1}{2}O_2(g) \quad E_0 = 1.23\,V \tag{A.3}$$
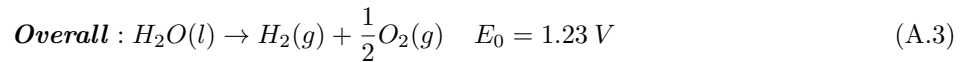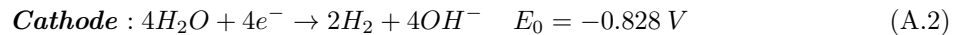
A.1.2 BG Modelling Basics for Multi-physics Systems

BG is a structure based modelling technique in which a system can be represented by predefined standard elements and junctions which in turn represent some physical phenomena. These elements are connected using the connectors known as power bonds that represent the power flow in the system. The BG is a unified approach as the elements are analogues irrespective of the physical domain to which the system belongs. The currency of interaction between the elements is power which is common to all the domains. This power exchange is labelled by two conjugated power variables named effort (e) and flow (f). However, the domains like chemical engineering can also be represented using this technique although the product of power variables is not power. Such models are known as pseudo bond graphs [15]. As shown in Fig. A.2(a), the power exchanged between two systems A and B is indicated by a bond and half arrow represents the direction of power flow. One key structural property of the BG is the concept of causality. In the bond graph, it is represented by a cross-stroke on indicating the direction of the effort. This means that system A imposes effort on B and B impose flow in return on A as shown by the block diagram in Fig. A.2 (b). Table A.2 represents the power variables for some energy domains.

Figure A.2: BG representation (a) and relative block diagram (b) [212]

Table A.2: Power variables for different energy domains [15]

Physical Domain	Effort (e)	Flow (f)
Electrical	Voltage (V)	Current intensity (A)
Fluidic	Pressure (Pa)	Volume flow rate ($m^3\,s^{-1}$)
Fluidic (Pseudo bond graph)	Pressure (Pa)	Mass flow ($kg\,s^{-1}$)
Thermal	Temperature (K)	Entropy flow ($J\,K^{-1}\,s^{-1}$)
Thermal (Pseudo bond graph)	Temperature (K)	Thermal flow ($J\,s^{-1}$)
Chemical (Transformation)	Chemical Potential ($J\,mol^{-1}$)	Molar flow ($mol\,s^{-1}$)
Chemical (Kinetic)	Chemical affinity ($J\,mol^{-1}$)	Reaction speed flow rate ($mol\,s^{-1}$)

A.2 BG Modelling Of AEM

In BG almost all systems can be represented using hand full elements. These elements can be represented as a set:S=$\{R \cup C \cup I \cup TF \cup GY \cup SE \cup SF \cup De \cup Df \cup J\}$ [213]. Here

R element represents energy dissipation. I and C elements represent the storage of kinetic and potential energy respectively.TF and GY are transformer and gyrator that represents the transformation of energy from one form to another. Se represents the source of effort and Sf represents the source of flow. De and Df are effort and flow sensors. J is junction which is used to connect the elements based on common effort (represented by 0) and common flow (represented by 1). It represents the law of conservation of energy. A multi-port RS element is also used for representing the resistance that also act like source. For example, a heating coil acts as a resistance for electricity bur also act as a source of thermal energy. Graphical model building using BG approach has been discussed in appendix B.

A.2.1 AEM Cell BG Modelling

AEM electrolysis cell is a multi-physics open system in which the physical inputs are electric current and electrolyte and the output is the hydrogen and oxygen gases. The modeling of such systems is not a trivial task and hence to simplify the modelling problem in hand following assumptions have been considered:

- The AEM cell operates under steady state conditions.

- The effect of diffusion is negligible on the cell voltage.

- The thermal capacity of the cell can be lumped into single parameter.

Figure A.3 shows the word BG for the AEM cell including the membrane electrode assembly (MEA), electrolyte supply tank, gas separators and the power source. Word BG represents the components of the system and the nature of power exchange between them. It can be seen that this power exchange in the system belongs to multiple physical domains such as electro-chemical, thermal, thermo-fluidic. The coupling between different domains make the modelling even more challenging. Fig 4 shows the BG for the considered system. Each phenomenon considered will be discussed one by one. The electro-chemical phenomenon is considered instantaneous and is responsible for the overall cell voltage. It is represented through an algebraic equation given by the 1_{ec} and 1_{ov} junctions.

$$E_{cell} = E_{rev} + E_{ohm} + E_{act,cat} + E_{act,ano} \tag{A.4}$$

where E_{cell} represents the overall cell voltage, E_{rev} reversible potential, E_{ohm} is ohmic overvoltage, $E_{act,cat}$ and $E_{act,ano}$ are activation overvoltages. The transformer element TF_{ec} represents the conversion of electricity into chemical energy which is expressed by the equations (A.5) and (A.6) [15].

$$\dot{\zeta} = \frac{I_{cell}}{2F} \tag{A.5}$$

$$E_{rev} = \frac{\Delta G}{2F} \tag{A.6}$$

The reversible potential is the minimum voltage to be applied along the cell in order to start the electrolysis. The value of it depends on temperature, molar concentration and vapour pressure of the KOH solution [214] and can be expressed by the equation (A.7)

$$E_{rev} = E_{rev,T}^o + \frac{R(T + 273.5)}{2F} ln \left(\frac{(P - P_{v,KOH})\sqrt{(P - P_{v,KOH})}}{a_{H_2O,KOH}} \right) \tag{A.7}$$

Here, the R is the ideal gas constant,F is the Faraday's constant, T is the temperature in ^oC, P is the operating pressure (in bar), $P_{v,KOH}$ is the vapour pressure of KOH and $a_{H_2O,KOH}$ is
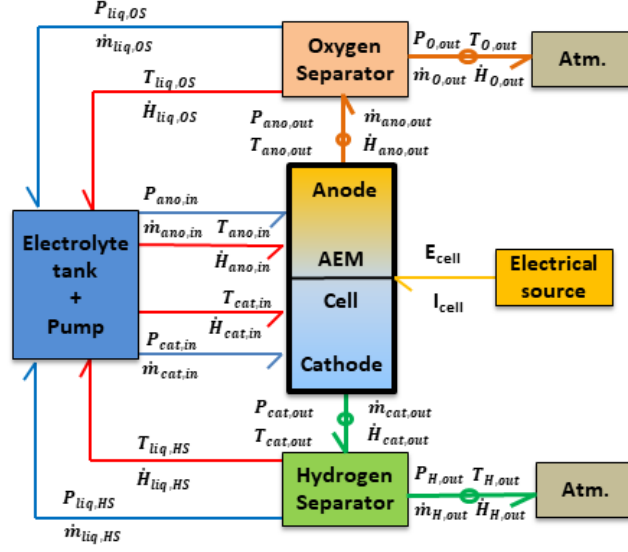
Figure A.3: Word BG for AEM cell

the water activity in the KOH solution. $E^o_{rev,T}$ is the reversible voltage as standard pressure (1bar). It is the function of temperature and is expressed as [214]

$$E^o_{rev,T} = 1.5184 - 1.5421 \times 10^{-3}(T+273.5) + 9.526 \times 10^{-5}(T+273.5)ln(T+273.5) + 9.84 \times 10^{-8}(T+273.15)^2 \tag{A.8}$$

Following equations are used to calculate vapour pressure of KOH solution [214]

$$P_{v,KOH} = exp(2.302\, a + b\, lnP_{v,H_2O}) \tag{A.9}$$

$$a = -0.0151m - 1.6788 \times 10^{-3}m^2 + 2.2588 \times 10^{-5}m^3 \tag{A.10}$$

$$b = 1 - 1.2062 \times 10^{-3}m + 5.6024 \times 10^{-4}m^2 - 7.8228 \times 10^{-6}m^3 \tag{A.11}$$

$$P_{v,H_2O} = exp81.6179 - \frac{7699.68}{T+273.15} - 10.9ln(T+273.5) + 9.5891 \times 10^{-3}(T+273.5) \tag{A.12}$$

where, m is the molar concentration of the KOH.

The water activity of KOH solution is given by the following expression [214]

$$a_{H_2O,KOH} = \left(-0.05192m + 0.003302m^2 + \frac{(3.177m - 2.131m^2)}{(T+273.5)}\right) \tag{A.13}$$

The activation overvoltages appear due to the kinetics of charge transfer between the electrode and the electrolyte. It is expressed by the Butler-Volmer equation [15].

$$J_{cell} = J_k \left[exp\left(\frac{\alpha_k.z.F.E_{act,k}}{R.T}\right) - exp\left(-\frac{(1-\alpha_k).z.F.E_{act,k}}{R.T}\right)\right] \tag{A.14}$$

where, J_{cell} is the current density, J_k is the current exchange density of the half reaction occurring at the two electrodes,α_k is the charge transfer coefficient and $E_{act,k}$ are the activation overvoltages for both electrodes. This equation is further simplified by considering equal charge transfer coefficient for both cathode and anode equal to 0.5 [15] which is true for low current
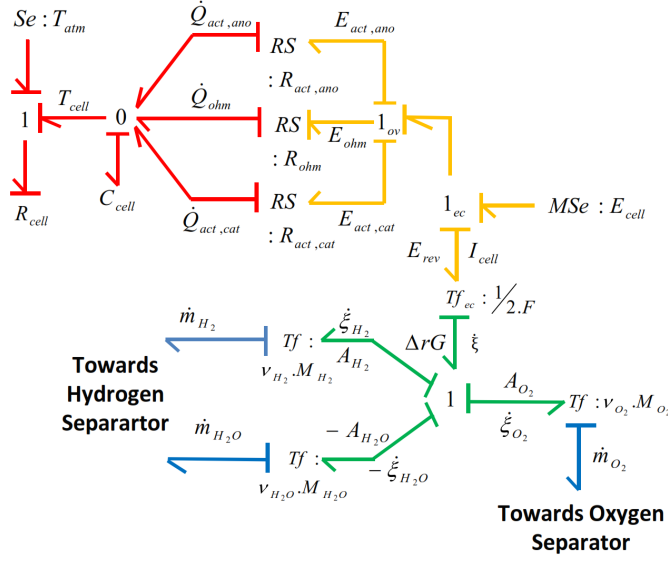
Figure A.4: BG for AEM cell

densities usually less than $2Acm^2$. This equation can be rewritten for calculating activation overvoltages as [15]

$$E_{act,k} = \frac{R(T + 273.15)}{F} sinh^{-1}\left(\frac{J_{cell}}{2J_k}\right) \tag{A.15}$$

These overvoltages are modelled as two non linear resistance elements (RS element) $R_{act,cat}$ and $R_{act,ano}$ which contributes towards increasing the temperature of the cell. The third RS element (R_{ohm} represents the ohmic resistance of the cell, the equation of which is written as [210]

$$R_{ohm} = \left(R_{contact} + \frac{L_M}{A_M \sigma_M}\right) \tag{A.16}$$

$$E_{ohm} = I.R_{ohm} \tag{A.17}$$

where, $R_{contact}$ is the resistance of the cell except membrane, L_M is the thickness, A_M is the area and σ_M is the ionic conductivity of the membrane. The value of σ_M (in $\Omega^{-1}m^{-1}$) depends on temperature and is given by the equation (A.18)

$$\sigma_M = 198.3exp\left(-\frac{11190}{R(T + 273.15)}\right) \tag{A.18}$$

In order to determine the current exchange densities an the resistance of the cell, these parameters are needed to be estimated using curve fitting of the polarisation curve. Due to lack of more experimental that at present such as Electrochemical Impedance Spectroscopy (EIS), it is not possible to identify the current exchange densities separately. Therefore it is assumed that the current exchange densities are equal for both half reactions so that we can see their overall effect on the polarisation curve. Also, these overvoltages act as the source of heat which tends to increase the temperature of the cell. To model this, lumped thermal capacity C_{cell} of the cell is considered. The equation for the cell temperature can be then written as

$$T_{cell} = \frac{1}{C_{cell}} \int \left(\dot{Q}_{act,ano} + \dot{Q}_{act,cat} + \dot{Q}_{ohm} - \frac{T_{cell} - T_{atm}}{R_{cell}}\right).dt \tag{A.19}$$

where, $\dot{Q}_j$ are the heat flows due to different overvoltages, T_{atm} is the ambient temperature and R_{cell} is the thermal resistance of the cell. Mass flows of the species produced and consumed is represented through TF elements as shown in Fig. A.4. The mass flows of the species are calculated as

$$\dot{m}_i = v_i.M_i.\dot{\zeta} = v_i.M_i\frac{I_{cell}}{2F} \tag{A.20}$$

where m_i represents mass flow of the species i, v_i and M_i are the stoichiometry coefficient and molar mass of the species i.

A.3 Parameters identification and model Validation

For validation and simulation, a MATLAB Simulink model has been deduced systematically from the graphical BG model. Parameters are identified by curve fitting the polarisation curve of an actual cell. The polarisation curve has been provided by University of Exeter for their newly developed AEM cell. The characteristics of this cell are shown in the table A.3

A.3.1 Parameters Identification

To achieve the curve fitting of the polarisation curve for the identification of the parameters, Levenberg-Marquardt algorithm has been used. The equation of the polarisation curve can be written as

$$E_{cell} = E^o_{rev,T} + \frac{R(T + 273.5)}{2F}ln\left(\frac{(P - P_{v,KOH})\sqrt{(P - P_{v,KOH})}}{a_{H_2O,KOH}}\right) + \frac{2R(T + 273.15)}{F}sinh^{-1}\left(\frac{J_{cell}}{2J_k}\right) + I.\left(R_{c}\right)$$

$$\tag{A.21}$$

Here the fitting parameters are J_k and $R_{contact}$. After fitting the values of J_k and $R_{contact}$ are found to be $4.337{\times}10^{-7}$ Acm^{-2} and 0.0518 Ω respectively.

A.3.2 Validation

Figure A.5 shows the plot of the actual and simulated polarisation curve. The model simulates the polarisation curve satisfactorily as the Mean Absolute Percentage Error (MAPE) of the model over considered data is 0.31%.

A.4 Simulation and Discussion

Figure A.6 shows the simulation of the polarisation curve for different temperatures and fixed concentration of 4M KOH. It can be seen that the voltage increases with increase in temperature. This phenomenon is probably due to the technology of membrane and need further experimental

Table A.3: Specifications of the AEM cell

Specification	Value
Thickness of the membrane	25-50 μm
Area of the membrane	9 cm^2
Operating Pressure	1 bar
Operating temperature range	20-80 ^oC
KOH Concentration	4M
Input and output flow rates	250 ml/min
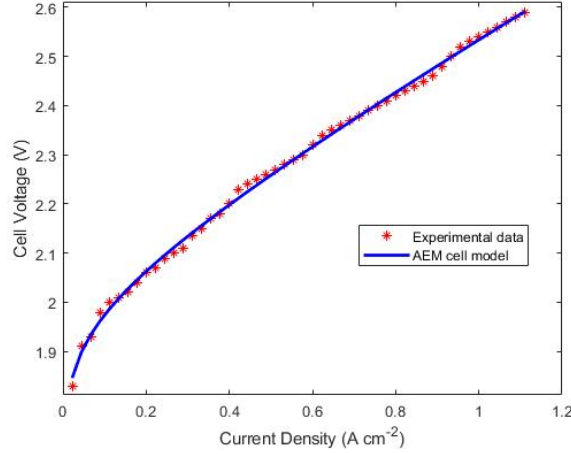
Figure A.5: Comparison of polarisation curve at 80 ºC and 4M KOH
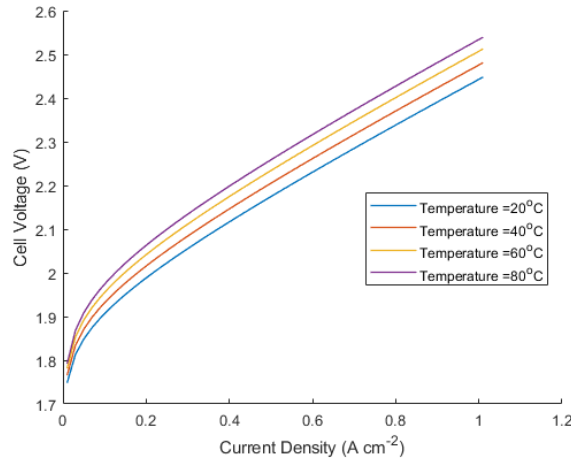
Figure A.6: Simulated polarisation curves for different temperatures at 4M KOH

investigation for the confirmation. Simulation of the polarisation curve for fixed temperature of 80 ºC and different concentrations of KOH is shown in the Fig.A.7. There is a negligible effect of the molar concentration on cell voltage as molar concentration appears in the equation of the reversible voltage only. Figure A.8 shows the qualitative simulation of temperature evolution for the AEM cell. These simulations shows that different operating conditions can be tested virtually. This can help in decreasing the cost and the time involved due to experimental testing and could prove as a great tool for design optimization.

A.5 Conclusion

AEM water electrolysis is a developing technology that requires lots of research to be a matured like PEM water electrolysis so as to see its commercial application. In an attempt to contribute towards this technology a BG based multi-physics model for AEM cell has been developed. The developed model is then used to systematically generate MATLAB Simulink model which is used for the simulations of polarisation curve at different operating conditions. The results shows that the model can predict the polarisation curve satisfactorily. Further improvement
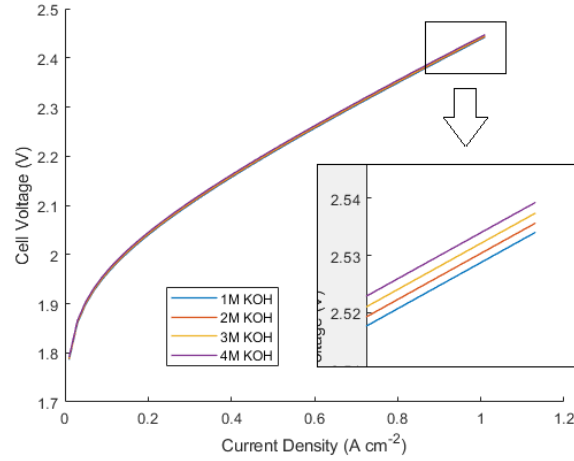
Figure A.7: Simulated polarisation curves for various conc. of KOH at 80°C
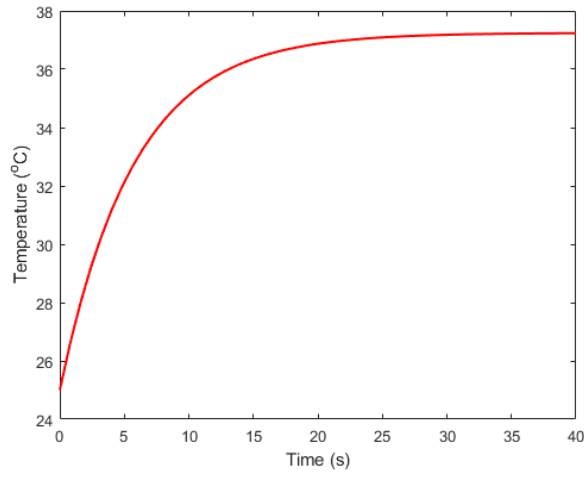
Figure A.8: Simulation of temperature evolution of the cell at constant current density of $0.5 Acm^{-2}$

in the model can be done by performing electrochemical impedance spectroscopy in order to identify current exchange densities for both anode and cathode separately. Also the model can be further enhanced by modeling the auxiliaries and other phenomenon like thermo-fluidic, mass transport etc. which can be then added into a single model. It will be really interesting to also test and validate the sizing of the model in order to see its implementation for AEM stack.

Bond Graph Approach

Contents

B.1 BG Technique for Model Building

BG is a well-adapted multi-disciplinary and unified graphical modelling approach to describe complex process having multiple energy exchanges[18, 215, 216]. A brief introduction to BG methodology for multi-physics systems is presented in this section.

B.1.1 BG Elements and BG Variables

BG can be denoted as G(N, B), where nodes N represent the BG elements that correspond to energetic physical elements (inertia, resistance and capacitance), source elements (battery, pump, etc.), power/energy constraint BG connecting elements and technological elements (subsystems) and bonds B represent the set of oriented edges that correspond to power/energy exchange among nodal elements. Bond is labeled by two power variables: called flow (f) and effort (e) variables whose product provides the value of physical power flow in that bond. Note that for some energy domains like chemical, the product of these variables on a bond may not be the representation of physical dimension of a power, however it is used for systematically model such energy domains, called pseudo BG model [197]. All the BG theory obviously remains valid in such cases also.

In figure B.1(a), a physical link between subsystem A and subsystem B using the half arrow power bond is presented that represents the direction of energy/power flow among them. In the represented configuration, energy flow is considered towards the destination node B, only when the product of power variables is positive; otherwise, energy flow is in the reverse direction, i.e. away from node B. In BG, causality (represented by cross-stroke) is an important structural property that determines the relationship between power/energy variables based on cause and effect analysis. The node which receives the effort information (or gives the flow information), cross-stroke is marked near to that node. For example, according to causality in figure B.1(a) and corresponding block diagram as in figure B.1(b), B receives effort information from A as cross-stroke is marked near B, while A receives flow information from B. In Table B.1, various flow and effort variables belonging to different energy domains are shown.

Different systems can be modelled in BG by employing a handful of elements (I, C, R, Sf, Df, Se, De, TF, GY and J) [218]. Here, I is the inertia element (stores kinetic energy); C is compliance element (stores potential energy); R is resistive element (represents dissipation phenomena); Sf and Se are, respectively, the source of flow and source of effort; Df and De
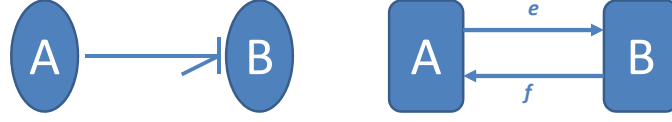
Figure B.1: (a) Causal BG and (b) corresponding block diagram representation.

Table B.1: Flow and effort for various energy domains [15, 217].

Energy Domain	Flow (f)	Effort (e)
Electrical	Current intensity (A)	Voltage (V)
Fluidic	Volume flow rate ($m^3.s^{-1}$)	Pressure (Pa)
Fluidic (Pseudo BG)	Mass flow ($kg.s^{-1}$)	Pressure (Pa)
Thermal	Entropy flow ($J.K^{-1}.s^{-1}$)	Temperature (K)
Thermal (Pseudo BG)	Thermal flow ($J.s^{-1}$)	Temperature (K)
Chemical (Transformation)	Molar flow ($mol.s^{-1}$)	Chemical potential ($J.mol^{-1}$)
Chemical (Kinetic)	Reaction flow rate ($mol.s^{-1}$)	Chemical affinity ($J.mol^{-1}$)

are, respectively, detectors for flow and effort (virtual sensors); TF is the transformer and GY is the gyrator. These elements represent the energy transformation between different domains. J represents the junction that accounts for energy conservation laws. These elements are presented briefly below:

B.1.1.1 I element

I is an inertia element that represents the storage of generalised kinetic energy of the system. The I element is shown in integral and differential causality with corresponding block diagrams in figure B.2. In integral causality, the element takes effort as input and returns flow to the system. The causal equation of the I element in this case is written as

$$f = \frac{1}{I} \int e \, dt \qquad (B.1)$$

In differential causality, the element takes flow as input and returns effort to the system. The causal equation of the I element in this case is written as

$$e = I \frac{\mathrm{d}f}{\mathrm{d}t} \qquad (B.2)$$

The value of I can be a constant value or a linear or non-linear function.

B.1.1.2 C element

C is a compliance element that represents the storage of generalised potential energy of the system. The C element is shown in integral and differential causality with corresponding block diagrams in figure B.3. In integral causality, the element takes flow as input and returns effort to the system. The causal equation of the C element in this case is written as

$$e = C \int f \, dt \qquad (B.3)$$

Integral causality

Differential causality
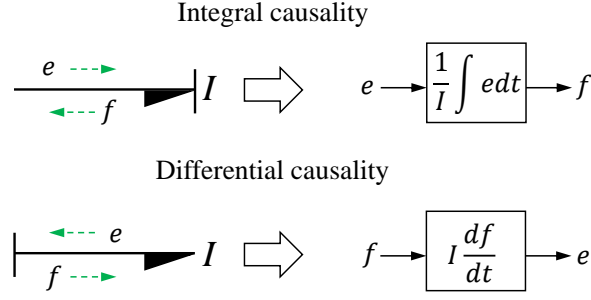
Figure B.2: BG and block diagram representation of inertia element

In differential causality, the element takes effort as input and returns flow to the system. The causal equation of the C element in this case is written as

$$f = \frac{1}{C}\frac{\mathrm{d}e}{\mathrm{d}t} \tag{B.4}$$

The value of C can be a constant value or a linear or non-linear function.

Integral causality

Differential causality
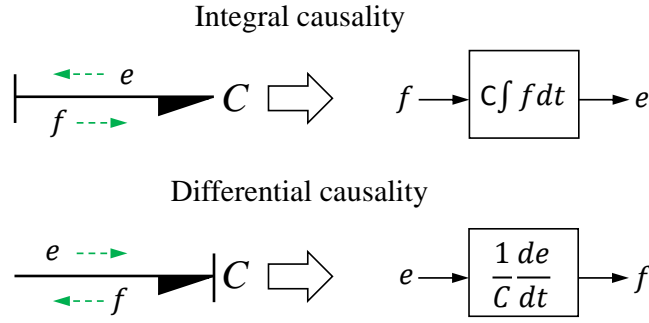
Figure B.3: BG and block diagram representation of capacitance element

B.1.1.3 R element

R is a resistive element that represents always represent the dissipation of energy in the system. Depending on the causality the R element can have resistive and conductive causality as shown in figure B.4. In resistive causality, the causal equation of the R element is given by

$$e = R.f \tag{B.5}$$

In conductive causality, the causal equation of the R element is given by

$$f = \frac{1}{R}e \tag{B.6}$$

The value of R can be a constant value or a linear or non-linear function. R element may also be used as a multi-port resistive-source element (noted RS) to represent the active resistance that generates entropy. For example, an electric coil that is used for heating acts as a resistance from electricity point of view, but also acts as a source of thermal energy from thermal viewpoint.
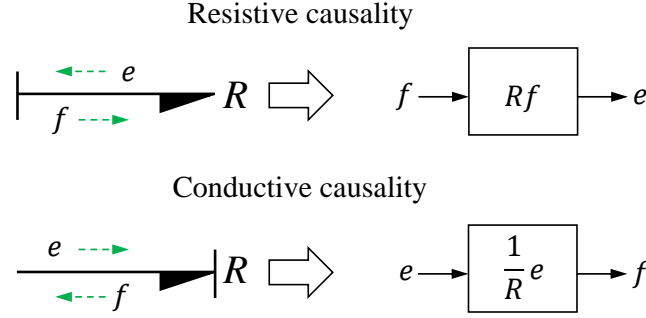
Figure B.4: BG and block diagram representation of resistive element
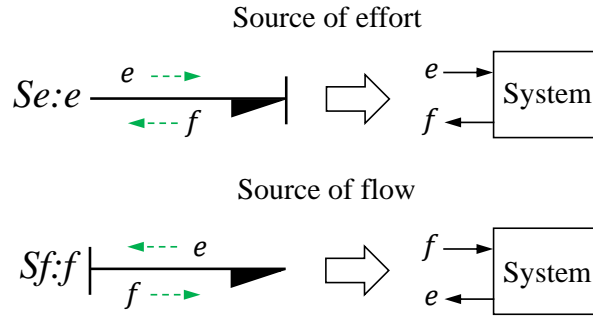
Figure B.5: BG and block diagram representation of source of effort and flow element

B.1.1.4 Se and Sf elements

Se and Sf represents the source of effort and source of flow respectively. Their BG and block diagram representation is shown in figure B.5. The Se element provides the information of effort to the system and there is no flow returned to the element from the system. The Sf element on the contrary provides the information of flow to the system and there is no effort returned to the element from the system. The value of the effort provided by Se and flow provided by Sf can be a constant or a linear or non-linear function.

B.1.1.5 Junctions

Junctions are the multi-port elements that can have any number of in and out ports to connect the elements based on their interaction with other elements or the sub-systems. The power coming in to the junction and going out of the junction is always equal. There are two types of junctions, 0-junction and 1-junction, based on the way the effort and flow are carried across the junction.

B.1.1.5.1 0-junction

The 0-junction is also known as flow sum junction. BG and block diagram representation of 0-junction is shown in figureB.6. All the bonds connecting to the 0-junction have same effort. As the total power flowing in to the junction is equal to the total power flowing out of the system. Therefore

$$e_1 f_1 + e_2 f_2 + e_3 f_3 ... + e_n f_n = 0 \tag{B.7}$$
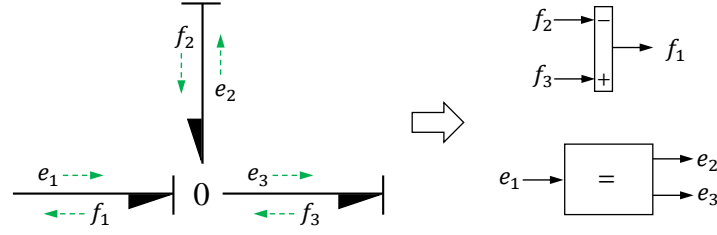
Figure B.6: BG and block diagram representation of 0-junction element

As for 0-junction all the efforts are equal,i.e.

$$e_1 = e_2 = e_3... = e_n \tag{B.8}$$

Equation B.7 can be rewritten as

$$f_1 + f_2 + f_3... + f_n = 0 \tag{B.9}$$

B.1.1.5.2 1-junction

The 1-junction is also known as effort sum junction. FigureB.7 shows the BG and block diagram representation of 1-junction. All the bonds connecting to the 1-junction carries same flow. As
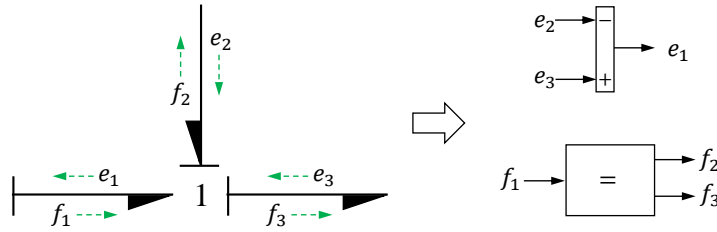
Figure B.7: BG and block diagram representation of 1-junction element

the total power flowing in to the junction is equal to the total power flowing out of the system. Therefore

$$e_1 f_1 + e_2 f_2 + e_3 f_3... + e_n f_n = 0 \tag{B.10}$$

As for 1-junction all the flows are equal,i.e.

$$f_1 = f_2 = f_3... = f_n \tag{B.11}$$

Equation B.10 can be rewritten as

$$e_1 + e_2 + e_3... + e_n = 0 \tag{B.12}$$

B.1.1.6 TF element

TF is a transformer element having two ports, which is used to proportionally transform the like power variables between the two ports. For example, in mechanical systems, a lever that is used for changing the force between two ends can be represented using transformer element. This transformation is governed by a modulus (m). Figure B.8 shows the two possible BG representations and their corresponding block diagram for a transformer element.

123
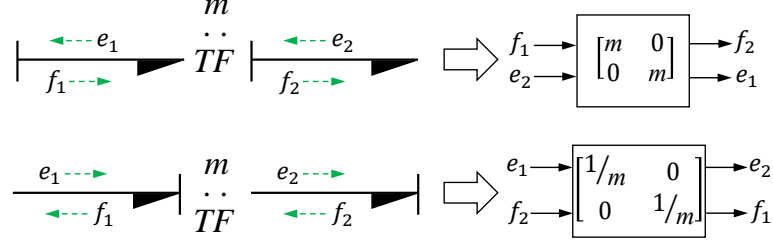
Figure B.8: BG and block diagram representation of transformer element

The causal equations of the TF element for first configuration (when the causal stroke is on right side) are written as:

$$f_2 = m.f_1 \tag{B.13}$$

$$e_1 = m.e_2 \tag{B.14}$$

The causal equations of the TF element for second configuration (when the causal stroke is on left side) are written as:

$$e_2 = \frac{1}{m}.e_1 \tag{B.15}$$

$$f_1 = \frac{1}{m}.f_2 \tag{B.16}$$

B.1.1.7 GY element

GY is a gyrator element having two ports, which is used to proportionally transform the dissimilar power variables between the two ports. For example, in case of a DC motor, the voltage (which is an effort variable in electric domain) is transformed into angular velocity (which is a flow variable in mechanical domain). This transformation is governed by a modulus (r). Figure B.9 shows the two possible BG representations and their corresponding block diagram for a GY element.
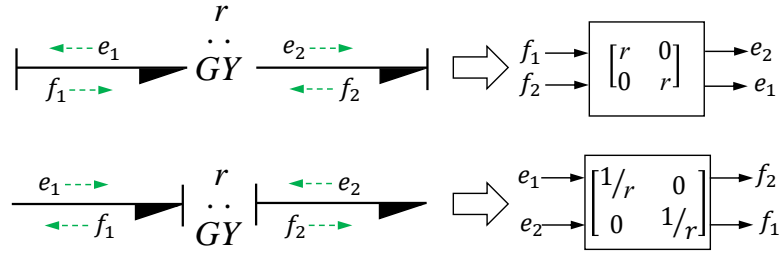
Figure B.9: BG and block diagram representation of gyrator element

The causal equations of the GY element for first configuration (when the causal strokes are away from the GY) are written as:

$$e_2 = r.f_1 \tag{B.17}$$

$$e_1 = r.f_2 \tag{B.18}$$

The causal equations of the GY element for second configuration (when the causal strokes are near to the DY) are written as:

$$f_2 = \frac{1}{r}.e_1 \tag{B.19}$$

$$f_1 = \frac{1}{r}.ef_2 \tag{B.20}$$

B.1.1.8 De and Df elements

De and Df are the detectors of effort and detector of flow respectively (BG and block diagram representation shown in figure B.10). These are the virtual sensors to measure the effort or flow in a junction.
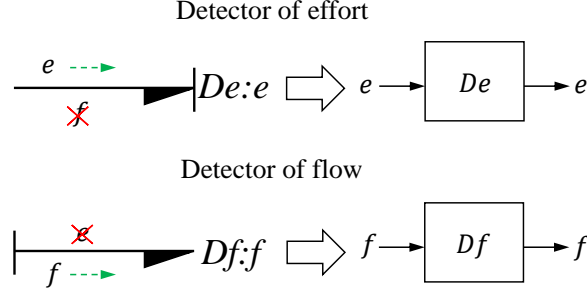
Figure B.10: BG and block diagram representation of detector of effort and flow element

De element can only be connected to 0-junction and Df element can only be connected to 1-junction. Their causal equations can be written as

$$De = e \tag{B.21}$$

$$Df = f \tag{B.22}$$

B.1.1.9   Vectorial representation

The vectorial representation is used to represent the coupling variables of a complex system. The coupled power variables in vectorial form are depicted as:

$$F = \begin{bmatrix} f_{fl} & f_{th} & f_{ch} \end{bmatrix}^T, E = \begin{bmatrix} e_{fl} & e_{th} & e_{ch} \end{bmatrix}^T \tag{B.23}$$

where F and E, respectively, are the flow and effort vectors. The suffices fl, th, ch, respectively, denote the fluidic/hydraulic, thermal and chemical energy domain. Figure B.11 shows different ways to illustrate a vector bond.
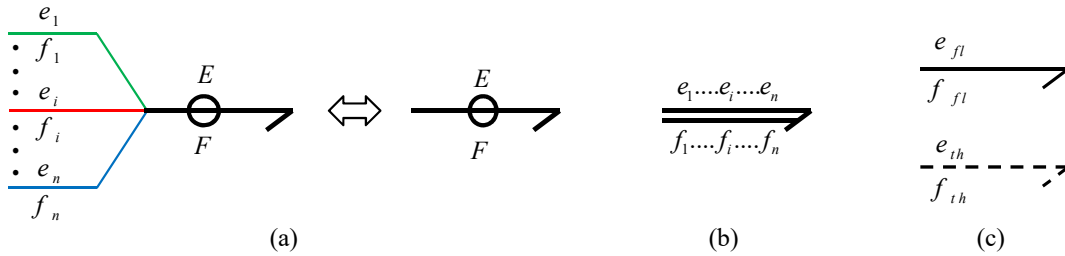
Figure B.11: BG and block diagram representation of detector of effort and flow element

B.1.2   Concept of Causality in BG

Causality connects one process (cause) to another process (effect) where the cause is fully or partially responsible for the effect. The concept of causality can be explained from physical or philosophical viewpoints. In both, the causes have to lie in the past and the effect lies in the

future. In a lumped parameter modeling framework, the velocity v of a point mass m at time t under application of a force F is mathematically written as

$$v\left(t\right) = \frac{1}{m}p\left(t\right) = \frac{1}{m}\int_{-\infty}^{t} F\left(\tau\right) d\tau = \frac{1}{m}\int_{0}^{t} F\left(\tau\right) d\tau + p\left(0\right) \tag{B.24}$$

where p denotes momentum, the time integration represents the past history and hence the force F is the cause and the velocity of the body v is the effect. This equation form representation where only one effect appears on the left hand side and one or more causes appear on the right hand side is called a computational or mathematical causality. The equation represents a model which may be logical, statistical, empirical, or derived from deep knowledge, i.e. the physics of the problem. In this work, equation models are based on physics. Thus, in the cited example, physical and computational causalities have the same meaning. The concept of causality in the Aristotelian philosophy assumes that the causes always lie in the past and it is good enough for building forward simulation models of physical systems. On the other hand, diagnosis task is different where the causes that lie in the past have to be inferred from the observed effects in the present. For the considered example where the force F acts on the point mass m, the equations in inverse causal form can be written as

$$F\left(t\right) = m\frac{\mathrm{d}v\left(t\right)}{\mathrm{d}t} \approx F\left(t - \Delta t\right) = m\frac{v\left(t\right) - v\left(t - \Delta t\right)}{\Delta t} \tag{B.25}$$

where Δt is a small time window corresponding to the measurement sampling interval. The velocity may be directly measured or an observable variable that can be computed from the other known measurements and states. Consequently, the velocity becomes the cause and the force becomes the effect as per the computational causality whereas the normal connotation of force as the cause and velocity as the effect remains valid as per the physical or Aristotelian philosophical causality.

In a BG model, causality decides the computational order of power variables $(e,\ f)$ based on cause and effect relation for mathematical equation generation. It defines whether the effort in a power bond is computed from the flow, or vice versa. The causality is represented by a vertical stroke at one end of a power bond. In the causalled power bond, the effort (e) variable is directed towards the causal stroke end, while the flow (f) variable is directed towards another end, i.e. opposite to causal stroke end. Generally, preferred integral causalities are assigned to the all energy storage elements (C and I) for dynamical behavior study where initial values of states have to be specified. On the other hand, preferred derivative causalities are assigned to C and I elements for diagnosis because values of initial states are unknown. A technique, called sequential causality assignment procedure (SCAP) is used to assign these causalities to a BG model[18]. A casual BG reveals the computational structure and is equivalent to a block diagram. However, unlike block diagram with fixed computation structure, a bond graph can be given new causality after any modification to it. The differential equations of state are generated from a bond graph model with storage elements in integral causality and those can be solved (simulated) using various types of integration methods.

B.1.3   Different Levels of Modelling Abstraction

To grasp complex systems, BG technique integrates the different levels of modelling, that is, technological, physical, mathematical and algorithmic levels using the common tool. In technological level, different subsystems of a dynamical system are first identified and then interconnected through energy or power variables. This level is represented by using word BG that shows the architecture of the system in a modularized form. In physical level, the system is

modelled in the form of lumped parameters (showing different physical phenomena such as energy storage, dissipation and transformation) using generalized BG elements with power/energy bonds. In mathematical level, dynamical behaviour of the system is represented in the form of mathematical equations such as differential and algebraic equations or in state-space form. The constitutive relations of the constraints and the components of the BG model provide these equations in mathematical form. In algorithmic level, the causal property of BG technique decides how these mathematical equations are algorithmically derived from the graphical BG model. Thus, the structural and causal properties of BG technique enable the dedicated software to systematically and algorithmically obtain the system dynamical equation either in the form of state-space equations or in the form of differential equations for the simulation and analysis purpose. Based on the BG approach, a number of software have been developed and are available for use such as Symbols-Shakti® and 20-Sim®. In this work, model builder of Symbol-Shakti® is used for developing the generic PEM electrolyser model where the structural integrity of different components and sub-systems for the global system modelling is checked. Once the models of different sub-systems (capsules) are built, their corresponding MATLAB® Simulink models are systematically derived from implementation point of view.

B.1.4 Modular Building (Capsules)

In Symbols-Shakti®, the capsules are properly modelled subsystems that have single or multiple input and output ports. They already have their partially derived equations. When the capsules are assembled to form the complete model, the equations are linked together to form behavioural equations for the complete model. For example, the capsule of PEM stack is developed by coupling the BG sub-models with different energy interactions (electro-chemical, thermal and fluidic). The internal model of the capsule in Symbols-Shakti® for a PEM stack is shown in figure B.12.

(a)

(b)
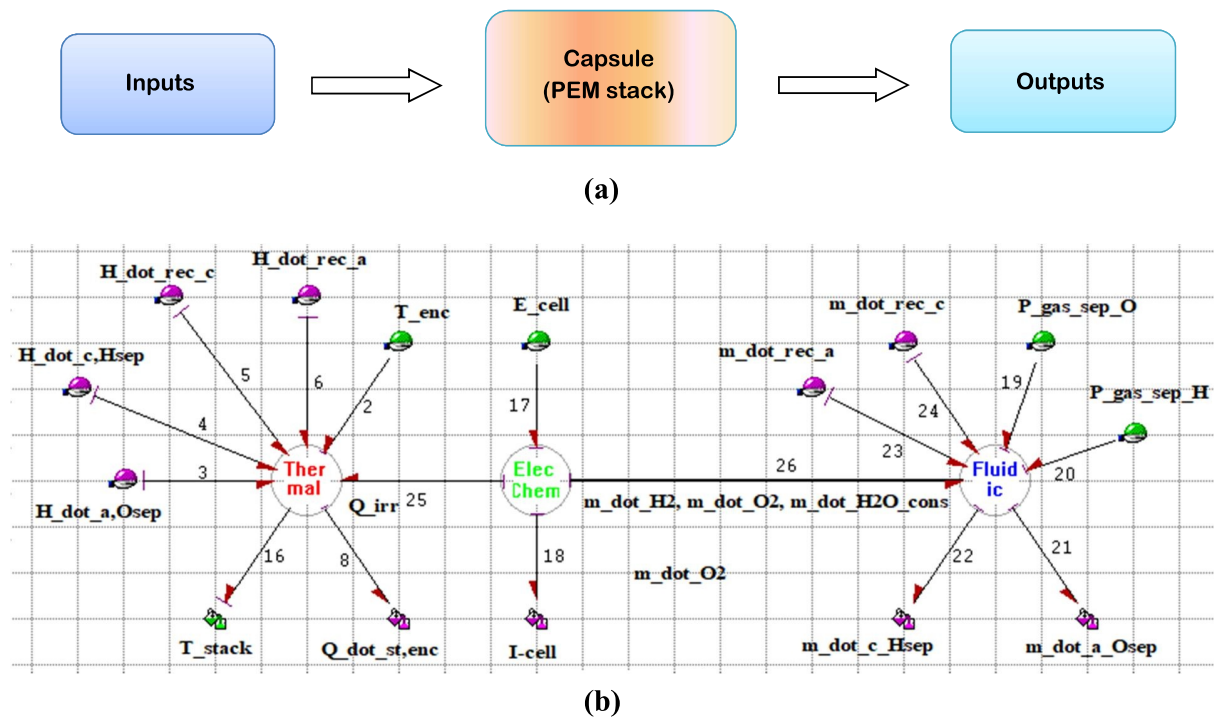
Figure B.12: (a) Schematic diagram and (b) BG model of PEM electrolyser stack capsule.

Depending upon the nature of interaction of the capsules with its environment, the ports can be defined as effort or flow input port and effort or flow output port. Based on the requirements these ports can be attributed as optional and hence are not needed to be connected in order to create the global model. Coupled energy interaction between the sub-models can be represented by a vector bond as shown by bond number 26 in figure B.12. A number of capsules are already available in the database of the software for the commonly used components such as tanks, valves, pipes, heaters and sensors. User defined capsules can be stored in the database and can be used and modified as per the model requirement. Figure B.13 shows the user defined capsules, developed for the PEM electrolyser system.
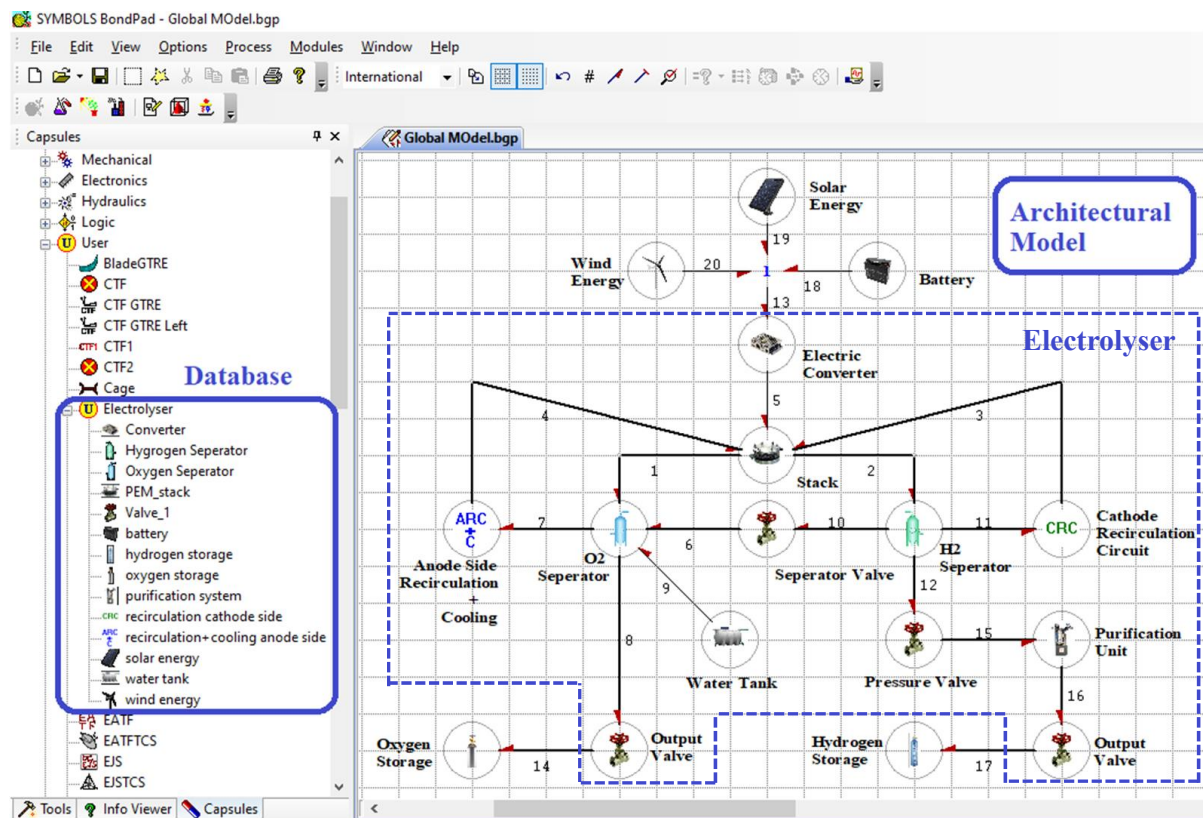
Figure B.13: Graphical user interface of the model builder.

B.1.5 Grammar and Connectivity Rules

Using the capsules, a global model of a complex system can be assembled in the model builder of the Symbols-Shakti® software. Figure B.13 shows the graphical user interface of the model builder. The global model is assembled in the form of piping and instrumentation diagrams using the capsules. For example, the architectural model of a PEM electrolyser is shown in figure B.13. The model builder also generates the behavioural equations for the whole system automatically.

To successfully connect the capsules with each other there are certain rules that have to be respected. The connectivity of the capsules is automatically checked by the software for validity. Only the like ports can be connected. The flow (resp. effort) output of a capsule can only be connected to the flow (resp. effort) input of the other capsule and vice versa. For example, figure B.14 demonstrates the requirement of the coherence of causality for the connection of the capsules of two tanks.
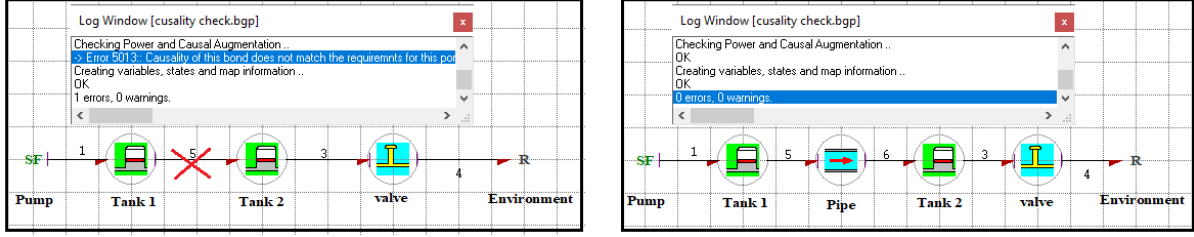
Figure B.14: (a) Invalid and (b) Valid connection of capsules.

From figure B.14(a), it can be seen that it is not possible to directly connect two tank capsules together as the input for the tank capsule is flow and the output is effort. In order to connect the two tank capsules the resistance of the pipe needs to be considered which takes effort as input and flow as output (as shown in figure B.14(b)). Published articles [199, 219, 220] and reference manual of the software can be referred to for further details.

B.2   Model-based Fault/degradation Diagnosis Methodology using BG

In model-based diagnosis, a residual is an indicator of the deviation of the behavior of a system from its expected/normal behavior. Various approaches can be used for the generation of residual which acts as a fault indicator in model-based diagnosis and those may be classified as observer-based, parity relation-based, parameter estimation/identification-based and ARRs based methods. The ARR s are usually manifestations of different conservation relations represented in the form of constraints or balance equations. For hydraulic system, these can be energy (Bernoulli equation), mass (continuity equation) and momentum (Navier-Stokes equation) conservation relations. For electrical circuits, these can be Kirchhoff's current and voltage laws, loop laws, element constitutive laws, and energy/power balance equations, etc.

BG being a graphical representation of the physics of dynamical systems offers a systematic approach to generate ARR s from the BG model. For simpler systems, ARR s can be written in closed symbolic form by eliminating the unknown power variables of the BG model while retaining the measurable system variables. BG causality provides the algorithm to eliminate the unknown variables from the model. The DBG model can be used for ARR generation from the DBG model in symbolic form. A DBG model of a system is obtained by changing the effort (or flow) sensors De (or Df) of BG model into modulated effort (or flow) sources MSe (or MSf), respectively, which are equivalent to changing the causality of different sensors. Such changes imply that for the diagnosis problem, measurements are known variables. The substitution of sensors by sources changes the causalities of junctions and elements in the BG model. Also, all the storage elements are assigned with derivative causalities so that unknown initial conditions are eliminated. Usually, for each sensor one ARR is generated, thus the number of ARR s is the same as the numbers of sensors in the plant. For instance, the BG model of an electric circuit (figure B.15(a)) is shown in figure B.15(b), where $Se : V_s$, $R : R_1$, $R : R_2$, $C : 1/C_1$ and $C : 1/C_2$ model the voltage source, resistances , R_1 and R_2, and capacitances C_1 and C_2, respectively. The current (flow) sensor is modeled by $Df : I$ and the two voltage (effort) sensors are modeled by $De : V_1$ and $De : V_2$. The 1-junctions in the model indicate common flow (current) or series connection and the 0-junctions indicate common effort (potential difference) or parallel connection. Note that flow detector Df always appears at 1 junction and effort detector De always appears at 0 junction. The causalities assigned in figure refelectrical circuit(b) have integral causality in storage (here C) elements and the sensors have usual causality. The model

in figure refelectrical circuit(b) has no causal conflict and can be used to simulate the behavior of the system for given inputs, parameter values and initial conditions (initial charges in the two capacitors).
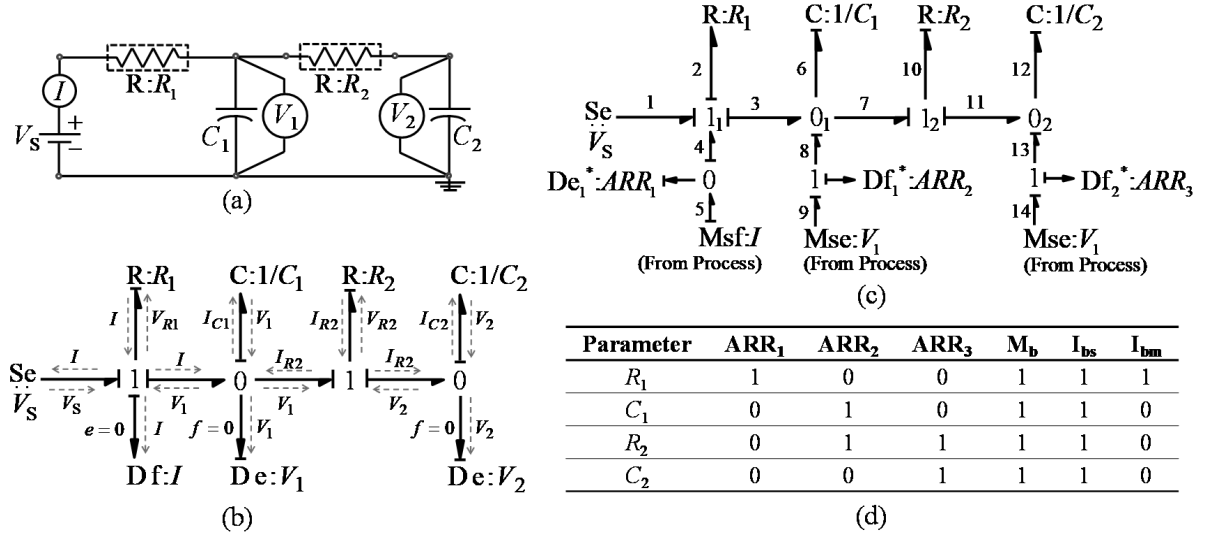
Figure B.15: (a) Example of an electric circuit, (b) BG model, (c) DBG model, and (d) corresponding FSM.

The DBG model of the system is shown in figure B.15(c), where the flow (current) sensor $Df : I$ and effort (voltage) sensors $De : V_1$ and $De : V_2$ of BG model (figure B.15(b)) are replaced by $Msf : I$ and $MSe : V_1$, $MSe : V_2$, respectively. In figure B.15(c), one imaginary effort detector (De_1^*) and two imaginary flow detectors (Df_1^* and Df_2^*) are introduced at new outputs. For a nominal plant with nominal parameters, these new outputs should be zero and hence the equations for these outputs give ARR s. Accordingly, one of the ARR s is derived from $De_1^* = e_4 = 0$ after eliminating the unknown variables by using the causality assignment. An ARR ($\mathbf{U}$, $\mathbf{Y}$, $\boldsymbol{\theta}$) is a constraint written in terms of input vector $\mathbf{U} \in (Se, Sf)$, known measurements imposed on DBG $\mathbf{Y} \in (MSe, MSf)$ in place of (De, Df) in original BG, and a parameter vector $\boldsymbol{\theta} = [\theta_1, \theta_2, ..., \theta_j, ..., \theta_p]^T$ comprising p number of known nominal parameters. For the causality assignment shown in figure B.15(c), at junction 1_1, $e_4 = -e_1 + e_2 + e_3$, where $e_1 = V_s$, $e_2 = f_2R_1 = f_4R_1 = f_5R_1 = IR_1$ and $e_3 = e_8 = e_9 = V_1$. Thus, after putting all known effort values in $De_1^* = 0$, it provides the ARR $_1$ as $V_s - IR_1 - V_1 = 0$ which is an expression containing only the known (measured) variables and parameter. Disregarding measurement faults, the constraint (or consistency check) expressed by ARR $_1$ is satisfied as long as the system operates without any deviation in the value of R_1. The evaluation of an ARR expression is called a residual. Here, the first residual $r_1(t) = \text{Eval}(\text{ARR}_1)$ at time t. If the value of R_1 has changed and the measurements have changed due to that, then, $r_1 \neq 0$ with new measurements and old/nominal value of R_1 and that indicates a degradation of R_1. The influence of parameter deviations on specific residuals is represented in a FSM. The FSM for the electrical system in figure B.15(a) is shown in Figure B.15(d) where only one residual r_1 (corresponding to ARR $_1$) would deviate with deviation of R_1 value and such a residual with one to one map is called a structured residual. In fact, to accommodate sensor noise and uncertainties, the residual consistency check is performed by specifying a threshold allowable deviation of residual, i.e. residual r_1 will be assumed to be consistent if $|r_1(t)| \leq \varepsilon_1(t)$ where ε_1 is a small threshold. In the prognosis problem, attempt is made to find the instantaneous true value of R_1 and the trend of its deviation which would keep $|r_1| \leq \varepsilon_1$ at all times, and then

postulate the time after which the true value of R_1 would violate a threshold limit of acceptable performance.

Likewise, the DBG in figure B.15(c) shows $Df_1{}^* = f_8 = 0$ and $Df_2{}^* = f_{13} = 0$, which provide the ARR $_2$ and ARR $_3$ after elimination of all unknown variables. Thus the ARR s of the electric circuit are expressed as

$$De_1^* : \mathrm{ARR}_1 = V_s - IR_1 - V_1 = 0 \tag{B.26}$$

$$Df_1{}^* : \mathrm{ARR}_2 = I - C_1\frac{\mathrm{d}}{\mathrm{d}t}V_1 - \frac{(V_1 - V_2)}{R_2} \tag{B.27}$$

$$\&Df_2{}^* : \mathrm{ARR}_3 = \frac{(V_1 - V_2)}{R_2} - C_2\frac{\mathrm{d}}{\mathrm{d}t}V_2 \tag{B.28}$$

In normal operation, ideally, residuals should be zero. However, due to modeling and process uncertainties, evaluated residuals show small non-zero values. In order to account for these uncertainties in a robust diagnosis/prognosis, the system is modelled in DBG-LFT form. For uncertain dynamic systems, nominal and uncertain parts of the ARR s are separated from the outputs of the DBG-LFT model and the uncertain parts are used to specify the residual thresholds, called adaptive thresholds. The adaptive thresholds should envelope the residuals evaluated by using the nominal ARR s during normal operation of the system or the system which has not degraded sufficiently.

Generally, the parameter uncertainty of any parameter value $\theta_j \in (I, C, R, TF, GY)$ can be represented either in a multiplicative form or an additive form as follow:

$$\begin{aligned}\theta_j &= \theta_{jn}(1 \pm \delta_{\theta_j})\\ \text{or}\,\theta_j &= \theta_{jn} \pm \Delta\theta_j\end{aligned} \tag{B.29}$$

where $\delta_{\theta_j} = (\Delta\theta_j/\theta_{jn})$ and $\Delta\theta_j$ are the relative and the absolute deviations of nominal parameter value θ_{jn}

In DBG-LFT form model, the nominal value of parameter θ_{jn} is decoupled from its uncertain part $\pm\Delta\theta_j$. The uncertain part is treated as a disturbance either in the form of additional flow or effort that depends on the type of BG element and its causality in the model. In DBG-LFT model, parameter $\theta_j \in (C)$ and $\theta_j \in (I)$, in differential causality, are modelled in the form as shown in figure B.16(a) and figure B.16(b), respectively, where J indicates a junction (0 or 1). Likewise, $\theta_j \in (R)$ is modelled in either form as shown in figure B.16(a) or figure B.16(b). Thus, the additional disturbance flow (or effort) due to uncertain part is brought to the junction 0 (or 1) by the uncertainty $\mp\delta_{\theta*}$ as shown in figure B.16(a) (or figure B.16(b)). This is achieved by introducing the virtual flow (or effort) sensor $Df' : z_{\theta*}$ (or $De' : z_{\theta*}$) and virtual modulated source of flow (or effort) input $MSf' : \pm w_{\theta*}$ (or$MSe' : \pm w_{\theta*}$) into the uncertain BG model. Note that subscript θ^* depends on the constitutive law of respective element. For instance, let us consider the linear R-element in the conductive causality (causal form in figure B.16(a)) with associated power variables e_R (effort) and f_R (flow). If the true parameter value of a resistor R-element is not known exactly then it can be expressed as $R_n \pm \Delta R = R_n(1 \pm \delta_R)$ where R_n denotes nominal parameter value and $\pm\Delta R = \pm\delta_R R_n$ is the uncertain part of R. The constitutive law of linear R-element modelled in conductive causality is given as

$$f_R = \frac{1}{R_n \pm \Delta R}e_R = \frac{1}{R_n}\left(1 \mp \delta_{1/R}\right)e_R = \frac{e_R}{R_n} \mp w_{1/R} = f_{Rn} \mp w_{1/R} \tag{B.30}$$

where f_{Rn} is nominal flow and $\mp\delta_{1/R}(e_R/R_n) = \mp w_{1/R}$ is the additional contribution of flow due to uncertain part of the parameter R and may be treated as a disturbance. Note that $\delta_{1/R}$ is the uncertainty in estimating the value of $1/R$.

131
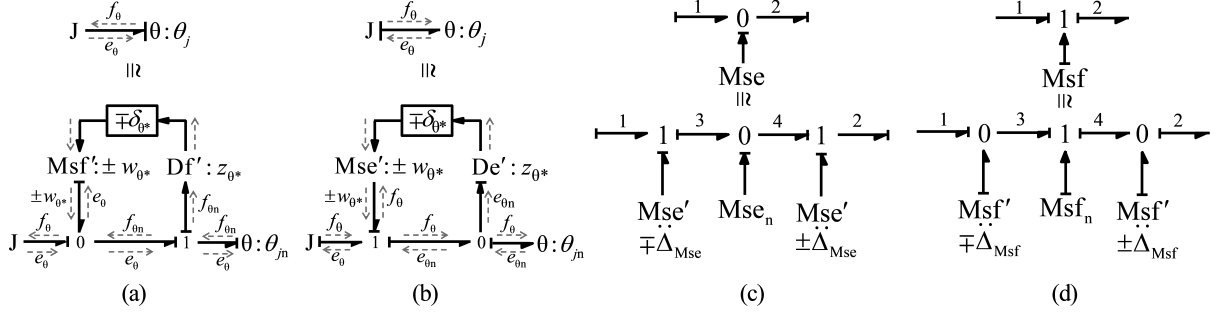
Figure B.16: (a)-(b) Modelling parameter uncertainty, and (c)-(d) modelling measurement uncertainty in DBG-LFT

Likewise, other BG elements (TF and GY) with uncertainties in the parameter values can be modelled by using BG-LFT form model. Also, the error in the measurement of effort (or flow) Δ_{MSe}(or Δ_{MSf}) may be detached from its nominal effort (or flow) part MSe_n (or MSf_n) and can be expressed as

$$MSe = MSe_n \pm \Delta_{MSe}$$
$$MSf = MSf_n \pm \Delta_{MSf}$$
(B.31)

These measurement errors Δ_{MSe} and Δ_{MSf} can be modelled by the virtual sources MSe' (shown in figure B.16(c))) and MSf' (shown in figure B.16(d))), respectively, in DBG-LFT form model at the respective junctions.

The DBG-LFT form model separates the nominal and uncertain parts of ARR s for robust fault diagnosis of an uncertain system. Without the loss of generality, the ARR $(\mathbf{U}, \mathbf{Y}, \boldsymbol{\theta})$ of an uncertain system may be expressed as

$$\mathrm{ARR}_{ni}\left(\mathbf{U}, \mathbf{Y}, \boldsymbol{\theta}\right) \pm \left(\lambda_i + \lambda_{Si}\right) = 0$$
(B.32)

where ARR_{ni}, λ_i and λ_{Si} represent the i-th nominal ARR that gives residual (r_i) $(i = 1, 2, ..., n; n$ is number of residuals), the uncertain part due to parameter uncertainties and the static uncertain part needed to account for measurement noise, respectively. Also, $\mathbf{U} \in (\mathbf{Se}, \mathbf{Sf})$ is the known input vector, $\mathbf{Y} \in (\mathbf{MSe_n}, \mathbf{MSf_n})$ is the nominal measurement vector, $\boldsymbol{\theta} = [\theta_1, \theta_2, ..., \theta_j, ..., \theta_p]^T$ is the nominal parameter vector comprising p parameters, $\lambda_i \in w_{\theta_j}$ and $\lambda_{Si} \in (\Delta_{MSe}, \Delta_{MSf})$.

Online evaluation of each nominal part, ARR_{ni}, and uncertain part,$(\lambda_i + \lambda_{Si})$, using $\mathbf{U}$, $\mathbf{Y}$, and $\boldsymbol{\theta}$ along with the different specified uncertainties bounds provides residual (r_i) and adaptive thresholds $(\varepsilon = \pm|(\lambda_i + \lambda_{Si})|)$, respectively. Note that as the absolute values of different uncertain parts contribution is added in the adaptive threshold, the small λ_{Si} part may be neglected. A coherence vector $(\mathbf{C})$ whose standard form is $\mathbf{C} = [\mathbf{c_1(t)}, \mathbf{c_2(t)}, ..., \mathbf{c_n(t)}]$, where $c_i(t) \in 0, 1 (i = 1, 2, ..., n)$ is used to generate the alarms during on-line supervision. The element $c_i(t)$ of coherence vector $(\mathbf{C})$ depends on the decision procedure, $\Theta\left(r_i(t)\right)$, and is obtained as

$$c_i(t) = \Theta\left(r_i(t)\right) = \begin{cases} 0, \text{if} - \varepsilon_i(t) \leq r_i(t) \leq \varepsilon_i(t), \\ 1, \text{otherwise}. \end{cases}$$
(B.33)

During normal operation of the system, all elements of coherence vector $(\mathbf{C})$ show zero values; otherwise non-zero value of any element of $\mathbf{C}$ indicates the abnormal behaviour of the system and it generates the alarm. In the present case, abnormal behaviour implies sufficient deviation of at least one parameter value from the corresponding nominal value. After an alarm is raised, the next step in the diagnosis is the isolation of the parameters whose values have deviated sufficiently (more than the uncertainty values), i.e. the components which have degraded beyond specified limits.

132

For isolation of degraded component, the standard FSM is used which includes the fault/degradation symptoms of different components of a system and it can be generated systematically by testing the sensitivity of each ARR with respect to each component's parameter. In FSM, columns represent the set of residuals and rows represent the set of components or parameters. Each row contains signature for the respective parameter in the form of a binary number (1 or 0) according to sensitivity of each ARR. If i-th ARR is sensitive to j-th parameter deviation then the entry in i-th column and j-th row of FSM is 1, which is otherwise 0. A degradation/fault of a component is monitorable if at least any one of the residuals is sensitive to it whereas it is isolatable only when the row vector corresponding to that component/parameter is different from the row vectors corresponding to all other components/parameters. So, monitorability index (M_{b}) and isolatability index (I_{bs}) are also included in the FSM to represent detectability and isolatability of the degradations/faults. These indices are shown as binary numbers 1 and 0, respectively, for TRUE and FALSE. The coherence vector ($\mathbf{C}$) is continuously evaluated at small time intervals during the system monitoring and if it is non-zero at any time then there is some fault/ degradation of a component and that particular component can be isolated by uniquely matching the coherence vector with rows of the FSM. For the detection and isolation of any degradation/fault, the corresponding monitorability index and isolatability index values must be 1. For instance, FSM of electric circuit example (figure B.15(a)) are obtained by analysing the ARR s and is shown in figure B.15(d) in the tabular form with isolatability indices I_{bs} for of single fault/degradation case and I_{bm} for multiple faults/degradations case. For isolation of multiple faults/degradations, FSM should be in diagonal or structured form. However, most often unstructured form of FSM is obtained due to the limitation of sensors placement in the plant. For example, from the FSM in figure B.15(d), fault/degrdation in R_1 belongs to structured part of the FSM and is always isolatable (both in single and multiple faults/degradations cases). However, other parameters (C_1, R_2 and C_2) belong to unstructured part of FSM and are not isolatable in multiple faults/degradations cases. Thus, for isolation of actual faults/degradations in such case of unstructured FSM, parameter estimation is required.

Bibliography

[1] Annalisa Savaresi. "The Paris agreement: a new beginning?" In: *Journal of Energy & Natural Resources Law* 34.1 (2016), pp. 16–26. DOI: 10.1080/02646811.2016.1133983.

[2] *Statistical review of world energy 2021*. Accessed on 10-08-2021. URL: https://www.bp.com/content/dam/bp/business-sites/en/global/corporate/pdfs/energy-economics/statistical-review/bp-stats-review-2021-full-report.pdf.

[3] Véronique Fröding and Stéphane Gasne. "France". In: *Renewable Energy 2021*. Global Legal Group Ltd, London, 2020, pp. 33–40. URL: https://iclg.com/practice-areas/renewable-energy-laws-and-regulations/france.

[4] *Année 2020*. Accessed on 10-08-2021. URL: http://www.deule-climat.net/2020.htm.

[5] I. P. Jain. "Hydrogen the fuel for 21st century". In: *International Journal of Hydrogen Energy* 34.17 (2009), pp. 7368–7378. DOI: 10.1016/j.ijhydene.2009.05.093.

[6] Pierre Olivier, Cyril Bourasseau, and Belkacem Ould-Bouamama. "Low-temperature electrolysis system modelling: a review". In: *Renewable & Sustainable Energy Reviews* 78 (2017), pp. 280–300. DOI: 10.1016/j.rser.2017.03.099.

[7] O. C. Onar, M. Uzunoglu, and M. S. Alam. "Dynamic modeling, design and simulation of a wind/fuel cell/ultra-capacitor-based hybrid power generation system". In: *Journal of Power Sources* 161.1 (2006), pp. 707–722. ISSN: 0378-7753. DOI: 10.1016/j.jpowsour.2006.03.055.

[8] IEA(2021). *Net zero by 2050*. Accessed on 11-08-2021. URL: https://www.iea.org/reports/net-zero-by-2050.

[9] IEA(2019). *The future of hydrogen*. Accessed on 11-08-2021. URL: https://www.iea.org/reports/the-future-of-hydrogen.

[10] Gregory A. DiLisi. "The Hindenburg disaster: combining physics and history in the laboratory". In: *The Physics Teacher* 55.5 (2017), pp. 268–273. DOI: 10.1119/1.4981031.

[11] Frano Barbir. "PEM electrolysis for production of hydrogen from renewable energy sources". In: *Solar Energy* 78.5 (2005), pp. 661–669. DOI: 10.1016/j.solener.2004.09.003.

[12] Marcelo Carmo et al. "A comprehensive review on PEM water electrolysis". In: *International Journal of Hydrogen Energy* 38.12 (2013), pp. 4901–4934. DOI: 10.1016/j.ijhydene.2013.01.151.

[13] Florian Josef Wirkert et al. "A modular design approach for PEM electrolyser systems with homogeneous operation conditions and highly efficient heat management". In: *International Journal of Hydrogen Energy* 45.2 (2020), pp. 1226–1235. DOI: 10.1016/j.ijhydene.2019.03.185.

[14] D. S. Falcão and A. M. F. R. Pinto. "A review on PEM electrolyzer modelling: guidelines for beginners". In: *Journal of Cleaner Production* 261 (2020), 121184:1–121184:10. DOI: 10.1016/j.jclepro.2020.121184.

[15] Pierre Olivier, Cyril Bourasseau, and Belkacem Ould-Bouamama. "Dynamic and multiphysic PEM electrolysis system modelling: a bond graph approach". In: *International Journal of Hydrogen Energy* 42.22 (2017), pp. 14872–14904. DOI: 10.1016/j.ijhydene.2017.03.002.

[16]   L. An et al. "Mathematical modeling of an anion-exchange membrane water electrolyzer for hydrogen production". In: *International Journal of Hydrogen Energy* 39.35 (2014), pp. 19869–19876. ISSN: 0360–3199. DOI: 10.1016/j.ijhydene.2014.10.025.

[17]   Ibrahim Abdallah, Anne-Lise Gehin, and Belkacem Ould-Bouamama. "Event driven hybrid bond graph for hybrid renewable energy systems part I: modelling and operating mode management". In: *International Journal of Hydrogen Energy* 43.49 (2018), pp. 22088–22107. DOI: 10.1016/j.ijhydene.2017.10.144.

[18]   Arun Kumar Samantaray and Belkacem Ould-Bouamama. *Model-based process supervision: a bond graph approach.* Springer Science & Business Media, 2008. DOI: 10.1007/978-1-84800-159-6.

[19]   Steven X. Ding. *Model-based fault diagnosis techniques: design schemes, algorithms, and tools.* Springer Science & Business Media, 2008. DOI: 10.1007/978-1-4471-4799-2.

[20]   Venkat Venkatasubramanian et al. "A review of process fault detection and diagnosis: part I: quantitative model-based methods". In: *Computers & Chemical Engineering* 27.3 (2003), pp. 293–311. ISSN: 0098–1354. DOI: 10.1016/S0098-1354(02)00160-6.

[21]   Venkat Venkatasubramanian, Raghunathan Rengaswamy, and Surya N. Kavuri. "A review of process fault detection and diagnosis: part II: qualitative models and search strategies". In: *Computers & Chemical Engineering* 27.3 (2003), pp. 313–326. ISSN: 0098–1354. DOI: 10.1016/S0098-1354(02)00161-8.

[22]   Venkat Venkatasubramanian et al. "A review of process fault detection and diagnosis: part III: process history based methods". In: *Computers & Chemical Engineering* 27.3 (2003), pp. 327–346. ISSN: 0098–1354. DOI: 10.1016/S0098-1354(02)00162-X.

[23]   K. Medjaher and N. Zerhouni. "Residual-based failure prognostic in dynamic systems". In: *IFAC Proceedings Volumes* 42.8 (2009). 7th IFAC Symposium on Fault Detection, Supervision and Safety of Technical Processes, pp. 716–721. ISSN: 1474-6670. DOI: 10.3182/20090630-4-ES-2003.00119.

[24]   George Vachtsevanos et al. *Intelligent fault diagnosis and prognosis for engineering systems.* Hoboken, New Jersey: John Wiley & Sons, Ltd, 2006. DOI: 10.1002/9780470117842.

[25]   Henry Edwardes-Evans. *Green hydrogen costs need to fall over 50% to be viable: S&P Global ratings.* Accessed on 30-08-2021. URL: https://www.spglobal.com/platts/en/market-insights/latest-news/electric-power/112020-green-hydrogen-costs-need-to-fall-over-50-to-be-viable-sampp-global-ratings.

[26]   Dmitri Bessarabov and Pierre Millet. *PEM water electrolysis.* Vol. 2. Hydrogen and Fuel Cells Primers. Academic Press, 2018. DOI: 10.1016/C2018-0-02127-1.

[27]   Nicola Briguglio and Vincenzo Antonucci. "Overview of PEM electrolysis for hydrogen production". In: *PEM Electrolysis for Hydrogen Production: Principles and Applications.* CRC Press, 2016, pp. 1–9. DOI: 10.1201/b19096.

[28]   Dmitri Bessarabov et al. *PEM electrolysis for hydrogen production: principles and applications.* 1st. Boca Raton: CRC Press: Boca Raton, 2016. ISBN: 9780429183607. DOI: 10.1201/b19096.

[29]   Ali Keçebaş, Muhammet Kayfeci, and Mutlucan Bayat. "Chapter 9 - electrochemical hydrogen generation". In: *Solar Hydrogen Production.* Ed. by Francesco Calise et al. Academic Press, 2019, pp. 299–317. ISBN: 978-0-12-814853-2. DOI: 10.1016/B978-0-12-814853-2.00009-6.

136

[30] Robert Phillips and Charles W Dunnill. "Zero gap alkaline electrolysis cell design for renewable energy storage as hydrogen gas". In: *RSC Advances* 6.102 (2016), pp. 100643–100651. DOI: 10.1039/C6RA22242K.

[31] Gernot Voitic et al. "Chapter 10 - hydrogen production". In: *Fuel Cells and Hydrogen.* Ed. by Viktor Hacker and Shigenori Mitsushima. Elsevier, 2018, pp. 215–241. ISBN: 978-0-12-811459-9. DOI: 10.1016/B978-0-12-811459-9.00010-4.

[32] Sarbjit Giddey, Sukhvinder P. S. Badwal, and HyungKuk Ju. "Polymer electrolyte membrane technologies integrated with renewable energy for hydrogen production". In: *Current trends and future developments on (Bio-) membranes.* Elsevier, 2019, pp. 235–259. ISBN: 978-0-12-813545-7. DOI: 10.1016/B978-0-12-813545-7.00010-6.

[33] Linsey C. Seitz et al. "Enhancement effect of noble mMetals on manganese oxide for the oxygen evolution reaction". In: *The Journal of Physical Chemistry Letters* 6.20 (2015), pp. 4178–4183. DOI: 10.1021/acs.jpclett.5b01928.

[34] Immanuel Vincent and Dmitri Bessarabov. "Low cost hydrogen production by anion exchange membrane electrolysis: a review". In: *Renewable and Sustainable Energy Reviews* 81 (2018), pp. 1690–1704. ISSN: 1364-0321. DOI: 10.1016/j.rser.2017.05.258.

[35] Aziz Nechache and Stéphane Hody. "Alternative and innovative solid oxide electrolysis cell materials: a short review". In: *Renewable and Sustainable Energy Reviews* 149 (2021), p. 111322. ISSN: 1364-0321. DOI: 10.1016/j.rser.2021.111322.

[36] O. Schmidt et al. "Future cost and performance of water electrolysis: an expert elicitation study". In: *International Journal of Hydrogen Energy* 42.52 (2017), pp. 30470–30492. ISSN: 0360-3199. DOI: 10.1016/j.ijhydene.2017.10.045.

[37] Yujing Guo et al. "Comparison between hydrogen production by alkaline water electrolysis and hydrogen production by PEM electrolysis". In: *IOP Conference Series: Earth and Environmental Science* 371 (2019), p. 042022. DOI: 10.1088/1755-1315/371/4/042022.

[38] Changqing Li and Jong-Beom Baek. "The promise of hydrogen production from alkaline anion exchange membrane electrolyzers". In: *Nano Energy* 87 (2021), p. 106162. ISSN: 2211-2855. DOI: 10.1016/j.nanoen.2021.106162.

[39] Hamish Andrew Miller et al. "Green hydrogen from anion exchange membrane water electrolysis: a review of recent developments in critical materials and operating conditions". In: *Sustainable Energy Fuels* 4 (5 2020), pp. 2114–2133. DOI: 10.1039/C9SE01240K.

[40] Pengzuo Chen and Xile Hu. "High-efficiency anion exchange membrane water electrolysis employing non-noble metal catalysts". In: *Advanced Energy Materials* 10.39 (2020), p. 2002285. DOI: 10.1002/aenm.202002285.

[41] Jaromír Hnát, Martin Paidar, and Karel Bouzek. "Chapter 5 - hydrogen production by electrolysis". In: *Current Trends and Future Developments on (Bio-) Membranes.* Ed. by Adolfo Iulianelli and Angelo Basile. Elsevier, 2020, pp. 91–117. ISBN: 978-0-12-817384-8. DOI: 10.1016/B978-0-12-817384-8.00005-4.

[42] Dimitris Ipsakis et al. "Power management strategies for a stand-alone power system using renewable energy sources and hydrogen storage". In: *International Journal of Hydrogen Energy* 34.16 (2009). 4th Dubrovnik Conference, pp. 7081–7095. ISSN: 0360-3199. DOI: 10.1016/j.ijhydene.2008.06.051.

[43] Tao Zhou et al. "Modeling and control design of hydrogen production process by using a causal ordering graph for wind energy conversion system". In: *In Proceedings of the IEEE International Symposium on Industrial Electronics, Vigo, Spain.* IEEE. 4–7 June 2007, pp. 3192–3197. DOI: 10.1109/ISIE.2007.4375126.

[44] Francisco da Costa Lopes and Edson H. Watanabe. "Experimental and theoretical development of a PEM electrolyzer model applied to energy storage systems". In: *2009 Brazilian Power Electronics Conference.* IEEE. 2009, pp. 775–782. DOI: 10.1109/COBEP.2009.5347619.

[45] Ozcan Atlam. "An experimental and modelling study of a photovoltaic/proton-exchange membrane electrolyser system". In: *International Journal of Hydrogen Energy* 34.16 (2009). 4th Dubrovnik Conference, pp. 6589–6595. ISSN: 0360-3199. DOI: 10.1016/j.ijhydene.2009.05.147.

[46] Tao Zhou and Bruno Francois. "Modeling and control design of hydrogen production process for an active hydrogen/wind hybrid power system". In: *International Journal of Hydrogen Energy* 34.1 (2009), pp. 21–30. ISSN: 0360-3199. DOI: 10.1016/j.ijhydene.2008.10.030.

[47] J. J. Hwang et al. "Dynamic modeling of a photovoltaic hydrogen fuel cell hybrid system". In: *International Journal of Hydrogen Energy* 34.23 (2009), pp. 9531–9542. ISSN: 0360-3199. DOI: 10.1016/j.ijhydene.2009.09.100.

[48] R. García-Valverde, N. Espinosa, and A. Urbina. "Optimized method for photovoltaic-water electrolyser direct coupling". In: *International Journal of Hydrogen Energy* 36.17 (2011), pp. 10574–10586. DOI: 10.1016/j.ijhydene.2011.05.179.

[49] S. M. Muyeen, R. Takahashi, and J. Tamura. "Electrolyzer switching strategy for hydrogen generation from variable speed wind generator". In: *Electric Power Systems Research* 81.5 (2011), pp. 1171–1179. ISSN: 0378-7796. DOI: 10.1016/j.epsr.2011.01.005.

[50] Abd El-Shafy A. Nafeh. "Hydrogen production from a PV/PEM electrolyzer system using a neural-network-based MPPT algorithm". In: *International Journal of Numerical Modelling: Electronic Networks, Devices and Fields* 24.3 (2011), pp. 282–297. DOI: 10.1002/jnm.778.

[51] Mustafa Ergin Şahin, Halil İbrahim Okumuş, and Mehmet Timur Aydemir. "Implementation of an electrolysis system with DC/DC synchronous buck converter". In: *International Journal of Hydrogen Energy* 39.13 (2014), pp. 6802–6812. ISSN: 0360-3199. DOI: 10.1016/j.ijhydene.2014.02.084.

[52] Raúl Sarrias-Mena et al. "Electrolyzer models for hydrogen production from wind energy systems". In: *International Journal of Hydrogen Energy* 40.7 (2015), pp. 2927–2938. ISSN: 0360-3199. DOI: 10.1016/j.ijhydene.2014.12.125.

[53] W. Saeed and Ghaith Warkozek. "Modeling and analysis of renewable PEM fuel cell system". In: *Energy Procedia* 74 (2015), pp. 87–101. DOI: 10.1016/j.egypro.2015.07.527.

[54] Blal Mohamed, Benattilah Alli, and Bellassri Ahmed. "Using the hydrogen for sustainable energy storage: designs, modeling, identification and simulation membrane behavior in PEM system electrolyser". In: *Journal of Energy Storage* 7 (2016), pp. 270–285. ISSN: 2352-152X. DOI: 10.1016/j.est.2016.06.006.

[55] Christoph Rakousky et al. "An analysis of degradation phenomena in polymer electrolyte membrane water electrolysis". In: *Journal of Power Sources* 326 (2016), pp. 120–128. DOI: 10.1016/j.jpowsour.2016.06.082.

[56] F. Fouda-Onana et al. "Investigation on the degradation of MEAs for PEM water electrolysers part I: effects of testing conditions on MEA performances and membrane properties". In: *International Journal of Hydrogen Energy* 41.38 (2016), pp. 16627–16636. ISSN: 0360-3199. DOI: 10.1016/j.ijhydene.2016.07.125.

[57] Domenico Ferrero and Massimo Santarelli. "Investigation of a novel concept for hydrogen production by PEM water electrolysis integrated with multi-junction solar cells". In: *Energy Conversion and Management* 148 (2017), pp. 16–29. ISSN: 0196-8904. DOI: 10.1016/j.enconman.2017.05.059.

[58] Kamaljyoti Talukdar. "Modeling and analysis of solar photovoltaic assisted electrolyzer-polymer electrolyte membrane fuel cell for running a hospital in remote area in Kolkata, India". In: *International Journal of Renewable Energy Development* 6.2 (2017), pp. 181–191. DOI: 10.14710/ijred.6.2.181-191.

[59] Vesa Ruuskanen et al. "PEM water electrolyzer model for a power-hardware-in-loop simulator". In: *International Journal of Hydrogen Energy* 42.16 (2017), pp. 10775–10784. DOI: 10.1016/j.ijhydene.2017.03.046.

[60] Mohamed Albarghot and Luc Rolland. "Comparison of experimental results with simulation of a PEM electrolyzer powered by a horizontal wind turbine". In: *2017 International Conference of Electrical and Electronic Technologies for Automotive*. 2017, pp. 1–6. DOI: 10.23919/EETA.2017.7993232.

[61] Vesa Ruuskanen et al. "Design and implementation of a power-hardware-in-loop simulator for water electrolysis emulation". In: *Renewable Energy* 119 (2018), pp. 106–115. ISSN: 0960-1481. DOI: 10.1016/j.renene.2017.11.088.

[62] A. Mraoui, B. Benyoucef, and L. Hassaine. "Experiment and simulation of electrolytic hydrogen production: case study of photovoltaic-electrolyzer direct connection". In: *International Journal of Hydrogen Energy* 43.6 (2018), pp. 3441–3450. ISSN: 0360-3199. DOI: 10.1016/j.ijhydene.2017.11.035.

[63] Steffen Henrik Frensch et al. "Influence of the operation mode on PEM water electrolysis degradation". In: *International Journal of Hydrogen Energy* 44.57 (2019), pp. 29889–29898. ISSN: 0360-3199. DOI: 10.1016/j.ijhydene.2019.09.169.

[64] Raffaele Petrone and Robin Roche. *Diagnostics and prognostics for the wind-hydrogen plant*. Accessed on 01-09-2021. URL: https://www.haeolus.eu/wp-content/uploads/2019/09/D6.5.pdf.

[65] Christian Schnuelle et al. "Dynamic hydrogen production from PV & wind direct electricity supply – modeling and techno-economic assessment". In: *International Journal of Hydrogen Energy* 45.55 (2020), pp. 29938–29952. ISSN: 0360-3199. DOI: 10.1016/j.ijhydene.2020.08.044.

[66] Boris Bensmann and Richard Hanke-Rauschenbach. "(Invited) Engineering modeling of PEM water electrolysis: a survey". In: *ECS Transactions* 75.14 (2016), p. 1065. DOI: 10.1149/07514.1065ecst.

[67] A. H. Abdol Rahim et al. "An overview of polymer electrolyte membrane electrolyzer for hydrogen production: modeling and mass transport". In: *Journal of Power Sources* 309 (2016), pp. 56–65. ISSN: 0378-7753. DOI: 10.1016/j.jpowsour.2016.01.012.

[68] Burin Yodwong et al. "Proton exchange membrane electrolyzer modeling for power electronics control: a short review". In: *C* 6.2 (2020). ISSN: 2311-5629. DOI: 10.3390/c6020029.

[69] Ángel Hernández-Gómez, Victor Ramirez, and Damien Guilbert. "Investigation of PEM electrolyzer modeling: electrical domain, efficiency, and specific energy consumption". In: *International Journal of Hydrogen Energy* 45.29 (2020), pp. 14625–14639. ISSN: 0360-3199. DOI: 10.1016/j.ijhydene.2020.03.195.

[70] Kazuo Onda et al. "Performance analysis of polymer-electrolyte water electrolysis cell at a small-unit test cell and performance prediction of large stacked cell". In: *Journal of The Electrochemical Society* 149.8 (2002), A1069. DOI: 10.1149/1.1492287.

[71] Pyoungho Choi, Dmitri G. Bessarabov, and Ravindra Datta. "A simple model for solid polymer electrolyte (SPE) water electrolysis". In: *Solid State Ionics* 175.1 (2004). Fourteenth International Conference on Solid State Ionics, pp. 535–539. ISSN: 0167-2738. DOI: 10.1016/j.ssi.2004.01.076.

[72] S. Sawada et al. "Solid polymer electrolyte water electrolysis systems for hydrogen production based on our newly developed membranes, part I: analysis of voltage–current characteristics". In: *Progress in Nuclear Energy* 50.2 (2008), pp. 443–448. ISSN: 0149-1970. DOI: 10.1016/j.pnucene.2007.11.029.

[73] S. A. Grigoriev et al. "High-pressure PEM water electrolysis and corresponding safety issues". In: *International Journal of Hydrogen Energy* 36.3 (2011), pp. 2721–2728. DOI: 10.1016/j.ijhydene.2010.03.058.

[74] Timothy D. Myles et al. "Species transport in a high-pressure oxygen-generating proton-exchange membrane electrolyzer". In: *International Journal of Hydrogen Energy* 37.17 (2012), pp. 12451–12463. DOI: 10.1016/j.ijhydene.2012.05.123.

[75] Luiz Fernando L. Oliveira, Christian Jallut, and Alejandro A. Franco. "A multiscale physical model of a polymer electrolyte membrane water electrolyzer". In: *Electrochimica Acta* 110 (2013). Electrochemistry for Advanced Materials, Technologies and Instrumentation, pp. 363–374. ISSN: 0013-4686. DOI: 10.1016/j.electacta.2013.07.214.

[76] A. H. Abdol Rahim et al. "Mathematical modelling and simulation analysis of PEM electrolyzer system for hydrogen production". In: *3rd IET International Conference on Clean Energy and Technology (CEAT) 2014*. 2014, pp. 1–7. DOI: 10.1049/cp.2014.1466.

[77] David L. Fritz, Jürgen Mergel, and Detlef Stolten. "PEM electrolysis simulation and validation". In: *ECS Transactions* 58.19 (2014). Accessed on 11-08-2021, p. 1.

[78] Ishanka Dedigama et al. "An experimentally validated steady state polymer electrolyte membrane water electrolyser model". In: *International Journal of Electrochemical Science* 9.5 (2014). Accessed on 15-08-2021, pp. 2662–2681. URL: http://electrochemsci.org/papers/vol9/90502662.pdf.

[79] M. Chandesris et al. "Membrane degradation in PEM water electrolyzer: numerical modeling and experimental evidence of the influence of temperature and current density". In: *International Journal of Hydrogen Energy* 40.3 (2015), pp. 1353–1366. DOI: 10.1016/j.ijhydene.2014.11.111.

[80] M. Chandesris et al. "Numerical modelling of membrane degradation in PEM water electrolyzer : influence of the temperature and current density". In: *6th International Conference on Fundamentals and Development of Fuel Cells, FDFC2015, Toulouse, FRANCE*. Accessed on 11-08-2021. 3–5 February 2015, pp. 3192–3197. URL: https://www.sintef.no/globalassets/project/novel/pdf/oral-presentations/numerical-modelling-of-membrane-degradation-in-pem-water-electrolyzer.pdf.

[81] AH Abdol Rahim and Alhassan Salami Tijani. "Modeling and analysis the effects of temperature and pressure on the gas-crossover in polymer electrolyte membrane electrolyzer". In: *World Academy of Science, Engineering and Technology, International Journal of Electrical, Computer, Energetic, Electronic and Communication Engineering* 10 (2015), 1e7. DOI: 10.5281/zenodo.1110517.

[82] Alhassan Salami Tijani and A. H. Abdol Rahim. "Numerical modeling the effect of operating variables on faraday efficiency in PEM electrolyzer". In: *Procedia Technology* 26 (2016). 3rd International Conference on System-Integrated Intelligence: New Challenges for Product and Production Engineering, pp. 419–427. ISSN: 2212-0173. DOI: 10.1016/j.protcy.2016.08.054.

[83] Bo Han et al. "Effects of membrane electrode assembly properties on two-phase transport and performance in proton exchange membrane electrolyzer cells". In: *Electrochimica Acta* 188 (2016), pp. 317–326. ISSN: 0013-4686. DOI: 10.1016/j.electacta.2015.11.139.

[84] Bo Han et al. "Modeling of two-phase transport in proton exchange membrane electrolyzer cells for hydrogen energy". In: *International Journal of Hydrogen Energy* 42.7 (2017), pp. 4478–4489. ISSN: 0360-3199. DOI: 10.1016/j.ijhydene.2016.12.103.

[85] F. Aubras et al. "Two-dimensional model of low-pressure PEM electrolyser: two-phase flow regime, electrochemical modelling and experimental validation". In: *International Journal of Hydrogen Energy* 42.42 (2017), pp. 26203–26216. ISSN: 0360-3199. DOI: 10.1016/j.ijhydene.2017.08.211.

[86] S. A. Grigoriev and A. A. Kalinnikov. "Mathematical modeling and experimental study of the performance of PEM water electrolysis cell with different loadings of platinum metals in electrocatalytic layers". In: *International Journal of Hydrogen Energy* 42.3 (2017). The 6th European Fuel Cell Technology & Applications Piero Lunghi Conference & Exhibition (EFC15), 16-18 December 2015, Naples, Italy, pp. 1590–1597. ISSN: 0360-3199. DOI: 10.1016/j.ijhydene.2016.09.058.

[87] M. F. Kaya and NESRİN Demir. "Numerical investigation of PEM water electrolysis performance for different oxygen evolution electrocatalysts". In: *Fuel Cells* 17.1 (2017), pp. 37–47. DOI: 10.1002/fuce.201600216.

[88] Alhassan Salami Tijani, Nur Afiqah Binti Kamarudin, and Fatin Athirah Binti Mazlan. "Investigation of the effect of charge transfer coefficient (CTC) on the operating voltage of polymer electrolyte membrane (PEM) electrolyzer". In: *International Journal of Hydrogen Energy* 43.19 (2018), pp. 9119–9132. ISSN: 0360-3199. DOI: 10.1016/j.ijhydene.2018.03.111.

[89] Alhassan Salami Tijani et al. "Electrochemical characteristics of (PEM) electrolyzer under influence of charge transfer coefficient". In: *International Journal of Hydrogen Energy* 44.50 (2019), pp. 27177–27189. ISSN: 0360-3199. DOI: 10.1016/j.ijhydene.2019.08.188.

[90] Faeze Moradi Nafchi et al. "A parametric study of polymer membrane electrolyser performance, energy and exergy analyses". In: *International Journal of Hydrogen Energy* 44.34 (2019), pp. 18662–18670. DOI: 10.1016/j.ijhydene.2018.11.081.

[91] Francesco Marangio, Massimo Santarelli, and M. Cali. "Theoretical model and experimental analysis of a high pressure PEM water electrolyser for hydrogen production". In: *International Journal of Hydrogen Energy* 34.3 (2009), pp. 1143–1158. DOI: 10.1016/j.ijhydene.2008.11.083.

[92] Zhenye Kang et al. "Effects of various parameters of different porous transport layers in proton exchange membrane water electrolysis". In: *Electrochimica Acta* 354 (2020), p. 136641. ISSN: 0013-4686. DOI: 10.1016/j.electacta.2020.136641.

[93] Fabian Scheepers et al. "Improving the efficiency of PEM electrolyzers through membrane-specific pressure optimization". In: *Energies* 13.3 (2020), 612:1–612:18. DOI: 10.3390/en13030612.

[94] Kyu Heon Rho et al. "Performance analysis of polymer electrolyte membrane water electrolyzer using OpenFOAM®: two-phase flow regime, electrochemical model". In: *Membranes* 10.12 (2020). ISSN: 2077-0375. DOI: 10.3390/membranes10120441.

[95] Zhuqian Zhang and Xiaohui Xing. "Simulation and experiment of heat and mass transfer in a proton exchange membrane electrolysis cell". In: *International Journal of Hydrogen Energy* 45.39 (2020). The 7th International Conference on Energy, Engineering and Environmental Engineering, pp. 20184–20193. ISSN: 0360-3199. DOI: 10.1016/j.ijhydene.2020.02.102.

[96] Jacob A. Wrubel et al. "Mathematical modeling of novel porous transport layer architectures for proton exchange membrane electrolysis cells". In: *International Journal of Hydrogen Energy* 46.50 (2021), pp. 25341–25354. ISSN: 0360-3199. DOI: 10.1016/j.ijhydene.2021.05.070.

[97] Farid Aubras et al. "Dimensionless approach of a polymer electrolyte membrane water electrolysis: advanced analytical modelling". In: *Journal of Power Sources* 481 (2021), 228858:1–228858:10. DOI: 10.1016/j.jpowsour.2020.228858.

[98] ZhiMing Wang et al. "Numerical investigation of water and temperature distributions in a proton exchange membrane electrolysis cell". In: *Science China Technological Sciences* 64.7 (2021), pp. 1555–1566. DOI: 10.1007/s11431-021-1810-9.

[99] A. A. Kalinnikov et al. "Two-phase mass transfer in porous transport layers of the electrolysis cell based on a polymer electrolyte membrane: analysis of the limitations". In: *Electrochimica Acta* 387 (2021), p. 138541. ISSN: 0013-4686. DOI: 10.1016/j.electacta.2021.138541.

[100] M. Santarelli, P. Medina, and M. Calì. "Fitting regression model and experimental validation for a high-pressure PEM electrolyzer". In: *International Journal of Hydrogen Energy* 34.6 (2009), pp. 2519–2530. ISSN: 0360-3199. DOI: 10.1016/j.ijhydene.2008.11.036.

[101] P. Medina and M. Santarelli. "Analysis of water transport in a high pressure PEM electrolyzer". In: *International Journal of Hydrogen Energy* 35.11 (2010). 3rd Argentinean and 2nd Latin American Congress inHydrogen and Sustainable Energy Sources, pp. 5173–5186. ISSN: 0360-3199. DOI: 10.1016/j.ijhydene.2010.02.130.

[102] A. B. Goldberg et al. "A hydrodynamic model for water decomposition in electrolyzers with a solid polymer electrolyte". In: *Journal of Applied Electrochemistry* 22.12 (1992), pp. 1147–1154. DOI: 10.1007/BF01297416.

[103] S. A. Grigor'ev et al. "Electrolysis of water in a system with a solid polymer electrolyte at elevated pressure". In: *Russian Journal of Electrochemistry* 37.8 (2001), pp. 819–822. DOI: 10.1023/A:1016735003101.

[104] Kevin W. Harrison et al. "Semiempirical model for determining PEM electrolyzer stack characteristics". In: *Journal of Fuel Cell Science and Technology* 3.2 (Nov. 2005), pp. 220–223. ISSN: 1550-624X. DOI: 10.1115/1.2174072.

[105] Meng Ni, Michael K. H. Leung, and Dennis Y. C. Leung. "Electrochemistry modeling of proton exchange membrane (PEM) water electrolysis for hydrogen production". English. In: *16th World Hydrogen Energy Conference 2006, WHEC 2006*. Vol. 1. 13–16 June 2006, pp. 33–39. ISBN: 9781622765409. URL: https://scholars.cityu.edu.hk/en/publications/publication(d3345447-369b-4390-9d0e-5117c259085c).html.

[106] Brahim Laoun, Bouziane Mahmah, and Lazhar Serir. "Theoretical investigation on solid polymer electrolyte water electrolysis". In: *WIH2'2007, The Second International Workshop on Hydrogen.* 19–21 March 2007.

[107] B. Laoun et al. "Electrochemical aided model to study solid polymer electrolyte water electrolysis". In: *Journal of Renewable Energies* 11.2 (2008). Accessed on 19-08-2021, pp. 267–276. URL: https://revue.cder.dz/index.php/rer/article/view/76.

[108] C. Y. Biaku et al. "A semiempirical study of the temperature dependence of the anode charge transfer coefficient of a 6 kW PEM electrolyzer". In: *International journal of hydrogen energy* 33.16 (2008), pp. 4247–4254. DOI: 10.1016/j.ijhydene.2008.06.006.

[109] N. V. Dale, M. D. Mann, and H. Salehfar. "Semiempirical model based on thermodynamic principles for determining 6kW proton exchange membrane electrolyzer stack characteristics". In: *Journal of Power Sources* 185.2 (2008), pp. 1348–1353. ISSN: 0378-7753. DOI: 10.1016/j.jpowsour.2008.08.054.

[110] Fabrizio Sossan et al. "A model predictive control strategy for the space heating of a smart building including cogeneration of a fuel cell-electrolyzer system". In: *International Journal of Electrical Power & Energy Systems* 62 (2014), pp. 879–889. ISSN: 0142-0615. DOI: 10.1016/j.ijepes.2014.05.040.

[111] S. A. Grigoriev et al. "Mathematical modeling of high-pressure PEM water electrolysis". In: *Journal of applied electrochemistry* 40.5 (2010), pp. 921–932. DOI: 10.1007/s10800-009-0031-z.

[112] Maximilian Schalenbach et al. "Pressurized PEM water electrolysis: efficiency and gas crossover". In: *International Journal of Hydrogen Energy* 38.35 (2013), pp. 14921–14933. ISSN: 0360-3199. DOI: 10.1016/j.ijhydene.2013.09.013.

[113] Markus Sartory et al. "Theoretical and experimental analysis of an asymmetric high pressure PEM water electrolyser up to 155 bar". In: *International Journal of Hydrogen Energy* 42.52 (2017), pp. 30493–30508. ISSN: 0360-3199. DOI: 10.1016/j.ijhydene.2017.10.112.

[114] Emile Tabu Ojong et al. "Development of an experimentally validated semi-empirical fully-coupled performance model of a PEM electrolysis cell with a 3-D structured porous transport layer". In: *International Journal of Hydrogen Energy* 42.41 (2017), pp. 25831–25847. ISSN: 0360-3199. DOI: 10.1016/j.ijhydene.2017.08.183.

[115] Amit C. Bhosale et al. "Modeling and experimental validation of a unitized regenerative fuel cell in electrolysis mode of operation". In: *Energy* 121 (2017), pp. 256–263. ISSN: 0360-5442. DOI: 10.1016/j.energy.2017.01.031.

[116] Meng Ni, Michael K. H. Leung, and Dennis Y. C. Leung. "Energy and exergy analysis of hydrogen production by a proton exchange membrane (PEM) electrolyzer plant". In: *Energy Conversion and Management* 49.10 (2008), pp. 2748–2756. ISSN: 0196-8904. DOI: 10.1016/j.enconman.2008.03.018.

[117] Amin Nouri-Khorasani et al. "Model of oxygen bubbles and performance impact in the porous transport layer of PEM water electrolysis cells". In: *International Journal of Hydrogen Energy* 42.48 (2017), pp. 28665–28680. ISSN: 0360-3199. DOI: 10.1016/j.ijhydene.2017.09.167.

[118] K. S. Agbli et al. "Multiphysics simulation of a PEM electrolyser: energetic macroscopic representation approach". In: *International Journal of Hydrogen Energy* 36.2 (2011), pp. 1382–1398. DOI: 10.1016/j.ijhydene.2010.10.069.

[119] F. Z. Aouali et al. "Modelling and experimental analysis of a PEM electrolyser powered by a solar photovoltaic panel". In: *Energy Procedia* 62 (2014). 6th International Conference on Sustainability in Energy and Buildings, SEB-14, pp. 714–722. ISSN: 1876-6102. DOI: 10.1016/j.egypro.2014.12.435.

[120] F. Z. Aouali et al. "Analytical modelling and experimental validation of proton exchange membrane electrolyser for hydrogen production". In: *International Journal of Hydrogen Energy* 42.2 (2017), pp. 1366–1374. ISSN: 0360-3199. DOI: 10.1016/j.ijhydene.2016.03.101.

[121] Dongqi Zhao et al. "Dynamic behaviour and control strategy of high temperature proton exchange membrane electrolyzer cells (HT-PEMECs) for hydrogen production". In: *International Journal of Hydrogen Energy* 45.51 (2020), pp. 26613–26622. ISSN: 0360-3199. DOI: 10.1016/j.ijhydene.2020.07.155.

[122] M. E. Lebbal and S. Lecœuche. "Identification and monitoring of a PEM electrolyser based on dynamical modelling". In: *International Journal of Hydrogen Energy* 34.14 (2009). 2nd International Conference on Hydrogen Safety, pp. 5992–5999. ISSN: 0360-3199. DOI: 10.1016/j.ijhydene.2009.02.003.

[123] R. García-Valverde, N. Espinosa, and A. Urbina. "Simple PEM water electrolyser model and experimental validation". In: *International Journal of Hydrogen Energy* 37.2 (2012), pp. 1927–1938. DOI: 10.1016/j.ijhydene.2011.09.027.

[124] Houcheng Zhang et al. "Efficiency calculation and configuration design of a PEM electrolyzer system for hydrogen production". In: *International Journal of Electrochemical Science* 7.4 (2012). Accessed on 7-08-2021, pp. 4143–4157. URL: http://www.electrochemsci.org/papers/vol7/7054143.pdf.

[125] Huiyong Kim, Mikyoung Park, and Kwang Soon Lee. "One-dimensional dynamic modeling of a high-pressure water electrolysis system for hydrogen production". In: *International Journal of Hydrogen Energy* 38.6 (2013), pp. 2596–2609. DOI: 10.1016/j.ijhydene.2012.12.006.

[126] Haluk Görgün. "Dynamic modelling of a proton exchange membrane (PEM) electrolyzer". In: *International Journal of Hydrogen Energy* 31.1 (2006), pp. 29–38. DOI: 10.1016/j.ijhydene.2005.04.001.

[127] A. Awasthi, Keith Scott, and S. Basu. "Dynamic modeling and simulation of a proton exchange membrane electrolyzer for hydrogen production". In: *International Journal of Hydrogen Energy* 36.22 (2011), pp. 14779–14786. DOI: 10.1016/j.ijhydene.2011.03.045.

[128] Vincenzo Liso et al. "Modelling and experimental analysis of a polymer electrolyte membrane water electrolysis cell at different operating temperatures". In: *Energies* 11.12 (2018), 3273:1–3273:18. DOI: 10.3390/en11123273.

[129] Petronilla Fragiacomo and Matteo Genovese. "Modeling and energy demand analysis of a scalable green hydrogen production system". In: *International Journal of Hydrogen Energy* 44.57 (2019), pp. 30237–30255. DOI: 10.1016/j.ijhydene.2019.09.186.

[130] Somayeh Toghyani et al. "Optimization of operating parameters of a polymer exchange membrane electrolyzer". In: *International Journal of Hydrogen Energy* 44.13 (2019), pp. 6403–6414. ISSN: 0360-3199. DOI: 10.1016/j.ijhydene.2019.01.186.

[131] Ozcan Atlam and Mohan Kolhe. "Equivalent electrical model for a proton exchange membrane (PEM) electrolyser". In: *Energy Conversion and Management* 52.8 (2011), pp. 2952–2957. ISSN: 0196-8904. DOI: 10.1016/j.enconman.2011.04.007.

[132] Mohan Kolhe and Ozcan Atlam. "Empirical electrical modeling for a proton exchange membrane electrolyzer". In: *2011 International Conference on Applied Superconductivity and Electromagnetic Devices*. IEEE. 2011, pp. 131–134. DOI: 10.1109/ASEMD.2011.6145085.

[133] Anissia Beainy, Nabil Karami, and Nazih Moubayed. "Simulink model for a PEM electrolyzer based on an equivalent electrical circuit". In: *International Conference on Renewable Energies for Developing Countries 2014*. IEEE. 26–27 November 2014, pp. 145–149. DOI: 10.1109/REDEC.2014.7038547.

[134] Rony Escobar-Yonoff et al. "Performance assessment and economic perspectives of integrated PEM fuel cell and PEM electrolyzer for electric power generation". In: *Heliyon* 7.3 (2021), e06506. DOI: 10.1016/j.heliyon.2021.e06506.

[135] Tevfik Yigit and Omer Faruk Selamet. "Mathematical modeling and dynamic Simulink simulation of high-pressure PEM electrolyzer system". In: *International Journal of Hydrogen Energy* 41.32 (2016), pp. 13901–13914. ISSN: 0360-3199. DOI: 10.1016/j.ijhydene.2016.06.022.

[136] Bo Han et al. "Electrochemical performance modeling of a proton exchange membrane electrolyzer cell for hydrogen energy". In: *International Journal of Hydrogen Energy* 40.22 (2015), pp. 7006–7016. ISSN: 0360-3199. DOI: 10.1016/j.ijhydene.2015.03.164.

[137] Bo Han et al. "Modeling of interfacial resistance effects on the performance and efficiency for electrolyzer energy storage". In: *13th International Energy Conversion Engineering Conference*. 2015, p. 3915. DOI: 10.2514/6.2015-3915.

[138] Zhenye Kang et al. "Performance modeling and current mapping of proton exchange membrane electrolyzer cells with novel thin/tunable liquid/gas diffusion layers". In: *Electrochimica Acta* 255 (2017), pp. 405–416. ISSN: 0013-4686. DOI: 10.1016/j.electacta.2017.09.170.

[139] J. C. Garcia-Navarro, M. Schulze, and K. A. Friedrich. "Measuring and modeling mass transport losses in proton exchange membrane water electrolyzers using electrochemical impedance spectroscopy". In: *Journal of Power Sources* 431 (2019), pp. 189–204. ISSN: 0378-7753. DOI: 10.1016/j.jpowsour.2019.05.027.

[140] Tim M. Brown et al. "Dynamic first principles model of a complete reversible fuel cell system". In: *Journal of Power Sources* 182.1 (2008), pp. 240–253. ISSN: 0378-7753. DOI: https://doi.org/10.1016/j.jpowsour.2008.03.077.

[141] Bonghwan Lee, Kiwon Park, and Hyung-Man Kim. "Dynamic simulation of PEM water electrolysis and comparison with experiments". In: *International Journal of Electrochemical Science* 8.1 (2013). Accessed on 7-08-2021, pp. 235–248. URL: http://www.electrochemsci.org/papers/vol8/80100235.pdf.

[142] Z. Abdin, C.J. Webb, and E. MacA Gray. "Modelling and simulation of a proton exchange membrane (PEM) electrolyser cell". In: *International Journal of Hydrogen Energy* 40.39 (2015), pp. 13243–13257. DOI: 10.1016/j.ijhydene.2015.07.129.

[143] Christiaan Martinson et al. "Equivalent electrical circuit modelling of a proton exchange membrane electrolyser based on current interruption". In: *2013 IEEE International Conference on Industrial Technology (ICIT)*. IEEE. 25–28 Feb. 2013, pp. 716–721. DOI: 10.1109/ICIT.2013.6505760.

[144] Sanghyun Yun, Jinyon Yun, and Gunyong Hwang. "Dynamic Model of Water Electrolysis for Prediction of Dynamic Characteristics of Cooling System". In: *Transactions of the Korean Hydrogen and New Energy Society* 32.1 (2021), pp. 1–10. DOI: `10.7316/KHNES.2021.32.1.1`.

[145] C. A. Martinson et al. "Characterisation of a PEM electrolyser using the current interrupt method". In: *International Journal of Hydrogen Energy* 39.36 (2014), pp. 20865–20878. ISSN: 0360-3199. DOI: `10.1016/j.ijhydene.2014.09.153`.

[146] Deju D. Nation and Kahlil L. Smith. "Modelling the dynamics of a polymer electrolyte membrane (PEM) electrolyser at start-Up". In: (2016). Accessed on 19-08-2021. URL: `https://www.researchgate.net/profile/Deju-Nation-2/publication/305777322_Modelling_the_Dynamics_of_a_Polymer_Electrolyte_Membrane_PEM_Electrolyser_at_Start-Up/links/5901ddfb4585156502a28c88/Modelling-the-Dynamics-of-a-Polymer-Electrolyte-Membrane-PEM-Electrolyser-at-Start-Up.pdf`.

[147] Mohamed Koundi and Hassan EL Fadil. "Mathematical modeling of PEM electrolyzer and design of a voltage controller by the SMPWM approach". In: *2019 International Conference on Power Generation Systems and Renewable Energy Technologies (PGSRET)*. 2019, pp. 1–6. DOI: `10.1109/PGSRET.2019.8882737`.

[148] Damien Guilbert and Gianpaolo Vitale. "Experimental validation of an equivalent dynamic electrical model for a proton exchange membrane electrolyzer". In: *2018 IEEE International Conference on Environment and Electrical Engineering and 2018 IEEE Industrial and Commercial Power Systems Europe (EEEIC / I CPS Europe)*. 2018, pp. 1–6. DOI: `10.1109/EEEIC.2018.8494523`.

[149] Damien Guilbert and Gianpaolo Vitale. "Dynamic emulation of a PEM electrolyzer by time constant based exponential model". In: *Energies* 12.4 (2019). ISSN: 1996-1073. DOI: `10.3390/en12040750`.

[150] Burin Yodwong et al. "Energy efficiency based control strategy of a three-level interleaved DC-DC buck converter supplying a proton exchange membrane electrolyzer". In: *Electronics* 8.9 (2019). ISSN: 2079-9292. DOI: `10.3390/electronics8090933`.

[151] Ángel Hernández-Gómez et al. "Development of an adaptive static-dynamic electrical model based on input electrical energy for PEM water electrolysis". In: *International Journal of Hydrogen Energy* 45.38 (2020), pp. 18817–18830. ISSN: 0360-3199. DOI: `10.1016/j.ijhydene.2020.04.182`.

[152] Ángel Hernández-Gómez et al. "Cell voltage static-dynamic modeling of a PEM electrolyzer based on adaptive parameters: development and experimental validation". In: *Renewable Energy* 163 (2021), pp. 1508–1522. ISSN: 0960-1481. DOI: `10.1016/j.renene.2020.09.106`.

[153] Damien Guilbert and Gianpaolo Vitale. "Variable parameters model of a PEM electrolyzer based model reference adaptive system approach". In: *2020 IEEE International Conference on Environment and Electrical Engineering and 2020 IEEE Industrial and Commercial Power Systems Europe (EEEIC / I CPS Europe)*. 2020, pp. 1–6. DOI: `10.1109/EEEIC/ICPSEurope49358.2020.9160615`.

[154] Damien Guilbert, Dario Sorbera, and Gianpaolo Vitale. "A stacked interleaved DC-DC buck converter for proton exchange membrane electrolyzer applications: design and experimental validation". In: *International Journal of Hydrogen Energy* 45.1 (2020), pp. 64–79. ISSN: 0360-3199. DOI: `10.1016/j.ijhydene.2019.10.238`.

[155] P. Olivier, C. Bourasseau, and B. Ould-Bouamama. "Modelling, simulation and analysis of a PEM electrolysis system". In: *IFAC-PapersOnLine* 49.12 (2016). 8th IFAC Conference on Manufacturing Modelling, Management and Control MIM 2016, pp. 1014–1019. ISSN: 2405-8963. DOI: 10.1016/j.ifacol.2016.07.575.

[156] P. S. Kauranen, P. D. Lund, and J. P. Vanhanen. "Development of a self-sufficient solar-hydrogen energy system". In: *International Journal of Hydrogen Energy* 19.1 (1994), pp. 99–106. ISSN: 0360-3199. DOI: 10.1016/0360-3199(94)90181-3.

[157] Jianhu Nie et al. "A photoelectrochemical model of proton exchange water electrolysis for hydrogen production". In: *Journal of Heat Transfer* 130.4 (Mar. 2008). 042409. ISSN: 0022-1481. DOI: 10.1115/1.2789722.

[158] Brahim Laoun et al. "Modeling of solar photovoltaic-polymer electrolyte membrane electrolyzer direct coupling for hydrogen generation". In: *International Journal of Hydrogen Energy* 41.24 (2016), pp. 10120–10135. ISSN: 0360-3199. DOI: 10.1016/j.ijhydene.2016.05.041.

[159] *Non-uniform velocity distributions in bipolar plate PEM electrolysis cell*. Vol. Volume 2: Fora, Parts A and B. Fluids Engineering Division Summer Meeting. July 2007, pp. 1339–1345. DOI: 10.1115/FEDSM2007-37299.

[160] *Numerical modeling of two-phase flow in a bipolar plate of a PEM electrolyzer cell*. Vol. Volume 10: Heat Transfer, Fluid Flows, and Thermal Systems, Parts A, B, and C. ASME International Mechanical Engineering Congress and Exposition. Oct. 2008, pp. 783–788. DOI: 10.1115/IMECE2008-68913.

[161] Jianhu Nie et al. "Numerical and experimental study of three-dimensional fluid flow in the bipolar plate of a PEM electrolysis cell". In: *International Journal of Thermal Sciences* 48.10 (2009), pp. 1914–1922. ISSN: 1290-0729. DOI: 10.1016/j.ijthermalsci.2009.02.017.

[162] Jianhu Nie and Yitung Chen. "Numerical modeling of three-dimensional two-phase gas–liquid flow in the flow field plate of a PEM electrolysis cell". In: *International Journal of Hydrogen Energy* 35.8 (2010), pp. 3183–3197. ISSN: 0360-3199. DOI: 10.1016/j.ijhydene.2010.01.050.

[163] N. Briguglio et al. "Design and testing of a compact PEM electrolyzer system". In: *International Journal of Hydrogen Energy* 38.26 (2013), pp. 11519–11529. DOI: 10.1016/j.ijhydene.2013.04.091.

[164] F. Arbabi et al. "Three-dimensional computational fluid dynamics modelling of oxygen bubble transport in polymer electrolyte membrane electrolyzer porous transport layers". In: *Journal of The Electrochemical Society* 163.11 (2016), F3062–F3069. DOI: 10.1149/2.0091611jes.

[165] Somayeh Toghyani, Ebrahim Afshari, and Ehsan Baniasadi. "Three-dimensional computational fluid dynamics modeling of proton exchange membrane electrolyzer with new flow field pattern". In: *Journal of Thermal Analysis and Calorimetry* 135.3 (2019), pp. 1911–1919. DOI: 10.1007/s10973-018-7236-5.

[166] S. Toghyani, E. Baniasadi, and E. Afshari. "Numerical simulation and exergoeconomic analysis of a high temperature polymer exchange membrane electrolyzer". In: *International Journal of Hydrogen Energy* 44.60 (2019), pp. 31731–31744. ISSN: 0360-3199. DOI: 10.1016/j.ijhydene.2019.10.087.

[167] Zhiwen Ma et al. "A comprehensive modeling method for proton exchange membrane electrolyzer development". In: *International Journal of Hydrogen Energy* 46.34 (2021). Special issue on the 2nd International Symposium on Hydrogen Energy and Energy Technologies (HEET 2019), pp. 17627–17643. ISSN: 0360-3199. DOI: 10.1016/j.ijhydene.2021.02.170.

[168] Steffen Becker and Vishy Karri. "Predictive models for PEM-electrolyzer performance using adaptive neuro-fuzzy inference systems". In: *International Journal of Hydrogen Energy* 35.18 (2010), pp. 9963–9972. ISSN: 0360-3199. DOI: 10.1016/j.ijhydene.2009.11.060.

[169] A. U. Chavez-Ramirez et al. "Dynamic model of a PEM electrolyzer based on artificial neural networks". In: *Journal of New Materials for Electrochemical System* 14 (2011), pp. 113–119. DOI: 10.14447/jnmes.v14i2.119.

[170] Jason Keonhag Lee and Aimy Bazylak. "Stochastic generation of sintered titanium powder-based porous transport layers in polymer electrolyte membrane electrolyzers and investigation of structural properties". In: *ECS Transactions* 80.8 (2017), pp. 1097–1106. DOI: 10.1149/08008.1097ecst.

[171] J. K. Lee, C. H. Lee, and A. Bazylak. "Pore network modelling to enhance liquid water transport through porous transport layers for polymer electrolyte membrane electrolyzers". In: *Journal of Power Sources* 437 (2019), p. 226910. ISSN: 0378-7753. DOI: 10.1016/j.jpowsour.2019.226910.

[172] P. Ayivor et al. "Modelling of large size electrolyzer for electrical grid stability studies in real time digital simulation". In: *Proceedings of the 3rd International Hybrid Power Systems Workshop, Tenerife, Spain.* Accessed on 10-08-2021. 2018, pp. 8–9. URL: https://hybridpowersystems.org/wp-content/uploads/sites/9/2018/05/TENE18_054_posterpaper_Ayivor_Patrick-1.pdf.

[173] Bart W Tuinema et al. "Modelling of large-sized electrolysers for real-time simulation and study of the possibility of frequency support by electrolysers". In: *IET Generation, Transmission & Distribution* 14.10 (2020), pp. 1985–1992. DOI: 10.1049/iet-gtd.2019.1364.

[174] Alexandre Tugirumubano et al. "Numerical simulation of the polymer electrolyte membrane electrolyzer". In: *IOSR* 13 (2016), pp. 94–97. DOI: 10.9790/1684-1305069497.

[175] Amalendu Mukherjee, Ranjit Karmakar, and Arun Kumar Samantaray. *Bond graph in modeling, simulation and fault identification.* IK International New Delhi, 2006. URL: https://www.ikbooks.com/books/book/engineering-computer-science/mechanical-production-industrial-engineering/bond-graph-modeling-simulation-fault-identification/9788188237968/.

[176] Wolfgang Borutzky. *Bond graph methodology: development and analysis of multidisciplinary dynamic system models.* Springer Science & Business Media, 2009. DOI: 10.1007/978-1-84882-882-7.

[177] B. Ould-Bouamama et al. "Bond graphs for the diagnosis of chemical processes". In: *Computers & Chemical Engineering* 36 (2012), pp. 301–324. ISSN: 0098-1354. DOI: 10.1016/j.compchemeng.2011.07.008.

[178] Ishanka Udeshini Dedigama. "Diagnostics and modeling of polymer electrolyte membrane water electrolysers". Accessed on 01-09-2021. PhD thesis. UCL (University College London), 2014. URL: https://discovery.ucl.ac.uk/id/eprint/1426127/.

[179] B. Verdin et al. "Operando current mapping on PEM water electrolysis cells. Influence of mechanical stress". In: *International Journal of Hydrogen Energy* 42.41 (2017), pp. 25848–25859. ISSN: 0360-3199. DOI: 10.1016/j.ijhydene.2017.08.189.

[180] Stefania Siracusano et al. "Electrochemical impedance spectroscopy as a diagnostic tool in polymer electrolyte membrane electrolysis". In: *Materials* 11.8 (2018). ISSN: 1996-1944. DOI: 10.3390/ma11081368.

[181] M. Bernt et al. "Analysis of gas permeation phenomena in a PEM water electrolyzer operated at high pressure and high current density". In: *Journal of The Electrochemical Society* 167.12 (2020), p. 124502. DOI: 10.1149/1945-7111/abaa68.

[182] Zhenye Kang et al. "In-situ and in-operando analysis of voltage losses using sense wires for proton exchange membrane water electrolyzers". In: *Journal of Power Sources* 481 (2021), p. 229012. ISSN: 0378-7753. DOI: 10.1016/j.jpowsour.2020.229012.

[183] P. Millet et al. "Cell failure mechanisms in PEM water electrolyzers". In: *International Journal of Hydrogen Energy* 37.22 (2012). HySafe 1, pp. 17478–17487. ISSN: 0360-3199. DOI: 10.1016/j.ijhydene.2012.06.017.

[184] M. Maier et al. "Operando flow regime diagnosis using acoustic emission in a polymer electrolyte membrane water electrolyser". In: *Journal of Power Sources* 424 (2019), pp. 138–149. ISSN: 0378-7753. DOI: 10.1016/j.jpowsour.2019.03.061.

[185] S.A. Grigoriev et al. "Failure of PEM water electrolysis cells: case study involving anode dissolution and membrane thinning". In: *International Journal of Hydrogen Energy* 39.35 (2014), pp. 20440–20446. ISSN: 0360-3199. DOI: 10.1016/j.ijhydene.2014.05.043.

[186] Shucheng Sun et al. "Investigations on degradation of the long-term proton exchange membrane water electrolysis stack". In: *Journal of Power Sources* 267 (2014), pp. 515–520. ISSN: 0378-7753. DOI: 10.1016/j.jpowsour.2014.05.117.

[187] Qi Feng et al. "A review of proton exchange membrane water electrolysis on degradation mechanisms and mitigation strategies". In: *Journal of Power Sources* 366 (2017), pp. 33–55. ISSN: 0378-7753. DOI: 10.1016/j.jpowsour.2017.09.006.

[188] Christoph Rakousky et al. "Polymer electrolyte membrane water electrolysis: restraining degradation in the presence of fluctuating power". In: *Journal of Power Sources* 342 (2017), pp. 38–47. ISSN: 0378-7753. DOI: 10.1016/j.jpowsour.2016.11.118.

[189] S. Siracusano et al. "Degradation issues of PEM electrolysis MEAs". In: *Renewable Energy* 123 (2018), pp. 52–57. ISSN: 0960-1481. DOI: 10.1016/j.renene.2018.02.024.

[190] Christoph Rakousky et al. "The stability challenge on the pathway to high-current-density polymer electrolyte membrane water electrolyzers". In: *Electrochimica Acta* 278 (2018), pp. 324–331. ISSN: 0013-4686. DOI: 10.1016/j.electacta.2018.04.154.

[191] Michel Suermann, Boris Bensmann, and Richard Hanke-Rauschenbach. "Degradation of proton exchange membrane (PEM) water electrolysis cells: looking beyond the cell voltage increase". In: *Journal of The Electrochemical Society* 166.10 (2019), F645–F652. DOI: 10.1149/2.1451910jes.

[192] F. N. Khatib et al. "Material degradation of components in polymer electrolyte membrane (PEM) electrolytic cell and mitigation mechanisms: a review". In: *Renewable and Sustainable Energy Reviews* 111 (2019), pp. 1–14. ISSN: 1364-0321. DOI: 10.1016/j.rser.2019.05.007.

[193] Georgios Papakonstantinou et al. "Degradation study of a proton exchange membrane water electrolyzer under dynamic operation conditions". In: *Applied Energy* 280 (2020), p. 115911. ISSN: 0306-2619. DOI: 10.1016/j.apenergy.2020.115911.

[194]   Mohand Arab Djeziri et al. "Robust fault diagnosis by using bond graph approach". In: *IEEE/ASME Transactions on Mechatronics* 12.6 (2007), pp. 599–611. DOI: 10.1109/TMECH.2007.912746.

[195]   Om Prakash, Arun Kumar Samantaray, and Ranjan Bhattacharyya. "Optimal adaptive threshold and mode fault detection for model-based fault diagnosis of hybrid dynamical systems". In: *Fault Diagnosis of Hybrid Dynamic and Complex Systems*. Springer, 2018, pp. 45–78. DOI: 10.1007/978-3-319-74014-0_3.

[196]   Sumit Sood et al. "Generic dynamical model of PEM electrolyser under intermittent sources". In: *Energies* 13.24 (2020). ISSN: 1996-1073. DOI: 10.3390/en13246556.

[197]   Rochdi Merzouki et al. *Intelligent mechatronic systems: modeling, control and diagnosis*. Springer: London, UK, 2012. ISBN: 978-1-4471-4628-5. DOI: 10.1007/978-1-4471-4628-5.

[198]   P. Vijay, Arun Kumar Samantaray, and A. Mukherjee. "A bond graph model-based evaluation of a control scheme to improve the dynamic performance of a solid oxide fuel cell". In: *Mechatronics* 19.4 (2009), pp. 489–502. DOI: 10.1016/j.mechatronics.2008.11.016.

[199]   Belkacem Ould-Bouamama. "Bond graph approach as analysis tool in thermofluid model library conception". In: *Journal of the Franklin Institute* 340.1 (2003), pp. 1–23. DOI: 10.1016/S0016-0032(02)00051-0.

[200]   Yunus Cengel and Afshin Ghajar. *Heat and mass transfer: fundamentals and applications*. 5th. McGraw Hill Education: New Delhi India, 2017. ISBN: 978-9339223199.

[201]   Rodney L. LeRoy, Christopher T. Bowen, and Donald J. LeRoy. "The thermodynamics of aqueous water electrolysis". In: *Journal of The Electrochemical Society* 127.9 (1980), pp. 1954–1962. DOI: 10.1149/1.2130044.

[202]   Dmitri Bessarabov and Pierre Millet. *PEM water electrolysis*. Vol. 1. Academic Press: Cambridge, Massachusetts, USA, 2017. DOI: 10.1016/C2016-0-00574-0.

[203]   S. Shiva Kumar and V. Himabindu. "Hydrogen production by PEM water electrolysis – a review". In: *Materials Science for Energy Technologies* 2.3 (2019), pp. 442–454. ISSN: 2589-2991. DOI: 10.1016/j.mset.2019.03.002.

[204]   Elena Borgardt et al. "Impact of clamping pressure and stress relaxation on the performance of different polymer electrolyte membrane water electrolysis cell designs". In: *International Journal of Hydrogen Energy* 44.42 (2019), pp. 23556–23567. ISSN: 0360-3199. DOI: 10.1016/j.ijhydene.2019.07.075.

[205]   Zhenye Kang et al. "In-situ and in-operando analysis of voltage losses using sense wires for proton exchange membrane water electrolyzers". In: *Journal of Power Sources* 481 (2021), p. 229012. ISSN: 0378-7753. DOI: 10.1016/j.jpowsour.2020.229012.

[206]   Ugljesa Babic. "Polymer electrolyte water electrolysis: development of diagnostics methods and mitigation strategies to tackle component degradation". PhD thesis. ETH Zurich, 2019. DOI: 10.3929/ethz-b-000361838.

[207]   Om Prakash, Arun Kumar Samantaray, and Ranjan Bhattacharyya. "Model-based diagnosis of multiple faults in hybrid dynamical systems with dynamically updated parameters". In: *IEEE Transactions on Systems, Man, and Cybernetics: Systems* 49.6 (2017), pp. 1053–1072. DOI: 10.1109/TSMC.2017.2710143.

[208]   Martín David, Carlos Ocampo-Martínez, and Ricardo Sánchez-Peña. "Advances in alkaline water electrolyzers: a review". In: *Journal of Energy Storage* 23 (2019), pp. 392–403. ISSN: 2352-152X. DOI: 10.1016/j.est.2019.03.001.

[209] Immanuel Vincent and Dmitri Bessarabov. "Low cost hydrogen production by anion exchange membrane electrolysis: a review". In: *Renewable and Sustainable Energy Reviews* 81 (2018), pp. 1690–1704. ISSN: 1364-0321. DOI: 10.1016/j.rser.2017.05.258.

[210] L. An et al. "Mathematical modeling of an anion-exchange membrane water electrolyzer for hydrogen production". In: *International Journal of Hydrogen Energy* 39.35 (2014), pp. 19869–19876. ISSN: 0360-3199. DOI: 10.1016/j.ijhydene.2014.10.025.

[211] Li Xiao et al. "First implementation of alkaline polymer electrolyte water electrolysis working only with pure water". In: *Energy & Environmental Science* 5.7 (2012), pp. 7869–7871. DOI: 10.1039/C2EE22146B.

[212] Hiroshi Ito et al. "Investigations on electrode configurations for anion exchange membrane electrolysis". In: *Journal of Applied Electrochemistry* 48.3 (2018), pp. 305–316. DOI: 10.1007/s10800-018-1159-5.

[213] Belkacem Ould-Bouamama, Ibrahim Abdalah, and Anne-Lise Gehin. "Bond graphs as mechatronic approach for supervision design of multisource renewable energy system". In: *IOP Conference Series: Materials Science and Engineering* 417 (2018), p. 012033. DOI: 10.1088/1757-899x/417/1/012033.

[214] Alfredo Ursúa and Pablo Sanchis. "Static–dynamic modelling of the electrical behaviour of a commercial advanced alkaline water electrolyser". In: *International Journal of Hydrogen Energy* 37.24 (2012). 2011 International Workshop on Molten Carbonates & Related Topics, pp. 18598–18614. ISSN: 0360-3199. DOI: 10.1016/j.ijhydene.2012.09.125.

[215] Henry M. Paynter. *Analysis and design of engineering systems*. The M.I.T. Press: Cambridge, Massachusetts, USA, 1961.

[216] Jean Thoma and Belkacem Ould-Bouamama. *Modelling and simulation in thermal and chemical engineering: a bond graph approach*. Springer-Verlag Berlin Heidelberg: Germany, 2000. ISBN: 978-3-642-08566-6. DOI: 10.1007/978-3-662-04181-9.

[217] Belkacem Ould-Bouamana and Jean-Philippe Cassar. "Integrated bond graph modelling in process engineering linked with economic systems". In: *In Proceedings of the 14th European Simulation Multiconference on Simulation and Modelling: Enablers for a Better Quality of Life*. Accessed on 10-08-2021. 2000, pp. 340–347. URL: https://dl.acm.org/doi/abs/10.5555/647917.739676.

[218] Belkacem Ould-Bouamama, Ibrahim Abdalah, and Anne-Lise Gehin. "Bond graphs as mechatronic approach for supervision design of multisource renewable energy system". In: *In Proceedings of the 5th International Conference on Mechanics and Mechatronics Research (ICMMR)*. IOP Publishing. 19–21 July 2018, 012033:1–012033:5. DOI: 10.1088/1757-899X/417/1/012033.

[219] Belkacem Ould-Bouamama et al. "Model builder using functional and bond graph tools for FDI design". In: *Control Engineering Practice* 13.7 (2005), pp. 875–891. DOI: 10.1016/j.conengprac.2004.10.002.

[220] Belkacem Ould-Bouamama, M. Staroswiecki, and Arun Kumar Samantaray. "Software for supervision system design in process engineering industry". In: *IFAC Proceedings Volumes* 39.13 (2006), pp. 646–650. DOI: 10.3182/20060829-4-CN-2909.00107.